Doctoral theses at NTNU, 2019:196

Trygve Olav Fossum

# Adaptive Sampling for Marine Robotics

Doctoral thesis

Trygve Olav Fossum

ISBN 978-82-326-3988-5 (printed ver.)
ISBN 978-82-326-3989-2 (electronic ver.)
ISSN 1503-8181

NTNU
Norwegian University of
Science and Technology

**NTNU**
Norwegian University of Science and Technology
Thesis for the Degree of
Philosophiae Doctor
Faculty of Engineering
Department of Marine Technology

Doctoral theses at NTNU, 2019:196

NTNU
Norwegian University of
Science and Technology

Trygve Olav Fossum

# Adaptive Sampling for Marine Robotics

Thesis for the Degree of Philosophiae Doctor

Trondheim, Juni 2019

Norwegian University of Science and Technology
Faculty of Engineering
Department of Marine Technology

NTNU
Norwegian University of
Science and Technology

**NTNU**
Norwegian University of Science and Technology

Thesis for the Degree of Philosophiae Doctor

Faculty of Engineering
Department of Marine Technology



ISBN 978-82-326-3988-5 (printed ver.)
ISBN 978-82-326-3989-2 (electronic ver.)
ISSN 1503-8181

Doctoral theses at NTNU, 2019:196

Printed by NTNU Grafisk senter

*“We should send machines and instruments out to sea, not people.”*
*- David Packard*

# Abstract

Maintaining a healthy ocean is of the utmost importance. Having only a limited set of resources available to study this vast domain requires research and science to focus on more efficient data collection. Determining *when and where to sample* is, in this regard, a crucial question. The introduction of robotic elements into ocean observation practices have augmented traditional ship-based sampling and provided efficient and reliable sensing platforms for autonomous sampling of oceanographic data, enabling measurements on scales logistically impossible using traditional techniques. However, robotic sampling still relies on deterministic pre-programmed sensing schemes, consisting of sequential waypoints scripted with mission planning tools. In this case, all relevant information is implemented into the mission *a priori*. This is problematic, since prior knowledge of oceanographic conditions is usually poor leading to substantial uncertainty; consequently, plans for sampling the oceans are suboptimal at best.

Alternatively, the platform can be programmed to adjust the sampling plan online during the mission, capitalizing on both prior and current (*in-situ*) information. In this setting, sampling happens sequentially over time, according to a conditional plan which changes online during the mission in response to observed data. This type of autonomous sampling scheme is typically referred to as *adaptive sampling* or *data-driven sampling*. Adaptive/data-driven strategies can operate on an a posterior knowledge base and react to current conditions. The impact of this is twofold: i) enabling the sensor platform to divert from the mission if favorable circumstances materialize (opportunistic behavior), and ii) increasing the prospect of retrieving pursued information more effectively. The latter aspect is often considered the most noteworthy, especially for resource intensive environmental sensing applications, having the potential to reduce time and cost.

This thesis presents different methods and applications in adaptive sampling for marine robotics, focusing on exploration of the upper ocean using single platform applications. The coastal ocean and the upper water column are characterized by substantial heterogeneity and spatio-temporal variation. Sampling can therefore benefit from access to synoptic marine data sources such as ocean models and remote sensing, but due to computational limitations and accuracy, these information sources must be used in combination with statistics. Gaussian Processes (GPs) offer a practical probabilistic approach for modeling spatial dependent data and uncertainty. The foundation for the approaches developed here is based on combining GPs with information-theoretic and data-driven criteria to evaluate potential sampling locations. A general problem related to optimization of choosing these sensing locations is the exponential combinatoric increase

in dimensionality. The problems are therefore often simplified using heuristics and greedy algorithms.

The principal contributions of this work are related to i) the design and analysis of information-theoretic approaches in upper water column sampling, coupled with intelligent control and ii) testing and validating these methods in the field. This includes a suite of greedy data-driven sampling strategies for the upper water column, developed and tested in full-scale experiments, with applications spanning thermal gradients and internal-waves, assessment of ocean model accuracy, 3-dimensional tracking of sub-surface chlorophyll, and dispersion dynamics in the water column. A proposed methodology for building compact proxy models from remote sensing SST images is also presented using machine learning tools, as well as an application for autonomous mapping of the seafloor. Field testing of these methods presents a considerable challenge given the harsh and dynamic state of the ocean, where large uncertainties and risk are usually the norm rather than the exception. The results show the benefits and potential of using marine data sources and incorporating adaptive sampling routines for exploration of the upper ocean. The emergence of autonomous systems and adaptive sampling does not displace ships or fixed observation stations, however, the introduction of data-driven sampling can greatly augment and increase the observational efficiency and resolution, helping to ensure scientific success.

This thesis is edited as a collection of papers.

# Preface

This thesis is submitted in partial fulfillment of the requirements for the degree of philosophiae doctor (PhD) at the Norwegian University of Science and Technology (NTNU). The work is a part of the Norwegian Centre of Excellence (SFF), Centre for Autonomous Marine Operations and Systems (AMOS), and the Applied Underwater Robotics Laboratory (AURLab). AMOS is part of the Research Council of Norway (RCN) funding scheme, RCN-223254.

The work was done at AMOS at the Department of Marine Technology (IMT) at NTNU, as well as the Monterey Bay Aquarium Research Institute (MBARI) and Stanford University in California, US. My main supervisors have been Professor Martin Ludvigsen and Professor Kanna Rajan, with support from Professor Jo Eidsvik. During my time in the US, my advisors were Dr. John Ryan, Professor Tapan Mukerji, and Thom Maughan.

## Acknowledgments

I would like to thank my supervisor, Professor Martin Ludvigsen for continuous support and encouragement, extending well beyond my thesis research. I will miss our trips and cruises together. Also, a great thanks to Professor Kanna Rajan for collaboration across all aspects of this work. I am especially grateful to him for sharing his foresightful perspective on ocean observation and overall knowledge, which has been of invaluable help in preparation of this thesis. Thank you also for providing opportunities and help beyond the call of duty. I would also like to thank Professor Jo Eidsvik, who played a central part during the course of my PhD. I could not have asked for a better collaborator, capable of sharing knowledge and helping me whenever I needed it. I look forward to our interactions in the future, Jo.

I am very grateful to RCN for providing the research grant making possible a research stay at MBARI and Stanford, and also to both institutions for inviting me. A significant portion of my thesis work has been carried out at the MBARI, where I had the privilege of working with a remarkable group of researchers. I am grateful to Dr. John Ryan for taking me in as a student and our interesting discussions and fruitful collaborations. I was also fortunate to meet my friend Thom Maughan, who deserves a big thank you. I cannot hope to give a true picture of your character here, so I will restrict myself to say that your spark in life is contagious.

Sharing this experience, the AURLab team deserves a special thank you. In particular, Petter Norgren, Øystein Sture, Tore Mo Bjøklund, Stein Melær Nornes, Øyvind Ødegaard, Frode Volden, Kay Skarpnes, Pedro De La Torre, and the unique team Geir Johnsen & Asgeir Sørensen. Thanks to my collaborators Stephanie Kemna (Maritime Robotics), Renato Mendes (Univ. Porto), Emlyn John Davies (SINTEF Ocean), Ingrid Ellingsen (SINTEF Ocean), Morten Omholt Alver (SINTEF Ocean), Jenny Ullgren (Runde Miljøsenter), Glaucia Fargoso (NTNU), Gunhild Elisabeth Berget (NTNU), and Tor Arne Johansen (NTNU). Thank you also to the Underwater Systems and Technologies Laboratory (LSTS) team at the University of Porto, and João Sousa, for providing support and advice throughout this work, as well as hosting me (always) on short notice.

Finally, I would like to thank my parents and brothers for their unconditional support on this journey. My great inspiration and mentor will always be my father, who led me to start a PhD in the first place. Last but not least, I am very grateful for all the support from my wonderful girlfriend Miriam; you are a remarkable person.

Trondheim, February $5^{th}$ 2019 *Trygve Olav Fossum*

# Contents

# Abbrevations and Conventions

We use the terms *data-driven* or *adaptive sampling* to refer to the act of making an intelligent and deliberate choice of *when and where* to gather data on the basis of informative and scientific metrics (measurements adjusted to purpose). Usually this also implies choices taken by an autonomous platform online and *in-situ*, where the term *in-situ* is used to refer to observations taken "in the environment". The term *upper ocean* refers to the water column.

| | |
|---|---|
| AMOS | Centre for Autonomous Marine Operations and Systems |
| AHRS | Attitude Heading Reference System |
| ASV/USV | Autonomous/Unmanned Surface Vehicle |
| AUV | Autonomous Underwater Vehicle |
| AURLab | Applied Underwater Robotics Laboratory |
| DVL | Doppler Velocity Logger |
| ENTiCE | Research project: ENabling Technology providing knowledge of structure, function and production in a complex Coastal Ecosystem. |
| ESA | European Space Agency |
| FFI | Norwegian Defence Research Establisment |
| GNSS | Global Navigation Satellite System |
| GPS | Global Positioning System |
| GSM | Global System for Mobile Communications |
| IMT | Department of Marine Technology |
| IMU | Inertial Measurement Unit |
| INS | Inertial Navigation System |
| LSTS | Underwater Systems and Technologies Laboratory at Univ. of Porto |
| MIT | Massachusetts Institute of Technology |
| NOAA | National Oceanic and Atmospheric Administration |
| NTNU | Norwegian University of Science and Technology |
| OOI | Object Of Interest |
| ROI | Region Of Interest |
| ROV | Remotely Operated Vehicle |
| R/V | Research Vessel |
| SSS | SideScan Sonar |
| UAV | Unmanned Aerial Vehicle |
| WHOI | Woods Hole Oceanographic Institution |

# List of Figures

# List of Tables

# Part I

# Thesis Overview

# Chapter 1

# Introduction & Motivation

CONSIDER the problem where the objective is to effectively measure a phenomenon or process taking place in the ocean. In this dynamic environment, observations are highly dependent on location and time, and relative to size of the oceanic domain, only a small number of sensors can be deployed, making it expensive and impractical – sometimes even impossible – to completely observe the entire domain in detail. A key question in this regard is

> *"Where and when should we measure in order to effectively retrieve relevant and useful information?"*

In spatial statistics this optimization problem is called *sampling* or *experimental design* (Krause et al., 2008), where the aim is to find the most informative locations given an optimization criterion or metric. Resolving these types of sensing problems depends on careful planning and understanding of the environmental characteristics. For an oceanographer, planning how to sample is often challenging as prior information is incomplete and uncertain. Trying to specify *when and where to sample* solely on the basis of prior data can therefore lead to redundant and ineffective data collection. Alternatively, one can make use of adaptive data collection systems and platforms capable of deciding where to sample online during the mission, in response to observed data. In this setting, sampling happens sequentially over time, according to a conditional plan that tries to capitalize on both prior and current (*in-situ*) information, providing potential for better allocation of sampling efforts and information recovery. This type of sampling is typically referred to as *adaptive sampling* and is encapsulated in Fig. 1.1, showing the fundamental premise that underlines this type of thinking, forming the basis for this thesis. This approach to sampling introduces a set of new challenges and topics that will be discussed in detail in the following subsections, in the context of sampling the upper ocean, using marine robotic platforms.

In this chapter, the motivation and background for the thesis is introduced together with the specific research questions and methodology. The goal is to explain adaptive sampling and related applications as plainly as possible, and build on this in the following chapters.

The structure and contributions of the thesis, as well as the relations between the papers, included in Part II of the thesis, are presented at the end of the chapter.

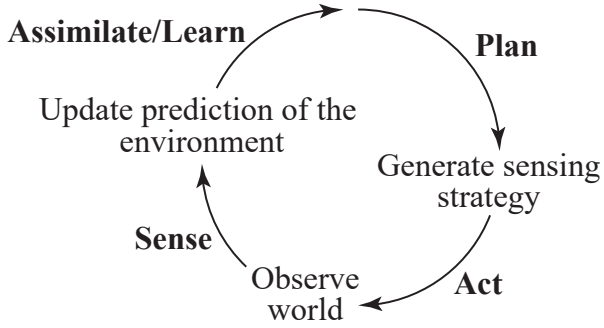


Figure 1.1: The adaptive sampling perspective of ocean observation underlining the approaches studied in this thesis. The cycle follows the *Sense→Plan→Act* control methodology.

## 1.1 Upper Ocean Observation: From Ships to Robots

Despite our reliance on the ocean, over 80% of the realm is unmapped, unobserved, and unexplored (National Oceanic and Atmospheric Administration, 2018). Starting with simple instruments, humans have studied and navigated the ocean throughout history. Although Charles Darwin set sail on the *HMS Beagle* and made many observations about ocean life in 1831 (Darwin and Keynes, 2001), modern oceanography first began as a field of science in the late 19th century with the *HMS Challenger* expedition in 1872-1876, which traveled more than 100,000 km and sampled all ocean basis except the Arctic (Bailey, 1953). The Norwegian scientist, Fridtjof Nansen, was an early, prominent figure for Arctic discovery and was responsible for valuable oceanographic, magnetic, and meteorological groundwork. He was studying the Arctic's current structure (Nansen, 1905) and was the inventor of the first widely used water sampling bottle (the "Nansen bottle"). Oceanographers and engineers have always looked for ways to improve ocean sampling systems and technologies. Much of this was driven by the fact that oceanographic exploration needed to both measure new parameters and reduce the cost of experiments - efforts that continue to this day

At a fundamental level, observing physical interactions in the ocean requires measuring across a moving mass of water and its constituents over time. Traditional ocean sampling methods were (and still are) ship-based, and included laborious data collection methods such as physical water sampling, net trawling, and vertical wire casting using various instruments. Such observations successfully led exploration of large-scale temperature, salinity, and density features associated with the dominant ocean currents until 1952 (Munk and Wunsch, 1982). An inherent problem with this form of observation was the lack of resolution in time and space, which masked observation of

a number of important processes and their variability. This lack of *synoptic*[1] observation prompted the renowned physical oceanographer, Walter Munk, to refer to this first period as the "century of undersampling". By the early 1970s the introduction of floating and fixed buoys resulted in increased temporal resolution, which soon demonstrated that the spatiotemporal variability of the water column was far more complex than previously assumed (Munk, 2002). The foundation for optimal synoptic sampling and exploration of this variability was later laid out in the pioneering work of Bretherton et al. (1976),whereby a moored array was specifically designed to reconstruct *mesoscale*[2] flow fields during the Mid-Ocean Dynamics Experiments (MODE-73 experiment). Gradually, a more nuanced understanding of ocean dynamics and scale-dependent variability became accepted. This led to an important realization among oceanographers that the current methods could not be sufficiently scaled to resolve the *aliasing*[3] problem linked to the traditional observational approach. Gathering data that can differentiate between spatial and temporal variations had always been a core challenge for oceanography; having a limited set of resources available to resolve this limitation, the marine scientific community felt compelled to focus on new and efficient data collection practices.

In the late 1970s, the first large-scale buoy network (Argo) and the first ocean satellite (Seasat) were launched. Like the introduction of the echosounder, satellite oceanography introduced a new and more synoptic perspective of the ocean. For the first time, some of the processes could be adequately measured with sufficient resolution to be *resolved*[4], such as tides (Munk, 2002); but unlike sound, the oceans are opaque to electromagnetic waves, thus only the very surface could be observed in this way. Synthetic ocean models were also rapidly becoming a useful tool, which could be used in conjunction with observations and satellite systems through assimilation (Munk and Wunsch, 1982). In response to an increasing need for *in-situ* characterization, the advent of marine robotics enabled data collection on scales logistically impossible using traditional techniques (Das et al., 2011), such as the ability to track individual organisms or resolve spatially-evolving gradients. The traditional form of ocean observation was by no means obsolete, but could now be complemented by data from a range of different sources. Numerous field programs involving coordinated robotic sampling, such as the Autonomous Ocean Sampling Network (AOSN-I/-II) (Curtin et al., 1993; Ramp et al., 2009), were conducted to study how ocean variability could be observed using a combined system of assets. In the wake of this and similar efforts, the need for coordinated, opportunistic, and targeted observations became more clear, leading the way for more sophisticated robotic sampling approaches.

[1] A synoptic observation is capable of capturing information in such a way that the measurements can more or less reconstruct the underlying process that created them.

[2] The term mesoscale describes the variability occurring at scales from ∼50-500 km, and ∼10-100 days; often referred to as the "internal weather of the ocean".

[3] Aliasing is an effect that arises from sampling information at a resolution/scale which is not sufficient for reconstruction (i.e., information that is lost when making observations).

[4] When we describe a process as resolved, we mean that the process is measured without aliasing.

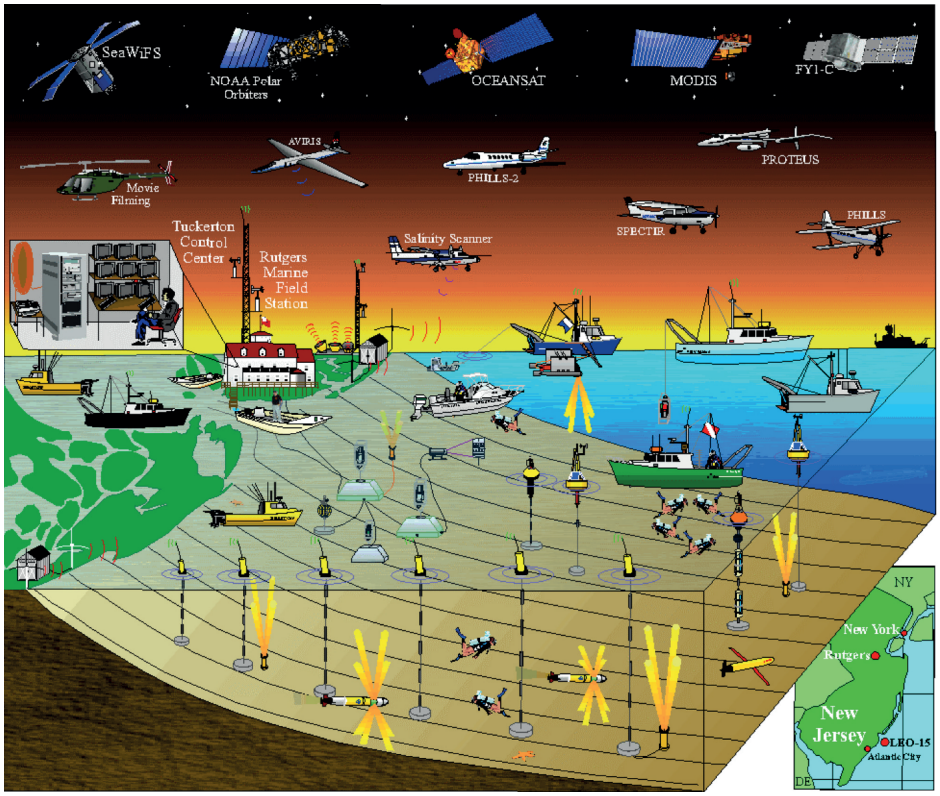


Figure 1.2: Schematic diagram illustrating the various platforms used for the Hyperspectral Coastal Ocean Dynamics Experiment (HyCODE) at the LEO-15 (von Alt and Grassle, 1992) study site off the coast of New Jersey, USA. Image courtesy: Scott Glenn, Rutgers University.

## 1.2 Adaptive Sampling of the Water Column

Present day ocean observation still builds on experiences from experiments such as AOSN-I/-II, where dominant practices have gradually shifted from ship-based ocean sampling to remote and robotic sensing using satellites, drifting floats, numerical ocean modeling, and autonomous underwater vehicles (AUVs). Oceanographic sensing practices have transformed from platform-based schemes towards networks of heterogeneous sensor nodes (Curtin et al., 1993)(see Fig. 1.2), measuring and sharing information across a range of different scales; this has prompted the need for effective allocation and coordination of these resources. Access to synoptic marine data sources such as ocean models and remote sensing can augment this process. However, the accuracy of ocean models is not at a level capable of making accurate predictions of these processes at scales sufficient for definite representation (Lermusiaux, 2006), and typical weather conditions make the use of remote sensing limited. As we will see, these information sources must therefore be used side-by-side with statistical tools and models, both to extract the best

possible information from the available data and provide the ability to generalize, model, and learn on the basis of prior and current data. The coastal ocean and the upper water column are domains where the need for more sophisticated robotic sampling approaches is critical. Being highly relevant to marine life and bio diversity, the study of the processes in the water column has broad ecological, scientific, and social-economical significance. Coastal influences from bathymetry, river discharge, land run-off, and complex oceanic circulation also cause additional heterogeneity and spatio-temporal variation that can only be adequately studied using *in-situ* assets. Determining what resources to deploy and *when and where to sample*, is therefore an essential question facing scientists in this domain. The fundamental non-deterministic nature of the ocean makes inference about sampling a task that cannot be fully determined prior to data collection – *ex-situ*. Regular grid ("lawnmower") or single-line surveys are still in use, but as ocean conditions imply both incomplete information and high uncertainty, such strategies often result in sub-optimal survey designs. These approaches are gradually being substituted by more effective sampling designs that can exploit background information, and adapt to changing conditions and observations (Frolov et al., 2014).

The potential for utilizing adaptive sampling approaches in the water column is significant. To illustrate this more clearly, examine Fig. 1.3a, which depicts a survey of a biomass layer distributed in the water column with an AUV. Let's imagine that we want to measure a property inherent to this biomass that implies placing the AUV within this layer. Starting with a non-adaptive strategy, a natural approach would be to base the survey depth on an average value calculated from prior data. Since this depth is dependent on conditions that may or may not be true for the current survey, the possibility of placing the AUV inside the biomass layer is low. Fig. 1.3a shows such a case, where a non-adaptive sampling plan (in red) ends up not measuring the biomass at all, except for a small region. Given the data from this survey, the conclusion might be that "there are little or no significant biomass in this area". In contrast, let's now imagine we use an adaptive strategy, capable of including information such as, "you are outside the patch→change the depth"; or rather, "you are inside the patch→keep the current depth". Incorporation of this type of information can lead to sampling plans such as the blue line in Fig. 1.3a, clearly superior in terms of placing the AUV at a more beneficial depth, on which a more correct conclusion about the biomass distribution could be drawn. This illustrates what can be achieved by exploiting information gathered in the field, as well as how different conclusions relate to sampling bias.

Adaptive sampling schemes also enable opportunistic behavior. Fig. 1.3b shows this aspect by presenting a case where two different distributions (i.e. yellow, green) are of interest. The AUV can in this context, if one or the other were to appear, choose to map either one of the distributions. Alt. A may be a good idea, as the AUV already has data from the other distribution, or if the previous distribution has more relevance, Alt. B may be the best option. Despite being a conceptual example, Fig. 1.3a and 1.3b clearly highlight the advantages of adaptation.

But there are some challenges. For the upper water column the bio-physical processes (interaction between biological parameters and physical forces in the ocean) being studied are often not directly measurable (e.g. phytoplankton via Chlorophyll *a*, photosynthesis via

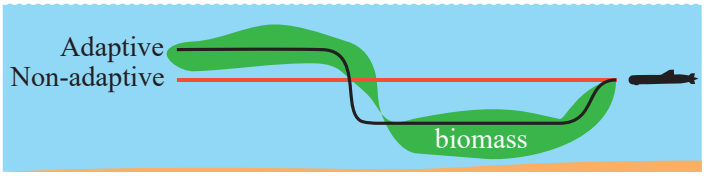


(a) Adaptive vs. non-adaptive sampling.

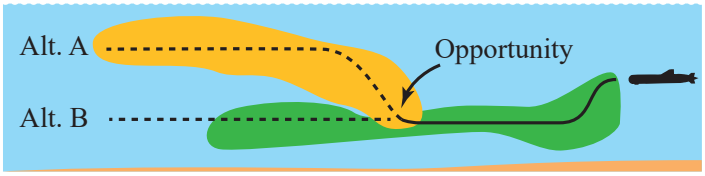


(b) Opportunistic behavior.

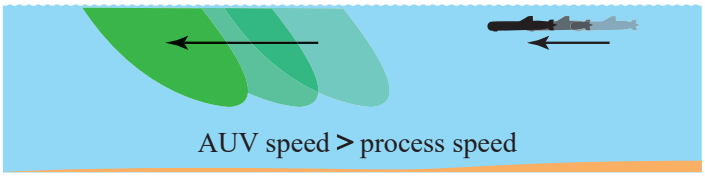


(c) Temporal constraints must be addressed to avoid undersampling.

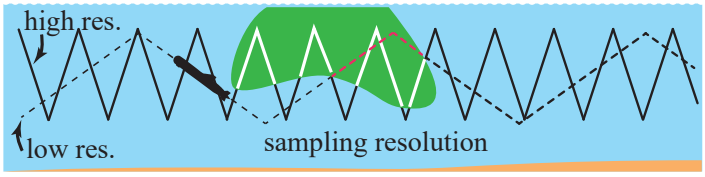


(d) Sampling resolution should be high enough to resolve the process characteristics.

Figure 1.3: Adaptive (data-driven) sampling of the upper water column showing the potential of using adaptive sampling and the associated spatio-temporal considerations, i.e. the influence of relative speed and spatial resolution on sampling efficiency and perception.

fluorometery, etc.), as sensors often only observe proxy variables, which means indirect information must be used to decide how to proceed with future sampling. Processes can also be highly dynamic, interacting on multiple scales, and even be episodic; this makes observation and mapping a considerable challenge. The sensor-carrying platform can itself try to quantify this and learn the distributional characteristics, but this can be both difficult and time consuming. Accordingly, it is important to identify the correct spatial and temporal scales at which to adequately sample the process of interest. Usually for water column surveys the platform is following a yoyo (sawtooth) pattern, as the vertical direction is more heterogeneous (i.e., contains more variability), compared to the horizontal. The main reason for this is stratification from gravitational pull, leading to a “layered” structure in the water column, with increased horizontal correlation. Although this undulating pattern is more efficient at resolving details in the water column, the speed over ground is reduced

thus affecting the spatial coverage along the horizontal plane. Temporal aspects are also important as currents, mixing, and other types of flow interaction continuously displaces the domain in which we are measuring. For example, given a non-stationary field, one would aim to visit dynamic locations more frequently than static locations to reduce the temporal errors. Or, in another instance, one would limit the survey area to a certain size (i.e. an enclosure criterion) in order to bound the time variable effects from currents. Fig. 1.3c and 1.3d illustrate some of the temporal and spatial aspects for making measurements in the water column, i.e. the influence of relative speed and spatial resolution on sampling efficiency and perception. As is evident from these illustrative examples, the speed of the platform has to be faster than the process speed (i.e. currents, vertical migration of zooplankton, plume dispersal speed, etc.) and the sampling resolution should be sufficient, in order to resolve the process structure. The sampling resolution should at least follow the Nyquist rate (see Section 2.1) to avoid aliasing.

## 1.3 Research Questions and Methodology

To achieve oceanography's overarching goal of better understanding of the world's oceans, it's necessary to develop cost effective tools, techniques, and processes for doing ocean based measurements using robotic platforms. From this broad perspective, the focal point of this thesis has been the development of adaptive sampling for marine robotics, with a principal focus on AUVs and coastal waters. The problem domain can be further divided into one of four categories of environmental sensing, given in Fig. 1.4.

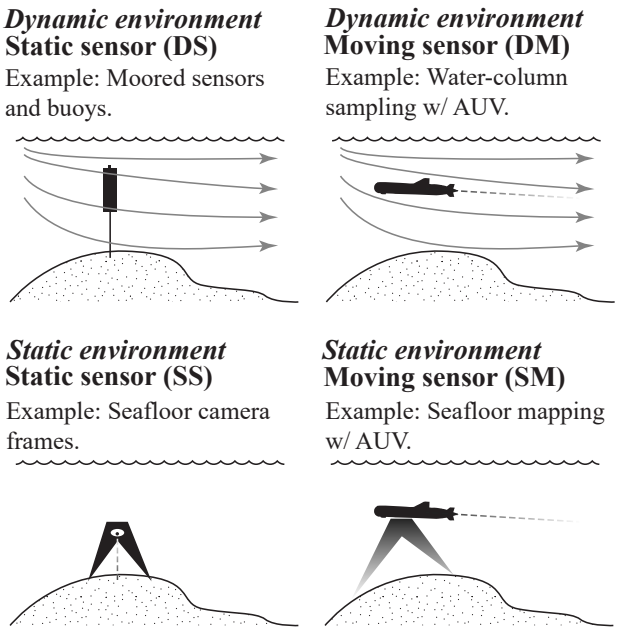


Figure 1.4: The types of environmental sensing problems in ocean science. This thesis concerns moving sensors in dynamic environments (DM), focusing on water column sampling with AUVs.

In a static or quasi-static environment, such as the sea-floor, the environment is stationary or slowly changing. In this context, the observations would not change significantly as time passes. In contrast, a dynamic environment, such as the water column, change happens regularly, often in an episodic and non-deterministic fashion. Determining a sampling design under these conditions is significantly more challenging, and planning ahead in time-dependent environments using only prior information would be prone to time evolving and unobserved uncertainty. Thus, the capacity to adjust sampling based on new observations is vital. Besides, it is also not possible to strive for complete coverage in the oceanic domain, so prioritization of sampling efforts must always be considered one way or another. Accordingly, the type of problems studied in this thesis concerns moving sensors in dynamic environments (DM), focusing on water column sampling with AUVs. Building on the current state of the science, the following research topics and methodologies have been raised to address the topic of adaptive sampling:

> *This thesis will describe the concepts involved in adaptive sampling and formulate methods that can demonstrate data-driven mission execution based on in-situ measurements for sampling applications in the water column. Additionally, verification and field testing of the proposed algorithms should be conducted, using AUVs as the main platform.*

**A:** ***Designing data-driven agents for ocean sampling:*** How can observed data be used to plan and retain an advantageous strategy for information recovery in the ocean using a data-driven agent?

**B:** ***Utilization of information-theoretic methods:*** How can we increase the prospect of retrieving the pursued data and make data collection more effective by integrating information-theoretic methods from spatial statistics and machine learning?

**C:** ***Utilization of marine data sources:*** How can marine data sources such as remote sensing and ocean models be used towards informing on board sampling strategies and planning?

The proposed research methodology includes theoretical analysis, simulation, modeling, and full-scale experiments. This process can vary greatly depending on the perspective of the end-users (e.g. oceanographers and biologists) and operational domain, whether one is in coastal waters, fjords, or high latitude locations such as the Arctic. The scientific foundation for autonomous ocean sensing also covers a range of different subfields and disciplines, including: robotics, control, spatial statistics, artificial intelligence (AI), machine learning, and the pure sciences (see Fig. 1.5). This work encompasses elements of all of these disciplines, building systems that can reason, plan, and strategize data collection in highly uncertain environments. Information-based metrics have largely been adopted from spatial statistics and Bayesian experimental design, with intersections between sensor networks and the sensor placement problem. The scientific context is also often multi-disciplinary including teams from biology, physical oceanography, and other environmental sciences. This is of particular relevance, as each field of study is exposed to different spatio-temporal scales depending on the processes in focus, each potentially requiring a different sampling approach. Finding a balance between practice and applicable theory is vital for success.

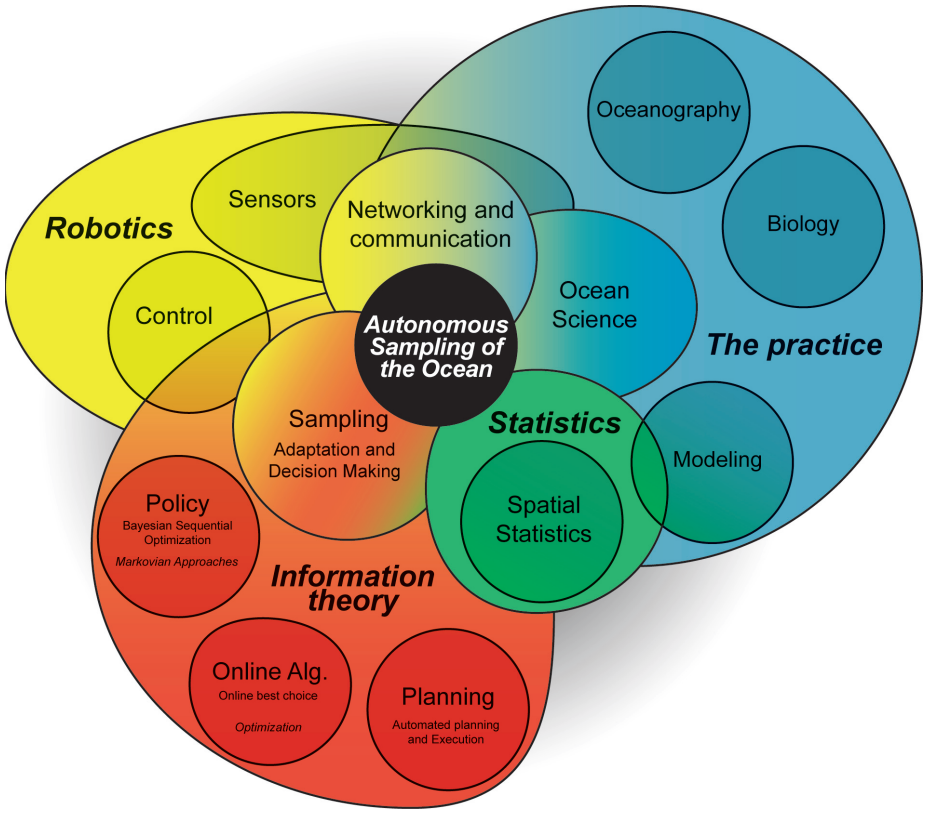


Figure 1.5: The disciplines and theory involved in autonomous sampling of the ocean: robotics, oceanography (the practice), spatial statistics, and information theory. This work encompasses elements of all of these disciplines, building systems that can reason, plan, and strategize data collection in highly uncertain environments.

Design and implementation have been conducted using the autonomous agent architecture T-REX (McGann et al., 2008b,a; Py et al., 2010) and the on board AUV control system DUNE (Pinto et al., 2012). The numerous sea trials (see Table A.1) have primarily been conducted in Svalbard, the Trondheimsfjord, and nearby coastal areas using the Light Autonomous Underwater Vehicle (Sousa et al., 2012) [LAUV Harald] – specialized for water column sampling. Real-world sensing applications and campaigns are not merely concerned about extending current sampling abilities of AUVs, but also retrieving the data itself. Failure to reconcile the two weakens the overall result, thus the aim must be to change the way we retrieve data for the benefit of the scientific context.

## 1.4 Thesis Contributions and Outline

The principal contributions of this work are related to i) the design and analysis of information-theoretic approaches in upper water column sampling, coupled with intel-

ligent control and ii) testing and validating these methods in the field. This includes development of greedy data-driven sampling strategies and formulation of compact proxy models for use in autonomous exploration of the water column using a single robotic platform. Details on the contributions per paper are listed in more detail in Ch. 6, Section 6.3, stated below the reference to each paper.

This thesis summarizes and complements a number of publications, and is organized as follows. The first part of the thesis presents an overview of the research with background information that helps to fit the individual papers into the broader context of adaptive sampling. There are six chapters whose content is briefly described below. Part II contains the papers, which support the discussion presented in Part I. Included here are four authored and two co-authored papers, of which three are journal papers and three are conference papers. The papers are listed in the same order as they appear below. The scientific contribution of each paper is given in Ch. 6 together with a summary and future work.

## Part I

**Chapter 2** gives an overview of sampling in the oceans and the space-time variability of the interacting processes before an overview over synoptic marine data sources is given, focusing on remote sensing and numerical ocean models. **Chapter 3** provides a brief introduction to spatial statistics and Gaussian processes. Applications and examples are given from the standpoint of modeling and inference in the ocean environment. Building on the basis from the preceding chapters, **Chapter 4** discusses information-theoretic and behavior-based adaptive sampling in detail, including theory, related work, applications, as well as some concrete examples of data-driven autonomous agents. The theory and concepts are further discussed in an operational context in **Chapter 5**, which provides a discussion about marine robotic platforms and practical aspects related to adaptive sampling, focusing on operational issues and deployment with AUVs in the upper water column. Finally, **Chapter 6** summarizes the thesis and specifies the scientific contributions before a discussion on potential future research directions. Lastly, **Appendix A** provides an overview of the field deployments undertaken during the PhD work.

## Part II

The papers included in this section cover different aspects of autonomous robotic sampling. **Papers A-B** present two adaptive sampling methods based on Gaussian processes for doing data collection in the water column. **Paper A** proposes a greedy adaptive sampling algorithm that uses an information-theoretic approach to select and plan sampling efforts. The strategy relies on a Gaussian process model for modeling the environment, formulated on the basis of regional data from an ocean model. **Paper B** employs a similar Gaussian model, but this time for modeling and mapping heterogeneous concentrations of water column parameters. This model is then used for adapting a volumetric AUV survey, targeting regions of interest. Results from field trials are shown, together with corresponding ship-based observations. **Paper C** presents a methodology for leveraging remote sensing data, specifically images of sea-surface temperature, towards developing compact on board models that can be used to inform sampling strategies for marine

sensing platforms. A case study using data from Monterey Bay and an autonomous surface vehicle is presented, together with statistical validation and analysis of the compact model. **Paper D** proposes an autonomous agent architecture for inspection, maintenance, and repair applications for ROVs, aided by control and computer vision techniques. Results from field deployment using a full scale integration on board a work class ROV is shown. In **Paper E**, the greedy and Gaussian framework from **Paper A** is re-applied to an industrial application for tracking and monitoring dispersion dynamics in the water column. **Paper F** presents an approach for autonomous mapping of the seafloor using Hidden Markov Random Fields. Backscatter is used to segment and automatically plan a more detailed camera survey; results from full-scale experiments are given.

## List of Included Papers

**A:** ***Peer-reviewed Journal Article***
**Trygve Olav Fossum**, Jo Eidsvik, Ingrid Ellingsen, Morten Omholt Alver, Glaucia Moreira Fragoso, Geir Johnsen, Renato Mendes, Martin Ludvigsen, and Kanna Rajan. **Information-driven Robotic Sampling in the Coastal Ocean**. *Journal of Field Robotics*, Volume 35, Issue 7, pages 1101–1121, 2018.

**B:** ***Peer-reviewed Journal Article***
**Trygve Olav Fossum**, Glaucia Moreira Fragoso, Emlyn J. Davies, Jenny Ullgren, Renato Mendes, Geir Johnsen, Ingrid Ellingsen, Jo Eidsvik, Martin Ludvigsen, and Kanna Rajan. **Towards Adaptive Robotic Sampling of Phytoplankton in the Coastal Ocean.** *Science Robotics*, Volume 4, Issue 27, eaav3041, 2019.

**C:** ***Peer-reviewed Journal Article***
**Trygve Olav Fossum**, John Ryan, Tapan Mukerji, Jo Eidsvik, Thom Maughan, Martin Ludvigsen and Kanna Rajan. **Compact models for Adaptive Sampling in Marine Robotics.** *Submitted to International Journal of Research Robotics*, $9^{th}$ November 2018.

**D:** ***Conference paper***
**Trygve Olav Fossum**, Martin Ludvigsen, Stein M. Nornes, Ida Rist-Christensen and Lars Brusletto. **Autonomous Robotic Intervention using ROV: An Experimental Approach.** *MTS/IEEE OCEANS 2016*, Monterey, CA, USA, $19^{th}$-$22^{th}$ September 2016.

**E:** ***Conference paper***
Gunhild Elisabeth Berget, **Trygve Olav Fossum**, Tor Arne Johansen, Jo Eidsvik and Kanna Rajan. **Adaptive Sampling of Ocean Processes Using an AUV with a Gaussian Proxy Model.** *11th IFAC Conference on Control Applications in Marine Systems, Robotics, and Vehicles (CAMS)* Opatija, Croatia, $10^{th}$-$12^{th}$ September 2018.

**F:** ***Conference paper***
Øystein Sture, **Trygve Olav Fossum**, Martin Ludvigsen and Martin Syre Wiig. **Autonomous Optical Survey Based on Unsupervised Segmentation of Acoustic Backscatter.** *MTS/IEEE OCEANS*, Kobe Techno-Oceans (OTO), Kobe, 2018.

The following works are not included in this thesis:

***Conference paper***
Martin Ludvigsen, Sigurd M. Albrektsen, Krzysztof Cisek, Tor Arne Johansen, Petter Norgren, Roger Skjetne, Artur Zolich, Paulo Sousa Dias, Sérgio Ferreira, João Borges de Sousa, **Trygve Olav Fossum**, Øystein Sture, Thomas Røbekk Krogstad, Øivind Midtgaard, Vegard Hovstein, and Erlend Vågsholm. **Network of heterogeneous autonomous vehicles for marine research and management.**
*In Proc. MTS/IEEE OCEANS*, Monterey, CA, USA, 2016.

***Technical Report***
Øystein Sture, Martin Syre Wiig, and **Trygve Olav Fossum**. **NTNU-FFI Cruise 2017-HUGIN Autonomy Integration (DUNE, T-REX).** *NTNU Cruise Reports*, The Norwegian University of Science and Technology (NTNU).

***Technical Report***
**Trygve Olav Fossum**. **Intelligent Autonomous Underwater Vehicles: A Review of AUV Autonomy and Data-Driven Sample Strategies** *IMT-AURLab-1*, Department of Marine Technology, Centre for autonomous marine operations and systems (AMOS), Norwegian University of Science and Technology (NTNU).

# Chapter 2

# Ocean Observation

*"Most of the previous century could be called a century of under-sampling."*
— Walter Munk, *Secretary of the Navy Research Chair in Oceanography*
*(Munk, 2002)*

THE ability to observe the ocean is rapidly improving. The use of high resolution ocean models, remote sensing, and robotic elements has moved oceanographic sensing practices towards a more holistic perspective, where increased presence and information sharing, across a range of different scales, is becoming more feasible (see Fig. 2.1). This chapter takes a closer look at ocean observation and the space-time variability of the interacting processes, followed by an overview over synoptic marine data sources focusing on remote sensing and numerical ocean models.

## 2.1 Observing Earth's Ocean

The study of the ocean covers a multitude of scales and space-time (spatiotemporal) variability, including processes that are episodic (see Fig. 2.2). The primary platform for observation has been – and still is – ships. However, the U.S. federal oceanographic fleet could be reduced to half its size by 2026 as a result of flat budgets and increased costs (Cressey, 2013); a trend that is indicative for the rest of the world. At the same time, trends in science and technology indicate that ship assets are still required (Board et al., 2009, Ch.5) and cannot be completely replaced by new sampling tools. These changes are also reflected in newly developing oceanographic sensing practices, where satellites, robotic elements, ocean models, and ocean sensor networks are increasingly being used as data-gathering tools (Kintisch, 2013). These networked sampling systems are not based on a single platform or observation scale, but rather a complementary ensemble covering a range of scales, building on the principle of sharing information to mutual advantage.

The introduction of remote sensing and large-scale sensor networks have provided a more synoptic perspective of the ocean; however, sensors measurement are still too far apart or cannot resolve the necessary details. The attenuation of radio waves also restrict satellite observation to the very surface. Ocean model accuracy is also not at a level where it can replace actual *in-situ* observation (Lermusiaux, 2006). Hence, we are still left with a significantly unobserved water column, where it is necessary to combine various individual marine data sources to close the gaps in coverage and resolution. Even

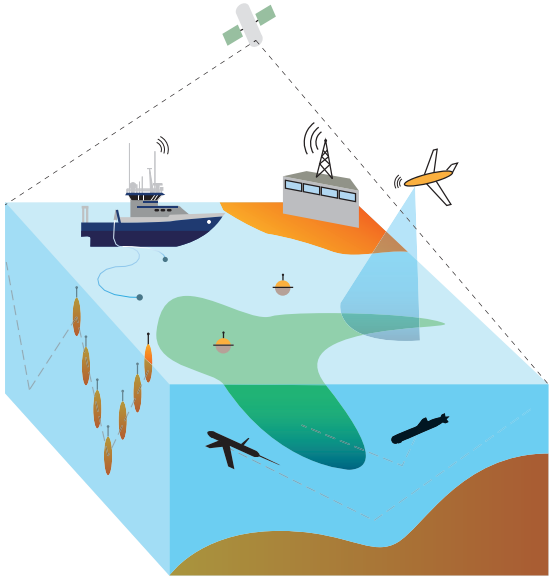

Figure 2.1: Conceptual view of a multi-scale, multi-platform field experiment using: ships, buoys, AUVs, glider, floaters, satellite, and aerial drones. Achieving the ambition of a synoptic understanding of the ocean requires a joint effort between a range of marine data sources.

with numerous deployed instruments, it will still not be conceivable to examine the entire environment in detail, and thus only *quasi-synoptic* (i.e. a semi-holistic recording of an event) coverage is usually possible (Curtin et al., 1993). Observation itself is also not straightforward; sensors are usually only capable of providing proxy measurements of the relevant processes, which means additional uncertainty is introduced. Observations also come at different scales, accuracy, are subject to spatial sampling bias (due to the inherent heterogeneity [patchiness] of the ocean), and cannot be readily transmitted with high bandwidth between sources – making cross-validation and comparison difficult. Additionally, currents, topography, tides, and turbulent flows constantly move information around, making all observations time dependent. In practice, this means that we are still inclined to *undersample* the environment in both time and space. The term "ground-truth" is therefore never really fully attainable in ocean sensing, except for very large scale processes (such as tides) or very local processes (such as determining run-off from rivers).

This is the *sampling conundrum* in oceanography and the lack of sufficient observations is the largest source of error in our understanding of the ocean (Stewart, 2009), making *when and where* to sample the key problem when designing oceanographic experiments. A guiding rule of thumb provided by the the Nyquist theorem is to sample at least twice in time for the shortest significant record period, and twice in space for the shortest significant length (Nyquist, 1928) to either resolve or eliminate (by filtering) scales of oceanic variability shorter than those being studied. In practice, this means mapping at an adequate spatial resolution faster than significant changes – in the phenomena – occur.

Summarizing the above, we can identify the following challenges:

**The challenges in ocean sampling (the *sampling conundrum*):**

- **Sparseness:** It is usually not possible or practical to observe the entire environment in detail both in terms of coverage (space) and resolution (space and time); usually only a quasi-synoptic coverage is possible.
- **Space-Time dependent environment:** The fundamental turbulent, heterogeneous, and episodic nature of the ocean makes observations time-dependent and sensitive to both location and scale (sampling bias); this also affects the ability to maintain up-to-date knowledge. Understanding and quantifying this influence is difficult.
- **Proxy measurements:** Sensor observations are rarely able to acquire direct measurements of the process or quantity we are interested in, introducing additional uncertainty. Certain instruments also affect the environment themselves (e.g. light and noise) that may cause instrument bias.
- **Sensing scales:** A multitude of sensors are used to fill observation gaps and to avoid undersampling, making cross-comparisons complex.
- **Harsh Environment:** Pressure, corrosion, and bio-fouling affect all equipment that goes into the ocean. Logistically, these instruments are expensive and complex to install. Once in place, wave motion, current, and wind subject the observation systems to varying loads and forces.

Addressing the sampling conundrum in the ocean requires understanding of the fundamental environmental characteristics, as well as new technological solutions and sensing practices that enable unification and augmentation of data from a range of sources and scales. From a sampling perspective, the combination of synoptic data sources such as ocean models and remote sensing with robotic platforms will be key, and will thus be covered in more detail in the following sections.

### 2.1.1 Space and Time Variability in the Ocean

The ocean is fundamentally turbulent. A multitude of oceanic processes interact to create variability in space and time, spanning many orders of magnitude from large scale oscillations exceeding 100 km, down to biogeochemical processes below 1 cm. This dynamical landscape is usually divided into the following scales: i) *Mesoscale: 50-500 km, 10-100 days* and ii) *Sub-mesoscale: 1-10 km, days-months*. Fig. 2.2 depicts some of the prominent oceanic events that occur in this vast dimension.

The energy of mesoscale processes, such as eddies, generally exceeds that of the mean flow by an order of magnitude or more (National Research Council, 2010), having a strong impact on the ecosystem. In operational oceanography, traditional techniques, like shipboard and moored measurements, can be effective at large spatial (**O**(100 km)) and temporal (**O**(week to months)) scales, but quickly become too sparse for sub-mesoscale variability (Graham et al., 2013). The introduction of satellite oceanography has also proved significant at these scales, capable of providing global coverage for variables such as sea level

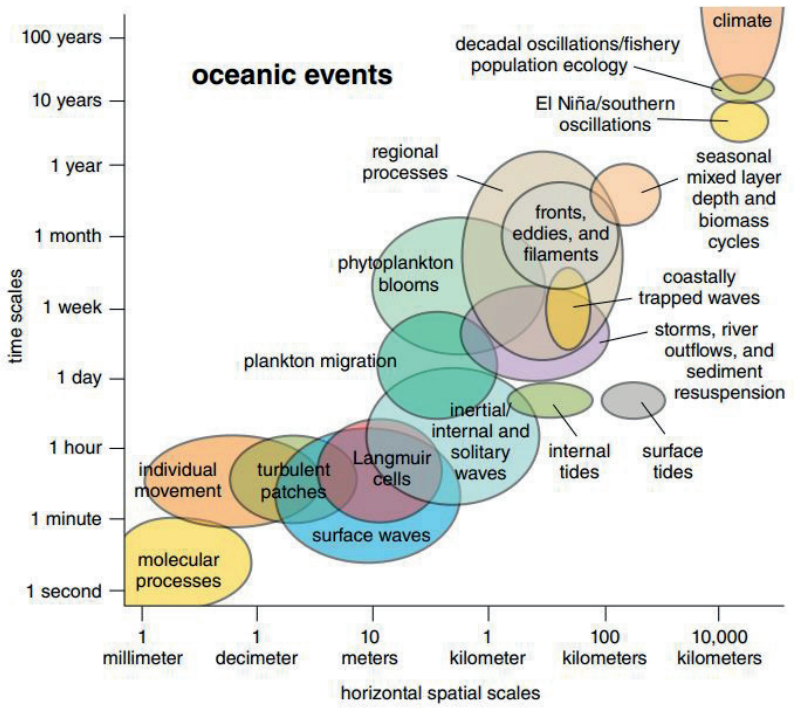


Figure 2.2: Some of the prominent oceanic processes and events, shown with their spatiotemporal extent. Image credit: (Schofield et al., 2013) and Tom Dunne.

height. Satellites also provide an overlap towards sub-mesoscale dynamics, whose importance is significant and directly influences events such as primary production (Lévy, 2003) or patch formation of biomass (Franks, 1992). For many years this variability was so *undersampled* that its impact was greatly misunderstood (Munk, 1997). One example is the spatial distribution of phytoplankton. Its intensity, morphology, and scale dependence are substantially driven by sub-mesoscale processes such as turbulent advection, upwelling, and vertical mixing (Mackas et al., 1985; Van Gennip et al., 2016). Local processes (such as upwelling zones) bring deep water nutrients to the surface/photic zone and nurture phytoplankton, creating regional hot spots (with high biomass concentration) at scales ranging from 5–10 km (Martin et al., 2002) or even $\leq$ 1 km for complex coastal zones (Hedger et al., 2003). In the open ocean, the same aggregation can range from 70–140 km (spatial correlation) in the horizontal plane; vertically, persistent upper water column stratification may lead to a layered structure with different subsurface maxima, where, for example, phytoplankton is concentrated in the bottom of a pycnocline (a density gradient) (Silsbe and Malkin, 2016). A vital point to note about stratification effects is the consequence that vertical correlation is much weaker compared to the horizontal, where the increase can be as high as factor of 111$\times$ for temperature and 800$\times$ for Chlorophyll *a* (Sahlin et al., 2014). This is important to consider when dealing with spatial interpolation and data assimilation, or when formulating proxy models for processes in the water column.

Accounting for spatiotemporal effects in the ocean can be difficult. As the ocean is non-stationary (correlation and mean structures can change in time, space, or both), common assumptions (e.g. non-changing statistical properties [stationarity]) that are used in statistical models such as Gaussian processes are strictly no longer valid (Eidsvik et al., 2015). Still, for moderate current, short survey times, or limited study regions (Das et al., 2012b), certain assumptions can hold (see Section 3.3). In cases where this is not true, solutions such as drifters (passive platforms floating at a fixed depth) can provide a relative Lagrangian position that can be used to mitigate these effects (for an example, see Graham et al. (2013)). Frolov et al. (2014) accounts for space-time covariance by employing a separable formulation, where space and time correlations are treated separately. Both separate and non-separable correlations are also compared in Graham et al. (2013), where real world tests showed that accounting for time is not necessarily straightforward. Ocean models have also been used to mitigate time effects in applications such as planning feature tracking (Smith et al., 2009) or accounting for ocean currents (Smith et al., 2011). Accounting for time can also be done by adding uncertainty of visited/measured regions as time progresses (for an example, see Ma et al. (2016); Fossum et al. (2018)).

## 2.2 Synoptic Ocean Data Sources

Synoptic data sources can be used to simulate, analyze, coordinate, and plan sampling strategies, in addition to predictive or *post-hoc* purposes. By leveraging this potential, sampling resources can better target the phenomenon/process or area of interest with sufficient detail and appropriate sensors. The increasing availability of high-end computational resources accessible to oceanographers has enabled high-resolution modeling modeling of the upper water column, and technological advancement in remote sensing applications and products is enabling new ways to study the ocean at a more synoptic scale. As numerical models can operate at various levels of spatial and temporal scales, this permits comparison, assimilation, and cross-validation between heterogeneous sampling resources. This perspective has been explored in the previously mentioned research project AOSN-I/-II, and the Controlled Agile and Novel Observation Network (CANON) field program (Das et al., 2010, 2012a), among others. Accordingly, these influences are changing the way we think about ocean sampling and field experiments, as there lie significant gains to be exploited where unification of: ocean models, remote sensing, and different robotic elements can provide a multi-resolution window into the sophisticated dynamical landscape of the oceanic interior. Fig. 2.3 combines the spatiotemporal coverage values from the major marine platforms with the main synoptic data sources to contextualize the forthcoming discussion.

However, there are two fundamental limitations to consider. First, numerical ocean models suffer from various sources of errors (for a more detailed discussion, see Lermusiaux (2006)), that degrade their ability to produce reliable predictions. Second, remote sensing sensors, such as infrared radiometers (which measure temperature), only cover the surface skin layer of the ocean (i.e. less than 1 mm thick). Information below this layer can sometimes be obtained, depending on optical attenuation. Remote sensing observations are also highly susceptible to cloud cover for certain measurements (see Fig. 2.4). The need to augment and cross-validate predictions is thus great. *In-situ* robotic as-

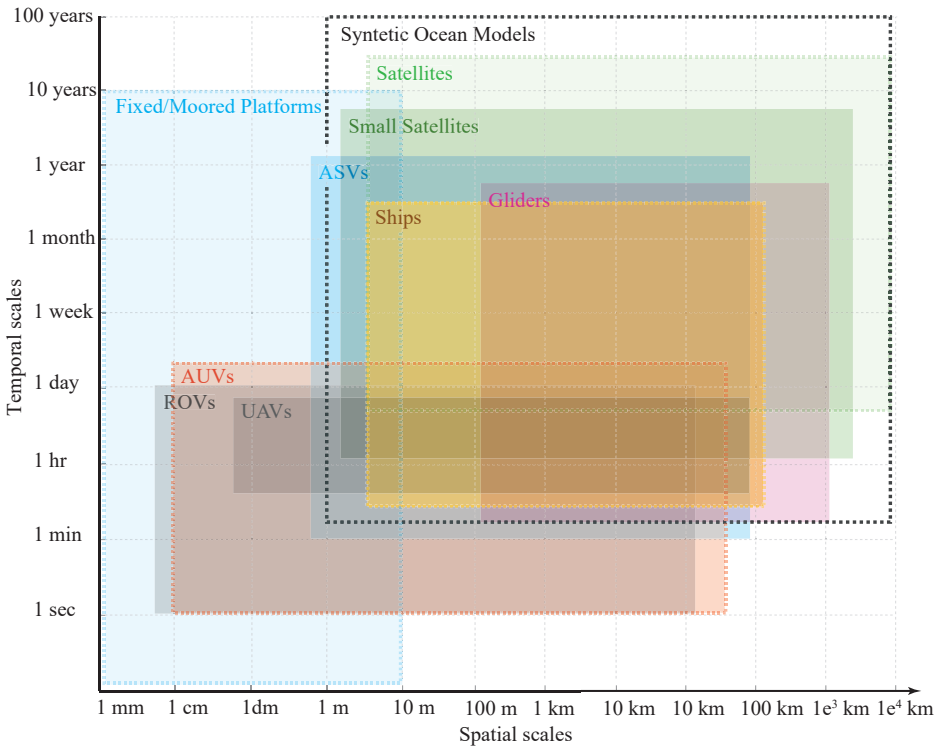


Figure 2.3: Common spatial and temporal characteristics for marine robotic platforms (exceptions exists). The lower axis represents resolution, while the vertical axis represent temporal coverage.

sets and adaptive sampling approaches are therefore essential in providing the necessary autonomous capabilities. However, before autonomy can be considered, the spatial and temporal coverage capacity of the platforms/data sources must be evaluated against the phenomena/process of interest. Fig. 2.3 illustrates this by showing the spatiotemporal capabilities across AUVs, glider and remote sensing resources in a space-time dimensional manner. Certain processes require a fast moving platforms (i.e. processes with a short time response, such as a advecting phytoplankton patch), while other require platforms capable of measuring for long time periods (i.e. processes with a slow time response, such as phytoplankton blooms), techniques and methods needs to be developed that can coordinate and determine sampling directives based on science goals. One example of a shore-based coordination system is the Oceanographic Decision Support System (ODSS)[1] developed at MBARI for online situational awareness, experiment planning, collaboration and data analysis (Gomes et al., 2013).

[1] http://odss.mbari.org

### 2.2.1 Remote Sensing

Alongside ocean models, remote sensing is a widely used source of synoptic information in ocean science. Remote sensing (the gathering of information at a distance) generally refers to satellite or radar-based data, but can also be used for any measurement that is made without physical contact with the relevant environment (hence this also includes acoustic [sonar] and magnetic [magnetometer] measurements). From the perspective of ocean-related satellite earth observation – which is the main focus here – we will use the definition given in Campbell and Wynne (2011):

> *"Remote sensing is the practice of deriving information about the Earth's land and water surfaces using images acquired from an overhead perspective, using electro-magnetic radiation in one or more regions of the electromagnetic spectrum, reflected or emitted from the Earth's surface."*

Satellite earth observation techniques provide a cost-effective way to monitor large coastal and marine habitats, human environmental impact, and climate change. The focus given here will be on remote sensing for applications in oceanography, and the basic ocean parameters: sea surface temperature (SST) (infrared radiometer) and ocean color (spectrometers). Sea surface height (altimeters), surface roughness generated from waves and wind (microwave), and other derived products will not be discussed in detail.

Remote sensing offers a way to synoptically study certain processes in the ocean through repeated large-scale ocean surface observations. Supplementing *in-situ* observation from marine platforms, remote sensing can also add to numerical ocean models by providing assimilation and cross-verification of model performance (Frolov, 2007). At present, only few assimilation methods are used operationally, partly due to low data reliability, inaccuracy, and insufficient coverage. Even if only the surface can be resolved, a number of ocean processes can still be *derived* from the observations, such as: current patterns, fronts, eddies, water mass distribution, water quality parameters such as chlorophyll, surface slicks, and suspended sediments (turbidity) (Johannessen et al., 2000). Fig. 2.4 gives an overview of the type of features that can be studied with remote sensing instruments. This has also been extended to include sea surface salinity (Le Vine et al., 2007), and – increasingly – remote detection of individual micro-organisms (Kudela et al., 2015). Being able to identify different types of organisms is important for understanding ecological dynamics and structure, as well as detection of harmful algal blooms (HALs), where algae produce toxins. Infrared and optical types of sensing are naturally sensitive to cloud cover which attenuate these signals. This can restrict use, especially at high latitudes, where cloud cover is more or less constant. Certain of the observations are, however, independent of weather conditions, such as synthetic aperture radar (SAR), but suffer from low resolution (1 km or more) (Johannessen et al., 2000). In addition to clouds, atmospheric correction must also be applied to reconstruct information that has been affected by the electromagnetic influence from the signal journey thorough the atmosphere.

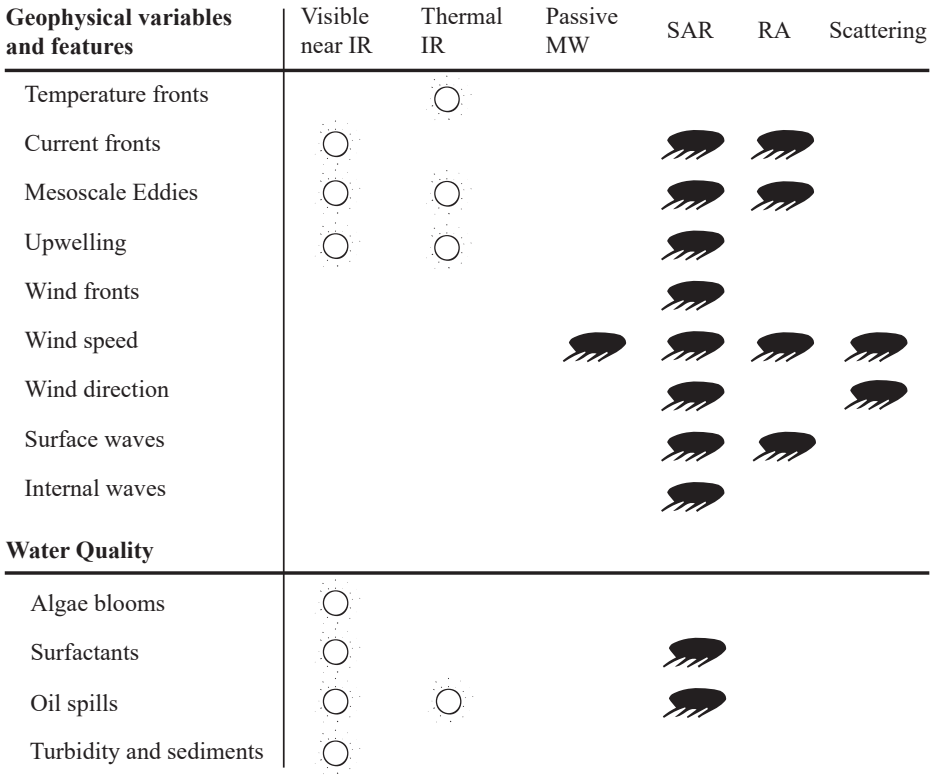


Figure 2.4: Ocean parameters and the remote sensing instrument/sensor that applies. The sun icon signifies that the observation can only be obtained in clear weather, while the cloud illustrate observations that may be derived given cloudy conditions. IR=Infrared, MW=Micro Wave, SAR=Synthetic Aperture Radar, RA=Radar Altimeter, Scatt.=Scattering. Modified from (Johannessen et al., 1993).

### Ocean Color and Chlorophyll *a*

Chlorophyll *a* (Chla) is used as a ”common currency” for biomass estimation, where the concentration of Chla is indicative of the phytoplankton biomass. Biomass is a broad and practical term used to describe the amount of living material in the water column. This bulk measurement is important, as processes controlling the growth and accumulation of phytoplankton are central to nutrient, carbon, and energy cycling. Observations of Chla are also an indicator for the process of *primary productivity* – the main source of energy and basis for the marine food web – and is thus of significant interest for studying ecosystem dynamics. Ocean-color based products, such as Chla, are calculated using an empirical relationship derived from in situ measurements of chlorophyll concentration and remote sensing reflectances in the *blue-to-green region* of the visible spectrum. Obtaining good results can be difficult in coastal areas (compared to open ocean), where sediments and color dissolved organic matter (cDOM) contribute to the measured signal (Johannessen et al., 2000).

Fig. 2.5a shows an image of a plankton bloom off the Norwegian coast ($10^{th}$ of June 2006), taken by Envisat's MERIS instrument (Rast et al., 1999), which is built to detect ocean color. The particular water discoloration shown here is also detectable with the human eye. The spatial resolution of standard chlorophyll products usually has the same order of magnitude as SST, which is rarely below $1 \times 1$ km. However, it is also possible to derive chlorophyll information from new satellite terrestrial-oriented missions, such as Landsat-8 (operational land imager sensor) and Sentinel-2 (multi-spectral instrument sensor) (see Fig. 2.5b), which provide data at more relevant spatial scales of 10 to 60 m (Vanhellemont and Ruddick, 2016). Ocean color satellite data does not cover the water column beyond the first optical attenuation length as defined by Beer's Law, where 90% of remotely-sensed radiance originates from (Werdell and Bailey, 2005); this can be too coarse for critical bio-physical ocean processes (Moses et al., 2016). An algal bloom may also have its peak activity below the surface, which may go undetected by satellite based sensors.

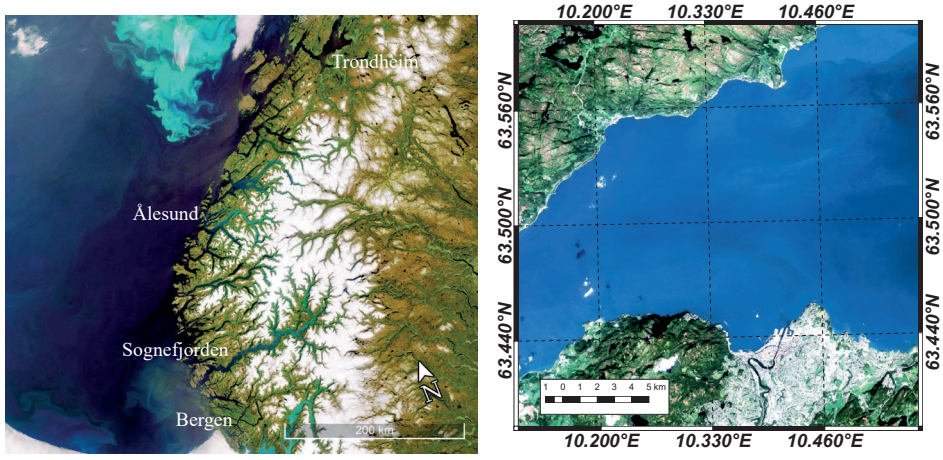


(a) Plankton bloom taken from Envisat.

(b) RGB image from Trondheimsfjord by Sentinel-2B.

Figure 2.5: (2.5a) False color image of a plankton bloom off the Norwegian coast $10^{th}$ of June 2006. Image taken by Envisat's Medium Resolution Imaging Spectrometerer (MERIS). (2.5b) An RGB image from Sentinel-2B and the Copernicus programme covering the Trondheimsfjord the $28^{th}$ of June 2018. Both images are courtesy of ESA, CC BY-SA 3.0 IGO.

### Sea Surface Temperature (SST)

SST can be used to provide information about a wide range of ocean processes such as currents, fronts, eddies, mesoscale eddies, and upwelling (Johannessen et al., 2000). SST satellite products are measured by infrared radiometers over the surface skin layer of the

ocean (i.e. less than 1 mm thick). The temperature of this skin layer is often cooler than the body of water below; this can potentially create a decoupled and decorrelated impression of the conditions below the surface. The gradients between these layers are highly dependent on meteorological conditions (Minnett and Kaiser-Weiss, 2012). Spatial resolution for SST is rarely below $1 \times 1$ km in ocean-oriented remote-sensing data, such as from NASA's MODIS-Aqua (Savtchenko et al., 2004), except for recent instruments such as the Sentinel-3 constellation mission as part of ESA's Copernicus programme (Donlon et al., 2012), which can yield resolutions down to about $300 \times 300$ m. An example of a SST data is shown in Fig. 2.6, covering the Monterey Bay.

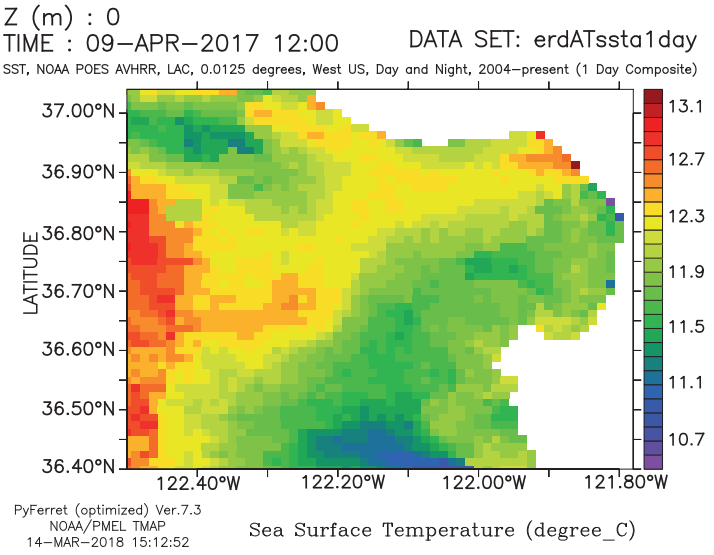


Figure 2.6: A one-day average SST image from NOAA NWS Monterey Regional Forecast Office showing Monterey Bay.

### 2.2.2 Ocean Models

Ocean models describe the state of the ocean at a given time based on a set of hydrodynamic and thermodynamic equations, commonly referred to as the *primitive equations* (see e.g. Beniston (1998)) that are solved using numerical techniques. These equations can be used to model currents, salinity, temperature, density, pressure, and their interaction. In implementations, the equations are discretized in different ways, utilizing either structured or unstructured model grids horizontally, and using horizontal terrain-following or hybrid discretization vertically. This discretization also influences the ability to resolve certain phenomena, which must be taken into account when planning the model grid. The spatial resolution of an ocean model represents a trade-off between the geographical area to be simulated and the availability of computer hardware and time. Running the model involves computation of a large set of equations, typically implemented with parallelization to optimize and reduce computing time. Since high resolution modeling can only be done for relatively small geographical areas, models are commonly *nested*. That is, one simulates

larger scale areas to produce boundary conditions for higher resolution models covering smaller areas. This process can be iterated several times to achieve the desired detail.

There are a number of inherent challenges to ocean modeling arising from: practical simplifications, inexact representations or parameterizations, numerical implementations (Lermusiaux, 2006), and the inability to resolve sub-grid features, i.e. treatment of turbulent dynamics (Troccoli, 2003). Models apply forcing by tides, sea level pressure, wind, heat exchange, and freshwater run-off. Defining these prescribed states and currents at the open boundaries pose a major challenge, as the quality and sensitivity of model input heavily depend on these initial conditions. A particular challenge for local scale ocean modeling is the accuracy of wind fields in coastal areas with strong topographic control of near-surface wind. Another major influence is the quality of bathymetric data, type of grid used, and choice of numerical techniques. Freshwater run-off can be assessed accurately for certain rivers, but the full distribution of run-off along the coast may be associated with large uncertainties and is usually based on climatological data (see (Berntsen, 2002)). Ocean models must also take into account atmospheric forcing. This can be based on meteorological model estimates, but these models will themselves contain model error. As all these errors become nested, the quality and resolution of ocean models can vary significantly. Model evaluation and correction using robotic assets is therefore valuable, but is limited by the cost of large-scale deployments in the ocean. Accordingly, sampling needs to be planned efficiently, taking into account model weaknesses and characteristics of poorly resolved processes to target areas for data collection.

### The SINMOD Ocean Model

SINMOD is a coupled 3D hydrodynamic and biological model system (Slagstad and McClimans, 2005; Wassmann et al., 2006). Its hydrodynamic component is based on the primitive equations that are solved using finite difference techniques using a z-coordinate regular grid with square cells. The model has been used for ocean circulation and ecosystem studies along the Norwegian coast and in the Barents Sea (Wassmann et al., 2010; Ellingsen et al., 2009; Skardhamar et al., 2007), in ecosystem risk assessment studies (Broch et al., 2013a), kelp cultivation potential (Broch et al., 2013b) and in climate change effect studies (Ellingsen et al., 2008; Slagstad et al., 2015).

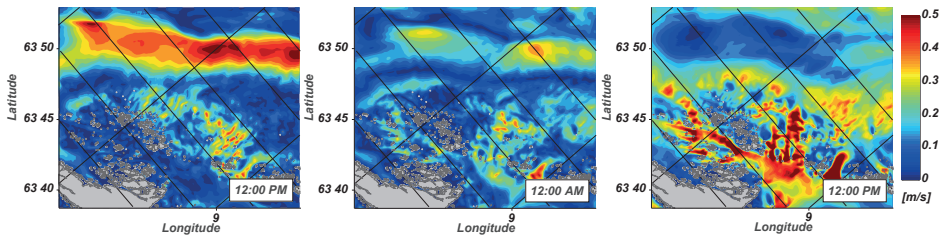


Figure 2.7: Snapshots of ocean surface current speeds in the Frøya region from simulated by the SINMOD ocean model. The snapshots are predictions from the $5^{th}$ to the $6^{th}$ of May, 2017.

In addition to forecasts, SINMOD is capable of providing hindcast, and short-term predictions (nowcasts) up to 48 hours. The term *hindcast* is used to describe an after-the-fact analysis or re-simulation, where initial conditions and other model input is taken from actual observations. For the production of forecast and nowcast data, SINMOD is using boundary conditions computed from the operational coastal model system Norkyst800[2] run by the Norwegian Meteorological Institute (MET)[3]. Norkyst800 is a model configuration using the Regional Ocean Model System (ROMS) ocean model (Shchepetkin and McWilliams, 2005b), applied to the Norwegian coast with a horizontal resolution of 800 m (Albretsen, 2011). Additionally, SINMOD uses atmospheric input from the MEPS operational weather forecast model (Müller et al., 2017), run by MET (2.5 km horizontal resolution). Freshwater run-off is based on climatological data. A snapshot of evolving current speed is shown in Fig. 2.7, as an example of model output.

## 2.3 Applications for Synoptic Ocean Data Sources

Achieving the ambition of a more detailed understanding of the ocean requires a joint effort between a range of marine data sources. An integral part of this is data assimilation between heterogeneous marine data sources. In the context of ocean models, data assimilation is in itself a modeling technique that uses sparse observations from marine data sources and platforms to constrain the dynamics of the model (Frolov, 2007). Full assessment of model accuracy is, however, not possible, as it requires measurement of temporal and spatial gradients in the ocean far exceeding current practical capabilities (Curtin et al., 1993). Surface data is usually assimilated into operational models from remote sensing sources, but is limited to the surface only. Evaluating model performance using observations from a range of different platforms is therefore advisable. In addition to *hindcast* model validation and correction, information from *in-situ* instrumentation can also improve near-real-time forecasting/*nowcasts* by assimilation of recent observations into the model. As shown by validation studies (e.g. Forristall (2011)) ocean models generally perform well with regard to statistical properties and tidal dynamics, although they show little skill in predicting currents from hour to hour in areas not dominated by tidal forces. AUVs will likely play an essential role in the process of data assimilation of water column properties in models that seek to describe detailed forecasts on critical events, such as harmful algae blooms, see e.g. Das et al. (2010); Scholin et al. (2006). AUV data could also be assimilated into predictive models to reduce uncertainties, which in turn can be used to guide subsequent AUV missions, thus closing the loop from measurements to modeling and back again (Howe et al., 2010). There is therefore a need to develop enabling technology that perform efficient and targeted sampling of the ocean. Capabilities such as adaptive sampling will thus be critical for finding and assimilating observations in regions prone to low model accuracy and skill, to correct and assess model shortcoming, and to reduce environmental uncertainty and characterization.

This synergy goes both ways, as model output can both be used in terms of prior specification and expectation of the environmental conditions, as well as proxy model characterization and analysis. An interesting application is shown in Das et al. (2010),

[2] https://goo.gl/H4Rbw2
[3] https://www.met.no

where ocean model forecasts are combined with remote sensing radar to predict hotspots and advection of harmful algae blooms, on which a subsequent sampling plan for an AUV is formulated. There are also applications for simulation and analysis of different ocean observing systems (OOS). Ocean model data is in this context treated as "truth" and virtual observations from the OOS is used to measure the performance of a given sampling strategy by comparing original model output and the posterior field resulting from the virtual observations, see e.g. Sakov and Oke (2008).

Formulation of proxy models and background statistics is a widely used application for ocean model data, see e.g. Frolov et al. (2014). Assuming that the ocean model is capable of capturing the long-time statistical properties of a region, formulation of priors and correlation structures can be extracted as long as sufficient data are available. The statistical characteristics of the synthetic data can also be augmented and checked with remote sensing data to ensure that weak modeling assumptions are not misrepresenting processes or containing strong bias effects. This is discussed in more detail in the next chapter (Section 3.2.1) covering Spatial Statistics, where a brief example using ocean model data is shown. This is later picked up in **Paper A**, which presents a real-world application of the methods from this chapter, where ocean model output is used to define the survey area, formulate a Gaussian process model, and analyze performance of the adaptive sampling agent.

# Chapter 3

# Spatial Statistics

STATISTICS naturally enters into sampling through requirements for generalization, modeling, and the ability to learn on the basis of prior and current data. Because ocean parameters are spatially correlated, this dependence also needs to managed by applying spatial process models. The field of statistics that describes such processes is called spatial statistics, see e.g. Cressie and Wikle (2011). A traditional model framework used in spatial statistics is the Gaussian (i.e. normal distributed) process (GPs) model, which is extensively used in environmental sensing applications and sampling design (Eidsvik et al., 2015). This chapter focuses on how spatial statistics can be used to analyze and model the ocean environment from the standpoint of GPs. We discuss the role of the controlling hyperparameters and the influence on model fitting, as well as regression using brief examples based on ocean model data.

## 3.1 Introduction to Gaussian Processes

A prerequisite for doing effective mission adaptation is to have accurate information about the spatial conditions, especially in highly dynamic environments. To identify the most relevant sampling locations in ocean processes, a model of the spatial phenomenon itself is necessary. This also includes formal measures of uncertainty, which is necessary for providing informative metrics used in sampling optimization, as we will see in Section 4.4.1. Running a high fidelity numerical ocean model on board a robotic platform is currently infeasible, as the required numerical resolution translates into computational demands that are too high for the platform to manage. To overcome this problem, different types of surrogate models (or proxy models) have been used instead, such as neural networks (van der Merwe et al., 2007) and linear combinations of static basis functions (Schwager et al., 2017). However, the more common modeling approach is stochastic modeling using GPs (Cressie and Wikle, 2011).

GPs are a widely used family of stochastic processes for modeling dependent data observed over time, space, or both (Richard A. Davis, 2001). GPs provide a practical probabilistic approach to modeling, making the approach popular across a wide range of environmental fields such as geology, hydrology, and atmospheric science. GPs have also been widely adopted in oceanographic sampling applications, see e.g. Binney et al. (2013),

Ma et al. (2017), Hitz et al. (2017), and Kemna (2018, Ch. 3.4) for instructive examples. The popularity of GPs stems primarily from four essential properties:

**Useful properties of GPs:**

- **Modeling and computational properties:** GPs unite a sophisticated modeling framework with computational tractability, allowing models to run on board the platforms themselves.
- **Model fitting:** as shown in Eq. (3.1), they can be fully expressed using only a *mean* and a *covariance function* (also known as a *kernel*). This alleviates model fitting to the first- and second-order moments of the relevant process (Richard A. Davis, 2001). Furthermore, as long as it is possible to estimate the covariance function, a GP can be used on the basis of sparse prior data.
- **Conditioning:** conditioning on data (updating the model based on measurements) is inherent to the fundamental equations of the model, making assimilation uncomplicated once the GP is formulated. The predicted posterior distribution can be used as input into the subsequent sensing strategy, enabling adaptation to observed changes during mission deployment.
- **Measure of uncertainty:** GPs can provide formal measures of predictive uncertainty (e.g. variance or entropy [mutual information] criterion), which can be used to quantify information gain as an uncertainty reduction.

A GP can be formally defined as a collection of random variables that have a *multivariate normal probability density function*. This provides analytical simplicity, since all finite subsets of this domain will follow this distribution. In environmental applications, a GP typically characterizes random variation at points in space, time, or both, discretized down to a grid map with a certain spatio-temporal resolution. For simplicity, we shall restrict attention to the case of 2D spatial models where we regard a location $\boldsymbol{s} = (East, North)$ in space. Consider therefore a real-valued stochastic process $\{x(\boldsymbol{s}),\ \boldsymbol{s} \in \mathcal{V}\}$[1], where $\mathcal{V}$ is an index set where $\mathcal{V} \subset \mathbb{R}^2$. This stochastic process is a GP if, for any finite choice of $n$ distinct locations $\boldsymbol{s}_1 \ldots, \boldsymbol{s}_n \in \mathcal{V}$, the random vector $\boldsymbol{x} = \big[x(\boldsymbol{s}_1), \ldots, x(\boldsymbol{s}_n)\big]$ has a multivariate normal probability density function

$$p(\boldsymbol{x}) = N(\boldsymbol{\mu}, \boldsymbol{\Sigma}) = \frac{1}{(2\pi)^{\frac{n}{2}} |\boldsymbol{\Sigma}|^{\frac{1}{2}}} e^{-\frac{1}{2}(\boldsymbol{x}-\boldsymbol{\mu})^T \boldsymbol{\Sigma}^{-1} (\boldsymbol{x}-\boldsymbol{\mu})}, \tag{3.1}$$

defined by the mean vector $\boldsymbol{\mu} = E(\boldsymbol{x})$, and the symmetric positive definite covariance matrix $\boldsymbol{\Sigma} = \text{cov}(\boldsymbol{x}, \boldsymbol{x})$. The mean vector $\boldsymbol{\mu} = [\mu_1, ..., \mu_n]$ is typically specified from existing data, for instance satellite images or outputs from ocean models. In the simplest case with replicates in time, the mean value at each location $i = 1, \ldots, n$ is set as

$$\mu_i = \frac{1}{m} \sum_{t=1}^{m} x_t(\boldsymbol{s}_i), \tag{3.2}$$

[1] Regarding the notation: some authors distinguish between the random variable using a capital letter $X(\boldsymbol{s})$ and the outcome or realization with a lowercase letter $\boldsymbol{x}$.

where $x_t(\boldsymbol{s}_i)$ is the value at location $\boldsymbol{s}_i$, over a timespan $t = 1, \ldots, m$. As the GP in our case is specified in two dimensions, the mean values constitute a surface of the expected value, which could be assigned to describe temperature, salinity, etc. The covariance matrix $\boldsymbol{\Sigma}$ is given as

$$\boldsymbol{\Sigma} = \begin{bmatrix} \Sigma_{11} & \Sigma_{12} & \ldots & \Sigma_{1n} \\ \Sigma_{21} & \Sigma_{22} & \ldots & \Sigma_{2n} \\ \vdots & \vdots & \ddots & \vdots \\ \Sigma_{n1} & \Sigma_{n2} & \ldots & \Sigma_{nn} \end{bmatrix}, \tag{3.3}$$

where, $\Sigma_{ij} = \sigma_i \sigma_j \mathcal{K}(i, j)$. Normally the variance terms $\sigma_i^2$ and $\sigma_j^2$ are taken to be the same for all locations and collected as $\sigma^2$, making the covariance independent of location (i.e. stationary). Without too much modification this can be augmented further to include a spatially varying local variance by leveraging available prior data, as

$$\sigma_i^2 = \frac{1}{m} \sum_{t=1}^{m} (x_t(\boldsymbol{s}_i) - \mu_i)^2. \tag{3.4}$$

The kernel $\mathcal{K}(i, j)$ function is defined as

$$\mathcal{K}(i, j) = (1 + \phi h_{ij}) e^{-\phi h_{ij}}, \tag{3.5}$$

where $h_{ij} = ||\boldsymbol{s}_i - \boldsymbol{s}_j||$ describes the Euclidean distance, and $\phi$ is indicative of the correlation range (Matérn, 2013). Capturing the correct spatial correlation distance is particularly important. Fig. 3.1 shows this influence graphically. By varying the correlation distance parameter $\phi$ in Eq. (3.5), for a simulated GP, different smooth fields are obtained (mean is set to zero). Due to the negative exponential, increasing $\phi$ reduces the correlation, and hence the process will be similar to noise (Fig. 3.1a).

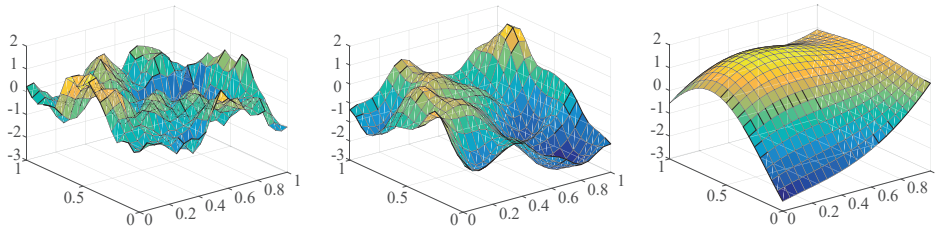

(a) $\phi = 100$ (b) $\phi = 20$ (c) $\phi = 0.5$

Figure 3.1: The effect of different correlation distances ($\phi$) on a GP.

GPs are, in many respects, closely related to the study of covariance functions. When variables are allocated to spatial locations, the covariance matrix models the spatial dependence between locations. Or, in the case of time, the covariance models the temporal dependence between observations. Both space and time relations can be built into the covariance matrix, and under certain assumptions, they can also be separated into different parts, see e.g. Frolov et al. (2014, App. A1).

## 3.2 Conditioning a Gaussian Processes

Once the mean and covariance function are defined, GPs follow basic probability theory, applied to multivariate Gaussian distributions. In this way, GPs can be used in a Bayesian setting where *Bayes' rule*, can be used to update the prior probability as more evidence or data becomes available. The model for Bayesian updating from data relies on finding the conditional probability $p(\boldsymbol{x}|\boldsymbol{y})$, where $\boldsymbol{x}$ is a distinction of interest (e.g. temperature), and $\boldsymbol{y}$ is data (e.g. measurements from an AUV). From the rules of conditional probability, the posterior is obtained according to Bayes' rule

$$p(\boldsymbol{x}|\boldsymbol{y}) = \frac{p(\boldsymbol{x},\boldsymbol{y})}{p(\boldsymbol{y})} = \frac{p(\boldsymbol{x})p(\boldsymbol{y}|\boldsymbol{x})}{p(\boldsymbol{y})} \tag{3.6}$$

where $p(\boldsymbol{x})$ is the prior model for $\boldsymbol{x}$, and $p(\boldsymbol{y}|\boldsymbol{x})$ is the *likelihood function*. The denominator $p(\boldsymbol{y})$ is the *marginal likelihood*, which is a normalizing constant that can be found from marginalizing over $\boldsymbol{x}$ as $p(\boldsymbol{y}) = \int p(\boldsymbol{x})p(\boldsymbol{y}|\boldsymbol{x})d\boldsymbol{x}$, or using sums in discrete situations. The assessment of the posterior probability density function (pdf) $p(\boldsymbol{x}|\boldsymbol{y})$ in Eq. (3.6), depends on the choice of prior and likelihood model. For GPs this has a practical implication, as the posterior will be Gaussian if both the prior and likelihood are Gaussian. In this setting, a tractable expression for the posterior can be found, which is presented in Eq. (3.10) and (3.11).

### 3.2.1 Example: Using Gaussian Processes

To illustrate how GPs can be practically applied to sampling, a short example of model fitting and prediction is demonstrated in this section using ocean model data. The model data that we will use is simulated surface temperature from a coastal area in Norway (Froan, Trøndelag). An imaged data collection survey with AUV will be the basis for illustrating conditioning (assimilation of data) within the GP framework.

We start by modeling the prior mean function using model output of surface temperature (at time 12:00 PM), presented in Fig. 3.2b. The mean function $\mu(\boldsymbol{s}_i)$ is found using 2D linear regression on the temperature data (see Fig. 3.2a), yielding the resulting regression vector $\boldsymbol{\beta}$=[5.42, ,0.0026, 0.0057]. This gives us a prior estimate of the temperature provided east-north location, as predicted values for $\mu$, shown in Fig. 3.3a. The covariance function $\text{cov}(x(\boldsymbol{s}_i), x(\boldsymbol{s}_j))$ is set to the *squared exponential* kernel. Consider then the GP given by

$$\mu(\boldsymbol{s}_i) = 5.40 + 0.0026\, e_i + 0.0058\, n_i, \tag{3.7}$$

$$\text{cov}(\boldsymbol{s}_i, \boldsymbol{s}_j) = \sigma^2 e^{(-\delta\, ||\boldsymbol{s}_i - \boldsymbol{s}_j||)}, \tag{3.8}$$

where $\boldsymbol{s}_i = (e_i, n_i)$ indicates location $i = 1, \ldots, n$. In the covariance function $\sigma^2$ and $\delta$ denote design parameters (hyperparameters) for variance and correlation distance, while $||\boldsymbol{s}_i - \boldsymbol{s}_j||$ may be recognized as the Euclidean distance between two sites $\boldsymbol{s}_i$ and $\boldsymbol{s}_j$. To obtain the correct correlation range $\delta$, a *variogram* analysis is conducted using multiple realizations of the surface temperature data from the ocean model. A variogram is a plot which is constructed to help relate the spatial distance

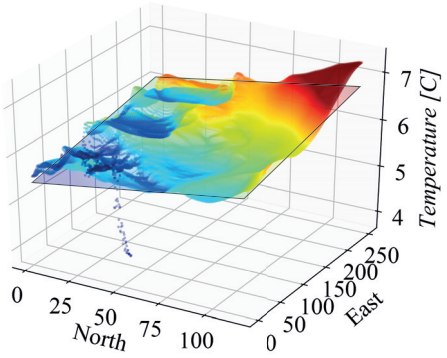


(a) 2D regression of ocean model data (temperature). Showing a fitted plane over the synthetic ground-truth data from (b).

(b) Synthetic temperature data generated from ocean model (12:00 PM), used as a simulated ground-truth, and AUV survey path (dashed line).

Figure 3.2: (3.2a) 2D regression of the simulated surface temperature, note the fitted 2D plane. (3.2b) The ocean model data showing the surface temperature used as ground-truth, and the simulated AUV survey (dashed line).

between points with the points variance. The formal definition follows the relation $\gamma(h) = \frac{1}{2}Var([x(s_i) - x(s_j)]) = Var(x(\boldsymbol{s})) - Cov(x(s_i), x(s_j))$, where $h$ is the lag vector (distance). Typically as the lag distance $h$ increases, the variance increases until a limit is reached and the variogram flattens out. At this limit, the points no longer yield any relation based on the data value and the variance can no longer grow indicating the correlation range $\delta$. The variogram for the ocean model data (many realizations covering one month) is displayed in Fig.3.3b.

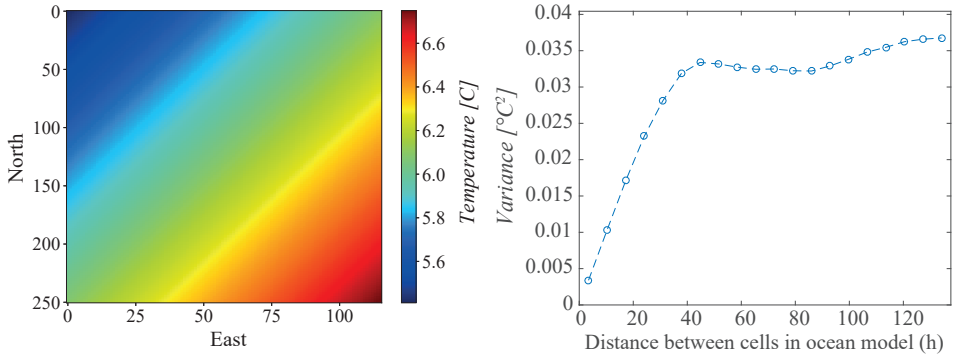


(a) Prior GP realization for $\boldsymbol{\mu}$ found using regression.

(b) Surface temperature variogram made using ocean model data.

Figure 3.3: (3.3a) The prior predicted temperature values in $\boldsymbol{\mu}$, before any observations are made. (3.3b) The one month variogram for the ocean surface temperature data.

The variogram curve in Fig.3.3b indicates a correlation distance of approx. 5-7 km (50-60 h). The correlation variance $\sigma^2$ can be set using Eq. (3.4), or to an average value. Here we use an average value of $\sim$0.035°C$^2$ based on the variogram. The prediction in Fig. 3.3a, found in Eq. (3.7), now constitute a prior estimate of the environment (which we will refer to as the *world model* in Section 4.3). We now proceed to simulate an AUV survey, using observations from the ocean model output (at time 12:00 PM), shown in Fig. 3.2b; observations are made as a location value pair. By assimilating these observations into the GP prior we can produce an updated GP posterior that can render updated values at all locations (including un-observed). The interpolated values are obtained using predictions delivered from the covariance functions, predicting the functional value at a given point by a weighted average of the values in the neighborhood of the point. Let **prior** be the prior function values at $\boldsymbol{s}_i$ based on out prior temperature function $\mu(\boldsymbol{s}_i) = 5.40 + 0.0026\, e_i + 0.0058\, n_i$, and **data** be measurements from the AUV that we want to assimilate. Using a matrix representation, there are four important matrices to consider in this regard, namely

**prior**: $\boldsymbol{\mu} = \mu(\boldsymbol{s}_i)$, for all locations $i = 1, \ldots, n$.

**observation matrix**: $\boldsymbol{F}$ = $m \times n$ matrix with fixed entries (0s and 1s) indicative of the survey design. $m$ is the number of observations/measurements.

**data**: $\boldsymbol{y} = \boldsymbol{F}\boldsymbol{x} + \boldsymbol{\varepsilon}$, where $\boldsymbol{x}$ is a process (ocean model), with Gaussian measurement noise $\boldsymbol{\varepsilon} \sim \mathcal{N}(\boldsymbol{0}, \boldsymbol{T})$; and $\boldsymbol{T} = \boldsymbol{\tau}^2\boldsymbol{I}$, where $\boldsymbol{\tau}$ is can be set manually.

**covariance**: $\boldsymbol{\Sigma}$ = cov$(\boldsymbol{s}_i, \boldsymbol{s}_j)$, for all locations pairs $i = 1, \ldots, n$ and $j = 1, \ldots, n$.

Using these matrices we can setup a joint Gaussian model as

$$p(\textbf{prior}, \textbf{data}) = \mathcal{N}\left(\begin{bmatrix} \textbf{prior} \\ \textbf{data} \end{bmatrix}; \begin{bmatrix} \boldsymbol{\mu} \\ \boldsymbol{F\mu} \end{bmatrix}, \begin{bmatrix} \boldsymbol{\Sigma} & \boldsymbol{\Sigma F}^T \\ \boldsymbol{F\Sigma} & \boldsymbol{F\Sigma F}^T + \boldsymbol{T} \end{bmatrix}\right). \tag{3.9}$$

The Gaussian posterior solution (ref. Eq. (3.6)) is defined by the conditional mean and covariance (posterior) as

$$\boldsymbol{\mu}_{posterior} = \boldsymbol{\mu} + \boldsymbol{\Sigma F}^T(\boldsymbol{F\Sigma F}^T + \boldsymbol{T})^{-1}(\boldsymbol{y} - \boldsymbol{F\mu}), \tag{3.10}$$

$$\boldsymbol{\Sigma}_{posterior} = \boldsymbol{\Sigma} - \boldsymbol{\Sigma F}^T(\boldsymbol{F\Sigma F}^T + \boldsymbol{T})^{-1}\boldsymbol{F\Sigma}, \tag{3.11}$$

where $\boldsymbol{F\mu}$ is the prior temperature prediction at the sampled locations $\mu(\boldsymbol{s}_k)$. Note that the posterior covariance $\boldsymbol{\Sigma}_{posterior}$ is reduced in comparison to the prior covariance, since the updated equation subtracts an always positive term representing the additional information gained from adding the new observations. Another factor which is important to notice is that the GP update requires inversion of the covariance matrix $(\boldsymbol{F\Sigma F}^T + \boldsymbol{T})$, which can be computationally expensive. This is can be a drawback for GP models; for large dimensional problems (i.e. many observations or points), sparse approximations need to be used, see e.g. Vanhatalo et al. (2010).

Using Eq. (3.10) and (3.11) the updated results (conditional mean and variance) can be seen in Fig. 3.4. The sampled locations are shown as dashed lines in Fig. 3.2b, illustrating the AUV path. The GP is conditioned on the data along this line to obtain the Fig. 3.4a. Comparing Fig. 3.4a to Fig. 3.2b, the GP has updated the prior mean field in Fig. 3.3a, into

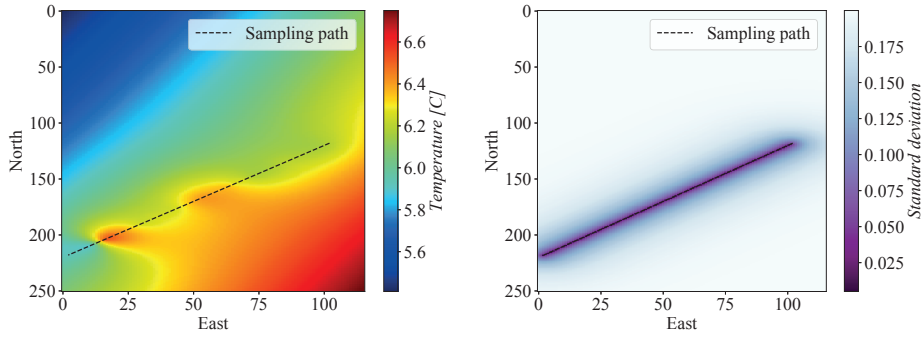


(a) Posterior prediction of Gaussian Process.

(b) Standard deviation estimation error.

Figure 3.4: The posterior mean and standard deviation after conditioning on the data gathered along the dashed line.

a more accurate representation of surface water temperature. The predicted temperature distribution can now be used as an input into the subsequent sensing strategy, enabling adaptation to observed changes during mission deployment. The standard deviation in Fig. 3.4b is small along the AUV observation sites (only sensor noise), and gradually increases to the level of the process noise as one gets further from the actual measurement site. The standard deviation (and variance) is independent of the actual measured data; only the spatial dependencies between the data provide influence, which can be checked by inspection of Eq. (3.11).

## 3.3 Considerations for Using GPs in the Ocean

Using GPs implies some assumptions regarding the environment, which we will briefly discuss from the basis of adaptive sampling.

Depending on the stationary properties of the random field, the covariance has different properties. In this context, the notion of *isotropy* is important to note. A covariance function which is isotropic is invariant to translations in the input space and is only a function of the distance between the respective sites (i.e. $||\boldsymbol{s}_i - \boldsymbol{s}_j||$). Isotropy is required for the random field to be *stationary* or *weakly stationary*. In stochastic process theory, a process which has constant mean and whose covariance function is invariant to translations is called *weakly stationary*. A process is *strictly stationary* if all of its finite dimensional distributions are invariant to translations. A spatial process is *anisotropic* if the correlation depends on direction. The ocean is fundamentally turbulent, and has episodic events such as tides or complicated processes like Langmuir circulation (Thorpe, 2004) which introduces heterogeneity, essentially making the ocean an anisotropic non-stationary process. However, to model and work with spatial models that are not too complicated, stationarity is often assumed. In practice, stationarity cannot be assumed to be true at all scales (Eidsvik et al., 2015). Trying to account for time varying uncertainty is complicated as

this weakens the underlying stationary properties. Integrating temporal dependence of the latent process is therefore often resolved by assuming approximate stationarity for a finite horizon using corrective measures to estimate the time dependent dynamics, such as separable integration into the covariance matrix (see e.g. Frolov et al. (2014, App. A1)), or even ignoring time variation completely.

Practical application of GPs depends, as always, on the type of data, model, and problem description. A reoccurring problem with GP models is the increased dimensionality that arises from large data sets, leading a lot of research into Sparse GPs for speeding up inference (Vanhatalo et al., 2010; Hoang et al., 2016). There is also a large body of work focusing on estimating and learning the hyperparameters for the GP, i.e. learning the covariance function parameters, see e.g. (Rasmussen and Williams, 2006). The notion here is that there is an underlying functional description of the studied process available through observation. In this setting, a problem arises. To deduce these parameters from observations, the system needs to be observed in such a way that the correlation structure can be extracted correctly, implying that a certain level of synoptic knowledge is attainable. Currents and other time varying processes make such observations difficult to measure on a synoptic timescale. However, at certain scales and time-frames, the ocean can exhibit *ergodic dynamics*, meaning that the time-averaged statistic does not drastically change over time. For most environmental sensing applications, the ergodic hypothesis is assumed to be valid. In such situations, it is possible to extract useful information, as demonstrated by Mathew and Mezić (2011) or Alvarez and Mourre (2012).

# Chapter 4

# Adaptive Sampling

ADJUSTING sampling decisions in response to observed data is a well known topic in geostatistics, atmospheric sciences, and other fields concerned with optimizing information gathering. Common to all these domains is the underlying limitation arising from finite sampling resources. Because of finite sampling resources, intensive sampling of the relevant domains is not possible. To obtain the most scientifically relevant measurements in an effective manner, adaptive approaches need to be used. In contrast to static/pre-planned schemes, adaptive/data-driven strategies can operate on a *posterior knowledge base* and react to current conditions, having access to both prior and current information; selecting sampling locations thus depends on past observations taken during exploration. Such schemes are preferable, since all the information available can be used to reason about the environment and compensate for partial or incorrect prior knowledge, as well as handling off-nominal conditions. The impact of this additional information is twofold; i) enabling the sensor platform to divert from the mission if favorable circumstances materialize (opportunistic behavior), and ii) increase the prospect of retrieving information more effectively. The latter aspect is often considered the most noteworthy, especially for resource intensive environmental sensing applications, having the potential to save time and cost.

This chapter provides an introduction to adaptive sampling and discusses related work in the context of ocean observation. Additional insight into this subject is given through a discussion of different adaptive methodologies, common autonomous architectures, and the underlying theoretical foundations with associated examples.

## 4.1 Introduction to Adaptive Sampling

The term *adaptive sampling* is used to refer to the act of making an intelligent and deliberate choice of *when and where* to gather data on the basis of informative and scientific metrics (measurements adjusted to purpose); this implies that choices need to be taken on line and *in-situ*. In this brief introduction we will look at the fundamental entities in this process, the theoretical principles involved, and the limitations that arises from the problem formulation.

### 4.1.1 Problem Solving Agents and Architectures

Given the high level of uncertainty in the ocean, the ability to learn and adapt is critical. In general terms, the aim of adaptive (data-driven) sampling is to effectively fuse observations with prior knowledge such that subsequent decisions can be made to refine the data collection strategy. The acting entity in this framework is the *agent*, as described in Russell and Norvig (1995):

> *"An agent is anything that can be viewed as perceiving its environment through sensors and acting upon that environment through effectors."*

A *agent* thus describes an autonomous system (robot) in which sensory data is used for synthesizing control and action selection. The agent can also, therefore, be thought of as a decision maker, where the internal structure and properties of the agent will be referred to as the *architecture*. The distillation of sensor information down to control actions or waypoints (sampling plan generation) differ based on the type of architecture and subsequent choice of method (see, for example, Chapter 5 and Fig. 5.1). A range of different architectures exists, as demonstrated by Russell and Norvig (1995); LaValle (2006). On the basis of the related work in Section 4.1.5 and the articles in Part II, we will restrict the discussion to model-based *information-theoretic* and state-based *subsumption-based* agents and corresponding architectures.

In *information-theoretic* systems, plan generation is conducted through utilization of information-based metrics and usually follow the ***Sense***→***Plan***→***Act*** control methodology. An example of an agent following this principle is the T-REX (Teleo-Reactive EXecutive) (McGann et al., 2008b) agent shown in Fig. 4.1. The essential part to note here is the *Plan* stage, in which distillation of one or several *actions* is formulated on the basis on available knowledge and problem constraints. The term "action" can have multiple meanings such as coordination (e.g. "turn the camera on", "keep distance to another AUV") or sampling optimization (e.g. should I sample at location A or B). The focus here is on the latter, where prioritization across different locations is conducted on the basis of information quantification. This quantification is typically established by borrowing metrics from Bayesian experiment design using uncertainty-based measures to evaluate, find, and differentiate between sampling locations, where the reduction of uncertainty constitutes a gain in information. For *subsumption-based* systems, the sampling decision does not originate from a plan, but is instead a series of discrete actions decomposed into different sets of *behaviors* (the term behavior-based architecture is therefore used interchangeably) that represent certain action-response pairs. These pairs are triggered by incoming data (e.g. "if temperature sensor reads below 5°C, turn 180°on current heading"), thus the control methodology becomes simply ***Sense***→***Act***, sometimes referred to as "the reactive paradigm".

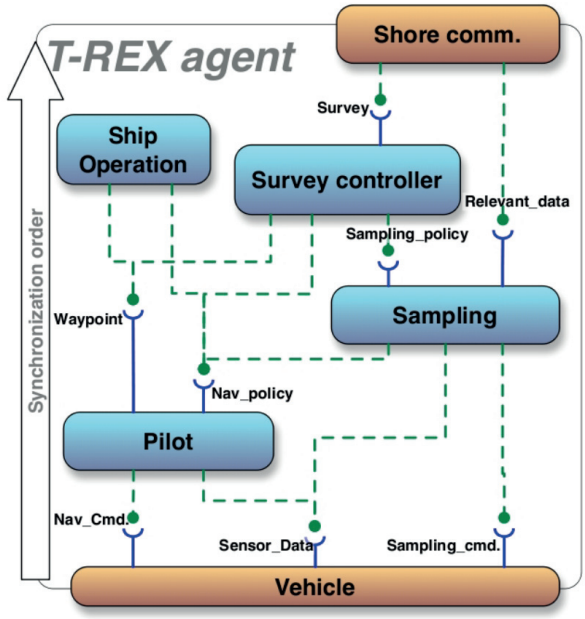


Figure 4.1: Internals of an instance of the autonomous T-REX sampling agent, using the *Sense→Plan→Act* control methodology (Rajan and Py, 2012). Multiple internal control loops (reactors) interact to create a sampling plan/behavior using relevant information that is shared across the internal network. The agent also features a chain of command, with low and high level control. Image courtesy of Rajan et al. (2012).

### 4.1.2 Static and Sequential Sensing Situations

When discussing different types of problem solving agents, it is also important to distinguish between *static* and *sequential* decision situations and the related sampling optimization. For sequential sensing situations, the decision maker (the agent) makes several decisions, one after another, about where to sample based on previous measurements (adaptive sampling). In contrast, a static decision is a pre-planned/one-time-only decision (*sensor placement problem*) using prior available data, which also applies to deterministic human-designed surveys (scripted plan with waypoints). Static decision problems take place "off-line," whereas sequential decisions are made "on-line" during execution. Consequently, the focus given here will be on sequential decision situations and data acquisition, where the agent would have the capability to adapt the plan based on observations. An example of such a situation is given in Fig. 4.2.

In practice, finding the optimal solution (described in Section 4.1.3) in these types of problems is not tractable because of the exponential growth in the number of combinations that has to be considered. This search has been shown to be NP-hard[1] for uncertainty-based

[1]NP (non-deterministic polynomial acceptable problems): problems are at least comparable to a non-deterministic polynomial-time (NP-problem), or more complex.

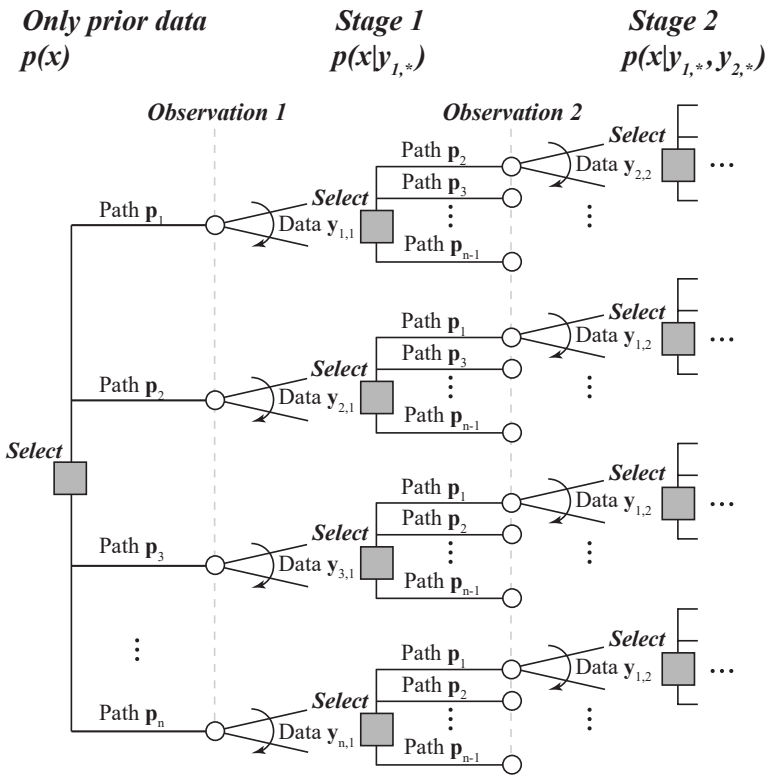


Figure 4.2: Illustration of sequential decisions for a spatial sampling problem. The grey box indicates a choice that needs to be taken by the agent. The dot and arrow indicate data $\boldsymbol{y}$ being observed after each choice of path. The subsequent decision about where to measure is a result of the gathered data and available locations; a problem that quickly grows due to the number path of combinations. If the path considered only has one element, then each path would equal a single location $\boldsymbol{s}$.

optimization schemes (e.g. entropy (Ko et al., 1995)), hence efficient exact solutions are likely not possible. Therefore, much of the focus is instead directed towards finding feasible solutions to these sequential problems, as opposed to more optimal *non-myopic* (non-greedy) solutions (see, for example, Singh et al. (2007); Zhang and Sukhatme (2007)). To find feasible solutions, different heuristics and *myopic* (greedy) approaches are typically used, more details are given in Section 4.1.5 and Krause (2008). It is also possible to regard Fig. 4.2 in the Bayesian context discussed in Section 3.2, where an update of the prior probability is done as more data becomes available. In this regard, the aim for the (data-driven) agent is now to traverse this graph in a manner that retains an advantageous strategy for information recovery.

### 4.1.3 Sampling Optimization: Coverage- vs. Feature-Based

What constitutes as optimal depends can be subjective, however, in this thesis we separate between *coverage-* and/or *feature-based* criteria. From the aspect of a coverage or sensor

placement standpoint, optimization can be classified as a problem deciding which locations to observe in order to effectively decrease the uncertainty about a phenomena. In this setting, the optimal solution does not depend on the data (only coverage), thus criteria measuring uncertainty such as *predictive variance* and *mutual information* (see Section 4.4.1) can be used in the objective function. Optimal locations can therefore be deterministically selected prior to making observations (i.e. non-adaptive), where the optimal/highly informal locations are those that reduce the uncertainty most. The sampling utility can then be quantified by measuring the total decrease in uncertainty across the different alternatives.

This can work well if the goal is simply restricted to sensor coverage (e.g. photogrammetry of a full coral reef), or in cases where the addition of actual measurements has little influence. However, in most environmental sampling applications, measurements provide an important source of information. Using observations enables more directed sampling metrics, which can be used to further reduce uncertainty and improve targeted sampling of features (e.g. fronts, temperature gradients, etc.) relevant for studying ocean processes (see, for example, the discussion in Low (2009, Ch. 2.1) about coverage- vs. feature-based sampling). Furthermore, optimizing sampling in environments characterized by the type of uncertainty that is hard to model and determine prior to sampling (such as the water column) is not well-suited for sensor placement approaches, which become sub-optimal in this context. The advantage of using adaptive and feature-based optimization is sometimes referred to as the *the adaptivity gap* (Krause, 2008). Criteria measuring uncertainty are vital for achieving solutions to sensing problems, however, it is important that data-driven terms are added to the optimization process in order to utilize all available information. This combination allows more complex interactions between *exploration and exploitation* influences. A more formal introduction to different optimization criteria is given further down in Section 4.4.1.

### 4.1.4 Exploration vs. Exploitation

The balance between exploration and exploitation is fundamental to decisions concerned with gathering information. This balance is split between i) decisions that allow us to explore and learn about our environment (exploration), and ii) decisions that focus on the most valuable options given current beliefs about the world (exploitation). Deciding what information to gather next also depends on the balance between prior and current knowledge. If all details about the environment are fully known, an approach that exploits such background information enables a more effective data gathering system. In contrast, if no prior information is available, an exploration-based strategy is more advantageous. However, as time passes by, and the domain gets "explored", this balance may shift back towards exploitation. The need to obtain new knowledge, and the need to use that knowledge to improve performance, is a trade-off that all adaptive systems need to address, either through a balance between coverage- and feature-based optimization, or coordination of competing behaviors. Optimal performance usually requires some balance between these two, at times contrasting, influences (Low, 2009). The trade-off is also heavily discussed in the machine learning literature within the *multi-armed bandit problem* (Audibert et al., 2009). Complex interactions between these influences can be

constructed, such as modeling curiosity, where one tries to quantify what is interesting in the environment, see e.g. (Girdhar and Dudek, 2015).

As identified in this brief introduction, the most important elements in adaptive sampling are summarized in the box below.

**Important elements in adaptive sampling:**

- **(Problem Solving) Agent:** The combined autonomous system and actor (decision maker).
  - **Architecture:** The internal structure and properties of the agent responsible for synthetization/optimization of the control actions and decisions (plan/policy), i.e information-theoretic- or subsumption-based architectures.
- **(Problem Domain) Sequential and Data-Dependent Sensing:** The type of problem structure that characterizes adaptive sampling is one in which the decision situation and information-gathering takes place sequentially over time.
- **(Method) Non-adaptive vs. Adaptive:** In cases where uniform sampling of the field at regular intervals is possible and the environmental field is smoothly varying, non-adaptive strategies can work well (Singh et al., 2006). However, faced with limited sampling resources, un-modeled uncertainty, or specific features of interest, adaptive sampling can exploit observational data to map the environmental more effectively.
- **(Optimization) Coverage- vs. Feature-Based:** Two types of criteria are usually considered in environmental sampling: i) coverage-based (uncertainty) criteria, associated with the sensor placement problem, and ii) feature-based (data-driven) criteria. A combination of both can also be considered.
  - **(Trade-Off) Exploration vs. Exploitation:** Combining coverage-based (uncertainty) and feature-based (data-driven) criteria involves finding a balance between exploration (reducing uncertainty) and exploitation (exploiting current knowledge).
  - **(Trade-Off) Optimality vs. Computability:** For this type of sampling problem, the number of choices (i.e. locations, paths, and candidate designs) makes the problem combinatorially large, creating a trade-off between optimization (finding the optimal design) and computability (arriving at a solution in reasonable time), which has to be considered in practice.

### 4.1.5 Related Work and Aspects of Adaptive Sampling

Partly fueled by the communication and information revolution of the last decades of the twentieth century, marine robotics are today a key element in environmental sensing and ocean observation applications (National Research Council, 1996). Along with increasing computational capabilities, a growing interest in developing systems to operate with a higher concept of autonomy have been introduced in light of the unique challenges posed by the oceanic domain. A vast range of approaches have been developed spanning several theoretic sub-fields, including: guidance and control theory, path planning, AI, machine

learning, and spatial statistics. Much of this can be traced back to the underlying problem of experiment design and sampling theory, demanding systems that can reason, plan, and strategize data collection in a highly uncertain environment. The scientific context is also often multi-disciplinary, including teams from biology, physical oceanography, and other environmental scientists. This is of particular relevance, as each field of study is exposed to different spatio-temporal scales depending on the processes under focus, each potentially requiring a different sampling approach. A more detailed discussion on the topic of space-time dependence in the ocean can be found in Lermusiaux (2006) and Graham et al. (2013).

Much of the classical underpinnings for information-theoretic sampling can be found in Guestrin et al. (2005) and Krause et al. (2006), building on traditional fields such as spatial statistics and work by Cressie and Wikle (2011). A central part of this influence is the use of GPs to model the environment, spatial dependence, and assimilation/conditioning of data. GPs also provide a formal measure of uncertainty, which connects to optimal sampling through information-theoretic criteria such as entropy (Thompson et al., 2011) and mutual information (Guestrin et al., 2005), reduction in variance (Binney et al., 2013), and root mean square error (RMSE) (Frolov et al., 2014). The use of variance and entropy as optimality criteria is further explained in Section 4.4.1. As discussed, finding optimal sampling locations can be either a static (selecting a finite set of appropriate stationary locations, e.g. deploying ocean buoys) or sequential problem (continuous selection and evaluation of sampling locations, e.g. AUV and glider based data collection). In a static or quasi-static environment, such as a copper mine or the sea-floor, the environment is stationary or slowly changing. In this context, the observations would not change significantly as time passes. In contrast, a dynamic environment, such as the water column or the atmosphere, change happens regularly, often in an episodic and non-deterministic fashion. Determining a sampling design under these conditions is significantly more challenging, and planning ahead in time-dependent environments using only prior information would be prone to time-evolving and unobserved uncertainty. Thus, the capacity to adjust sampling based on new observations is vital. Besides, it is also not possible to strive for complete coverage in the oceanic domain, so prioritization of sampling efforts must always be considered one way or another.

Even at a basic level the problem of information gathering is difficult. Solving a static sensor placement problem, a well-known problem in the sensor-network community, has been shown to be NP-hard (Ko et al., 1995). Another factor is the influence of spatial dependence, which makes the information gain of each sensor depend on the proximity of all other sensors. This interconnectedness makes for a vast increase in problem complexity as one has to account for the fact that the information is not *modular*[2], but shared instead. Correlation implies that measurements that are close yield less information than measurements taken far apart, as samples taken close to each other are likely to share information. In the context of a fixed size area, initial (and non-proximal) samples give a lot of information, while as the number of samples increase (i.e. samples has to be taken closer together), the information value of each new measurement decreases. This is characteris-

[2]Can be explained as an "additive" property. Euclidean distance satisfies this as the sum of two segments is equal to the sum of the combined segments.

tic of a diminishing returns property, often expressed in relation to the objective function, as *submodularity*[3]. Since information is shared, observations carry redundant information and it is necessary to gather additional information to achieve the same knowledge as if they where uncorrelated. For a static network of sensors, identifying submodularity in a problem is actually useful, as submodular functions have very similar properties to convex and concave functions. Just as convexity makes continuous functions more amenable to optimization, so does submodularity in the case of combinatorial problems (Krause, 2008, Ch.5). Furthermore, a fundamental result from Nemhauser et al. (1978) proves that a simple greedy algorithm (iteratively selecting the location which most increases the utility) can achieve a near-optimal solution obtaining a constant fraction of 63% of the optimal value of this NP-hard optimization problem (Krause, 2008, p.33), if the submodularity property is present.

**Myopic (Greedy) vs. Non-myopic/Synoptic Sampling**

Given the added complexity of studying spatial sampling in a dynamic (non-stationary) system and the combinatorial growth of the parameter space in sequential settings (see Fig. 4.2), assumptions and simplifications often need to be made in order to attain a feasible solution, leaving room for various approaches. One intuitive approach is to discretize the problem by assigning potential measurement locations to a graph and then evaluating the problem along the graph edges (see example in Section 4.5.1). Evaluation can be *myopic* (greedy), using a fixed and usually short planning/evaluation horizon, or be more synoptic, planning over several sequential steps (*non-myopic*). One important aspect to consider in this regard is that greedy strategies are subject to the *local minima* problem of optimization. Non-myopic schemes can avoid this by looking further ahead (several sampling steps) and more elaborate searching criteria. There is however a fundamental difficulty specifically related to environmental sampling in the ocean, and especially the water column, namely the fact that it is difficult to attain and maintain synoptic up-to-date knowledge. Planning ahead only makes sense if you can trust the quality of the information.

When discussing myopic vs. non-myopic approaches the previously mentioned result from Nemhauser et al. (1978) is of interest, providing a measure of the expected performance for greedy algorithms. Chekuri and Pal (2005) explored this in the setting of a graph using a recursive greedy algorithm, providing near-optimal solutions depending on the planning horizon and graph resolution. Transferring from the (static) aforementioned work by Guestrin, Krause, and Singh et al. (2007), Low et al. (2008) showed a sequential approach for multiple robots that incorporated assimilation of newly gathered data using dynamic programming, GPs, and log-GPs[4], using the sum of posterior variances and entropy as the information metric. The same metric and mutual information was later used in Binney et al. (2010) and Binney et al. (2013), adapted to a recursive greedy approach, with a finite horizon, a generalization of Chekuri and Pal (2005). Trying to move away

[3]Submodularity is usually explained as an diminishing returns property where adding a sensor to an existing deployment helps more if we have placed few sensors so far, and less if we have already placed many sensors (Krause, 2008, p.4).

[4]Log-Gaussian Processes assume data follow a log-normal distribution, which correspond better to data that is clustered in hotspots (Crow and Shimizu, 1988).

from greedy and myopic strategies introduces issues with scalability, running time, and computational load typically arising from increasing dimensionality in the problem space, such as increasing the graph size or resolution. Different types of heuristics (see Low et al. (2009)), Markov properties, and Monte Carlo approaches are typically used to alleviate the computational burden and find feasible solutions. Branch and bound methods have also been used to limit dimensionality growth, for example, to allow handling of larger graphs (Binney and Sukhatme, 2012). Greedy approaches avoid this problem entirely by using a limited look-ahead (see Hitz et al. (2014)), sacrificing optimality and/or completeness. In this context, the term *anytime algorithm* is often used to describe algorithms that can deliver solutions (partial answers) in real time, even with interruption. Another solution for dealing with computational complexity is to assume modularity in the objective function. This simplification enabled Zhang and Sukhatme (2007) to obtain good results, given a certain graph resolution. Similarly, Yilmaz et al. (2008) uses this in a classical example using cost functions and constraints (communication, available energy, etc.) to maximize the sum of probabilities along paths with mixed integer linear programming.

For a number of applications, the aim is not only to gain information (explore), but also to exploit information, a trade-off fundamental to robotic exploration, reinforcement learning, and active learning. Exploitation comes in as a factor when there is a specific interest, e.g. either sampling above a certain concentration or hotspots (areas of high value measurements) or, more generally, a set of particular conditions connected to a feature. In a sense, this captures the motivation for data-driven approaches, as one can act opportunistically if favorable conditions arises. A concrete example of this is the work by Das et al. (2015), where both GPs and *ex-situ* supervised learning is used, aiming to learn optimal sampling points, for an AUV with water sampling capabilities. Building a semantic prediction of the environment under spatio-temporal variation is also explored in Girdhar and Dudek (2015), focusing on modeling curiosity to elevate the utility for long term missions with mobile robots.

**Environmental Modeling in Ocean Sampling**

As previously mentioned, spatio-temporal dynamics are complicating the data-collection strategy. To address this, various types of environmental models have been applied trying to estimate different aspects of this variability. With the increasing availability of high-end computational resources accessible to oceanographers, multi-resolution modeling of the upper water column, for predictive or post-hoc purposes is a new and viable tool to understand complex interactions between physical and biological features. However, current synthetic ocean models (see e.g. Shchepetkin and McWilliams (2005a); Dag Slagstad (2005)) still lack the detail necessary for adequate predictions of change necessary for detailed planning of sampling efforts (Griffies et al., 2000; Lermusiaux, 2006). Nevertheless, forecasts from ocean models have been used to efficiently guide underwater gliders (see Chang et al. (2015)) using the predicted current field to minimize energy and improve navigation. Coupling adaptation and modeling was also studied in Smith et al. (2010), Smith et al. (2011) and Smith et al. (2016), where prior information from models was used to plan sampling of frontal systems and phytoplankton blooms. This concept was further studied in Fossum et al. (2018), where utilization of ocean model data was combined with

GPs and information theoretic metrics (reduction of variance) towards developing a data-driven greedy adaptive sampling algorithm (GASA) for use in coastal waters. Statistical prediction of surface currents using satellite data have also been suggested as an effective aid for underwater vehicles (Frolov et al., 2012).

**Moving Away from Graphs**

As discussed, the discretization of the workspace, i.e. a graph, has a large impact on the result, computability, and attainable solutions. Consequently, by omitting graphs these methods try to work in continuous space. To overcome the aforementioned problem with dimensionality, some approaches use *genetic algorithms* (GAs) that can iteratively evolve the path according to a defined measure of reward/score by relying on bio-inspired operators such as mutation, crossover and selection (Mitchell, 1998). Frolov et al. (2014) serves as a excellent example of this approach, where the mean square error (MSE) is used as an information metric to evaluate the GAs path evolution, comparing performance with both lawnmower and A* solutions. More recently, Hitz et al. (2017) investigate methods for data-driven sampling in 3D using GAs, taking into account constraints such as path budget. Even if GAs tend to have less computational cost compared to a similar dense graph, the cost of the GAs increases exponentially with the path length (Frolov et al., 2014), due to the number of calls to the cost function. GAs also have problems relating inconsistency (may provide different solutions each time) and incompleteness (do not always produce a feasible path when one exists) when searching for the optimal path (Zeng et al., 2015). Sampling-based methods for path planning, such as rapidly exploring random trees (RRT) variations, have also been used (see Hollinger and Sukhatme (2014)). Sampling-based methods can find solutions more quickly, but require submodularity properties for pruning away alternatives in the correct manner.

**Autonomous Sampling Networks**

In addition to a multitude of platform-specific approaches, numerous field programs involving robotic sampling have been conducted, including work on multi-vehicle coordination. Much of the foundation for optimal synoptic sampling was laid in the seminal work by Bretherton et al. (1976) and the associated MODE-73 experiment, where the objective was to study the mesoscale motion on spatial scales from 50 to 500 km, and time scales of 1 week to a few months. More recently, campaigns like the Autonomous Ocean Sampling Network (AOSN-I/-II) (Curtin et al., 1993; Ramp et al., 2009), the Adaptive Sampling and Prediction (ASAP) field experiment (Leonard et al., 2010), the Keck Institute for Space Studies (KISS) field program (Chao et al., 2017), the Controlled Agile and Novel Observation Network (CANON) field program (Das et al., 2010, 2012a), and associated activity at Monterey Bay Research Institute (MBARI) (Chavez et al., 2017), have tested several of the aforementioned methods in practice on a large scale with multiple platforms and ships in the water simultaneously. The persistent focus of these efforts and the increasing complexity of doing fleet coordination in such campaigns has prompted the development of a few widely used autonomous agent architectures used for scientific AUV applications, namely the previously presented T-REX agent (McGann et al., 2008b) developed at MBARI, shown in Fig. 4.1, and the MOOS-IvP (Mission Oriented Operating Suite) (Benjamin et al., 2010) from Massachusetts Institute of Technology (MIT). In

regular operation, the T-REX framework explores adaptive data-collection using multiple control loops together with a "divide-and-conquer" problem-solving strategy. A thorough overview of T-REX is given in Py et al. (2010), Rajan and Py (2012), and Rajan et al. (2012), with the latter including examples from field trials.

**Multi-Vehicle Coordination**

In addition to single craft controlling agents, multi-vehicle coordination of platforms has also been extensively investigated. Following work related to the AOSN-II (Ramp et al., 2009), Leonard et al. (2007b), Alvarez et al. (2007), and Leonard et al. (2010) addresses collective synoptic sampling and provides a solution by optimizing spacing between multiple platforms along elliptical pathways (chosen to simplify the trajectory planning). While impressive, the approach assumes homogeneous spatial correlation and uniform prior uncertainty, which later is addressed in Frolov et al. (2014). Coordination is not only restricted to a single domain, but across mediums such as land, ocean, and air, see e.g. Py et al. (2016), Ludvigsen et al. (2016), Ferreira et al. (2018), and Costa et al. (2018). For human-in-the-loop applications, the previously mentioned Oceanographic Decision Support System (ODSS) (Gomes et al., 2013) developed at MBARI is an example of an online tool for multi-platform coordination and control that supports situational awareness, experiment planning, collaboration, and data analysis between platforms and decision makers. Multi-platform observation and coordination can also help address issues related to overly simplistic assumptions about the field statics. In Das et al. (2012b), coordinated sampling using Lagrangian drifters and AUVs is explored to address the problem of tagging and tracking an advection patch of water. The same platforms are also used in Graham et al. (2013), where the aim is to assess the use of different spatio-temporal correlation models. An overview of information-theoretic approaches and related multi-platform efforts can be found in Kemna (2018).

## 4.2 Subsumption-Based Architectures

Subsumption architectures (Brooks, 1986) constitute the most rudimentary form of problem solving agents, where sensory information couples directly to action selection (*Sense*→*Act*). Subsumption-based agents usually feature a simplistic model of the environment, using only a finite number of states. Since there is no planning or deliberation involved – only actions corresponding to sensor values – there is no need for a complex internalized model that includes values at unobserved locations. Rather than featuring a planning stage, the sampling behavior is decomposed into different sets of behaviors that represent certain action-response pairs that are triggered by incoming data, see Fig. 4.3.

In this sense subsumption-based architectures share similarities with expert systems (see Jackson (1998)). A clear limitation of this setup is that all sampling behavior needs to be determined in advance (hand-tailored to each problem), and reconciliation of different behaviors may lead to both sub-optimal solutions and complexity. In comparison to information-theoretic approaches, on which the model plays a central role, subsumption architectures cannot (in their traditional form) rely on re-planning to handle off-nominal situations. Another limitation is that subsumption architectures, in their classical form (hybrid architectures exists), only react to their immediate environment (e.g. passing through a temperature gradient), disregarding impacts to future actions or states (Rajan and Py,

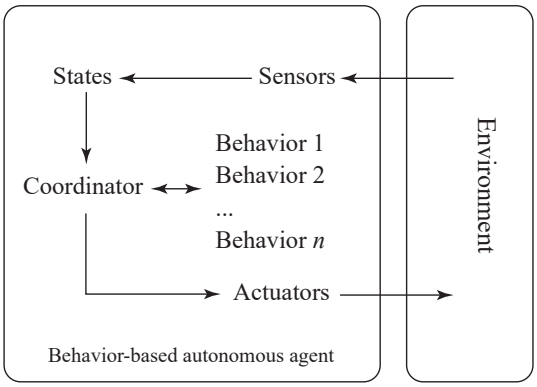


Figure 4.3: Behavior-based autonomous agent structure with the *Sense→Act* autonomy structure.

2012). Still, these behavior-based approaches provide a direct way of partitioning data collection into specific routines that reflect a desired sampling reaction. Feature tracking (Petillo et al., 2010), obstacle avoidance (Fossum et al., 2016), and rendezvous/directed homing control (Bellingham and Leonard, 1994) are all examples of this type of subsumption-based architecture. More complex behaviors can, however, be built into the system to include more complicated and predictive behavior (see Petillo (2015)), in which case the system can operate as a hybrid.

## 4.3 Information-Theoretic Architectures

The structure of information-theoretic architectures may appear, at first sight, similar to that of subsumption systems (see Fig. 4.4). However, the architectures differ considerably in their abilities and methodology for formulating sampling behavior and control. Information-theoretic architectures typically feature a more involved model of the environment, as well as extended learning, planning, and decision making capabilities; this makes the system more *deliberative*[5]. Also, as there is no predefined and direct mapping between sensor values and actions, such that finding a suitable sampling action (location) needs to be computed – rather than specified – using formalized rules, metrics, and algorithms. This process sets the architecture apart and results in a *Sense→Plan→Act* control methodology, where the inclusion of a "Plan" stage signify this. The *in-situ* performance of this additional deliberation, has been criticized as being too slow for certain dynamic and fast changing environments. However, algorithmic and implementational advances have made this less of an issue (Rajan et al., 2012), but is still something that should be noted, especially for moving AUVs doing continuous observations. The upside is that the system can be programmed to handle a wider range of unforeseen events and

[5]Deliberative systems (agents) articulate more informed control and conscious behavior by searching through a space of alternative actions, maintains a detailed internal state, and tries to predict the effects of actions on future states.

opportunities that may arise during execution by re-planning accordingly.

To plan and evaluate optimal actions, there need to exist an updated description of the environment; the more accurate description is the better. The models associated with information-theoretic architectures are usually referred to as *world models*, and are more elaborate than the single state representation used in typical subsumption systems. This model is usually a type of map representation that incorporates both prior and posterior information about the environment (including unobserved locations). The common form is typically a gridded map of value-location pairs (e.g. a discretized 2D GP model). However, depending on the application and implementation choice, different declarative representations can be used to serve varying functional requirements (science optimization, path planning, behavior coordination, collision avoidance, cooperative planning, etc.). Typical representations are in this regard: potential fields, statistical and parametric models; roadmaps, and different classes of value-based grids. The world model can also be extended to include co-variates and other relevant mechanisms relevant for the specific domain (e.g. risk and fault diagnosis). The model representation acts as a workspace across the different components of an autonomous agent (e.g. different sub-routines can access the map structure for waypoint inference). Using a predictive model of the environment can be useful when trying to understand and prioritize sampling resources, making the agent more attuned to the environment. As the model typically also includes information at unobserved locations, the impact of sampling can be evaluated against metrics that include this information, such as the global reduction of uncertainty. The formulation or refinement of a sampling plan (the interaction between planner, algorithms, and objective functions shown in Fig. 4.4) will be described in more detail in the following section.

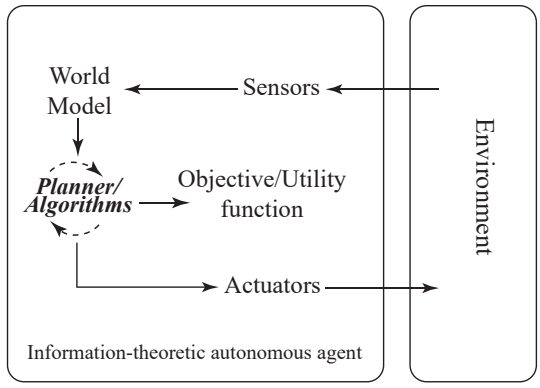


Figure 4.4: Information-theoretic autonomous agent architecture, following the *Sense→Plan→Act* autonomy structure.

## 4.4 Information-Theoretic Adaptive Sampling

For information-theoretic approaches, formulation or refinement of a sampling plan can be an complex task due to the number of parameters and alternatives involved. Additionally, a compromise must usually also be found between a set of objectives and constraints related to the overarching research question, while simultaneously reaching agreement with the entities already integrated into the plan. Complications such as resource limitations (e.g. balance between sensor coverage and battery life), competing objectives, off-nominal conditions, fault tolerance, and synchronization have to be settled according to a quantitative understanding built into the agent's planning system. Even so, the cyclic process of formulating an adaptive sampling plan, shown in Fig. 4.5, is fairly general and builds on the initial Fig. 1.1, where continuous assimilation of data allows information to be retained across time and decisions. In this regard, we will now address the major influences in information-theoretic adaptive sampling, using the steps shown in Fig. 4.5 as reference.

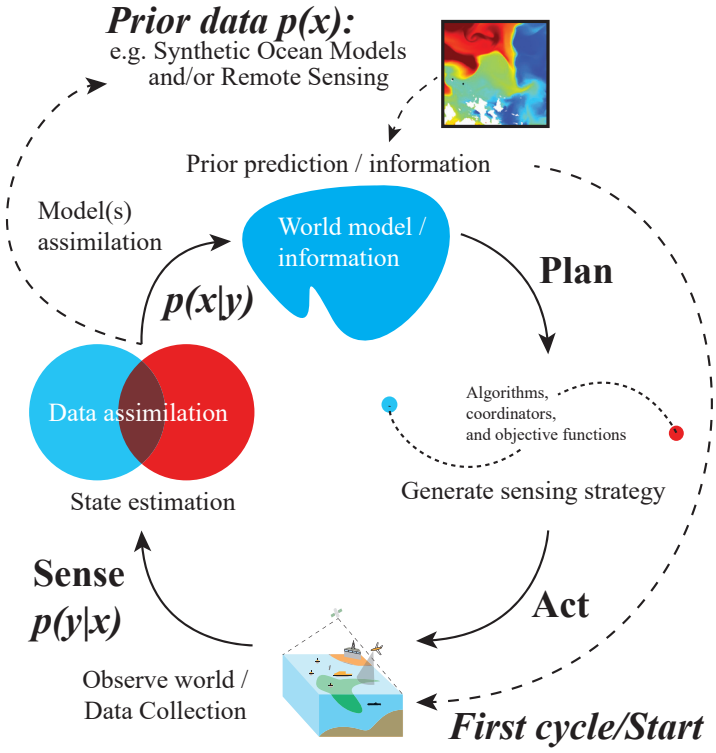


Figure 4.5: The data-driven/adaptive sampling cycle, where continuous assimilation and refinement of a sampling strategy follows the *Sense*→*Plan*→*Act* control methodology.

We start a cycle with a predefined data collection plan based on the *prior prediction*, $p(\boldsymbol{x})$ where $\boldsymbol{x}$ is a distinction of interest (e.g. temperature, salinity, chlorophyll, etc.). Starting without any predefined plan is of course possible, but is not often practical, leaving all planning to the agent. Typically a set of waypoints is selected and used as "lead

in" for the agent, chosen as a "best guess" optimal launch route. Despite being based on scientific expertise, the degree of discrepancy will likely be large for early points of comparison with the prior prediction. The risk of confusion and long-term sub-optimal performance is therefore high in early phases of deployment. This is typical when the effective number of observations are small, since the bias is much larger than the variance in the beginning, dominating the mean square error.

Retaining an advantageous strategy for information recovery requires favorable reconciliation of recovered data with the world model, continuously adding and refining current knowledge. Consequently, assimilation (conditioning) must run in parallel, fusing information in such a way that an updated representation of the environment is maintained. This can be performed in numerous ways, but usually consists of a statistical update procedure, often based on Bayesian approaches (the conditional $p(\boldsymbol{x}, |\boldsymbol{y})$ given in Eq. (3.6). The generated posterior belief is then used as the current world model, yielding an updated and, hopefully, improved conception of the environmental state/world evolution. In the strictest sense of the word, knowledge can only be about the past, yet the environment can in certain situations change faster than the agent can plan (the plan becoming obsolete or degraded too fast). However, given that the process dynamics are resolvable from the standpoint of the platform limitations (depth rating, speed, etc.), information is accumulated faster than it is lost. Once a new world state is available, the strategy for information recovery can be re-evaluated and potentially refined, enabling adaptation to observed changes during mission deployment – the last step in Fig. 4.5, "Generate sensing strategy". In this step decisions are made on where and when to sample. Different criteria can be used to evaluate the best action forward, and we will in the next sections see how this can be done from an information-theoretic perspective.

### 4.4.1 Objective Functions and Different Optimization Criteria

Information-theoretic sampling utilizes models and informative metrics to find and differentiate between different sampling locations. Generating a sampling plan usually relies on optimization of a *utility function*, which is an objective function that computes a score, either maximizing or minimizing a form of metric. This metric is often a value function based on the uncertainty reduction (e.g. variance or mutual information), feature-based context (gradients, concentrations, etc.), or a combination of both. The problem of choosing the path that maximizes this utility within an underlying field of interest, is often described as *informative path planning* (IPP). IPP stands in contrast to *path planning*, which seeks to optimize criteria such as distance. For path planning, typical algorithms such as *Dijkstra's* algorithm can be applied due to the modularity property of the objective function that usually builds on Euclidean distance. IPP problems and many environmental sensing problems on the other hand are usually submodular. Submodularity arises from the fact that spatial data are correlated, which connects back to spatial statistics and correlated data. Observations made close to each other in space (or time) are likely to share mutual information. It is therefore necessary to gather additional information to achieve the same knowledge as if they were uncorrelated, a diminishing return effect that needs to be included in the objective function. As previously mentioned, this submodularity property can be systematically exploited in order to efficiently obtain provably near-optimal

solutions to sensing problems (see Nemhauser et al. (1978) and Krause (2008)). IPP can formally be defined as:

$$P^* = \text{argmax}_{P \in \Omega_e} \{\mathcal{O}(\mathcal{S}(P))\}, \tag{4.1}$$

where $P$ is a path from the set of possible paths $\Omega_e$ within the environment, the function $\mathcal{S}(\cdot)$ provides the finite set of sampling locations given $P$, and $\mathcal{O}(\cdot)$ is an objective function. There will also be an associated cost function $\mathcal{C}(P) \leq B$, which allows constraints such as energy, time, or other resources to be included into the problem.

For information-theoretic agents the objective function, $\mathcal{O}(\cdot)$ in Eq. (4.1) is of fundamental importance for determining which observations should be prioritized, operating as a sensing quality function. Following the introduction given in Section 4.1.3, optimization criteria can be purely location based (e.g. sensor placement), aiming to reduce uncertainty, or be combined with feature-based (data-driven) criteria. A few aspects concerning the objective functions will be discussed here, from the standpoint of GPs. We re-use the notation from GPs and Section 3.1, to formally quantify uncertainty in this context.

Consider therefore a real-valued stochastic process $\{x(\boldsymbol{s}), \boldsymbol{s} \in \mathcal{V}\}$, where $\mathcal{V}$ is an index set where $\mathcal{V} \subset \mathbb{R}^2$, describing the subset of locations $\boldsymbol{s}$ where we can sample. Assume further that for this finite choice of locations that the random vector $\boldsymbol{x} = \big[x(\boldsymbol{s}_1), \ldots, x(\boldsymbol{s}_n)\big]$ has a multivariate normal probability density function defining the GP. For a subset $\mathcal{A} \subseteq \mathcal{V}$, let $\boldsymbol{x}_\mathcal{A}$ denote a set of random variables associated with some candidate locations given by $\mathcal{A}$. These candidate locations can be seen in relation to the alternative paths $P^*$, discussed in Eq. (4.1). To evaluate the informative value of the candidate locations, it is necessary to estimate a conditional distribution $p(\boldsymbol{x}(\boldsymbol{s})|\boldsymbol{x}_\mathcal{A})$ over the unobserved locations $\boldsymbol{s} \in \mathcal{V}/\mathcal{A}$, which is given in Eq. (3.10) and (3.11).

**Uncertainty-driven Criteria**

For many sensing applications, the goal is to reduce the uncertainty in unobserved variables. Using the notation above, it is now possible to evaluate this in terms of different criteria such as *predictive variance* and *mutual information* using the GP formulation. In this case, both criteria rely on $\boldsymbol{\Sigma}$, and selection depends on how one wishes to express uncertainty. Here, $\mathcal{A}$ should be considered the subset of potential sampling locations compatible with logistic constraints such as the number of platforms, available time, depth rating, etc.

First used by Caselton and Zidek (1984) for spatial prediction, ***mutual information*** is a measure of the shared information between two variables, quantifying the information gain about one random variable through observing the other. This criterion, using the determinant, is also known under the name of Bayesian *D-optimality* (Chaloner and Verdinelli, 1995). A criterion using mutual information can be expressed in closed form solution for a GP as

$$\begin{aligned} \mathcal{O}_{MI}(\mathcal{A}) &= I(\boldsymbol{x}_\mathcal{A}; \boldsymbol{x}_{\mathcal{V}/\mathcal{A}}), \\ &= H(\boldsymbol{x}_{\mathcal{V}/\mathcal{A}}) - H(\boldsymbol{x}_{\mathcal{V}/\mathcal{A}}|\boldsymbol{x}_\mathcal{A}), \end{aligned} \tag{4.2}$$

where $I(\cdot)$ is the mutual information expressed by the entropy $H(\cdot)$. This can be thought of as trying to reduce the uncertainty at the unobserved locations/variables. The optimal subset of sampling locations, $\mathcal{A}^*$, with maximal mutual information is then

$$\mathcal{A}^*_{MI} = \underset{\mathcal{A}\subseteq\mathcal{V}}{\operatorname{argmax}} \ \frac{1}{2}\log((2\pi e)^n\,(\det \boldsymbol{\Sigma}_{\mathcal{V}/\mathcal{A}} - \det \boldsymbol{\Sigma}_{\mathcal{V}/\mathcal{A}|\mathcal{A}})), \tag{4.3}$$

where $\boldsymbol{\Sigma}_{\mathcal{V}/\mathcal{A}|\mathcal{A}}$ can be inferred from Eq. (3.11). Similarly, ***variance*** can be used to quantify the reduction of uncertainty by measuring the reduction of prior vs. posterior variance. If $\boldsymbol{\Sigma}_0$ denotes the prior covariance matrix for a set of locations $\boldsymbol{s} \in \mathcal{V}$ is defined in Eq. (3.3), while the posterior is given as $\boldsymbol{\Sigma}_{s|\mathcal{A}}$ defined in Eq. (3.11). From this we can express a variance criterion as

$$\mathcal{O}_V(\mathcal{A}) = \text{Var}(\boldsymbol{x}(\boldsymbol{s})) - \text{Var}(\boldsymbol{x}(\boldsymbol{s}|\mathcal{A})). \tag{4.4}$$

The optimal subset of sampling locations $\mathcal{A}^*$, that maximizes reduction of uncertainty can be expressed as

$$\mathcal{A}^*_V = \underset{\mathcal{A}\subseteq\mathcal{V}}{\operatorname{argmax}} \ \frac{1}{N}(\text{tr}(\boldsymbol{\Sigma}_0) - \text{tr}(\boldsymbol{\Sigma}_{s|\mathcal{A}})), \tag{4.5}$$

where $\text{tr}(\cdot)$ is the trace of a matrix, and $N$ is the total number of possible measurement locations (a constant number). This criterion, using the trace, is also known under the name of Bayesian *A-optimality* (Chaloner and Verdinelli, 1995).

Given Eq. (4.3) and (4.5), an optimal design can in this context, with respect to potential sampling locations $\mathcal{A}$, be generically defined by

$$\mathcal{A}^* = \underset{\mathcal{A}\subseteq\mathcal{V}}{\operatorname{argmax}} \ \{\phi_{\mathcal{A}}(\boldsymbol{\Sigma})\}, \tag{4.6}$$

where $\phi_{\mathcal{A}}$ is a scalar function. Note that the difference in $\phi$ between entropy using the determinant (D-optimality) of $\boldsymbol{\Sigma}$, and variance using the trace (A-optimality), is that the trace only considers elements along the diagonal. Hence, the trace covers only the overall level of uncertainty and does not take into account the correlation between variables. Taking the determinant measures a different type of variability, sometimes referred to as generalized variance (Sen Gupta, 2004). In general, a design based on a measure of variance results in more globally uniform sampling strategies, while designs based on mutual information lump observations in areas of high uncertainties (Alvarez and Mourre, 2012). These tendencies, of course, depend on the particular spatio-temporal correlation and variability structure of the region under consideration. In addition to A- and D-optimal designs, there are several other optimality criteria (see Chaloner and Verdinelli (1995)) that can lead to different sampling strategies. For example, using the eigenvectors of $\boldsymbol{\Sigma}$, the uncertainty can be studied through the eigenvalues corresponding to coherent spatial patterns of variability, known as *E-optimality*. Thus, an E-optimal design will seek to minimize the variance of the worst estimated spatial pattern (dominant error modes) of this variability. There is no clear criterion that performs better for sensing applications in the marine environment (Alvarez and Mourre, 2012), but both A- and D-optimality are commonly used. More about spatial models and different optimality criteria can be found in Müller (2007).

### Data-Driven Criteria

Both Eq. (4.3) and (4.5) do not depend on the actual value of the observations, only their location through $\mathbf{\Sigma}$. The optimal strategy is therefore deterministic and can be calculated *a priori*. As previously discussed, this is useful in applications where one wishes to focus on optimizing sensor placement, e.g. placing a network of temperature sensors in an office building. However, in uncertain and dynamic domains such as the ocean where prior information is limited, it makes more sense to develop criteria that also utilize information from observed values. An example of this is given below, showing a ***data-driven criterion*** (V+G) where the objective function is formulated as a balance between gradient intensity (data-driven) and reduction of variance (uncertainty)

$$\mathcal{O}_{V+G}(\mathcal{A}) = (\text{Var}(\boldsymbol{x}(\boldsymbol{s})) - \text{Var}(\boldsymbol{x}(\boldsymbol{s}|\mathcal{A}))) + \nabla(\boldsymbol{x}(\mathcal{A})). \tag{4.7}$$

The formulation defines a set of sampling locations $\mathcal{A}$ that both reduces the posterior variance and prioritizes paths indicative of having large gradients over the potential sampling locations. Sampling strong gradients can be useful as they arise from the number of ocean processes. Thermal gradients are one example where large changes in temperature can be associated with frontal zones, upwelling, currents, etc. The optimal subset of sampling locations $\mathcal{A}^*$, for this objective function can be formulated as

$$\mathcal{A}^*_{V+G} = \underset{\mathcal{A}\subseteq\mathcal{V}}{\text{argmax}}\{\theta_1 \frac{1}{N}(\text{tr}(\mathbf{\Sigma}) - \text{tr}(\mathbf{\Sigma}_{s|\mathcal{A}})) + \theta_2 \frac{1}{N}\nabla(\boldsymbol{\mu}(\mathcal{A}))\}, \tag{4.8}$$

where $\theta$ is a weighting parameter balancing the influence of each term, $\nabla$ denotes the gradient, and $\boldsymbol{\mu}(\mathcal{A})$ is the expected mean evaluated at locations $\mathcal{A}$. In a sequential setting, a conditional plan (a selection policy) could be developed that selects one location after another, utilizing the metric in Eq. (4.8). As uncertainty and gradient utilities may prefer different locations, a balance between exploration vs. exploitation must be found (ref. the weighting parameter $\theta$); this balance may be constant or change during the course of the sampling activity. As initial assumptions about gradients may be highly uncertain in the beginning of the survey, it may be more advantageous to favor the reduction of variance. However, as the consumption and assimilation of observations proceed, there is a gradual reduction of uncertainty. Reducing all uncertainty might not be a beneficial strategy in the long run, and advantageous behavior can instead be inferred on the basis of an approximately known environment (driven by data). These strategies may be myopic or non-myopic, looking several steps ahead and thus considering paths rather than points. Yet, planning far ahead is not always better, as large uncertainties degrade the quality of long term plans; this a problem which often is encountered in the ocean environment.

As previously discussed, it is also useful to consider limitations such as time or energy. This can be encoded as a ***cost function*** $\mathcal{C}(\mathcal{A}) \leq B$, such that the optimal subset reads

$$\mathcal{A}^* = \underset{\mathcal{A}\subseteq\mathcal{V}}{\text{argmax}}\ \{\phi_{\mathcal{A}}(\mathbf{\Sigma}, \boldsymbol{\mu})\} \quad s.t. \quad \mathcal{C}(\mathcal{A}) \leq\ B. \tag{4.9}$$

To better understand the practical use of these criteria, the next section presents examples using both uncertainty- and data-driven criteria.

## 4.5 Examples of Autonomous Agents

The difference between the ***Sense→Plan→Act*** and ***Sense→Act*** control methodology, makes a clear distinction between information-theoretic and behavior-based agents. Still, both architectures are capable of performing adaptive sampling. This section presents two examples of this through: i) a simulated survey using an information-theoretic agent, and ii) a concrete, real-world case study using a behavior-based autonomous agent.

### 4.5.1 Information-Theoretic agent

A brief example of an information-theoretic agent is given here using both uncertainty-(variance) and data-driven criteria (variance and gradient) from Section 4.4.1. In a simulated setup, the goal is to map an area with a patchy temperature distribution using a GP model. The approach is based on discretization of a GP to a waypoint graph, and assigning potential measurement locations along the graph edges for route evaluation. The goal is to sequentially select the node that maximizes the score of the objective function given your position in the graph, using the different criteria and horizons.

**Formulating a GP Model**

The model framework from Section 3.1 is used to formulate a GP model of a temperature distribution over locations $\boldsymbol{s}_i$. The temperature is modeled to increase squared radially (this to attain a more box like distribution, as seen in Fig. 4.6a), originating from a source $\boldsymbol{s}_{source}$. The covariance is isotropic and depends only on distance, given as

$$\mu(\boldsymbol{s}_i) = \beta_{t,0} + \beta_{t,1}||\boldsymbol{s}_i - \boldsymbol{s}_{source}||^2, \tag{4.10}$$

$$\text{cov}(\boldsymbol{s}_i, \boldsymbol{s}_j) = \sigma^2 e^{(-\gamma\,||\boldsymbol{s}_i - \boldsymbol{s}_j||)}, \tag{4.11}$$

where $\beta_{t,0}, \beta_{t,1} = [3.0, 0.007]$, specifies a temperature covariate parameter, and the remaining parameters are defined in Section 3.2.1, Eq. (3.7). The GP is now fully determined by collecting the mean $\boldsymbol{\mu} = [\mu(\boldsymbol{s}_1), ..., \mu(\boldsymbol{s}_n)]$ and covariance $\Sigma_{ij} = \text{cov}(\boldsymbol{s}_i, \boldsymbol{s}_j)$ following Eq. (3.3). Discretization into a $50 \times 50$ grid yields the prior model that can be seen in Fig. 4.6a. The true underlying temperature distribution is a realization of the GP model, seeded by Gaussian noise, and shown in Fig. 4.6b.

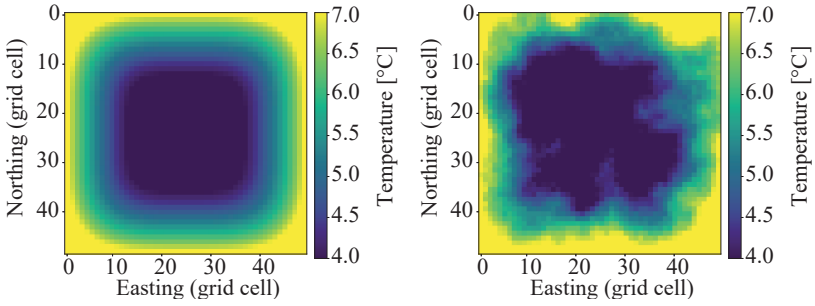


(a) Prior temperature estimate. (b) True temperature field.

Figure 4.6: (4.6a) The prior GP mean. (4.6b) The true underlying temperature.

**Waypoint Graph and Objective Functions**
The available locations are given in Fig. 4.7, showing a waypoint graph $G = (V, E, D)$. Each cell consists of a four corner node/vertex (red dot) that can be visited, with arrows illustrating the possible sampling routes (edges E) that can be selected.

A large number of routes can be extracted from this graph, as each node (except for the corner nodes) connects to eight neighboring nodes; this makes up the first column of choices in Fig. 4.2. Using a brute force (evaluating all routes) 1-step horizon, the routes to evaluate at each graph node equal the number of nodes (eight); for a 2-step horizon this increases to 64, and so on. Some routes can, however, be pruned out, e.g. going back and fourth. Evaluating which route to take is done using the objective functions $\mathcal{O}_V$ or $\mathcal{O}_{V+G}$ given below. Eq. (4.12) is not dependent on data, as it only considers reduction in the (posterior) error covariance.

$$\mathcal{O}_V = \frac{1}{N}(\text{tr}(\boldsymbol{\Sigma}) - \text{tr}(\boldsymbol{\Sigma}_{s|\mathcal{A}})), \tag{4.12}$$

In Eq. (4.13), a gradient term is added to the objective function. This enables the agent to evaluate in which direction the temperature changes the most and use this in planning.

$$\mathcal{O}_{V+G} = \frac{1}{N}(\theta_1 \ (\text{tr}(\boldsymbol{\Sigma}) - \text{tr}(\boldsymbol{\Sigma}_{s|\mathcal{A}})) - \theta_2 \ \nabla(\boldsymbol{\mu}_{s|\mathcal{A}})). \tag{4.13}$$

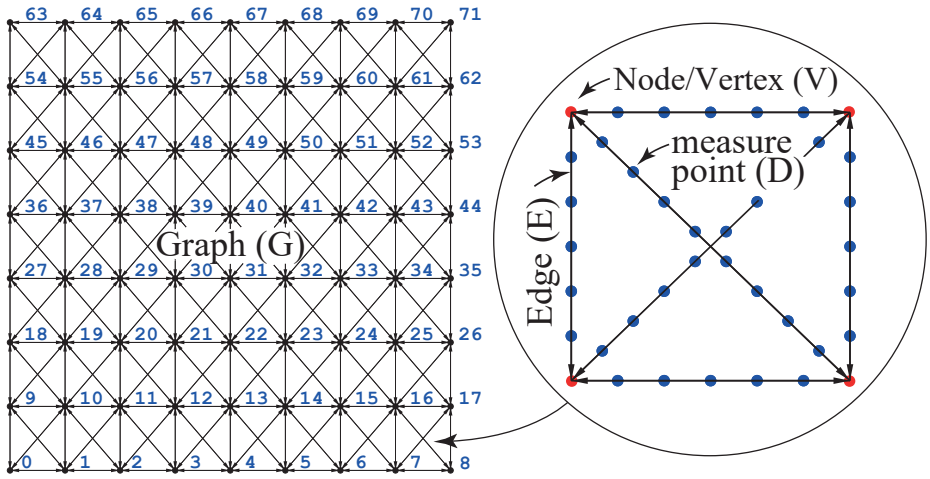


Figure 4.7: The different paths for an AUV are encapsulated in a waypoint graph $G = (V, E, D)$ with four corner nodes/vertexes $v \in V$, $v = \{0, 1, 2, 3\}$, edges between the nodes given as $e \in E$, and measurement points $\boldsymbol{x}(\boldsymbol{s}_i) \in D$.

**Simulation Setup and Performance Metrics**
To simulate a survey, the agent is given 20 nodes to visit in the graph $G$ using either Eq. (4.12) or (4.13), with different planning horizons. In a oceanographical context the simulated temperature in Fig. 4.6b, could represent a patch of temperature which we

wish to sample. To evaluate performance between the utilities, one can use either RMSE or $\boldsymbol{R}^2$, which is a statistic that computes the percentage of the prior variance captured by observations as: $\boldsymbol{R}^2 = 100 * (1 - (\boldsymbol{\Sigma}_{posterior}/\boldsymbol{\Sigma}_{initial}))$. Performance could also be set according to the behavior itself, which in this case could be a desire from the scientist to follow the edges of the patch. The edges are of interest, as this is where the patch interaction with the surroundings occur, which is where biological activity in a real scenario would be high (e.g. fronts).

**Results and Discussion**

Fig. 4.8 show the results from the simulated survey, using both variance (V), as well as variance and gradient (V+G). Both functions are evaluated using a 1-step horizon (greedy). The prior uncertainty is initially evenly distributed (all yellow background), but as the agent progresses through the graph, the uncertainty is lowered around the agent route (in red color). The V-approach (Fig. 4.8a) only depends on $\boldsymbol{\Sigma}$ and seeks to minimize the (posterior) error covariance. The resulting route ends up following a spiraling path that first trends toward the middle. The trend toward the middle leads to sub-optimal performance, as one later has to cross over previously covered regions where posterior covariance is already low; this can be thought of as a "myopic-trap". Using a V+G-approach (Fig. 4.8b) the agent becomes dependent on data and quickly changes behavior. As gradients are high along the edges of the patch, the agent tracks along these and avoids getting drawn into the middle, as well as crossing over previously mapped areas.

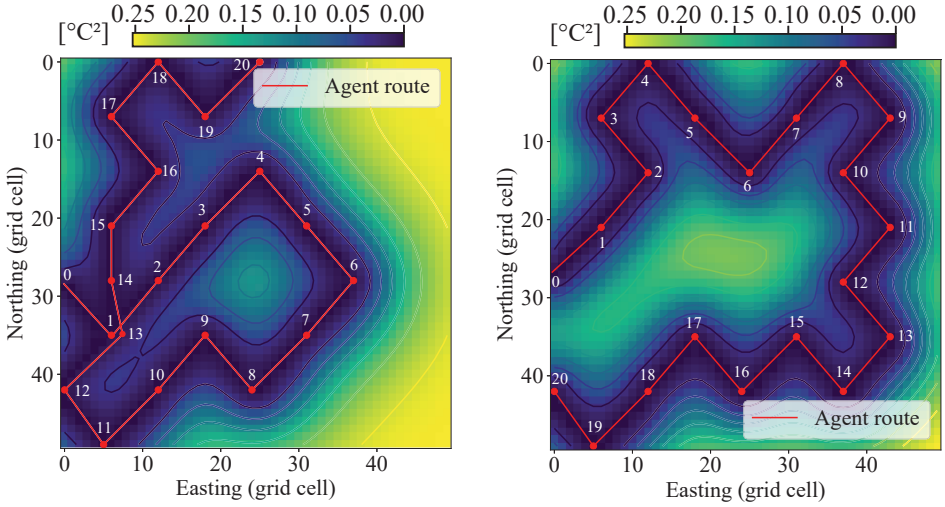


(a) Variance based utility (greedy).

(b) Data-driven (V+G) based utility (greedy).

Figure 4.8: The agent routes using variance- and variance+gradient objective functions. The posterior error covariance is shown in the background, with the agent route superimposed in red. Note that the variance based utility initially seeks into the middle, leading to a path cross-over later in the route.

Finding a more optimal strategy that initially avoids the "myopic-trap" temptation

of visiting the middle point, one can try to increase the planning horizon. Increasing the planning horizon to 2-steps, the V-approach performs slightly better (Fig. 4.9a), but still seeks into the middle. Increasing the planning horizon to 3-steps, evaluating a maximum 512 routes at each planning instance, does not improve the result (Fig. 4.9b). Why do we not get an increase in performance? Increasing the horizon of the brute force planner[6] does not always improve performance. This is an important and counterintuitive result. Even if a route appears better, looking further ahead, the route can turn out to be worse over an even longer horizon. For the case shown here, the 2- and 3-step horizon is not long enough to detect that visiting the middle, leads to a sub-optimal strategy. For this to be detected, the horizon would need to be something around 11-steps, where middle-seeking paths could be compared to paths that encircle the middle instead. Furthermore, the only way to find the globally optimal route, using a brute force planner such as the one considered here, is to use a full horizon (Binney et al., 2013); which in this case would be a 71-node horizon, requiring an impractical amount of computation time.

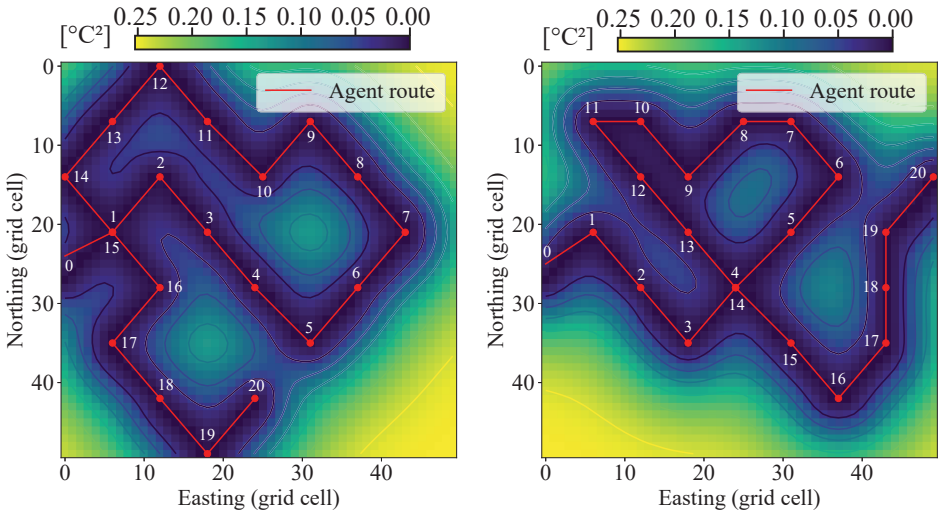


(a) Variance based utility (2-step horizon).

(b) Variance based utility (3-step horizon).

Figure 4.9: The effect of increasing planning horizon (2- and 3-step) for the V-approach. A longer planning horizon does not always improve the result.

The results are summarized in Table 4.1, where deliberation (computation) time, RMSE, $\boldsymbol{R}^2$, and behavior is presented. As shown in Fig. 4.8 and 4.9, different solutions are obtained by including data-driven criterion or extending planning horizon. For example, low RMSE is achieved using a 2-step V-approach, while the strategy that yields the route with lowest explained variance ($\boldsymbol{R}^2$) is 1-step V+G approach. This latter results is attributed to the gradient influence, pulling the agent away from the "myopic-trap" explained earlier, yet the RMSE is not better than the V-approach. The counterintuitive effect

[6] A brute force planner considers all options, one by one.

of increasing the planning horizon is also evident in the results for strategy 3 and 5, where performance is diminished. One could also use behavior for evaluating the performance of the different strategies, as scientists may want edge tracking rather than optimal coverage. In this example, strategy 4 is a good choice, featuring both edge tracking and low $\boldsymbol{R}^2$.

Table 4.1: Simulation results using different informative sampling strategies.

| **Strategy** | **Delib. time** | **RMSE** | **R$^2$** | **Behavior** |
|---|---|---|---|---|
| 1) Variance (greedy) | 40 sec | 0.36 | 62% | Inward spiral |
| 2) Variance (2-step) | 3 min | 0.32 | 67% | Inward spiral |
| 3) Variance (3-step) | 10 min | 0.38 | 65% | Inward spiral |
| 4) Variance + Gradient (greedy) | 40 sec | 0.36 | 72% | Tracks gradient |
| 5) Variance + Gradient (2-step) | 3 min | 0.35 | 70% | Tracks gradient |

### 4.5.2 Subsumption Agent

This last example cover tracking of fronts in an Arctic environment using a behavior-based agent architecture. The results are from a real deployment conducted in Arctic Ocean September 2018 (see overview of field deployments in Table A.1). Contrary to an information-theoretic approach, the agent illustrated here uses only a few states to perform adaptive sampling of an evolving front feature (similar to Pinto et al. (2018)). Oceanographic features, such as fronts, are both episodic and highly dynamic, posing a challenge for traditional pre-planned sampling surveys. As their location is constantly moving, prior estimates are usually too poorly resolved and uncertain for deterministic planning. An adaptive sampling strategy is therefore used to autonomously follow this feature as it moves. A simplified state space graph is shown to illustrate the interaction between the different behaviors built into the architecture.

**Autonomous Tracking of an Arctic Front With an AUV**
Oceanic fronts are dynamic regions forming a boundary where different water masses meet and interact. Large changes in water properties (such as temperature, salinity, oxygen concentration, etc.) result in elevated horizontal gradients that can be used to detect their presence. These regions are of interest to scientists as high biological activity is coupled with strong physical interaction. Hence, mapping the frontal processes are of vital importance for understanding the ecosystem dynamics.

A simplified illustration of the behavior-based architecture is shown in Fig. 4.10. The agent switches between the states, “Search” and “Track,” where the agent is either exploring to find the front (Search), constantly checking whether it has crossed a thermal shift (the green box [front detected?]), or if the front is detected the agent plans a zig-zag maneuver to cross the front, and enters tracking mode (Track). The thermal shift (the trigger for proceeding to the next state) is a predefined temperature hysteresis (threshold with a defined “dead-zone”), set based on the expected gradient conditions at the front.

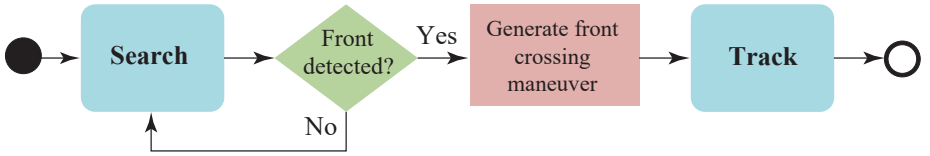


Figure 4.10: Example of a rudimentary behavior-based state machine used to track frontal processes. Two behaviors, "Search" and "Track" are shown, with sensor input (front detected) and coordination and control (generate front crossing maneuver).

The goal of the adaptive agent was to track back and forth across the front edge to increase the sampling resolution of the frontal process and document the different physical and ecosystem dynamics across the feature. In experiments conducted at 82°North (Norgren et al., 2018), north to Svalbard in the Arctic Ocean, an extended version of the agent was used to autonomously detect and track a thermal front, close to the ice edge. The front was characterized by cooled Arctic and warmer Atlantic water creating a temperature difference of almost 5°C. The detection trigger for detection was centered around 1.5°C, with a hysteresis of 0.5°C. The resulting behavior is shown in Fig. 4.11 and displays the AUV survey path crossing and tracking the thermal front a number of times, as intended.

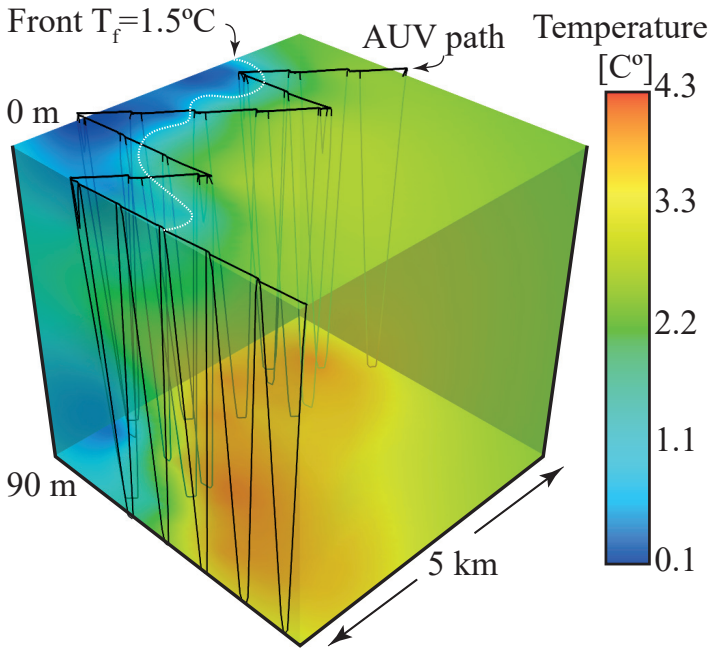


Figure 4.11: An interpolated 3D volume using the CTD measurements from the AUV. Note the AUV path crosses the front a number of times, recording the physical and ecosystem changes across the feature.

# Chapter 5

# Operational Aspects in Adaptive Sampling

In a chaotic and complex environment such as the ocean, the challenge of robotic sampling is as much practical as theoretic. The method and design depend upon a range of different design and risk considerations, which vary depending on the environment type (e.g. coastal waters, fjords, or high latitude locations such as the Arctic). The researcher has to account for this in the development methodology, finding a balance between practice, practical knowledge, and applicable theory. This chapter provides a discussion about marine robotic platforms and practical aspects related to adaptive sampling, focusing on operational issues and deployment with AUVs in the upper water column. The field deployments undertaken during this thesis, with associated papers and comments, can be found in Appendix A.

## 5.1 A Methodological Approach to Sampling

Planning and optimizing sampling activity is a process consisting of several steps. An example model of the different levels of abstraction, common to robotic sampling, is shown in Fig. 5.1. Note that proceeding from one step to another may require several iterations up and down in abstraction level (e.g. make a simple test program and see if simulations suggest a change of method). In the proposed model we separate between the *planning phase*, and the *development and execution phase*. The planning phase sets the basic parameters for the decisions that follow, which start with the scientific motivation and capacities available to the scientist. The subsequent aspects relating to domain, platforms, and choice of method all depend on these initial constraints. Once this initial construct is in place, one proceeds into the development and execution phase. This is where the actual work is done, finding and solving specific practical details of the problem; this also includes development of programming code, simulation, and field-testing. Interaction with the real world is vital and several iterations are usually necessary for arriving at a robust and functional system. Much time can be spent in this last phase, constantly discovering and resolving conflicts relating to off-nominal conditions and events. The final stage is the execution step (step 6), where the conclusive experiment takes place. In practice, this step can further be

sub-divided into its own planning and execution step, which considers more near-term decisions relating to operational risks such as weather, deployment and recovery, logistics, etc. The setup in Fig. 5.1 is a generic example, providing an overview of the common steps involved for developing a sensing strategy and deploying it in the ocean. In the following sections, more details will be provided on operational aspects relating to adaptive sampling approaches.


Figure 5.1: An example model of the different levels of abstraction for determining a robotic sampling strategy/approach, from high level science considerations to lower-level method selection, implementation, and testing.

## 5.2 Marine Robotic Platforms

There are three major types of aquatic robots used for sampling the ocean: propelled and glider based autonomous underwater vehicles (AUVs), autonomous surface vehicles (ASVs), and remotely operated vehicles (ROVs) (see Fig. 5.2). ROVs need ship support for navigation, power, and control. In contrast, AUVs and ASVs are capable of operating independently having internal power, data storage, and navigation solutions. AUVs and

ASVs can both have active or passive propulsion. Passive types of transportation include buoyancy (glider AUVs), wavefoil (wave energy ASVs), and currents (drifter ASVs). Passive transportation is naturally less mobile and slower compared to active locomotion, but can sustain longer operations as energy is harvested from the environment.


(a) ROV - Minerva, NTNU.


(b) ASV - Otter, Maritime Robotics.


(c) AUV - Remus 100, Kongsberg Maritime.

(d) AUV (Glider) - Seaglider, Kongsberg Maritime.

Figure 5.2: The major types of marine robotic platforms: remotely operated vehicles (ROVs), autonomous surface vehicles (ASVs), autonomous underwater vehicles (AUVs), and gliders.

Each platform has a particular coverage capacity and resolution, which has to be considered when planning and coordinating oceanographic sampling. As shown in Fig. 2.2, this is driven by the resolution demands arising from the dynamics of the ocean process being studied. This can span several orders of magnitude from sub-centimeter identification of phytoplankton, to mesoscale studies of bloom dynamics. Capturing the process at an adequate resolution is thus often only possible using a range of different sources. The unification of ocean models, remote sensing resources, different robotic elements, and ship-based sampling is therefore essential in order to address this. Before we can address the operational aspect related to adaptive sampling of the water column, a brief introduction to AUVs is given.

### 5.2.1 Autonomous Underwater Vehicles

Applications of robotics to marine science and industry started in the post-World-War II era. The first AUV arrived on the scene in 1957, pioneered by the University of Washington, USA. This was the Self Propelled Underwater Research Vehicle (SPURV), carrying a conductivity-temperature-depth (CTD) for observing internal wave structures, which was of interest to the US Navy. According to Busby's 1987 Undersea Vehicle Directory (Busby Associates, 1987), there were 6 AUVs in operation and 15 under development by

the end of the 1980s. By the end of the 1990s the number had increased dramatically and vehicles such as the MIT Odyssey, WHOI Autonomous Benthic Explorer (ABE) (Yoerger et al., 1991) and Remote Environmental Monitoring Unit(s) (REMUS) (Allen et al., 1997), South Hampton Oceanography Center's Autosub (Griffiths et al., 1999), and Kongsbergs Simrads HUGIN (Kristensen and Vestgard, 1998) were launched in the wake of increasing industrial and scientific activity (Von Alt, 2003). Increased modularity, battery capacity, long range communication, and depth rating have enabled AUVs to explore new reaches of the ocean, and the development of software tools have allowed scientists to program and use the AUVs themselves, making AUVs an essential tool for conducting ocean science.

For the AUVs that are discussed in this work, one can define AUVs as self-contained crafts designed for covering large areas effectively with high maneuverability and built for collecting sensor data in the water column or at the seafloor. Propulsion can be electric- or buoyancy-driven, in which case the AUVs is referred to as a *Glider*; hybrid types of AUVs have also been developed (see Hobson et al. (2012)). AUVs are trimmed to be slightly buoyant so they will float to the surface if a critical error is encountered; others also employ a drop weight, or are capable of hovering. This also means that AUV needs to be in constant motion to stay at a fixed depth. Typical AUV operations are based on running pre-programmed missions consisting of sequential behaviors and waypoints. Waypoints are locations specified in latitude, longitude, and depth that the AUVs are programmed to visit. Most commercial AUVs are therefore paired with a mission planning software that help operators to program the survey using a map. Example of an AUV mission planning software is shown in Fig. 5.3.

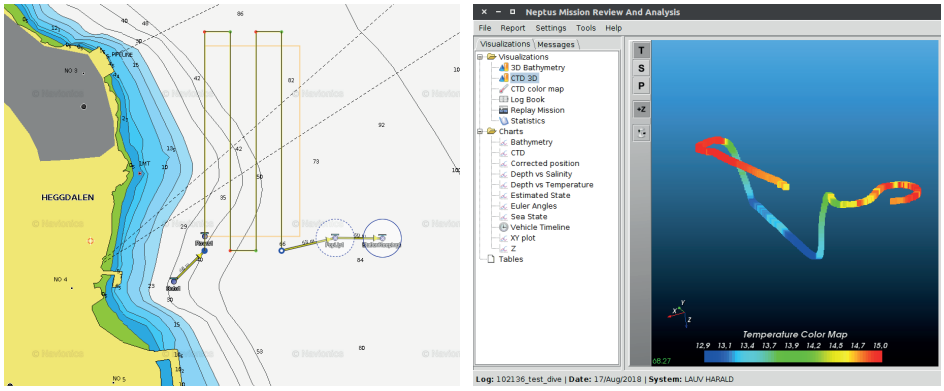


(a) Waypoints in an AUV plan.

(b) Review data and logs from AUV.

Figure 5.3: Examples of the *Neptus* AUV planning software, part of the LSTS-toolchain (Pinto et al., 2013) by the Underwater Systems and Technology Laboratory (LSTS), Univ. of Porto.

Navigation is limited while submerged due to the attenuation of radio waves and, therefore, GNSS signals. Underwater navigation is therefore based on inertial navigation systems, acoustic baseline navigation, or a combination of both. Acoustic positioning

systems such as Long baseline (LBL) or Ultra-short baseline (USBL) (Kinsey et al., 2006) are examples of such systems, where position is determined from acoustically measured metrics, such as range and bearing from either one or several known distinct sources (transponders). LBL usually uses two or more transponders to achieve different accuracies, while USBL operates with only one transducer-transponder pair. LBL and USBL only provide a relative navigation reference dependent on the accuracy of the placement of the transponders. More details are given in Milne (1983).

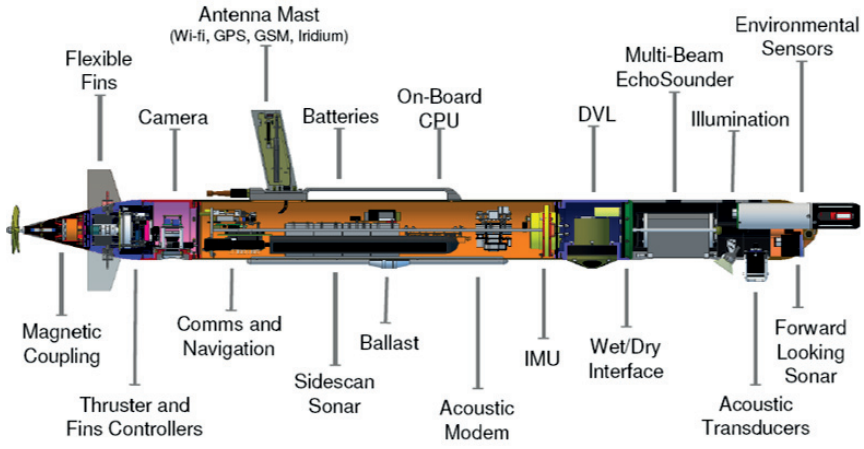


Figure 5.4: Example of an AUV platform (light autonomous underwater vehicle [LAUV]), shown with sensors, payload, and instrument locations. Image courtesy of the Underwater Systems and Technology Laboratory, Univ. of Porto.

Inertial navigation can traditionally be based on either an Attitude Heading Reference System (AHRS), or an Inertial Navigation System (INS); in both cases an Inertial Measurement Unit (IMU) is used. While a AHRS can be based on a low cost IMU, an INS requires a high end IMU (characterized by low gyro bias). Navigation grade IMUs are based on one of two principles: Fiber Optic Gyro (FOG) or Ring Laser Gyro (RLG), both of which are expensive, take a large footprint and have a high power consumption. Micro Electro Mechanical Systems (MEMS) IMUs are much smaller, cheaper, and have lower power consumption at the cost of accuracy. Even with inertial navigation, a build up of position error will be unavoidable without supporting systems. Both systems are therefore usually aided by a Doppler Velocity Logger (DVL) that provides a measurement of the vehicle speed relative to the seafloor or surrounding water mass. This allows the craft to restrict error build-up arising from velocity estimates. The DVL can often also be configured to run as an acoustic Doppler current profiler (i.e. using acoustic backscatter to detect currents). Still, traditional AUV surveys usually contain surfacing events that restores an absolute position from GNSS.

In addition to payload and navigation sensors, AUVs usually carry one or more communication systems on board including: Wi-Fi (2,4 GHz radio), Acoustic modem

(acoustic transducer), satellite communication (e.g. Iridium Short Burst Data (SBD) Transceiver), and mobile (GSM). Due to radio attenuation AUVs communicate using radio at the surface and acoustics while underwater. Wi-Fi and mobile can provide high-throughput communication, while the acoustic modem and satellite usually operate with low data rates. The acoustic modem is also a central part of acoustic navigation in cases where accurate position is necessary (e.g. seafloor mapping or under ice operations). To summarize this brief introduction to AUVs, some common, fundamental limitations of using AUVs are given in Table 5.1, modified from Nornes (2018).

| **Pros:** | **Cons:** |
|---|---|
| + Small environmental footprint, low level of intrusion. | – Operation risks, including loss of data or vehicle. |
| + Capable of reaching difficult, harsh, and remote areas (e.g. under-ice operations). | – Limited weather window for launch and recovery of AUV due to sensitivity to waves and current. |
| + Unique 3D mobility capabilities. | – Limited power supply and energy capacity on-board (does not apply to Gliders). |
| + High survey area coverage per time. | – Limited navigation quality unless supported by a ship or seafloor infrastructure. |
| + Can provide high resolution spatial data for seafloor mapping. | – Need for competence on personnel for launch and recovery, planning of operation, troubleshooting during different operational scenarios. |
| + Ship independence. | |
| + Configurable payload capacity (less capacity compared to ROV). | |
| + Autonomous and adaptive capabilities. | |

Table 5.1: Pros and cons of using AUVs. Modified from Nornes (2018).

In addition to Table 5.1, the reliance on underwater communications, computational capacity, and underwater navigation, are vital limitations which need to be accounted for when developing autonomous sampling capabilities. Keeping track of the asset and its course through acoustic link is not a given in the ocean, as strong thermocline and pycnocline gradients may corrupt the acoustic propagation through water, and currents may force the AUV off route.

## 5.3 Operational Aspects for Using Adaptive Sampling

Deploying non-deterministic sampling agents is, in practice, rarely a straightforward task. The added operational complexity is expressed in terms of increased risks related to autonomy, deployment, recovery, and supervision. For pre-determined operations following a scripted sequence of tasks/waypoints, the operator can easily maintain predictability (e.g. know where the AUV is expected to surface, maximum depth), which

is important for effective risk control. As mission decisions and control are instead managed by complex and deliberative systems on board the robotic platform itself, some of this predictability is lost in favor of autonomy. Experience from simulation and testing is therefore vital for keeping these risks under control.

In the beginning of the operation, a set of waypoints is usually selected and used as "lead in" for the agent, chosen as a "best guess" optimal launch route. Despite being based on scientific expertise, the degree of discrepancy will likely be large for early points of comparison with the predicted world state (see Fig. 4.5). The high level of initial uncertainty can result in sub-optimal performance and undesirable behavior in early phases of deployment. This is typical when the effective number of observations is small, since the bias is much larger than the variance in the beginning, dominating the mean square error, thereby motivating the use of bias correcting methods, as presented in **Paper A**.

Another pitfall for adaptive approaches is the potential for the agent to get stuck in a loop or local minima. This is a typical drawback when using greedy or reactive behaviors (Binney et al., 2013). There are a number of ways to deal with this problem, such as using more non-myopic approaches (Zhang and Sukhatme, 2007; Low et al., 2009; Hoang et al., 2014), complete or entire paths (Binney et al., 2013), or different types of higher order logic added on top of the architecture that can detect and avert such situations (see Fig. 4.1).

The computational nature associated with optimizing sampling (as discussed in Section 4.1) also adds challenges related to available computational resources. In general, this only applies to information-theoretic adaptive sampling, where more deliberative approaches (***Sense***→***Plan***→***Act***) are used. This problem includes path planning where planning and re-planning often produce large scale optimization problems, whose solutions may take considerable time to compute, affecting the reaction time of the autonomous agent. Traditional subsumption approaches (***Sense***→***Act***) do not spend time planning, as there is direct mapping between action and observation, thus alleviating both problems.

Introduction of adaptive and non-deterministic surveys can, due to their adaptive programming (e.g. surveying around a drifter), potentially result in highly irregular and erratic survey patterns which can be hard to interpret and post-process. A general question to ask in this regard is: can adaptive strategies "outperform" regular lawnmower or single transect surveys? The practical answer to this question is far from straightforward, and closing the gap between simulation/theory and real world experiments is always challenging (see Graham et al. (2013) and Frolov et al. (2014)). (Out)performance can in this context typically be measured with RMSE, detection rate, or simply coverage duration. As previously mentioned, in cases where uniform sampling of the field is possible (complete coverage) and the environmental field is smoothly varying, non-adaptive strategies can work well (Singh et al., 2006). Additionally, some applications or conditions are irreconcilable with non-deterministic behavior (e.g. fixed historical survey transect and highly trafficked port monitoring scenarios). However, in most cases, faced with limited sampling resources, unmodeled uncertainty, or specific features of interest, adaptive sampling can exploit obser-

vational data towards mapping the environmental field with improved performance (Low, 2009). Additionally, adaptive sampling offers opportunistic behavior, which, in terms of feature-tracking, is absolutely necessary. Thus for most practitioners and ocean observation scenarios, adaptive sampling is still a better and more preferable approach if resources and expertise are available.

# Chapter 6

# Summary of Thesis

THE key question through the course of this work has been *when and where to sample*? Addressing this question, from the perspective of robotic sampling, involves formulating and optimizing data collection using data-driven agents. This dissertation has discussed several methods for adaptive sampling for marine robots, including information-theoretic and behavior-based agents. The approaches presented in this thesis have mainly focused on science applications in the coastal ocean with AUVs. Practical implementation, and field testing, where reconciliation of convoluted science objectives, changing weather, platform deployment and recovery, communications, loss of asset, and the lack of synoptic and absolute measurements has also been discussed. A general comment in this regard is the inevitable gap between synthetic and real world results which, due to off-nominal conditions, reaffirms the need for approaches that builds on field experiments. This point further emphasizes the benefits of synergistic approaches to ocean science using marine data sources such as remote sensing and ocean models in simulation, analysis, planning, and design of potential sampling methods. Real-world sensing applications and campaigns are not concerned about merely extending current sampling abilities of AUVs, but also retrieving the data itself. The aim has therefore been to change the way we retrieve data for the benefit of the scientific context. On this note, a recapitulation of the research topics and methodologies guiding this work is given:

> *This thesis has described the concepts involved in adaptive sampling and formulated methods that can demonstrate data-driven mission execution based on in-situ measurements for sampling applications in the water column. Verification and field testing of the proposed algorithms have been conducted, using AUVs as the main platform.*
>
> This work aimed to explore the following research questions:

**A:** ***Designing data-driven agents for ocean sampling:*** How can observed data be used to plan and retain an advantageous strategy for information recovery in the ocean using a data-driven agent?

**B:** ***Utilization of information-theoretic methods:*** How can we increase the prospect of retrieving the pursued data and make data collection more effective by integrating information-theoretic methods from spatial statistics and machine learning?

**C:** ***Utilization of marine data sources:*** How can marine data sources such as remote sensing and ocean models be used towards informing on board sampling strategies and planning?

## 6.1 Conclusions

The emergence of autonomous systems and adaptive sampling does not displace ships or fixed observation stations, however, the introduction of data-driven sampling can greatly augment and increase the observational efficiency and resolution, helping to ensure scientific success.

This thesis has presented different methods and applications for adaptive sampling in the ocean using marine robots, with a special focus on coastal waters and AUV applications. The principal contributions of this work are related to i) the design and analysis of information-theoretic approaches in upper water column sampling, coupled with intelligent control (*topic A,B*) and ii) testing and validating these methods in the field (*topic A*). This also includes methods for combining adaptive sampling with synoptic data sources such as ocean models and remote sensing (*topic C*).

In addressing *topic A*, a general problem related to optimization of sensing locations is the exponential combinatoric increase in dimensionality that needs to be considered when the set of possible sampling locations grows, and thus an efficient exact solution is generally not available (Krause, 2008). Solving such problems usually involves computationally intensive techniques that do not scale well to larger problems. The problems are therefore often simplified using heuristics (e.g. myopic algorithms, such as the greedy approach in **Paper A** and **E**). Non-myopic approaches attempt to solve more general forms of the problem, and are specifically designed to deal with the problem of high dimensionality. Even if non-myopic approaches try to solve a more complete form of the original problem, for many practical applications, it is hard to find an algorithm that performs significantly better than a greedy approach (Krause and Guestrin, 2009), which can partly be traced back to the submodularity property, which is characteristic for spatial depend data. Additionally, planning over an extended horizon will, in the ocean, also be challenging as current, turbulence, etc. change the environment and introduce uncertainty. This makes it difficult to both attain and maintain synoptic up-to-date knowledge upon which the assumptions underpinning the sampling plan is based. Planning ahead only makes sense if you can trust the quality of the information. This discussion is raised in **Paper A** and describes the choices made for using a greedy approach.

**Paper A** and **C** also describe the synergies to be exploited between data-driven sampling and marine data, which was the focus of *topic C*. **Paper A** introduced a greedy data-driven sampling strategy for the upper water column combining information from ocean models and *in-situ* measurements, focusing sampling to regions indicative of

high uncertainty and thermal gradients. This involved formulation and modification of a GP model using ocean model data from the SINMOD ocean model (Slagstad and McClimans, 2005) to develop a non-stationary correlation kernel and a bias correcting mean. Experimental validation was performed at a highly prolific and complex coastal zone (Frøya) and shown together with other marine data. The field tests showed that the algorithm differentiated between alternative survey strategies, having reasonable agreement with model forecasts. The recorded data indicated correspondence between ocean model and AUV in determining a thermocline shift from influx of Atlantic Water. The sampling strategy was further contextualized with supporting data from remote sensing, buoy, and ship-based measurements, effectuating the aim of *topic C*; both to understand the sampling behavior and how the combined data sources could be used improve ocean models.

Accounting for time variability is a recurring problem related to both modeling and planning, as currents and mixing degrade information over time. Handling this type of uncertainty is therefore an important aspect of addressing both *topic A* and *topic B*, where also finding a balance between exploration and exploitation is vital. In this regard, **Paper B** presents a practical, real-world implementation of a sampling approach for the upper water column. The method is capable of volumetrically estimating distributions of water column parameters using GPs, on which a sampling plan is generated in 3D. The method, demonstrated in a field experiment scenario together with a ship, aimed to map sub-surface phytoplankton distributions. The proposed method presents a solution to bound the associated time-variability effects by splitting the survey into two dedicated phases, as well as an enclosure criterion similar to Das et al. (2012b). Given moderate current conditions, the method provides a sampling strategy capable of attaining quasi-synoptic information about water column features. The results from this work showed that the method could be used on platforms like AUVs to focus sampling to fine-scale features inside a volume, where a clear spatial coherence was apparent in the volumetric estimate throughout the mission.

Addressing *topic C* directly, **Paper C** shifted focus from sampling algorithms to modeling the environment, and proposed a methodology for building compact models from remote sensing SST images in order to increase the predictive capabilities of robotic sampling platforms on large spatio-temporal scales (kilometers, hours). Dictionary learning and Hierarchical clustering was used to derive conditional means from SST images, on which basis the compact model was built. The model results were later compared and verified using historical wind measurements. As both data sources were actual synoptic recordings taken over three years, the statistical characteristics were easier to use compared to using ocean model data (which may contain different biases). Results from a case study using WaveGlider data was used to illustrate how such compact models could be used to aid sampling, by supporting reconstruction of synoptic information based on local *in-situ* measurements. Bayesian modeling was subsequently used together with Monte Carlo approximation to evaluate model prediction error, as well as a discussion on practical planning of sampling campaigns. The paper thus covered a process from data to model, and from model to sampling, touching upon all three the research topics (*topic A, B, and C*).

**Paper D** was the only article focused on ROVs and proposed a subsumption-based autonomous agent architecture for inspection, maintenance, and repair applications. The autonomous agent was aided by sensor readings and computer vision techniques to help switch between the different mission states. Results from field deployment using a full scale integration on board a work class ROV demonstrated that certain aspects of these operations can be automated (addressing *topic A*), and that computer vision techniques can be used for obstacle avoidance.

In addressing *topic A*, **Paper E** used the greedy and Gaussian framework from **Paper A**, re-applied towards tracking and monitoring dispersion dynamics in the water column. The objective function was rewritten to prioritize sampling locations that are proximal, with high variance and high concentration to better resolve plume type phenomena originating from one source.

Finally, **Paper F** presented an approach for autonomous mapping of the seafloor. Using a Hidden Markov Random Field model, observations of backscatter was used to classify different types of seafloor, on which a subsequent camera survey was automatically planned (addressing *topic A and B*). Results from full-scale experiments using a HUGIN AUV showed that the method successfully identified and planned sampling online.

## 6.2 Future Research Directions

The transition from traditional human-developed plans to more autonomous oceanic sampling is something that is still underway in oceanography. We want to briefly touch on topics of further investigation which we deliberately side-stepped, and/or that are a natural extension of the current research.

**Optimization:** and problems related to the use of suboptimal planning algorithms.

**Non-myopic approaches:** Extending from a greedy planning perspective, non-myopic approaches could be evaluated by using model, science-based heuristics, and more synoptic path planning algorithms with a limited computational footprint (see Hoang et al. (2014)). Challenges with long term planning, such as non-modeled time-variability, could be addressed using support from ocean models and remote sensing assets.

**Optimization constraints:** In this work, we have deliberately ignored the aspect of operational constraints, such as available energy and time in the objective function. This has been possible as the planning horizon has been greedy, which allowed us to manage traditional operational constraints by restricting survey time or the number of locations to visit (the agent would simply stop given a predetermined condition). In the process of evaluating more elaborate non-myopic approaches, restricting survey time would not be a practical solution, as plans are optimized over a longer time horizon. See e.g. Leonard et al. (2007a) for an example deriving optimal paths for a network of mobile sensors.

**Modeling:** and problems related to overly simplistic assumptions about the field statics.

**Spatio-temporal variability and uncertainty:** Only information from specific depth regions are currently utilized in the proposed GP models. Extending the integration to multiple depths can be done without significantly increasing the complexity of the system. This is also the case for extending the current GP model to include more complex spatio-temporal dynamics such as time-dependent correlations (Frolov et al., 2013, 2014). Large sources of sampling uncertainty comes from the effects of currents (speed and direction), making the observations time dependent. The correlation scales used in this work are based on the variogram from either ocean model data, or work such as Hedger et al. (2003). Accounting for time or anisotropic factors in the GP model could improve the model accuracy, and subsequently the approach. This correction is, however, not advantageous unless a good model and/or measurement (e.g. Lagrangian drifters) for the time variability can be provided.

**GP hyperparameters:** Initializing the GPs hyperparameters has been done on the basis of ocean model data, and online re-evaluation has not been explored because the statistical properties are likely to be captured by the ocean model. However, in cases where this data is not available, the hyperparameters must be learned online (active learning). Consequently, exploring new methods for determining the background statistical representations can extend the usability of the GP model.

**Inclusion of co-variates:** In **Paper A**, a bias-correcting mean function was proposed. The prior mean would be corrected if the mean temperature discrepancy was more than 1°C. More elaborate adjustments on the basis of different co-variates are possible and should be investigated in future applications.

**Multi-platform collaboration and planning:** At the cost of increased operational complexity, additional assets such as another AUV could be used to increase coverage capacity and sampling density, as well as providing shared knowledge. This also includes heterogeneous platforms such as remote-sensing satellites, research vessels, moorings, ASVs, and airplanes that could be used together in a coordinated sampling system, e.g. ODSS (Gomes et al., 2013).

## 6.3 List of Publications and Scientific Contributions

This final section summarizes the publications included in Part II and their scientific contribution. Included in these publications are four authored and two co-authored papers, of which three are journal papers and three conference paper. The papers are listed in the same order as they appear in Part II, journal papers first, followed by the conference papers. The context and scientific contribution of each paper is stated below the reference to the paper. A last section, presents the public presentations of the work.

**A:** ***Peer-reviewed Journal Article***
**Trygve Olav Fossum**, Jo Eidsvik, Ingrid Ellingsen, Morten Omholt Alver, Glaucia Moreira Fragoso, Geir Johnsen, Renato Mendes, Martin Ludvigsen, and Kanna Rajan. **Information-driven Robotic Sampling in the Coastal Ocean**. *Journal of*

*Field Robotics*, Volume 35, Issue 7, pages 1101–1121, 2018.

***Context:*** The paper combines ocean models, Gaussian process modeling, and information-theoretic sampling to address the challenges related to sampling dynamic coastal processes and ocean model assimilation. The work presents an end-to-end, real-world implementation of an information-theoretic adaptive sampling agent, specifically for observation of upwelling and internal waves processes in the upper water column. The system is shown to be capable of directing sampling efforts to regions in accordance with these processes using a utility metric balancing uncertainty reduction and thermal gradients.

***Scientific contributions:*** i) Development of an greedy, data-driven sampling algorithm (GASA), that balances variance and gradient based influences; implementation of the computer code and supporting algorithms on board an AUV. ii) Integration and utilization of ocean model data into a Gaussian process model, developing a locally-varying correlation kernel and a bias-correcting mean. iii) Design of a survey campaign, based on spatial analysis of ocean model data. iv) Results from field experiments with AUV, specifically tracking sub-surface coastal processes. v) Analysis and verification of AUV results using data from remote sensing, buoys, and ship-based sampling.

**B:** ***Peer-reviewed Journal Article***
**Trygve Olav Fossum**, Glaucia Moreira Fragoso, Emlyn J. Davies, Jenny Ullgren, Renato Mendes, Geir Johnsen, Ingrid Ellingsen, Jo Eidsvik, Martin Ludvigsen, and Kanna Rajan. **Towards Adaptive Robotic Sampling of Phytoplankton in the Coastal Ocean.** *Science Robotics*, Volume 4, Issue 27, eaav3041, 2019.

***Context:*** Currents, wind, bathymetry, and freshwater run-off are some of the factors that makes coastal waters heterogeneous and patchy, and an environment of scientific interest where it is challenging to resolve the spatio-temporal variation within the water column. Motivated by this, a practical real-world implementation of a sampling approach for the upper water column, capable of adapting to distributions in 3D, is presented. Trying to resolve this in a dynamic environment requires a trade-off between exploration and exploitation. The proposed method presents a solution to this by splitting the survey into two dedicated phases given a limited volume, bounding time-variability effects. Under these conditions the AUV first estimates and then maps (based on the learned information) the most interesting region of the water column in a fast and focused way: towards attaining a quasi-synoptic snapshot of the feature. Results from field experiments, conducted together with a ship showcase the potential of collaborative mapping of phytoplankton distributions in a dynamic coastal environment; the sensitivity of time-varying processes (such as currents) are also discussed.

***Scientific contributions:*** i) Development of a volumetric (3D) data-driven sampling algorithm for water column surveys; implementation of the computer code and supporting algorithms on board an AUV. ii) Development of a Gaussian process model

for estimating distributions of high concentrations in 3D. iii) Results from field experiments with AUV, specifically tracking sub-surface chlorophyll distributions. iv) Results from analysis and verification of AUV behavior using data from a particle camera and fluorometery.

**C:** ***Peer-reviewed Journal Article***
**Trygve O. Fossum**, John Ryan, Tapan Mukerji, Jo Eidsvik, Thom Maughan, Martin Ludvigsen and Kanna Rajan. **Compact models for Adaptive Sampling in Marine Robotics.** *Submitted to International Journal of Research Robotics*, 9th November 2018.

***Context:*** Information-theoretic sampling driven by machine learning techniques can have a substantial impact to the *undersampled* oceans. The paper presents a methodology for building compact ocean models using data from remote sensing to increase the predictive capabilities of robotic sampling platforms; combining machine learning, statistics, and robotics with physical and biological oceanography. The integrity of the compact model is documented by cross-verification with historical wind data. Results from a case study using WaveGlider data is shown, to illustrate how models can be used to reconstruct synoptic information based on local *in-situ* measurements. Finally, a statistical analysis of the model sensitivity is presented together with practical implications for survey- and resource-planning.

***Scientific contributions:*** i) Development of an unsupervised methodology for building compact on board models from remote sensing data; creation of model and implementation of the computer code, including supporting algorithms. ii) Verification of the method using historical wind measurements. iii) Results and model prediction using data collected during from field experiments by an unmanned surface vehicle. iv) A statistical analysis of model prediction error.

**D:** ***Conference paper***
**Trygve O. Fossum**, Martin Ludvigsen, Stein M. Nornes, Ida Rist-Christensen and Lars Brusletto. **Autonomous Robotic Intervention using ROV: An Experimental Approach.** *MTS/IEEE OCEANS 2016*, Monterey, CA, USA, 19-22 September 2016.

***Context:*** A semi-autonomous agent architecture for robotic intervention with an ROV is proposed. The system is tested both in simulations and in field experiments. The ROV agent is able to execute an inspection-type mission, navigating to an object of interest (subsea structure) from the surface while avoiding obstacles aided by computer vision. This demonstrates the architecture's feasibility in an environment similar to an operational situation.

***Scientific contributions:*** i) Contributed to development and field testing of a subsumption-based autonomous agent architecture for ROV inspection, maintenance, and repair operations. ii) Contributed to integration of a computer vision detection and avoidance scheme. iii) Participation in field experiments and data collection.

**E:** ***Conference paper***
Gunhild Elisabeth Berget, **Trygve O. Fossum**, Tor Arne Johansen, Jo Eidsvik and Kanna Rajan. **Adaptive Sampling of Ocean Processes Using an AUV with a Gaussian Proxy Model.** *11th IFAC Conference on Control Applications in Marine Systems, Robotics, and Vehicles (CAMS)* Opatija, Croatia, $10^{th}$-$12^{th}$ September 2018.

***Context:*** The goal is to monitor dispersion dynamics related to industrial applications such as oil and mine tailings. A spatial proxy model using Gaussian processes is developed for robotic sampling with an AUV. Results and verification are done using simulated data. An objective function to maximize the value of the collected information is designed that uses a greedy adaptive sampling strategy. The objective function prioritizes proximal locations with high variance and high concentration, focusing the AUV sampling effort along tracking and exploring a simulated particle plume.

***Scientific contributions:*** i) Contributed to development of the Gaussian process model, data assimilation, and sampling algorithm – based on the approach and method in Paper A. ii) Ideas and formulation of overarching research goals and aims. iii) Contributed to writing and proofreading the published work.

**F:** ***Conference paper***
Øystein Sture, **Trygve O. Fossum**, Martin Ludvigsen and Martin Syre Wiig. **Autonomous Optical Survey Based on Unsupervised Segmentation of Acoustic Backscatter.** *MTS/IEEE OCEANS 2016*, Kobe, Japan, May-June 2018.

***Context:*** Design and integration of a Hidden Markov Random Field (HMRF) model to perform unsupervised segmentation of the backscatter response for the purpose of determining different seabed types. This is valuable information to possess as it can be used to optimize seabed coverage. The model output is directly used to plan and conduct an autonomous near-seabed camera survey to verify the classification results, whilst also augmenting the acoustical data set with increased detail. Results from a full-scale experiment on board a Kongsberg HUGIN 1000 AUV are presented.

***Scientific contributions:*** i) Contributed to the development of the HMRF model for seabed classification and mapping. ii) Ideas and formulation of overarching research goals and aims. iii) Participation and results from field experiments in a fjord using an AUV. iv) Contributed to writing and proofreading the published work.

The following presentations have been held based on the work in this thesis:

***Conference paper***
Martin Ludvigsen, Sigurd M. Albrektsen, Krzysztof Cisek, Tor Arne Johansen, Petter Norgren, Roger Skjetne, Artur Zolich, Paulo Sousa Dias, Sérgio Ferreira, João Borges de Sousa, **Trygve O. Fossum**, Øystein Sture, Thomas Røbekk Krogstad, Øivind Midtgaard, Vegard Hovstein, and Erlend Vågsholm. **Network of heterogeneous autonomous vehicles for marine research and management.**
*In Proc. MTS/IEEE OCEANS*, Monterey, CA, USA, 2016.

***Technical Report***
Øystein Sture, Martin Syre Wiig, and **Trygve O. Fossum**. **NTNU-FFI Cruise 2017-HUGIN Autonomy Integration (DUNE, T-REX).** *NTNU Cruise Reports*, The Norwegian University of Science and Technology (NTNU).

***Technical Report***
**Trygve O. Fossum**. **Intelligent Autonomous Underwater Vehicles: A Review of AUV Autonomy and Data-Driven Sample Strategies** *IMT-AURLab-1*, Department of Marine Technology, Centre for autonomous marine operations and systems (AMOS), Norwegian University of Science and Technology (NTNU).

### 6.3.1 Presentations

During the course of this work, the following presentations have been held based on the work in this thesis:

***A Dive Into Artificial Intelligence and Underwater Robotics***, *Nor-Fishing Conference*, Trondheim, Norway, $18^{th}$ of August 2016.

***Coupling Robotic Sampling with Ocean Models***, *SINMOD 30 year anniversary*, SINTEF Ocean AS, Trondheim, Norway, $17^{th}$ of January 2017.

***Adaptive Data Collection: What Robots can do for Ocean Science***, *AMOS-days*, Trondheim, Norway, $9^{th}$ of November 2017.

***The Faces of Monterey Bay - Compact Remote Sensing Ocean Models***, *Monterey Bay Aquarium Research Institute (MBARI) weekly seminars*, Moss Landing, California, $28^{th}$ of June 2018.

***Searching for Information at Sea: Adaptive Sampling with AUVs***, *AMOS-days*, Trondheim, Norway, $23^{rd}$ of October 2018.

***Compact Remote Sensing Ocean Models for Adaptive Sampling in the Coastal Ocean***, *Ocean Data Analytics Symposium*, Trondheim, Norway, 28-$30^{th}$ of November 2018.

# References


J. Albretsen. NorKyst-800 Report No. 1: User Manual and technical descriptions. *Institute of Marine Research: Fisken og havet*, 2011.

B. Allen, R. Stokey, T. Austin, N. Forrester, R. Goldsborough, M. Purcell, and C. von Alt. Remus: a small, low cost auv; system description, field trials and performance results. In *OCEANS'97. MTS/IEEE Conference Proceedings*, volume 2, pages 994–1000. IEEE, 1997.

A. Alvarez and B. Mourre. Optimum sampling designs for a glider–mooring observing network. *Journal of Atmospheric and Oceanic Technology*, 29(4):601–612, 2012. doi: 10.1175/JTECH-D-11-00105.1. URL https://doi.org/10.1175/JTECH-D-11-00105.1.

A. Alvarez, B. Garau, and A. Caiti. Combining networks of drifting profiling floats and gliders for adaptive sampling of the ocean. In *Proceedings 2007 IEEE International Conference on Robotics and Automation*, pages 157–162, April 2007. doi: 10.1109/ROBOT.2007.363780.

J. Y. Audibert, R. Munos, and C. Szepesvári. Exploration–exploitation tradeoff using variance estimates in multi-armed bandits. *Theoretical Computer Science*, 410(19): 1876–1902, 2009.

H. S. Bailey. The voyage of the challenger. *Scientific American*, 188(5):88–95, 1953.

J. G. Bellingham and J. J. Leonard. Task configuration with layered control. In *IARP Workshop on Mobile Robots for Subsea Environments*, 1994.

M. Beniston. *From Turbulence to Climate: Numerical Investigations of the Atmosphere With a Hierarchy of Models*. Springer, 1998. ISBN 9783540634959. URL https://books.google.no/books?id=MBqbSi9WMvcC.

M. R. Benjamin, H. Schmidt, P. M. Newman, and J. J. Leonard. Nested autonomy for unmanned marine vehicles with MOOS-IvP. *Journal of Field Robotics*, 27(6):834–875, 2010.

J. Berntsen. Internal pressure errors in sigma-coordinate ocean models. *Journal of Atmospheric and Oceanic Technology*, 19(9):1403–1414, 2002. doi: 10.1175/1520-0426(2002)019⟨1403:IPEISC⟩2.0.CO;2. URL https://doi.org/10.1175/1520-0426(2002)019<1403:IPEISC>2.0.CO;2.

J. Binney and G. S. Sukhatme. Branch and bound for informative path planning. In *Robotics and Automation (ICRA), 2012 IEEE International Conference on*, pages 2147–2154. IEEE, 2012.

J. Binney, A. Krause, and G. S. Sukhatme. Informative Path Planning for an Autonomous Underwater Vehicle. *Proc. IEEE Int. Conf. Robotics and Automation*, pages 4791–4796, 2010. ISSN 1050-4729. doi: 10.1109/ROBOT.2010.5509714. URL http://cres.usc.edu/cgi-bin/print{_}pub{_}details.pl?pubid=642.

J. Binney, A. Krause, and G. S. Sukhatme. Optimizing waypoints for monitoring spatiotemporal phenomena. *The International Journal of Robotics Research*, 32(8):873–888, 2013. ISSN 0278-3649. doi: 10.1177/0278364913488427. URL http://ijr.sagepub.com/cgi/doi/10.1177/0278364913488427.

O. S. Board, N. R. Council, et al. *Science at sea: meeting future oceanographic goals with a Robust Academic Research Fleet*. National Academies Press, 2009.

F. P. Bretherton, R. E. Davis, and C. Fandry. A technique for objective analysis and design of oceanographic experiments applied to mode-73. In *Deep Sea Research and Oceanographic Abstracts*, volume 23, pages 559–582. Elsevier, 1976.

O. J. Broch, I. H. Ellingsen, S. Forbord, X. Wang, Z. Volent, M. O. Alver, A. Handå, K. Andresen, D. Slagstad, K. I. Reitan, et al. Modelling the cultivation and bioremediation potential of the kelp saccharina latissima in close proximity to an exposed salmon farm in norway. *Aquaculture Environment Interactions*, 4(2):187–206, 2013a.

O. J. Broch, D. Slagstad, and M. Smit. Modelling produced water dispersion and its direct toxic effects on the production and biomass of the marine copepod calanus finmarchicus. *Marine Environmental Research*, 84(Supplement C):84 – 95, 2013b. ISSN 0141-1136. doi: https://doi.org/10.1016/j.marenvres.2012.12.003. URL http://www.sciencedirect.com/science/article/pii/S0141113612002218.

R. Brooks. A robust layered control system for a mobile robot. *IEEE journal on robotics and automation*, 2(1):14–23, 1986.

I. Busby Associates. *Undersea Vehicles Directory*. Busby Associates, Inc., 1987.

J. B. Campbell and R. H. Wynne. *Introduction to Remote Sensing, Fifth Edition*, volume 39. Guilford Press, 2011. ISBN 978-1-60918-176-5. doi: 10.1007/s13398-014-0173-7.2. URL https://books.google.com/books?id=NkLmDjSS8TsC{&}pgis=1.

W. F. Caselton and J. V. Zidek. Optimal monitoring network designs. *Statistics & Probability Letters*, 2(4):223–227, 1984.

K. Chaloner and I. Verdinelli. Bayesian experimental design: A review. *Statistical Science*, pages 273–304, 1995.

D. Chang, F. Zhang, and C. R. Edwards. Real-time guidance of underwater gliders assisted by predictive ocean models. *Journal of Atmospheric and Oceanic Technology*, 32(3):562–578, 2015. ISSN 15200426. doi: 10.1175/JTECH-D-14-00098.1.

Y. Chao, S. Chien, J. Kinsey, M. M. Flexas, Z. K. Erickson, J. Farrara, D. Fratantoni, A. Branch, S. Chu, M. Troesch, B. Claus, and T. O. Society. Satellites to Seafloor: Towards fully autonomous ocean sampling. *Oceanography*, 30(2):160–168, 2017.

F. P. Chavez, P. G. Brewer, and C. A. Scholin. From the guest editors: Celebrating 30 years of ocean science and technology at the Monterey Bay Aquarium Research Institute. *Oceanography*, 30, December 2017. URL `https://doi.org/10.5670/oceanog.2017.420`.

C. Chekuri and M. Pal. A recursive greedy algorithm for walks in directed graphs. In *Foundations of Computer Science, 2005. FOCS 2005. 46th Annual IEEE Symposium*, pages 245–253. IEEE, 2005.

M. J. Costa, J. Pinto, P. S. Dias, J. Pereira, K. Lima, M. Ribeiro, J. B. Sousa, T. Lukaczyk, R. Mendes, M. P. Tomasino, C. Magahlaes, I. Belkin, F. Lopez-Castejon, J. Gilabert, K. A. Skarpnes, M. Ludvigsen, K. Rajan, Z. Mirmalek, and A. Chekalyuk. Field report: Exploring fronts with multiple robots. In *IEEE AUV*, Porto, 2018.

D. Cressey. Us science fleet's future is far from ship-shape. *Nature*, 2013. doi: 10.1038/nature.2013.13164. URL `https://www.nature.com/news/us-science-fleet-s-future-is-far-from-ship-shape-1.13164`.

N. A. C. Cressie and C. K. Wikle. *Statistics for Spatio-Temporal Data.* Wiley Series in Probability and Statistics. Wiley, 2011. ISBN 9780471692744.

E. L. Crow and K. Shimizu. *Lognormal Distributions - Theory and Applications*. Marcel Dekker, New York, 1988.

T. B. Curtin, J. G. Bellingham, J. Catipovic, and D. Webb. Autonomous oceanographic sampling networks. *Oceanography*, 6(3):86–94, 1993. ISSN 10428275, 2377617X. URL `http://www.jstor.org/stable/43924649`.

S. Dag Slagstad. Sinmod - a physical, chemical, and biological model system. technical report, SINTEF, Trondheim, 2005.

C. Darwin and R. Keynes. *Charles Darwin's Beagle Diary*. Cambridge University Press, 2001. ISBN 9780521003179. URL `https://books.google.no/books?id=MFUZsb5PPIoC`.

J. Das, K. Rajan, S. Frolov, J. P. Ryan, F. Py, D. A. Caron, G. S. Sukhatme, J. P. Ryan, D. A. Caron, and G. S. Sukhatme. Towards marine bloom trajectory prediction for AUV mission planning. *Proceedings - IEEE International Conference on Robotics and Automation*, pages 4784–4790, 2010. ISSN 10504729. doi: 10.1109/ROBOT.2010.5509930.

J. Das, T. Maughan, M. McCann, M. Godin, T. O'Reilly, M. Messié, F. Bahr, K. Gomes, F. Py, J. G. Bellingham, G. S. Sukhatme, and K. Rajan. Towards mixed-initiative, multi-robot field experiments: Design, deployment, and lessons learned. In *2011 IEEE/RSJ International Conference on Intelligent Robots and Systems*, pages 3132–3139, Sept 2011. doi: 10.1109/IROS.2011.6095068.

J. Das, F. Py, T. Maughan, M. Messie, T. O'Reilly, J. Ryan, G. S. Sukhatme, and K. Rajan. Coordinated Sampling of Dynamic Oceanographic Features with AUVs and Drifters. *The International Journal of Robotics Research*, 31:626-646, 2012a. April.

J. Das, F. Py, T. Maughan, T. O'Reilly, M. Messié, J. Ryan, G. S. Sukhatme, and K. Rajan. Coordinated sampling of dynamic oceanographic features with underwater vehicles and drifters. *International Journal of Robotics Research*, 31(5):626–646, 2012b. ISSN 02783649. doi: 10.1177/0278364912440736.

J. Das, F. Py, J. B. J. Harvey, J. P. Ryan, A. Gellene, R. Graham, D. A. Caron, K. Rajan, and G. S. Sukhatme. Data-driven robotic sampling for marine ecosystem monitoring. *The International Journal of Robotics Research*, 34(12):1435–1452, 2015. ISSN 0278-3649. doi: 10.1177/0278364915587723. URL http://ijr.sagepub.com/content/34/12/1435.full.

C. Donlon, B. Berruti, A. Buongiorno, M.-H. Ferreira, P. Féménias, J. Frerick, P. Goryl, U. Klein, H. Laur, C. Mavrocordatos, et al. The global monitoring for environment and security (gmes) sentinel-3 mission. *Remote Sensing of Environment*, 120:37–57, 2012.

J. Eidsvik, T. Mukerji, and D. Bhattacharjya. *Value of Information in the Earth Sciences: Integrating Spatial Modeling and Decision Analysis*. Cambridge University Press, Cambridge, 008 2015. ISBN 9781139628785. doi: 10.1017/CBO9781139628785. URL https://www.cambridge.org/core/books/value-of-information-in-the-earth-sciences/61119AB2F707D557E49E00BF9FD6FE39.

I. Ellingsen, P. Dalpadado, D. Slagstad, and H. Loeng. Impact of present and future climatic conditions on the physical and biological environment of the barents sea. *Climate Change*, 10, 2008. doi: https://doi.org/10.1007/s10584-007-9369-6.

I. Ellingsen, D. Slagstad, and A. Sundfjord. Modification of water masses in the barents sea and its coupling to ice dynamics: a model study. *Ocean Dynamics*, 59(6):1095–1108, Dec 2009. ISSN 1616-7228. doi: 10.1007/s10236-009-0230-5. URL https://doi.org/10.1007/s10236-009-0230-5.

A. S. Ferreira, M. Costa, F. Py, J. Pinto, M. A. Silva, A. Nimmo-Smith, T. A. Johansen, J. B. de Sousa, and K. Rajan. Advancing multi-vehicle deployments in oceanographic field experiments. *Autonomous Robots*, Oct 2018. ISSN 1573-7527. doi: 10.1007/s10514-018-9810-x. URL https://doi.org/10.1007/s10514-018-9810-x.

G. Forristall. Lofoten and Vesteralen currents (LOVECUR): Comparison of hindcasts with measurements. Technical report, Forristall Ocean Engineering Inc., Camden, ME, USA, 2011.

T. O. Fossum, M. Ludvigsen, S. M. Nornes, I. Rist-Christensen, and L. Brusletto. Autonomous robotic intervention using ROV: An experimental approach. In *OCEANS 2016 MTS/IEEE*, pages 1–6, Monterey, USA, Sept 2016. doi: 10.1109/OCEANS.2016.7761178.

T. O. Fossum, J. Eidsvik, I. Ellingsen, M. O. Alver, G. M. Fragoso, G. Johnsen, R. Mendes, M. Ludvigsen, and K. Rajan. Information-driven robotic sampling in the coastal ocean. *Journal of Field Robotics*, 35(7):1101–1121, 2018. doi: 10.1002/rob.21805. URL https://onlinelibrary.wiley.com/doi/abs/10.1002/rob.21805.

P. J. S. Franks. Sink or swim: Accumulation of biomass at fronts. *Marine Ecology Progress Series*, 82:1–12, 1992. ISSN 01718630. doi: 10.3354/meps082001.

S. Frolov. *Enabling technologies for data assimilation in a coastal-margin observatory*. Phd thesis, Oregon Health & Science University, 2007. URL papers2://publication/uuid/AD417354-9648-4DFF-BA97-5AA82A3CE8B0.

S. Frolov, J. Paduan, M. Cook, and J. Bellingham. Improved statistical prediction of surface currents based on historic HF-radar observations. *Ocean Dynamics*, 62(7):1111–1122, 2012. ISSN 16167341. doi: 10.1007/s10236-012-0553-5.

S. Frolov, R. M. Kudela, and J. G. Bellingham. Monitoring of harmful algal blooms in the era of diminishing resources: A case study of the U.S. West Coast. *Harmful Algae*, 21-22:1–12, 2013. ISSN 15689883. doi: 10.1016/j.hal.2012.11.001. URL http://dx.doi.org/10.1016/j.hal.2012.11.001.

S. Frolov, B. Garau, and J. Bellingham. Can we do better than the grid survey: Optimal synoptic surveys in presence of variable uncertainty and decorrelation scales. *Journal of Geophysical Research: Oceans*, 119:5071–5090, 2014. ISSN 21699291. doi: 10.1002/2013JC009521.

Y. Girdhar and G. Dudek. Modeling curiosity in a mobile robot for long-term autonomous exploration and monitoring. *Autonomous Robots*, 2015. ISSN 09295593. doi: 10.1007/s10514-015-9500-x.

K. Gomes, D. Cline, D. Edgington, M. Godin, T. Maughan, M. McCann, T. O'Reilly, F. Bahr, F. Chavez, M. Messié, et al. Odss: A decision support system for ocean exploration. In *Data Engineering Workshops (ICDEW), 2013 IEEE 29th International Conference on*, pages 200–211. IEEE, 2013.

R. Graham, F. Py, J. Das, D. Lucas, T. Maughan, and K. Rajan. Exploring Space-Time Tradeoffs in Autonomous Sampling for Marine Robotics. In *Experimental Robotics*, volume 88, pages 819–839. Spinger, 2013. ISBN 978-3-319-00064-0. doi: 10.1007/978-3-319-00065-7. URL http://link.springer.com/10.1007/978-3-319-00065-7.

S. M. Griffies, C. Böning, F. O. Bryan, E. P. Chassignet, R. Gerdes, H. Hasumi, A. Hirst, A.-M. Treguier, and D. Webb. Developments in ocean climate modelling. *Ocean Modelling*, 2(3-4):123–192, 2000. ISSN 14635003. doi: 10.1016/S1463-5003(00)00014-7.

G. Griffiths, P. Stevenson, A. T. Webb, N. W. Millard, S. D. McPhail, M. Pebody, and J. R. Perrett. Open ocean operational experience with the autosub-1 autonomous underwater vehicle. In *International symposium on unmanned untethered submersible technology*, pages 1–12. University of new hampshire-marine systems, 1999.

C. Guestrin, A. Krause, and A. P. Singh. Near-optimal sensor placements in gaussian processes. *Proceedings of the 22nd International Conference on Machine Learning*, 1(January 2005):1–8, 2005. ISSN 15324435. doi: 10.1145/1102351.1102385. URL http://dl.acm.org/citation.cfm?id=1102385.

R. D. Hedger, T. J. Malthus, and A. M. Folkard. Spatial dynamics of chlorophyll-$\alpha$ and sea surface temperature in a coastal zone as revealed by high-resolution remote sensing. In *Remote Sensing of the Ocean*, volume 4880, pages 146–158. International Society for Optics and Photonics, 2003. doi: 10.1117/12.462413. URL https://doi.org/10.1117/12.462413.

G. Hitz, A. Gotovos, M.-É. Garneau, C. Pradalier, A. Krause, R. Y. Siegwart, et al. Fully autonomous focused exploration for robotic environmental monitoring. In *Robotics and Automation (ICRA), 2014 IEEE International Conference on*, pages 2658–2664. IEEE, 2014.

G. Hitz, E. Galceran, M.-E. Garneau, F. Pomerleau, and R. Siegwart. Adaptive continuous-space informative path planning for online environmental monitoring. *Journal of Field Robotics*, 34(8):1427–1449, 2017. doi: 10.1002/rob.21722. URL https://onlinelibrary.wiley.com/doi/abs/10.1002/rob.21722.

T. N. Hoang, K. H. Low, P. Jaillet, and M. Kankanhalli. Nonmyopic Epsilon-Bayes-Optimal Active Learning of Gaussian Processes. *Proceedings of the International Conference on Machine Learning*, pages 739–747, 2014. ISSN 16113349. doi: 10.1007/978-3-662-44845-8_43.

T. N. Hoang, Q. M. Hoang, and B. K. H. Low. A distributed variational inference framework for unifying parallel sparse gaussian process regression models. In *International Conference on Machine Learning*, pages 382–391, 2016.

B. W. Hobson, J. G. Bellingham, B. Kieft, R. McEwen, M. Godin, and Y. Zhang. Tethys-class long range auvs-extending the endurance of propeller-driven cruising auvs from days to weeks. In *Autonomous Underwater Vehicles (AUV), 2012 IEEE/OES*, pages 1–8. IEEE, 2012.

G. A. Hollinger and G. S. Sukhatme. Sampling-based robotic information gathering algorithms. *The International Journal of Robotics Research*, 33(9):1271–1287, 2014.

B. M. Howe, Y. Chao, P. Arabshahi, S. Roy, T. McGinnis, and A. Gray. A smart sensor web for ocean observation: Fixed and mobile platforms, integrated acoustics, satellites and predictive modeling. *IEEE Journal of Selected Topics in Applied Earth Observations and Remote Sensing*, 3(4):507–521, 2010.

P. Jackson. *Introduction to expert systems*. Addison-Wesley Longman Publishing Co., Inc., 1998.

J. A. Johannessen, L. Røed, O. M. Johannessen, G. Evensen, B. Hackett, L. H. Pettersson, P. M. Haugan, S. Sandven, and R. Shuchman. Monitoring and modeling of the marine coastal environment. *Photogrammetric engineering and remote sensing*, 59(3):351–361, 1993.

O. M. Johannessen, S. Sandven, A. D. Jenkins, D. Durand, L. H. Pettersson, H. Espedal, G. Evensen, and T. Hamre. Satellite earth observation in operational oceanography. *Coastal Engineering*, 41(1-3):155–176, 2000. ISSN 03783839. doi: 10.1016/S0378-3839(00)00030-2.

S. Kemna. *Multi-Robot Strategies for Adaptive Sampling with Autonomous Underwater Vehicles*. Phd thesis, University of Southern California, 2018. URL http://digitallibrary.usc.edu/cdm/ref/collection/p15799coll89/id/76169.

J. C. Kinsey, R. M. Eustice, and L. L. Whitcomb. A survey of underwater vehicle navigation: Recent advances and new challenges. In *IFAC Conference of Manoeuvering and Control of Marine Craft*, volume 88, pages 1–12, 2006.

E. Kintisch. A sea change for u.s. oceanography. *Science*, 339(6124):1138–1143, 2013. ISSN 0036-8075. doi: 10.1126/science.339.6124.1138. URL http://science.sciencemag.org/content/339/6124/1138.

C.-W. Ko, J. Lee, and M. Queyranne. An exact algorithm for maximum entropy sampling. *Operations Research*, 43(4):684–691, 1995.

A. Krause. *Optimizing Sensing: Theory and Applications*. Phd thesis, Carnegie Mellon University, 2008.

A. Krause and C. Guestrin. Optimizing sensing: From water to the web. *Computer*, 42(8):38–45, 2009. ISSN 00189162. doi: 10.1109/MC.2009.265.

A. Krause, C. Guestrin, A. Gupta, and J. Kleinberg. Near-optimal sensor placements: maximizing information while minimizing communication cost. In *2006 5th International Conference on Information Processing in Sensor Networks*, number January 2006 in IEEE, pages 2–10, 2006. ISBN 1-59593-334-4. doi: 10.1109/IPSN.2006.244031. URL http://ieeexplore.ieee.org/lpdocs/epic03/wrapper.htm?arnumber=1662434.

A. Krause, A. Singh, and C. Guestrin. Near-Optimal Sensor Placements in Gaussian Processes: Theory, Efficient Algorithms and Empirical Studies. *Journal of Machine Learning Research*, 9:235–284, 2008. ISSN 15324435. doi: 10.1145/1102351.1102385.

J. Kristensen and K. Vestgard. Hugin - an untethered underwater vehicle for seabed surveying. In *OCEANS'98 Conference Proceedings*, volume 1, pages 118–123. IEEE, 1998.

R. M. Kudela, S. L. Palacios, D. C. Austerberry, E. K. Accorsi, L. S. Guild, and J. Torres-Perez. Application of hyperspectral remote sensing to cyanobacterial blooms in inland waters. *Remote Sensing of Environment*, 167:196 – 205, 2015. ISSN 0034-4257. doi: https://doi.org/10.1016/j.rse.2015.01.025. URL http://www.sciencedirect.com/science/article/pii/S0034425715000437.

S. M. LaValle. *Planning algorithms*. Cambridge university press, 2006.

D. M. Le Vine, G. S. Lagerloef, F. R. Colomb, S. H. Yueh, and F. A. Pellerano. Aquarius: An instrument to monitor sea surface salinity from space. *IEEE Transactions on Geoscience and Remote Sensing*, 45(7):2040–2050, 2007.

N. E. Leonard, D. A. Paley, F. Lekien, R. Sepulchre, D. M. Fratantoni, and R. E. Davis. Collective Motion, Sensor Networks, and Ocean Sampling. *Proceedings of the IEEE*, 95(1):48–74, jan 2007a. ISSN 0018-9219. doi: 10.1109/JPROC.2006.887295.

N. E. Leonard, D. A. Paley, F. Lekien, R. Sepulchre, D. M. Fratantoni, and R. E. Davis. Collective motion, sensor networks, and ocean sampling. *Proceedings of the IEEE*, 95 (1):48–74, Jan 2007b. ISSN 0018-9219. doi: 10.1109/JPROC.2006.887295.

N. E. Leonard, D. A. Paley, R. E. Davis, D. M. Fratantoni, F. Lekien, and F. Zhang. Coordinated control of an underwater glider fleet in an adaptive ocean sampling field experiment in Monterey Bay. *Journal of Field Robotics*, 27(6):718–740, 2010.

P. F. J. Lermusiaux. Uncertainty estimation and prediction for interdisciplinary ocean dynamics. *Journal of Computational Physics*, 217(1):176–199, sep 2006. ISSN 00219991. doi: 10.1016/j.jcp.2006.02.010. URL `https://doi.org/10.1016/j.jcp.2006.02.010`.

M. Lévy. Mesoscale variability of phytoplankton and of new production: Impact of the large-scale nutrient distribution. *Journal of Geophysical Research: Oceans*, 108(C11), 2003. ISSN 2156-2202. doi: 10.1029/2002JC001577. URL `http://dx.doi.org/10.1029/2002JC001577`.

K. H. Low. *Multi-Robot Adaptive Exploration and Mapping for Environmental Sensing Applications*. Phd thesis, Carnegie Mellon University, 2009. URL `http://www.comp.nus.edu.sg/{~}lowkh/pubs/final.pdf`.

K. H. Low, J. M. Dolan, and P. Khosla. Adaptive multi-robot wide-area exploration and mapping. In *Proceedings of the 7th international joint conference on Autonomous agents and multiagent systems-Volume 1*, pages 23–30. International Foundation for Autonomous Agents and Multiagent Systems, 2008.

K. H. Low, J. M. Dolan, and P. K. Khosla. Information-Theoretic Approach to Efficient Adaptive Path Planning for Mobile Robotic Environmental Sensing. *Proceedings of the International Conference on Automated Planning and Scheduling*, pages 233–240, 2009.

M. Ludvigsen, S. M. Albrektsen, K. Cisek, T. A. Johansen, P. Norgren, R. Skjetne, A. Zolich, P. S. Dias, S. Ferreira, J. B. de Sousa, T. O. Fossum, Ø. Sture, T. R. Krogstad, Ø. Midtgaard, V. Hovstein, and E. Vågsholm. Network of heterogeneous autonomous vehicles for marine research and management. In *OCEANS 2016 MTS/IEEE Monterey*, pages 1–7, Sep. 2016. doi: 10.1109/OCEANS.2016.7761494.

K.-C. Ma, L. Liu, and G. S. Sukhatme. An Information-Driven and Disturbance-Aware Planning Method for Long-Term Ocean Monitoring. *Intelligent Robots and Systems (IROS), 2016 IEEE/RSJ International Conference on*, pages 2102–2108, 2016.

K.-C. Ma, L. Liu, and G. S. Sukhatme. Informative planning and online learning with sparse gaussian processes. In *Robotics and Automation (ICRA), 2017 IEEE International Conference on*, pages 4292–4298. IEEE, 2017.

D. L. Mackas, K. L. Denman, and M. R. Abbott. Plankton patchiness: biology in the physical vernacular. *Bulletin of Marine Science*, 37(2):653–674, 1985. ISSN 00074977.

A. P. Martin, K. J. Richards, A. Bracco, and A. Provenzale. Patchy productivity in the open ocean. *Global Biogeochemical Cycles*, 16(2):9–1–9–9, 2002. ISSN 1944-9224. doi: 10.1029/2001GB001449. URL http://dx.doi.org/10.1029/2001GB001449.

B. Matérn. Spatial variation. *Meddelanden från Statens Skogsforskningsinstitut*, 36(5): 1–144, 2013.

G. Mathew and I. Mezić. Metrics for ergodicity and design of ergodic dynamics for multi-agent systems. *Physica D: Nonlinear Phenomena*, 240(4-5):432–442, 2011.

C. McGann, F. Py, K. Rajan, J. P. Ryan, and R. Henthorn. Adaptive Control for Autonomous Underwater Vehicles. In *AAAI*, pages 1319–1324, Chicago, IL, 2008a.

C. McGann, F. Py, K. Rajan, H. Thomas, R. Henthorn, and R. McEwen. A Deliberative Architecture for AUV Control. In *IEEE International Conference on Robotics and Automation (ICRA)*, Pasadena, May 2008b.

P. H. Milne. *Underwater acoustic positioning systems*. Gulf Publishing Co., Houston, TX, 1983.

P. Minnett and A. Kaiser-Weiss. Near-surface oceanic temperature gradients. *GHRSST Discussion Doc*, 2012. URL www.ghrsst.org/files/download.php?m=documents&f=120113121306-SSTDefinitionsDiscussion.pdf.

M. Mitchell. *An introduction to genetic algorithms*. MIT press, 1998.

W. J. Moses, S. G. Ackleson, J. W. Hair, C. A. Hostetler, and W. D. Miller. Spatial scales of optical variability in the coastal ocean: Implications for remote sensing and in situ sampling. *Journal of Geophysical Research: Oceans*, 121(6):4194–4208, 2016. ISSN 2169-9291. doi: 10.1002/2016JC011767. URL http://dx.doi.org/10.1002/2016JC011767.

M. Müller, M. Homleid, K.-I. Ivarsson, M. A. Køltzow, M. Lindskog, K. H. Midtbø, U. Andrae, T. Aspelien, L. Berggren, D. Bjørge, et al. Arome-metcoop: a nordic convective-scale operational weather prediction model. *Weather and Forecasting*, 32 (2):609–627, 2017.

W. G. Müller. *Collecting spatial data: optimum design of experiments for random fields*. Springer Science & Business Media, 2007.

W. Munk. Sampling the oceans from above and beneath, 8 1997. IAPSO President's Invited Lecture, Melbourne, Australia.

W. Munk. The evolution of physical oceanography in the last hundred years. *Oceanography*, 15, 2002. URL https://doi.org/10.5670/oceanog.2002.45.

W. H. Munk and C. I. Wunsch. Observing the ocean in the 1990s. *Philosophical Transactions of the Royal Society of London. Series A, Mathematical and Physical Sciences*, 307(1499):439–464, 1982.

F. Nansen. *The Norwegian North polar expedition, 1893-1896: scientific results*, volume 6. Longmans, Green and Company, 1905.

National Oceanic and Atmospheric Administration. How much of the ocean have we explored?, 2018. URL `https://oceanservice.noaa.gov/facts/exploration.html`.

National Research Council. *Undersea vehicles and national needs*. National Academies Press, 1996.

National Research Council. *Precise Geodetic Infrastructure: National Requirements for a Shared Resource*. National Academies Press, 2010. ISBN 9780309163293. URL `https://books.google.no/books?id=C24AIaT9MW4C`.

G. L. Nemhauser, L. A. Wolsey, and M. L. Fisher. An analysis of approximations for maximizing submodular set functions—i. *Mathematical programming*, 14(1):265–294, 1978.

P. Norgren, T. O. Fossum, and L. Martin. Intelligent robots as a tool to understand climate changes in the arctic ocean, 2018. URL `https://arvenetternansen.com/?p=2535`.

S. M. . Nornes. *Guidance and Control of Marine Robotics for Ocean Mapping and Monitoring*. PhD thesis, Norwegian University of Science and Technology, 2018.

H. Nyquist. Certain topics in telegraph transmission theory. *Transactions of the American Institute of Electrical Engineers*, 47(2):617–644, 1928.

S. Petillo. *Autonomous & Adaptive Oceanographic Feature Tracking On Board Autonomous Underwater Vehicles*. Phd thesis, Massachusetts Institute of Technology and the Woods Hole Oceanographic Institution, 2015.

S. Petillo, A. Balasuriya, and H. Schmidt. Autonomous adaptive environmental assessment and feature tracking via autonomous underwater vehicles. In *OCEANS'10 IEEE SYDNEY*, pages 1–9, May 2010. doi: 10.1109/OCEANSSYD.2010.5603513.

J. Pinto, P. Calado, J. Braga, P. Dias, R. Martins, E. Marques, and Sousa. Implementation of a control architecture for networked vehicle systems. *IFAC Proceedings Volumes*, 45 (5):100–105, 2012.

J. Pinto, P. S. Diasand, R. Martins, J. Fortuna, E. Marques, and J. Sousa. The LSTS toolchain for networked vehicle systems. In *MTS/IEEE Oceans*, pages 1–9. IEEE, 2013.

J. Pinto, R. Mendes, J. C. B. da Silva, J. M. Dias, and J. B. de Sousa. Multiple autonomous vehicles applied to plume detection and tracking. In *2018 OCEANS - MTS/IEEE Kobe Techno-Oceans (OTO)*, pages 1–6, May 2018. doi: 10.1109/OCEANSKOBE.2018.8558802.

F. Py, K. Rajan, and C. McGann. A Systematic Agent Framework for Situated Autonomous Systems. In *9th International Conf. on Autonomous Agents and Multiagent Systems (AAMAS)*, Toronto, Canada, May 2010.

F. Py, J. Pinto, M. Silva, T. A. Johansen, J. B. Sousa, and K. Rajan. EUROPtus: A Mixed-initiative Controller for Multi-Vehicle Oceanographic Field Experiments. In *Intnl. Symp. on Experimental Robotics (ISER)*, Tokyo, 2016.

K. Rajan and F. Py. T-REX: Partitioned Inference for AUV Mission Control. In G. N. Roberts and R. Sutton, editors, *Further Advances in Unmanned Marine Vehicles*. The Institution of Engineering and Technology (IET), August 2012. ISBN 978-1849194792.

K. Rajan, F. Py, and J. Berreiro. Towards Deliberative Control in Marine Robotics. In M. Seto, editor, *Marine Robot Autonomy*. Springer Verlag, 2012.

S. R. Ramp, R. E. Davis, N. E. Leonard, I. Shulman, Y. Chao, A. R. Robinson, J. Marsden, P. F. Lermusiaux, D. M. Fratantoni, J. D. Paduan, F. P. Chavez, F. L. Bahr, S. Liang, W. Leslie, and Z. Li. Preparing to predict: The Second Autonomous Ocean Sampling Network (AOSN-II) experiment in the Monterey Bay. *Deep-Sea Research Part II: Topical Studies in Oceanography*, 56(3-5):68–86, 2009. ISSN 09670645. doi: 10.1016/j.dsr2.2008.08.013.

E. C. Rasmussen and C. K. I. Williams. *Gaussian Processes for Machine Learning*. MIT Press, 1 edition, 2006. ISBN 026218253X. doi: 10.1142/S0129065704001899.

M. Rast, J. Bezy, and S. Bruzzi. The esa medium resolution imaging spectrometer meris a review of the instrument and its mission. *International Journal of Remote Sensing*, 20 (9):1681–1702, 1999.

Richard A. Davis. Gaussian processes. *Encyclopedia of Environmetrics, Section on Stochastic Modeling and Environmental Change*, 2001.

S. J. Russell and P. Norvig. *Artificial Intelligence: A Modern Approach, Third Edition*. Prentice-Hall, 1995. ISBN 0131038052. doi: 10.1007/s11894-010-0163-7.

J. Sahlin, M. A. Mostafavi, A. Forest, and M. Babin. Assessment of 3d spatial interpolation methods for study of the marine pelagic environment. *Marine geodesy*, 37(2):238–266, 2014.

P. Sakov and P. R. Oke. Objective array design: Application to the tropical Indian Ocean. *Journal of Atmospheric and Oceanic Technology*, 25(5):794–807, 2008. ISSN 07390572. doi: 10.1175/2007JTECHO553.1.

A. Savtchenko, D. Ouzounov, S. Ahmad, J. Acker, G. Leptoukh, J. Koziana, and D. Nickless. Terra and Aqua MODIS products available from NASA GES DAAC. *Advances in Space Research*, 34(4):710–714, 2004.

O. Schofield, S. Glenn, and M. Moline. The robot ocean network. *American Scientist*, 101 (6):434–440, 2013. doi: 10.1511/2013.105.434.

C. Scholin, S. Jensen, B. Roman, E. Massion, R. Marin, C. Preston, D. Greenfield, W. Jones, and K. Wheeler. The environmental sample processor (esp)-an autonomous robotic device for detecting microorganisms remotely using molecular probe technology. In *OCEANS 2006*, pages 1–4. IEEE, 2006.

M. Schwager, M. P. Vitus, S. Powers, D. Rus, and C. J. Tomlin. Robust adaptive coverage control for robotic sensor networks. *IEEE Transactions on Control of Network Systems*, 4(3):462–476, Sept 2017. ISSN 2325-5870. doi: 10.1109/TCNS.2015.2512326.

A. Sen Gupta. Generalized variance. *Encyclopedia of Statistical Sciences*, 4, 2004.

A. F. Shchepetkin and J. C. McWilliams. The regional oceanic modeling system (roms): a split-explicit, free-surface, topography-following-coordinate oceanic model. *Ocean modelling*, 9(4):347–404, 2005a.

A. F. Shchepetkin and J. C. McWilliams. The regional oceanic modeling system (ROMS): a split-explicit, free-surface, topography-following-coordinate oceanic model. *Ocean Modelling*, 9(4):347–404, 2005b.

G. M. Silsbe and S. Y. Malkin. Where light and nutrients collide: The global distribution and activity of subsurface chlorophyll maximum layers. In *Aquatic microbial ecology and biogeochemistry: A dual perspective*, pages 141–152. Springer, 2016.

A. Singh, R. Nowak, and P. Ramanathan. Active learning for adaptive mobile sensing networks. *Proceedings of the fifth international conference on Information processing in sensor networks - IPSN '06*, page 60, 2006. doi: 10.1145/1127777.1127790. URL `http://portal.acm.org/citation.cfm?doid=1127777.1127790`.

A. Singh, A. Krause, C. Guestrin, W. Kaiser, and M. Batalin. Efficient planning of informative paths for multiple robots. In *Proceedings of the 20th International Joint Conference on Artifical Intelligence*, IJCAI'07, pages 2204–2211, San Francisco, CA, USA, 2007. Morgan Kaufmann Publishers Inc. URL `http://dl.acm.org/citation.cfm?id=1625275.1625631`.

J. Skardhamar, D. Slagstad, and A. Edvardsen. Plankton distributions related to hydrography and circulation dynamics on a narrow continental shelf off northern norway. *Estuarine, Coastal and Shelf Science*, 75(3):381 – 392, 2007. ISSN 0272-7714. doi: https://doi.org/10.1016/j.ecss.2007.05.044. URL `http://www.sciencedirect.com/science/article/pii/S0272771407002041`. Hydrodynamic control of aquatic ecosystem processes.

D. Slagstad and T. A. McClimans. Modeling the ecosystem dynamics of the Barents Sea including the marginal ice zone: I. Physical and chemical oceanography. *Journal of Marine Systems*, 58(1-2):1–18, Oct. 2005. ISSN 0924-7963. URL `http://www.sciencedirect.com/science/article/B6VF5-4H98T19-1/2/e4b73b9ffefe92c45c7b28e227ffcde1`.

D. Slagstad, P. F. Wassmann, and I. Ellingsen. Physical constraints and productivity in the future arctic ocean. *Frontiers in Marine Science*, 2:85, 2015.

R. N. Smith, Y. Chao, B. H. Jones, D. a. Caron, P. P. Li, and G. S. Sukhatme. Trajectory design for autonomous underwater vehicles based on ocean model predictions for feature tracking. *Proceedings of the 7th International Conference on Field and Service Robotics*, pages 1–10, 2009. URL http://www.springerlink.com/index/916X02P6P77WT128.pdf.

R. N. Smith, J. Das, C. Yi, D. A. Caron, B. H. Jones, and G. S. Sukhatme. Cooperative multi-AUV tracking of phytoplankton blooms based on ocean model predictions. In *IEEE Oceans*, Sydney, 2010. ISBN 9781424452217. doi: 10.1109/OCEANSSYD.2010.5603594.

R. N. Smith, M. Schwager, S. L. Smith, B. H. Jones, D. Rus, and G. S. Sukhatme. Persistent ocean monitoring with underwater gliders: Adapting sampling resolution. *Journal of Field Robotics*, 28(5):714 – 741, 2011. URL http://cres.usc.edu/cgi-bin/print_pub_details.pl?pubid=710.

R. N. Smith, F. Py, P. Cooksey, G. Sukhatme, and K. Rajan. Adaptive Path Planning for Tracking Ocean Fronts with an Autonomous Underwater Vehicle. In *International Symposium on Experimental Robotics (ISER)*, Morocco, June 2016. doi: 10.1007/978-3-319-23778-7_50.

A. Sousa, L. Madureira, J. Coelho, J. Pinto, J. Pereira, J. B. Sousa, and P. Dias. Lauv: The man-portable autonomous underwater vehicle. *IFAC Proceedings Volumes*, 45(5):268 – 274, 2012. ISSN 1474-6670. doi: https://doi.org/10.3182/20120410-3-PT-4028.00045. URL http://www.sciencedirect.com/science/article/pii/S1474667016306140. 3rd IFAC Workshop on Navigation, Guidance and Control of Underwater Vehicles.

R. Stewart. *Introduction to physical oceanography*. University Press of Florida, 2009. ISBN 9781616100452. doi: 10.1119/1.18716.

D. R. Thompson, D. S. Wettergreen, and F. J. C. Peralta. Autonomous science during large-scale robotic survey. *Journal of Field Robotics*, 28(4):542–564, 2011.

S. Thorpe. Langmuir circulation. *Annual Review of Fluid Mechanics*, 36(1):55–79, 2004. doi: 10.1146/annurev.fluid.36.052203.071431. URL https://doi.org/10.1146/annurev.fluid.36.052203.071431.

A. Troccoli. A proposal for correcting the wind stress forcing of an ocean model. In *EGS-AGU-EUG Joint Assembly*, 2003.

R. van der Merwe, T. K. Leen, Z. Lu, S. Frolov, and A. M. Baptista. Fast neural network surrogates for very high dimensional physics-based models in computational oceanography. *Neural Networks*, 20(4):462–478, 2007.

S. Van Gennip, A. P. Martin, M. A. Srokosz, J. T. Allen, R. Pidcock, S. C. Painter, and M. C. Stinchcombe. Plankton patchiness investigated using simultaneous nitrate and chlorophyll observations. *Journal of Geophysical Research: Oceans*, 121(6):4149–4156, 2016.

J. Vanhatalo et al. *Speeding up the inference in Gaussian process models*. Phd thesis, Aalto University School of Science and Technology, 2010. URL http://lib.tkk.fi/Diss/2010/isbn9789526033815/isbn9789526033815.pdf.

Q. Vanhellemont and K. Ruddick. Acolite for sentinel-2: Aquatic applications of msi imagery. In *Proceedings of the ESA Living Planet Symposium, Pragur, Czech Republic*, pages 9–13, 2016.

C. Von Alt. Autonomous underwater vehicles. In *Autonomous Underwater Lagrangian Platforms and Sensors Workshop*, volume 3, 2003.

C. J. von Alt and J. Grassle. Leo-15, an unmanned long-term environmental observatory. In *Proc. Oceans*, volume 92, pages 849–854, 1992.

P. Wassmann, D. Slagstad, C. W. Riser, and M. Reigstad. Modelling the ecosystem dynamics of the Barents Sea including the marginal ice zone: II. Carbon flux and interannual variability. *Journal of Marine Systems*, 59(1-2):1–24, Jan. 2006. ISSN 0924-7963. URL http://www.sciencedirect.com/science/article/B6VF5-4J140YJ-1/2/14301cbdd82f300a5035491d9e072b35.

P. Wassmann, D. Slagstad, and I. Ellingsen. Primary production and climatic variability in the european sector of the arctic ocean prior to 2007: preliminary results. *Polar Biology*, 33(12):1641–1650, Dec 2010. ISSN 1432-2056. doi: 10.1007/s00300-010-0839-3. URL https://doi.org/10.1007/s00300-010-0839-3.

P. J. Werdell and S. W. Bailey. An improved in-situ bio-optical data set for ocean color algorithm development and satellite data product validation. *Remote sensing of environment*, 98(1):122–140, 2005.

N. K. Yilmaz, C. Evangelinos, P. F. Lermusiaux, and N. M. Patrikalakis. Path Planning of Autonomous Underwater Vehicles for Adaptive Sampling Using Mixed integer Linear Programming. *IEEE Journal of Oceanic Engineering*, 33(4):522–537, 2008. ISSN 0364-9059. doi: 10.1109/JOE.2008.2002105.

D. R. Yoerger, A. M. Bradley, and B. B. Walden. The autonomous benthic explorer (abe): A deep ocean auv for scientific seafloor survey. *Oceanogi. aphic*, page 79, 1991.

Z. Zeng, L. Lian, K. Sammut, F. He, Y. Tang, and A. Lammas. A survey on path planning for persistent autonomy of autonomous underwater vehicles. *Ocean Engineering*, 110: 303–313, 2015. ISSN 00298018. doi: 10.1016/j.oceaneng.2015.10.007. URL http://dx.doi.org/10.1016/j.oceaneng.2015.10.007.

B. Zhang and G. S. Sukhatme. Adaptive Sampling for Estimating a Scalar Field using a Robotic Boat and a Sensor Network. *Proceedings of the IEEE Conference on Robotics and Automation*, 4(April):3673 – 3680, 2007.

# Appendix A

# Field Deployments

Field testing and implementation has been an important factor in this Thesis, where a number of experiments have been conducted across a wide range of locations and environments. The important efforts are listed below in Table A.1, listed chronologically, with a brief comment on the type of activity and associated paper.

Table A.1: Field deployments, associated papers, and activities. Abbreviations and conventions used in the table can be found on page *ix*.

| Paper | Location | Year | Duration | Activity |
|---|---|---|---|---|
| - | Svalbard, Longyearbyen | 2016 | 12 days | Deployment with REMUS 100 type AUV. Oceanographic and benthic survey activity in Adventsfjorden. |
| - | Norway, Trondheim, Rissa | 2016 | 3 days | Deployment with REMUS 100 type AUV and SeaBotix ROV. Benthic survey of landslide. |
| D | Norway, Trondheim Fjord | 2016 | 1 week | Deployment with Sperre 30k work class ROV. Field trials for autonomous intervention activity with ROVs. |
| - | Norway, Agdenes | 2016 | 3 days | Deployment of multi-vehicle operation with AUV, USV, UAV for heterogeneous long range radio networks (Ludvigsen et al., 2016). |
| A | Norway, Froya | 2016 | 3 days | Deployment with REMUS 100 type AUV. Preliminary study and planning for the ENTiCE oceanographic project. |
| - | Norway, Slettvik | 2016 | 3 days | Deployment of new type of water column and benthic AUV (LAUV). Work shop on LAUVs (responsible for training NTNU crew on new crafts). |
| - | Svalbard, Ny-Ålesund | 2017 | 5 weeks | Deployment of LAUV (oceanographic and benthic AUVs) during the polar night. Testing of adaptive surveys and data collection in harsh environments. |
| - | Portugal, Porto | 2017 | 1 week | Deployment of LAUV (oceanographic AUV). Adaptive data collection strategies for tracking river plumes (Pinto et al., 2018). LSTS organized project. |

| | | | | |
|---|---|---|---|---|
| A | Norway, Froya | 2017 | 2 weeks | Deployment of LAUV (oceanographic AUV). Adaptive data collection strategies for reducing error in synthetic ocean models. ENTiCE project. |
| B | Norway, Runde | 2017 | 1 week | Deployment of LAUV (oceanographic AUV). Adaptive data collection strategies for mapping chlorophyll distributions in 3D. |
| - | Svalbard, Longyearbyen | 2017 | 8 days | Deployment with LAUV (oceanographic and benthic AUVs). Oceanographic and benthic survey activity in Adventsfjorden and Tempelfjorden. |
| - | Norway, Trondheim Fjord | 2017 | 3 days | Deployment of multi-vehicle operation with LAUV and USV (Jetyak). |
| F | Norway, Trondheim Fjord | 2017 | 4 days | Testing of backseat driver for FFI HUGIN AUV, autonomous tracking of fronts in Korsfjorden. |
| C | US, Monterey | 2018 | 2 weeks | MBARI's CANON project, June 2018. Multiple deployments in Monterey Bay, with WaveGlider and other assets. |
| - | Svalbard, Arctic Ocean | 2018 | 2 weeks | Deployment with LAUV (oceanographic) autonomous tracking of polar fronts. The Nansen Legacy Project. |

# Part II

# Articles

# Article A

## Information-Driven Robotic Sampling in the Coastal Ocean

**Trygve Olav Fossum**, Jo Eidsvik, Ingrid Ellingsen, Morten Omholt Alver, Glaucia Moreira Fragoso, Geir Johnsen, Renato Mendes, Martin Ludvigsen and Kanna Rajan



This article is published in
*Journal of Field Robotics* Volume 8, Issue 7, pages 1101-1121, 2018.
doi: 10.1002/rob.21805

Received: 26 October 2017 | Revised: 13 April 2018 | Accepted: 8 June 2018

DOI: 10.1002/rob.21805

REGULAR ARTICLE

WILEY

# Information-driven robotic sampling in the coastal ocean

Trygve Olav Fossum[1,2] | Jo Eidsvik[3] | Ingrid Ellingsen[4] | Morten Omholt Alver[4] | Glaucia Moreira Fragoso[5] | Geir Johnsen[2,5,6] | Renato Mendes[7,8,9] | Martin Ludvigsen[1,2,6] | Kanna Rajan[2,7,10]

[1]Department of Marine Technology, Norwegian University of Science and Technology (NTNU), Trondheim, Norway

[2]Centre of Autonomous Marine Operations and Systems (AMOS), Trondheim, Norway

[3]Department of Mathematical Sciences, Norwegian University of Science and Technology (NTNU), Trondheim, Norway

[4]SINTEF Ocean AS, Trondheim, Norway

[5]Department of Biology, Norwegian University of Science and Technology (NTNU), Trondheim, Norway

[6]University Centre in Svalbard (UNIS), Longyearbyen, Norway

[7]Underwater Systems and Technology Laboratory, Faculty of Engineering, University of Porto (UP), Portugal

[8]Interdisciplinary Center for Marine and Environmental Research (CIIMAR), UP, Portugal

[9]Physics Department, CESAM, University of Aveiro, Portugal

[10]Department of Engineering Cybernetics, Norwegian University of Science and Technology (NTNU), Trondheim, Norway

**Correspondence**
Trygve Olav Fossum, Department of Marine Technology, Norwegian University of Science and Technology (NTNU), Otto Nielsens Veg 10, NO-7491, Trondheim, Norway.
Email: trygve.o.fossum@ntnu.no

**Funding information**
Nansen Legacy Program, Grant/Award Number: 27272; Senter for Autonome Marine Operasjoner og Systemer, Grant/Award Number: 223254; Norges Forskningsråd, Grant/Award Number: 255303/E40; European Union's Seventh Framework Programme (FP7/2007–2013), Grant/Award Number: 270180

## Abstract

Efficient sampling of coastal ocean processes, especially mechanisms such as upwelling and internal waves and their influence on primary production, is critical for understanding our changing oceans. Coupling robotic sampling with ocean models provides an effective approach to adaptively sample such features. We present methods that capitalize on information from ocean models and in situ measurements, using Gaussian process modeling and objective functions, allowing sampling efforts to be concentrated to regions with high scientific interest. We demonstrate how to combine and correlate marine data from autonomous underwater vehicles, model forecasts, remote sensing satellite, buoy, and ship-based measurements, as a means to cross-validate and improve ocean model accuracy, in addition to resolving upper water-column interactions. Our work is focused on the west coast of Mid-Norway where significant influx of Atlantic Water produces a rich and complex physical–biological coupling, which is hard to measure and characterize due to the harsh environmental conditions. Results from both simulation and full-scale sea trials are presented.

**KEYWORDS**

Gaussian processes, marine robotics, ocean modeling, ocean sampling, robotic sampling

## 1 | INTRODUCTION

The coastal waters (CWs) of Middle Norway, and the Froan archipelago is influenced by Atlantic Water (AW),* local water masses from the Trondheim Fjord (FW), and CW transported by Norwegian coastal current (NCC; Sætre, 2007). The elevated levels of mixing that occur increase the nutrient transport necessary for primary production—the main source of energy and basis for the marine food web. In addition to the influx of AW, complex coastal topography makes the region exceptionally productive and important in terms of marine life and biodiversity, with a broader ecological, scientific, and social-economical significance (Sætre, 2007). Despite this, little is known about the basic



* AW is defined by a salinity ≥35.0 and temperature >3 °C, CW has a salinity ≥34.7 and a wider temperature range (Sakshaug, Johnsen, & Kovacs, 2009), while FW is related to salinities below 34.7.

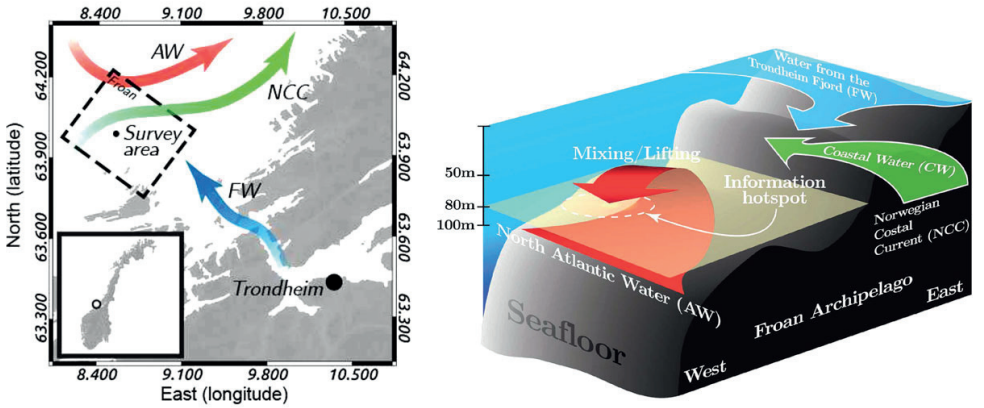


**FIGURE 1** (a) The Middle-Norway coastal region and the Froan archipelago. The location of the survey area and its relation to the Norwegian coastline (inset). (b) The physical driving forces in the Froan area, the coastal region of investigation. The convergence of different currents at the Froan archipelago, where influx of Atlantic Water (AW) is predicted to provide nutrient rich deep water, which accentuates primary productivity. In order to understand the region's significance it is essential to sample this influx, which is an "information hotspot"

driving mechanisms and their effect on the marine ecosystem (Asplin, Salvanes, & Kristoffersen, 1999). The spatial and temporal scales of ocean processes make it unrealistic to deploy vast resources to record these dynamics in detail. Consequently, the use of ocean models to represent the dynamics is critical for realizing sampling strategies that return information with high scientific quality. Together with the complex bio-geophysical interactions involved, this forms the motivation for the development of information-driven sampling strategies, which is the focus of this paper.

With the increasing availability of high-end computational resources accessible to oceanographers, multiresolution modeling of the upper water-column, for predictive or post hoc purposes, has been a new and viable tool to understand complex interactions between physical and biological features. However, modeling skill is still at a level where physical, biological, and chemical features related to ocean structure and circulation cannot be used to make accurate predictions at scales sufficient for definite representation (Lermusiaux, 2006). To understand these upper water-column biogeochemical processes, scientists have to resort to direct observations (Stewart, 2009), which are typically sparsely distributed in both time and space leading to *undersampling*. Making intelligent and targeted observations is therefore becoming exceedingly important for oceanography, which is an expensive and demanding enterprise, restricted to static sensors placed on buoys, or measurements taken by personnel on ships.

Recently, mobile robotic platforms, such as autonomous underwater vehicles (AUVs), have become more affordable, robust and viable for scientific exploration, with greater functionality, increased scientific payload, and in-water duration, providing an efficient platform for autonomous collection of in situ oceanographic data.

Increasingly, ocean models and AUVs are being combined to address this common problem of undersampling and uncertainty. We describe one methodology involved in combining these resources toward developing sampling methods that can capitalize on the expressiveness of the model and in situ information. Having access to both prior (model) and current (sensor) information, AUVs can operate on an a posterior knowledge, allowing execution to be adjusted according to the geographical context and the upper ocean feature(s) of interest. This leads to a sampling strategy that can both improve model accuracy and exceed traditional approaches in locating and mapping oceanographic phenomena. To support and verify such an approach, data inputs from multiple sources, including remote sensing satellite data, ship-based measurements, near real-time data from buoys, drifters, and other robotic platforms are necessary. This in turn enables cross-verification, assimilation, and adjustment of model parameters, as well as analysis of AUV performance.

The unification of models, remote sensing resources, and different robotic elements is essential in order to increase the predictive power of models for effective autonomous ocean sampling. Our work is motivated from campaigns such as the Autonomous Ocean Sampling Network (`AOSN-I/-II`; Curtin, Bellingham, Catipovic, & Webb, 1993; Ramp et al., 2009), and the Controlled Agile and Novel Observation Network (`CANON`) field program (Das et al., 2010, 2012), both from Monterey Bay, California. It brings together biological and physical oceanography with autonomous robotic control while providing focus on the Froan archipelago, located outside the CWs of Middle Norway, see Figure 1. In addition to AUVs, data were collected from satellites, buoys, surface autonomous platforms (WaveGlider[†]), and ship-based surveys, primarily as a means to ground truth in situ robotic data. Data collection in the Froan area is particularly challenging due to inclement weather, narrow straights, complex bathymetry, and its remote location. An overview of the system setup for the campaign is shown in Figure 2.

The paper is organized as follows. Section 2 provides the context of this work in relation to other efforts. Section 3 provides definitions and reviews background information on ocean sampling, modeling, methods, and data assimilation. Section 4 is the core of our paper

[†] The WaveGlider and payload storage was damaged upon recovery, and is therefore not included in this work.

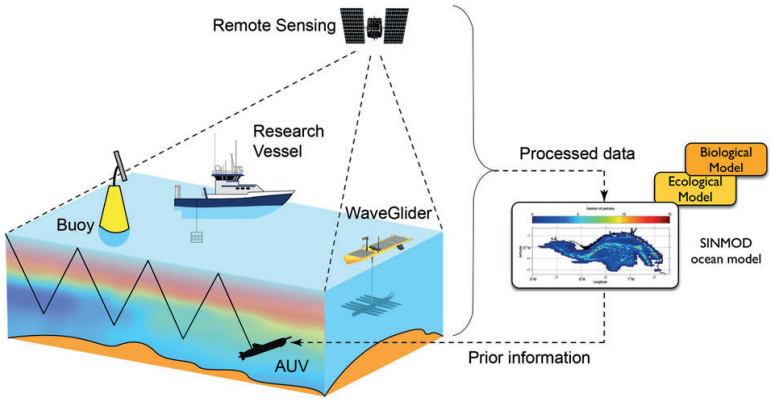


**FIGURE 2** System block diagram of the platforms used in the sampling campaign: Ocean model SINMOD, moored buoy (temperature, salinity, and biological measurements), research vessel (biological and physical measurements), remote sensing (temperature and chlorophyll *a*), autonomous surface vehicle (temperature, salinity, and weather data), and an AUV (biological and physical measurements)

and articulates the approach and the specific algorithm we have developed. Section 5 provides an in-depth perspective on the field experiments and the subsequent analysis from various data sources. Finally, Sections 6 and 7 conclude with a summary discussion, conclusions, and future work.

## 2 | RELATED WORK

Our work is related to informative sampling strategies and autonomous data collection in the ocean. There is a large body of literature on maximizing information gain from in situ measurements to characterize phenomena, or providing estimation of a scalar field. Zhang and Sukhatme (2007) showed adaptive sampling schemes for reconstructing a temperature field using a sensor network of both static and mobile sensors, while Graham et al. (2012) discussed the use of Gaussian processes (GPs) and the problems relating to environment reconstruction in the ocean with different correlation kernels. Yilmaz, Evangelinos, Lermusiaux, and Patrikalakis (2008) used a mixed integer programming utility combining reduction of uncertainty and physical constraints. Chekuri and Pal (2005) optimized informative paths using a recursive greedy approach with mutual information in directed graphs. Although adaptation is not the focus, the authors explore the utility of sampling a dynamic field in space and time. This concept is further studied for an application with multiple robots in Singh, Krause, Guestrin, and Kaiser (2009). Minimizing estimation error of a sampled field using optimal distribution of mobile sensors in the ocean is presented in Leonard et al. (2007). Low et al. (2011) discussed efficient information-theoretic path planning for sampling of GP-based fields using a Markov policy based on entropy, with empirical results on real-world temperature and plankton density field data. This is expanded to include anisotropic fields in Cao, Low, and Dolan (2013). Nonparametric optimization is explored in Zamuda, Hernandez Sosa, and Adler (2016), where a self-adaptation path planning scheme for a glider is developed for exploration of submesoscale eddies.

Ocean models are used to estimate the underlying current field toward improving energy efficiency and navigation for AUVs and gliders in Chang, Zhang, and Edwards (2015) and Rao and Williams (2009). Statistical estimation of surface currents using satellite data have also been suggested as an effective aid for handling dynamics in Frolov, Paduan, Cook, and Bellingham (2012). Online algorithms and decision strategies can also be trained and tuned using ocean models and Markov decision processes, and have been applied to AUVs influenced by spatial and temporal uncertainty in Ma, Liu and Sukhatme (2016). In situ identification of features using GP regression and supervised learning is presented in Das et al. (2015), with the aim to select optimal sampling points, for an AUV with water sampling capabilities. Similar approaches are also used in Bayesian optimization, where for instance Marchant et al. (2014) formulate a Monte Carlo tree search for robot path planning. Ling, Low, and Jaillet (2016) have developed an approximate dynamic programming approach in a similar vein, where the reward function includes the posterior mean and not only variance terms (which do not depend on the data).

The work presented here is also associated with sensor placement problems that have been explored for GPs in Guestrin, Krause, and Singh (2005), Krause, Guestrin, Gupta, and Kleinberg (2006), and Krause, Singh, and Guestrin (2008) who use a greedy algorithm for maximizing mutual information. Coupling adaptation and modeling is studied in Smith et al. (2010, 2011), Smith, Py, Cooksey, Sukhatme, and Rajan (2016) employing prior information from ocean models and adaptive approaches for the characterization of a frontal system and sampling phytoplankton blooms. Binney, Krause, and Sukhatme (2010) use the measure of *mutual information* and Gaussian approximation techniques to relate the sampled and unsampled locations, optimizing information gain along a 2D path for a glider. This is further elaborated considering time variation with a surface vehicle in Binney, Krause, and Sukhatme (2013).

Our work presents an end-to-end, real-world implementation, of an information-theoretic sampling system for environmental sensing of the upper water-column that combines information from ocean models and in situ measurements, using a balance between variance and gradient based measures. We show how integration and utilization of ocean model data can be leveraged in GP modeling and used for

directing sampling efforts to regions of high scientific interest. Specifically, this involves modifying the probabilistic model using data to develop a nonstationary correlation kernel and a bias correcting mean. Finally, we present experimental validation and correlation with other marine data.

## 3 | BACKGROUND

### 3.1 | The SINMOD ocean model

Ocean models describe the state of the ocean at a given time based on a set of hydrodynamic and thermodynamic equations, commonly called the *primitive equations*, that are solved using numerical techniques. These equations provide information about currents, salinity, temperature, density, and pressure. In implementations, the equations are discretized in different ways, utilizing either structured or unstructured model grids horizontally, and using horizontal terrain-following or hybrid discretization vertically. The spatial resolution of an ocean model represents a trade-off between the geographical area to be simulated and the availability of computer hardware and time. Running the model involves computation of a large number of equations, typically implemented with parallelization in order to utilize more CPUs to reduce computing time. Because high-resolution modeling can only be done for relatively small geographical areas, models are commonly nested, that is, one simulates larger scale areas to produce boundary conditions for higher resolution models covering smaller areas. This process can be iterated several times, to achieve the desired detail. Models apply forcing by tides, sea-level pressure, wind, heat exchange, and freshwater runoff. Regional models additionally need prescribed states and currents at the open boundaries. Errors in the forcing data also impact the quality of the model output. This can typically be the accuracy of wind fields in coastal areas with strong topographic steering of near-surface wind. The quality of bathymetric data, type of grid used, and choice of numerical techniques are other factors that influence ocean model output.

Model performance can be evaluated using observations from different platforms such as AUVs, buoys, or ship-based sampling. Due to the chaotic nature of the processes in the upper water-column, the scale and accessibility of the ocean makes it difficult to obtain sufficient measurements, both for validation purposes and for model correction. In addition to hindcast model validation and correction, information from in situ instrumentation can also improve the near-real-time forecast using persistent data assimilation into the oceanic model. Surface data are usually assimilated in operational models, mostly from satellite imagery. With advancing technology, AUVs will likely play an essential role in the process of data assimilation of water-column properties in such models. AUV data could also be assimilated into predictive models to reduce uncertainties, and in turn be used to guide subsequent AUV missions, thus closing the loop from measurements to modeling and back again (Howe et al., 2010). As shown by validation studies, for example, Forristall (2011), ocean models generally perform well with regard to statistical properties and tidal dynamics, while they show little skill in predicting currents from hour to hour in areas not dominated by tidal forces. There is therefore a need to develop enabling technology that performs efficient and targeted sampling of the ocean. Robotic methods in sampling are therefore critical for assessing model accuracy and shortcomings, as well as reducing environmental uncertainty and characterization.

SINMOD is a coupled 3D hydrodynamic and biological model system (Slagstad & McClimans, 2005; Wassmann, Slagstad, Riser, & Reigstad, 2006). Its hydrodynamic component is based on the primitive equations that are solved using finite difference techniques using a *z*-coordinate regular grid with square cells. The model has been used for ocean circulation and ecosystem studies along the Norwegian coast and in the Barents Sea (Wassmann, Slagstad, & Ellingsen, 2010; Ellingsen, Slagstad, & Sundfjord, 2009; Skarðhamar, Slagstad, & Edvardsen, 2007), in ecosystem risk assessment studies (Broch et al., 2013), kelp cultivation potential (Broch, Slagstad, & Smit, 2013) and in climate change effect studies (Ellingsen, Dalpadado, Slagstad, & Loeng, 2008; Slagstad, Wassmann, & Ellingsen, 2015).

In addition to forecasts, SINMOD is capable of providing hindcast and short-term predictions (nowcasts) up to 48 hr. The term *hindcast* is used to describe an after-the-fact analysis or resimulation, where initial conditions, and other model inputs are taken from actual observations. For the production of forecast and nowcast data for the Frøya and Froan region, SINMOD has been set up in a 160-m resolution mode using boundary conditions computed from the operational coastal model system Norkyst800[‡] run by the Norwegian Meteorological Institute (MET).[§] This is a configuration with the Regional Ocean Model System ocean model (Shchepetkin & McWilliams, 2005) for the Norwegian coast with a horizontal resolution of 800 m (Albretsen, 2011). Additionally, SINMOD uses atmospheric input from MEPS 2.5 (Müller et al., 2017) operational weather forecast, by MET (2.5 km horizontal resolution), as well as climatological data for freshwater runoff. For our sampling area in the Froan archipelago, the boundary conditions mediate the tidal circulation and the regional features such as the NCC. They determine the fluxes into and out of the model area, and thereby have a strong influence on model values computed within the area. A snapshot of evolving current speed is shown in Figure 3 as an example of model output.

### 3.2 | Ocean sampling

Sampling in the ocean is subjected to a broad range of spatial and temporal (including episodic) variability. Often, it is not possible to examine the entire environment in detail, and only a quasi-synoptic (i.e., a non-holistic recording of an event) coverage is possible. This is the sampling problem in oceanography and the lack of sufficient observations is the largest source of error in our understanding (Stewart, 2009), making *when and where* to sample the key problem for designing oceanographic experiments.

Addressing these questions requires a detailed and holistic perspective of the ocean and the interacting processes within. Field experiments, when augmented by ocean models, such as SINMOD, can be

[‡] https://goo.gl/H4Rbw2.

[§] https://www.met.no.

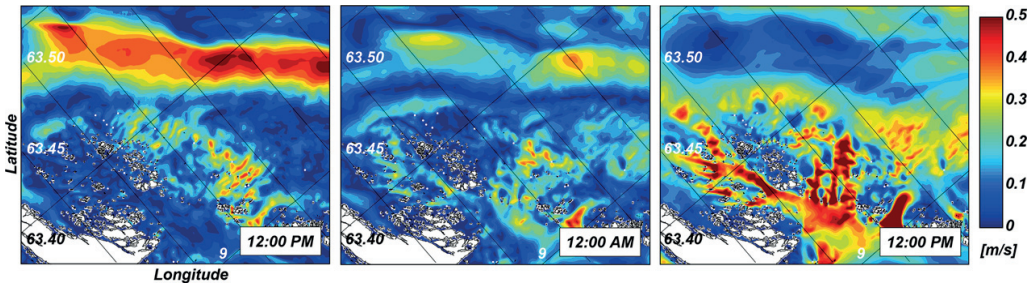


**FIGURE 3** Snapshots of typical ocean surface current speeds in the Frøya–Froan region from SINMOD forecasts (nowcasts) from the 5th to 6th of May 2017

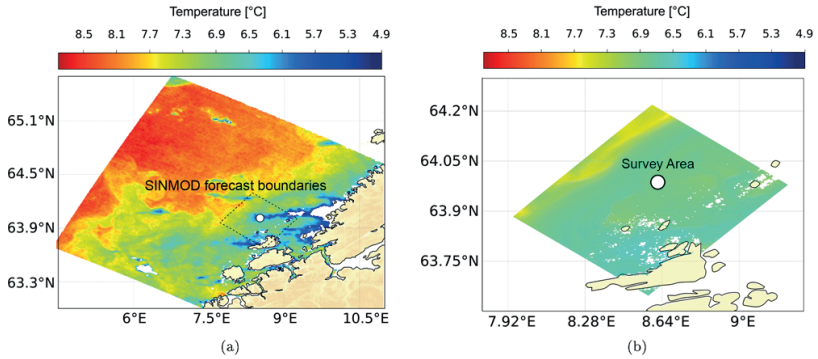


**FIGURE 4** L2 products from MODIS-Aqua (https://oceancolor.gsfc.nasa.gov/, $1 \times 1$ km$^2$ resolution) for our operational area in the Frøya–Froan region. (a) Sea surface temperature (SST) from Mid-Norway on May 5 at 02:55 a.m. SINMOD SST forecast at 03:00 a.m. The operational area in satellite images is often affected by cloud cover, masking the true underlying ocean temperature

used to simulate, analyze, and plan sampling strategies prior to full-scale deployment. By doing so, sampling resources can target the phenomenon, or the area, of interest in sufficient detail with appropriate sensors. However, numerical ocean models suffer from several sources of errors: practical simplifications, inexact representations or parameterizations, numerical implementations (Lermusiaux, 2006), and the inability to resolve subgrid features, that is, treatment of turbulent dynamics (Troccoli, 2003). This prompts the need for in situ measurements and direct characterization to augment and cross-validate predictions.

Sampling the ocean environment and the latent ecosystem is therefore ideally a joint effort between a range of sources, much as we do in this work, as coincident information about physical (i.e., temperature, salinity, and currents) and biological variables (i.e., light regime, fluorescence, and plankton species) can span multiple temporal and spatial scales. Remotely sensed satellite data can provide repeated large-scale surface observations, such as sea surface temperature (SST), as illustrated in Figure 4, and products of chlorophyll *a* concentration—which represents a phytoplankton biomass indicator. SST satellite products are measured by infrared radiometers over the surface skin layer of the ocean (i.e., <1 mm thick). The temperature of this skin layer is often cooler than the body of water below commonly measured by in situ instruments due to heat flux, with the direction of flux typically from the ocean to the atmosphere. The gradients between these layers are highly dependent on meterological conditions (Minnett & Kaiser-Weiss, 2012). The spatial resolution is rarely below $1 \times 1$ km in ocean-oriented remote sensing data such as from NASA's MODIS-Aqua (Savtchenko et al., 2004) and about $300 \times 300$ m in the Sentinel-3 constellation mission as part of ESA's Copernicus program (Donlon et al., 2012). Ocean color based products, such as chlorophyll *a*, are calculated using an empirical relationship derived from in situ measurements of chlorophyll concentration and remote sensing reflectances in the blue-to-green region of the visible spectrum. The spatial resolution of the standard chlorophyll products has the same order of magnitude as SST. However, it is possible to derive chlorophyll information from new satellite terrestrial oriented missions as Landsat-8 (OLI sensor) and Sentinel-2 (MSI sensor), which provide data at more relevant spatial scales of 10–60 m (Vanhellemont & Ruddick, 2016). Ocean color satellite data do not cover the water column beyond the first optical attenuation length as defined by Beer's Law, where 90% of remotely sensed radiance originates from (Werdell & Bailey, 2005); this can be too coarse for critical biophysical ocean processes (Moses, Ackleson, Hair, Hostetler, & Miller, 2016). Further, optical remote sensing observations are highly susceptible to cloud cover for certain measurements.

Traditional techniques, like shipboard and moored measurements, can be effective at large spatial (**O**(100 km)) and temporal (**O**(week to months)) scales, but have proved difficult for submesoscale (smaller

than an internal Rossby radius of (**O**(10 km))) variability (Graham et al., 2012). The importance of these dynamics for physical ocean processes is significant (Barth, Hebert, Dale, & Ullman, 2004) and directly influences primary production (Lévy, 2003) and patch formation (Franks, 1992) of biological signatures.

The use of autonomous and adaptive capabilities allows for responsiveness to interactions as they occur, the opportunity to alter the sampling strategy based on the data available, as well as the sampling resolution in regions of high interest. These factors coupled with the *gaps in observations*, left by other marine data sources, have made marine robotic platforms an integral part of ocean observation.

### 3.3 | Spatial models and gaussian processes

A prerequisite for doing adaptation and to determine suitable future actions is to have information about the spatial conditions in the area of interest, especially in dynamic environments. Having a high-fidelity numerical ocean model operating onboard a robotic platform is currently infeasible, as the required numerical resolution in both time and space translates into high computational demands. To overcome this problem, a stochastic surrogate model (also known as a proxy or a reduced order model) based on GPs can be used. Apart from having a smaller computational footprint, GPs are conventional tools for dealing with statistical modeling of spatial data and have been widely adopted in oceanographic applications (Binney et al., 2013).

A GP is in essence a collection of random variables that have a *multivariate normal probability density function*. When variables are allocated to spatial locations, a GP is a model that allows spatial dependence to be modeled using covariance functions. Due to its representational flexibility, it is often a popular way to represent environmental processes (see, e.g., Banerjee, Carlin, and Gelfand, 2014; Cressie & Wikle, 2011). Formally

> *Consider a real-valued stochastic process* $\{X(s),\ s \in \Omega\}$, *where* $\Omega$ *is an index set where* $\Omega \subset \mathbb{R}^2$. *This stochastic process is a GP if, for any finite choice of n distinct locations* $\boldsymbol{s}_1 \ldots, \boldsymbol{s}_n \in \Omega$, *the random vector* $\boldsymbol{x} = [x(\boldsymbol{s}_1), \ldots, x(\boldsymbol{s}_n)]$ *has a multivariate normal probability density function:*

$$p(\boldsymbol{x}) = N(\boldsymbol{\mu}, \boldsymbol{\Sigma}) = \frac{1}{(2\pi)^{\frac{n}{2}} |\boldsymbol{\Sigma}|^{\frac{1}{2}}} e^{-\frac{1}{2}(\boldsymbol{x}-\boldsymbol{\mu})^T \boldsymbol{\Sigma}^{-1}(\boldsymbol{x}-\boldsymbol{\mu})}, \tag{1}$$

> *defined by the mean vector* $\boldsymbol{\mu} = E(\boldsymbol{x})$, *and the symmetric positive definite covariance matrix* $\boldsymbol{\Sigma} = cov(\boldsymbol{x}, \boldsymbol{x})$.

The popularity of GPs is often attributed to two essential properties. First, as shown in Equation 1, they can be fully expressed using only a *mean* and a *covariance function* (also known as a *kernel*). This alleviates model fitting, as only the first- and second-order moments need to be specified (Davis, 2014). Second, the procedure for prediction and assimilation is inherent to the fundamental equations of the model, making this step uncomplicated once the GP is formulated. Furthermore, as long as it is possible to estimate the covariance function, a GP can be used on the basis of sparse prior data. In environmental applications, a GP typically characterizes random variation at points in space, time, or both, discretized down to a grid map with a certain spatiotemporal resolution.

The focus of the statistical model applied in this work is to approximate the underlying distribution of ocean temperature, specified from hindcast data from SINMOD. Using a GP to model temperature as a spatial phenomenon has been studied before (e.g., Cressie & Wikle, 2011; Graham et al., 2012). Based on the characteristics of our ocean model data, the GP is a reasonable model to use for temperatures, as no heavy tails or skewness was significant in the temperature data used for modeling. Furthermore, the GP we use here has a random bias parameter that allows the entire temperature field to be corrected up or down to account for errors in the priors, more details are given in Section 4.1. Such hierarchical GPs (Banerjee et al., 2014) can be useful for adding flexibility in modeling, and therefore viable as a primary building block. The motivation for using temperature is related to a number of factors, which are explained in detail next.

### 3.4 | Temperature as an information utility

In addition to salinity (S), water temperature (T) plays an outsize role in a variety of oceanographic processes. Together, they provide a strong coupling between physical and biological factors, which are at the heart of the marine life-cycle. In addition, T can be cross-validated using remote sensing data. Physical phenomena such as upwelling, vertical mixing, eddies, fronts, and currents can coincide with temperature variation and gradients (Sverdrup, Duxbury, & Duxbury, 2006), as well as the distribution and accumulation of biological activity (Gordoa, Masó, & Voges, 2000). For example, high variability in T would be visible in frontal zones, where having a T front gliding by a Lagrangian point, would result in a greater gradient in T compared to a region with more stable dynamic conditions. Consequently, T and S play a central role in ocean models, and their broad influence as physical parameters on these nonlinear processes makes them a useful tool for exploring the model error (Holt, Allen, Proctor, & Gilbert, 2005). Using T and S to guide robotic data collection is not new (see, e.g., Zhang, Sukhatme, and Requicha, 2004; Smith, Py, Cooksey, Sukhatme, and Rajan, 2016).

Off the Froan archipelago, results from SINMOD show a combination of stratified and mixed waters, with periodic mixing and lifting of warm and dense AW (Figure 5), creating underwater fronts with higher T gradients, most prominent at 70–90 m depth. The sampling strategy was therefore to concentrate on data collection from this zone with the assumption that the temperature at these depths would be fairly homogeneous, except in areas influenced by AW. Lifting and mixing of AW is important not only for primary productivity, as the AW brings nutrient rich waters to the euphotic zone (0–75 m), but also for the structure and function of the ecosystem. The local bathymetry in the area results in narrowing and strengthening of the NCC outside the Froan archipelago (Sætre, 2007). In combination with high internal wave activity modeled by SINMOD, this results in a dynamic environment and with high variability in S and T, making these *information hot spots* for ocean scientists.

These complex dynamics make the area challenging to model and thus highly relevant for assessing model accuracy. Further, strong dynamics are usually hard to model, especially at smaller scales, and

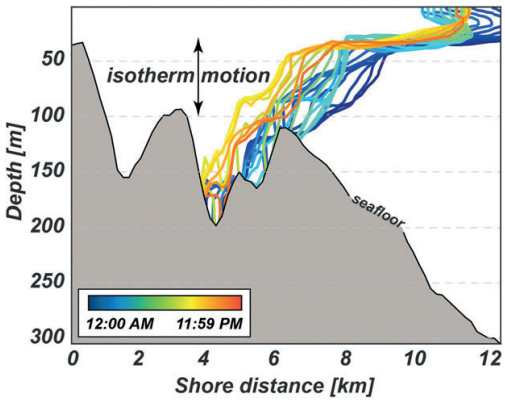


**FIGURE 5** Atlantic Water 6.8 °C thermal contour (isotherm) motion from SINMOD simulations, showing the interface shift at the Froan archipelago, for a 24-hr period for May 5th. Note the isotherm shift from 70 to 90 m consistent with our assumptions for data assimilation (see Section 4.2)

resolving sharp temperature gradients is challenging in ocean models (Trenberth, 1992). Sampling the water structure and associated temperature dynamics would, therefore, augment the model and in addition provide vital phenomenological context.

## 4 | METHODS

Coupling sampling with model-derived information is necessary to improve the capability to study and understand ocean processes that involve physical and biological interactions. Our comprehension of biogeochemical interactions in the upper ocean is, to a large extent, dependent on how ocean models render related processes. Exploring sampling from an ocean model perspective requires us to focus on model shortcomings and inaccuracies, in addition to in situ measurements. The method below is motivated by the characteristics for the Froan archipelago, with temperature as the primary variable of focus for the sampling strategy. However, the approach is general in nature, with a pipeline that can be used to approach sampling, while leveraging data from an ocean model. The following section articulates the approach starting with (a) the discretization and spatial modeling of the phenomena using model data, (b) formulation of the objective function toward a scientific context, and (c) algorithmic implementation. The approach presented here is a *greedy/best-first* search, using a one-node horizon, that is, the method is myopic. This is assumed to be sufficient as the model data have substantial uncertainty that is inherited by the sensing strategy. Moreover, due to control, actuation, and navigational errors in part due to ocean currents, the position of the AUV will deviate from any "optimal" route—a more detailed discussion about myopic versus nonmyopic approaches are given in Section 6.

### 4.1 | Gaussian process specification

Referring to the definition given in Equation 1, the prior mean $\boldsymbol{\mu} = [\mu_1, \ldots, \mu_n]$ is established by simply extracting the statistical mean temperature for each location $i = 1, \ldots, n$. In our case, the data used are a 160-m resolution SINMOD hindcast data set from May 2016, taken at the planned deployment time (~10 a.m.) as

$$\mu_i(\beta_0) = \frac{1}{m}\sum_{j=1}^{m} x_{ij} + \beta_0 = \bar{x}_i + \beta_0, \tag{2}$$

where $x_{ij}$ is the temperature at location $i$ for the current day $j$, $m$ is the number of days evaluated from the model, and $\beta_0$ is a bias correction term, enabling the AUV to, in situ, correct the prior mean toward the true underlying temperature field, based on the first measurements. As the GP is specified in two dimensions, the mean values constitute a 2D temperature surface. Correction of this surface, using a bias term, allows the AUV to shift all temperatures in unison toward the true mean ocean temperature. The covariance matrix $\boldsymbol{\Sigma}$ is given as

$$\boldsymbol{\Sigma} = \begin{bmatrix} \Sigma_{11} & \Sigma_{12} & \cdots & \Sigma_{1n} \\ \Sigma_{21} & \Sigma_{22} & \cdots & \Sigma_{2n} \\ \vdots & \vdots & \ddots & \vdots \\ \Sigma_{n1} & \Sigma_{n2} & \cdots & \Sigma_{nn} \end{bmatrix},$$

where $\Sigma_{ij} = \sigma_i \sigma_j \mathcal{K}(i,j)$. Normally, the variance terms $\sigma_i^2$ and $\sigma_j^2$ are taken to be the same for all locations and collected as $\sigma^2$, making the covariance independent of location (i.e., stationary). Following Stein (2005), these variances are augmented further to include a spatially varying local variance to better suit the local variability—doing so makes measurements at high variance locations have less influence on neighboring locations. We then define the spatially varying variance as

$$\sigma_i^2 = \frac{1}{m}\sum_{k=1}^{m}(x_{ik} - \bar{x}_i)^2, \tag{3}$$

where $x_{ik}$, is the temperature at location $i$ for the current day $k$ and $\bar{x}_i$ is the average temperature for location $i$. We used the same 160-m resolution SINMOD hindcast temperature data from May 2016, to calculate the local temperature variance for the survey area. The kernel function is defined as

$$\mathcal{K}(i,j) = (1 + \phi h_{ij})e^{-\phi h_{ij}},$$

where $h_{ij} = |\boldsymbol{s}_i - \boldsymbol{s}_j|$, and $\phi$ is indicative of the correlation range (Matérn, 2013). Capturing the correct spatial correlation distance is particularly important. Formulating an accurate surrogate GP model depends on getting this parameter as correct as possible. One could also add anisotropy in this kernel, with correlations depending on north–east directions between locations, and the methodology presented next would still work. However, based on the ocean model data, there was no significant anisotropy in the current case.

A standard tool for estimating correlation range is the *variogram*. Given spatially dependent data, the variogram can estimate the degree of spatial correlation as a function of distance (Cressie & Wikle, 2011). The same hindcast temperature data from SINMOD was used to find $\phi$ using this procedure, as shown in Figure 6. The derived variogram is fitted from the residuals after the trend in the input data has been subtracted, under the assumption of smooth, slow-changing, spatial variance terms—this is necessary to obtain a correct evaluation of the

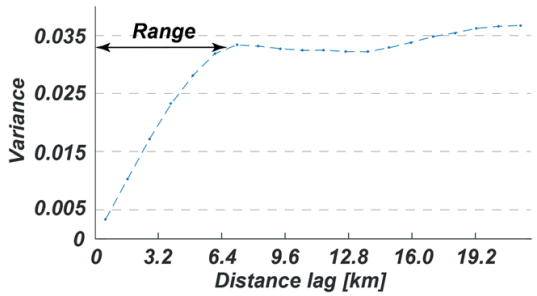


**FIGURE 6** The final variogram from analyzing SINMOD temperature data

underlying variability. As the distances increase along the *x*-axis, the spatial dependence decreases, increasing the variogram, until a limit is reached (horizontal black line on *y*-axis in Figure 6). At this limit, the points no longer yield any correlation based on data values, and it is therefore possible to provide the lag distance/range for the correlation at around 5–7 km. The parameter estimates could be improved using maximum likelihood estimation based on the density function in Equation 1 for the ocean model data, see e.g., Stein, Chi, and Welty (2004).

The GP we use, therefore, has a nonstationary kernel function and a bias correcting mean function, based on temperature data from SINMOD. Exploratory data analysis shows residual plots that are approximately Gaussian, justifying using a GP for temperature data in the current setting. The process $\boldsymbol{x}$ is assumed to be relatively constant over the data gathering period. To account for minor time variations, we add process noise $\boldsymbol{Q}_t$, that is accumulated over the survey period, to capture minor variability from sea currents (current velocity is typically 0.2 m/s on average (Figure 3), while vehicle speed over ground is about 1.5 m/s), see Equation 5.

## 4.2 | Data assimilation

Measurements are acquired sequentially for time steps $1, \ldots, T_f$, where $T_f$ is typically mission duration. Only measurements from a specific depth layer (70–90 m) are used for assimilation, to focus on the dynamics related to the characteristics of the Froan archipelago (see Section 3.4 and Figure 5 for further details).

A sampling design is defined by $d_1, \ldots, d_{T_f}$, where $d_t$ is a survey location at time $t$. The successive survey design until time $t$ is denoted by $\boldsymbol{d}_t = (d_1, \ldots, d_t)$. The measurement model for design $d_t$ at time $t$ is given by

$$\boldsymbol{y}_{t,d_t} = \boldsymbol{G}_{t,d_t}\boldsymbol{x} + \boldsymbol{v}_t, \tag{4}$$

where $\boldsymbol{y}_{t,d_t}$ is a $m_{t,d_t} \times 1$ vector of observations along a survey line, and the matrix $\boldsymbol{G}_{t,d_t}$ of size $m_{t,d_t} \times n$ contains "1" entries only at the designated $d_t$ indices, and 0 otherwise. The error term $\boldsymbol{v}_t \sim N(0, \boldsymbol{R}_{t,d_t})$ is measurement noise. The covariance matrix $\boldsymbol{R}_{t,d_t}$ is typically set to a constant matrix with only diagonal elements (Wunsch & Heimbach, 2007), and there is no dependence of measurement error terms over time.

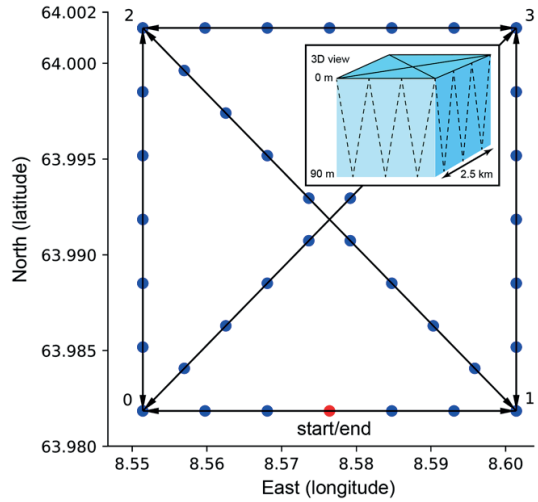


**FIGURE 7** The waypoint graph $G$ used in experiments in the Froan region, with the depth range 0–90 m. Because the AUV is undulating, the graph takes 4 hr to survey, visiting five nodes

Under Gaussian linear modeling assumptions, the sequential updating of data leads to the Gaussian distribution $p(\boldsymbol{x}|\boldsymbol{y}_{1,d_1}, \ldots, \boldsymbol{y}_{t,d_t})$. The common Gaussian equations for conditioning give the updated mean $\boldsymbol{m}_{t,d_t} = E(\boldsymbol{x}|\boldsymbol{y}_{1,d_1}, \ldots, \boldsymbol{y}_{t,d_t})$ and variance $\boldsymbol{P}_{t,d_t} = Var(\boldsymbol{x}|\boldsymbol{y}_{1,d_1}, \ldots, \boldsymbol{y}_{t,d_t})$ at every stage. These equations are recursive over the data gathering steps:

$$\begin{aligned}
\bar{\boldsymbol{P}}_{t,d_t} &= \boldsymbol{P}_{t-1,d_{t-1}} + \boldsymbol{Q}_t I(t = t_{wp}),\\
\boldsymbol{S}_{t,d_t} &= \boldsymbol{G}_{t,d_t}\bar{\boldsymbol{P}}_{t,d_t}\boldsymbol{G}^t_{t,d_t} + \boldsymbol{R}_{t,d_t},\\
\boldsymbol{K}_{t,d_t} &= \bar{\boldsymbol{P}}_{t,d_t}\boldsymbol{G}^t_{t,d_t}\boldsymbol{S}^{-1}_{t,d_t},\\
\boldsymbol{m}_{t,d_t} &= \boldsymbol{m}_{t-1,d_{t-1}} + \boldsymbol{K}_{t,d_t}(\boldsymbol{y}_{t,d_t} - \boldsymbol{G}_{t,d_t}\boldsymbol{m}_{t-1,d_{t-1}}),\\
\boldsymbol{P}_{t,d_t} &= \bar{\boldsymbol{P}}_{t,d_t} - \boldsymbol{K}_{t,d_t}\boldsymbol{G}_{t,d_t}\bar{\boldsymbol{P}}_{t,d_t}.
\end{aligned} \tag{5}$$

The first equation above, contains the step where the accumulated process noise $\boldsymbol{Q}_t$ is added, when reaching the waypoint goal (finishing a survey line) and activated by the indicator function $I(t = t_{wp})$, where $t_{wp}$ indicates the arrival time at a waypoint goal.

## 4.3 | Waypoint graph

The different paths for an AUV are encapsulated in a waypoint graph $G = (V, E, D)$ with four corner nodes $v \in V$, $v = \{0, 1, 2, 3\}$ and edges between the nodes given as $e \in E$, $e = \{(0, 1), (0, 2), (0, 3), (1, 0), (1, 2), \ldots, (3, 2)\}$, represented as arrows, as shown in Figure 7. Each edge $e_j$, $j = 1, \ldots, n_e$, where $n_e$ is the number of edges in $e$, is referred to as a *survey line* or graph edge. These lines also contain a set of *sample points* (the dots on the lines in Figure 7) collected for each survey line $e_j$ in the vector $\boldsymbol{d}_j \in D$, $\boldsymbol{d}_j = \{D \mid e_j\}$, where $D$ is the set containing all the sample points in the graph. As

noted, variability in the water column tends to be greater along the vertical dimension—to appropriately measure this variation, the AUV undulates (with a fixed angle) up and down, in what is known as a "yo-yo" pattern throughout the mission. The sample points (used to evaluate the objective function) are spaced out according to the depth, angle of the yoyo, and the distance of the survey line, having twice the number of sampling points as the number of crossings of the given depth layer. For the configuration used here, this results in a sample point spacing of 416 m. Measuring the entire water column is important (rather than only undulate between the 70 and 90 m depth band), as both surface phenomena (i.e., SST, surface warming effects, chlorophyll, etc.) and deeper processes (influx of AW) are of interest. The AUV then traverses the graph going from one node to another: for example, going from node 1 → node 2, along the survey line $e_5 = (1, 2)$, contains the sample points $\boldsymbol{d}_5$.

## 4.4 | The objective function

The aim of an objective function is to evaluate and prioritize the different survey alternatives (graph edges), accounting for prior (model) and in situ information. Focusing solely on reducing uncertainty in the ocean model, one solution would be to bias locations yielding the largest reduction in variance, or to use mutual information (Krause et al., 2006), to determine the graph edge having the largest information gain (highest entropy reduction). However, neither of these criteria are capable of readily using incoming measurement data $\boldsymbol{y}_{t,d_t}$, consequently making the strategy deterministic (Eidsvik, Mukerji, & Bhattacharjya, 2015). Given the large uncertainty in oceanographic sampling, the informative value of in situ measurements cannot be overlooked. Still, the conundrum of exploration versus exploitation continues to persist, and finding a functional balance is necessary.

The GP representation is well suited for this purpose because it holds prior information about the temperature variance (uncertainty), in addition to assimilating the incoming measurements into the mean parameter.

For achieving effective adaptability, the upper ocean temperature variability and trends derived from the GP are used to guide the data collection process through variance and gradient measures. Temperature is a prominent factor in the Froan region, because measurements associated with CW and FW are different from AW (Sætre, 2007), with a well-defined front between the cold and low-salinity NCC and the warm and dense AW (Ikeda, Johannessen, Lygre, & Sandven, 1989). These temperature-laden fronts are found all year; horizontal gradients of 0.5°C/km can be observed, depending on the season (Sætre, 1999) and increased variability and levels of primary productivity is expected in areas where these water masses meet. Faced with high model uncertainty, variance is preferred over entropy as the metric for uncertainty in our approach, because of its simpler form and wider acceptance as a measure of spread in a numerical model (Baafi & Schofield, 1997).

The objective function is formulated as a balance between gradient intensity and reduction of variance—the rationale being that in cases with uniform temperature conditions, the strategy would prioritize navigating according to the variance. Or in the opposite case, if a thermal gradient is discovered, using the gradient as a means to steer toward locations indicative of these changes, directing the AUV toward nonuniform conditions. The objective function is evaluated using the surrogate GP model formulated in the preceding sections. The objective function is evaluated on the sample points $k_j$ related to each alternative survey line $\boldsymbol{d}_j$ given as

$$f(\boldsymbol{d}_j) = \text{argmin}_{\boldsymbol{d}_j} \left\{ \frac{\omega_p}{n} \text{trace}(\boldsymbol{P}_{t,\boldsymbol{d}_j}) - \frac{\omega_g}{n_k} \sum_{k_j=1}^{n_k} \nabla g_{t,k_j} \right\}. \tag{6}$$

The first term expresses variability at all locations, with $n$ being the total number of locations. The second term provides the weighted gradient summed over the sample points $k_j$, where the number of points along the line is $n_k$. Both terms are normalized prior to subtraction, in order to allow reconciliation between the variance and gradient term. The influence between the variance and gradient can be adjusted using the weights $\omega_p$ and $\omega_g$. For simplicity, we have set the weights to 1; depending on the application, these may be adjusted. The gradient is calculated for the mean value at the survey points, weighted by their uncertainty as

$$g_{t,k_j} = \frac{\boldsymbol{m}_{t,\boldsymbol{d}_j}(k_j)}{\boldsymbol{P}_{t,\boldsymbol{d}_j}(k_j, k_j)},$$

where $\boldsymbol{m}_{t,\boldsymbol{d}_j}$ and $\boldsymbol{P}_{t,\boldsymbol{d}_j}$ are terms from Equation 5. Before calculating the scaled gradient, the term $\boldsymbol{P}_{t,\boldsymbol{d}_j}$ is normalized using the global minimum as follows $(\min_{k_j}[\boldsymbol{P}_{t,\boldsymbol{d}_t}(k_j, k_j)]/\boldsymbol{P}_t, \mathbf{d}_j(\mathbf{k}_j, \mathbf{k}_j))$ and has a lower limit to avoid over emphasis on already visited locations. The best node to visit will be the node with the connecting survey line yielding the lowest objective value. Explorative survey lines would reduce diagonal elements of $\boldsymbol{P}_{t,\boldsymbol{d}_j}$ more than the lines previously surveyed. And finally, $\nabla$ in Equation 6 is the operator using second order central differences to compute the actual gradient value.

Note that several other criteria are possible. Entropy measures or average variance reduction are commonly used, but for GP these will not depend on the data (Eidsvik et al., 2015). The criterion in Equation 6, which includes the temperature gradients, allows adaptive sampling where the survey paths can depend on the realized data. In simulations we also ran tests with a criterion aiming to classify significantly large temperature gradients in the main current direction, that is, $E[\nabla_\theta x_t|\cdot] - \sqrt{Var[\nabla_\theta x_t|\cdot]}$, where the conditioning represents currently available data, and $\theta$ is a predefined direction. One could also go further to account for the uncertainty in future data along the next sample line that entails an integral over the data (Bhattacharjya, Eidsvik, & Mukerji, 2013; Eidsvik, Martinelli, & Bhattacharjya, 2018), or even use the expectation over future lines, with additional computational complexity for nonmyopic approaches. But the simple weighting in Equation 6 is a practical solution which gave reasonable results for our field tests, and we leave more complex objective functions for future work.

Because the path of the AUV only considers one node into the future, the approach is a greedy/best-first search. Using such a myopic approach, with a one node horizon, is assumed to be sufficient as the ocean model skill is typically low, resulting in substantial uncertainty when executing the sensing strategy. Additionally, due to control,

actuation, and navigational errors in part due to ocean currents, the position of the AUV will deviate from the optimal route—more details are given in Section 6. Note that the information utility used here is a single objective function with only one solution. Extension into multiobjective functions would be possible to account for other environmental or operational parameters such as energy, safety zones, and operation of other vehicles; or more decision analytic criteria related to algal bloom treatment, fishing policies, and dynamic placement of fish farms.

## 4.5 | The GASA algorithm

The GP model, objective function, and the waypoint graph $G$ are then collected in an algorithm, which is to run onboard during execution. Using the different survey alternatives the algorithm iterates through possible survey lines and calculates their objective value, utilizing the variance and mean estimates from the GP model. The details of these steps are given in the greedy adaptive sampling algorithm (GASA) in Algorithm 1.

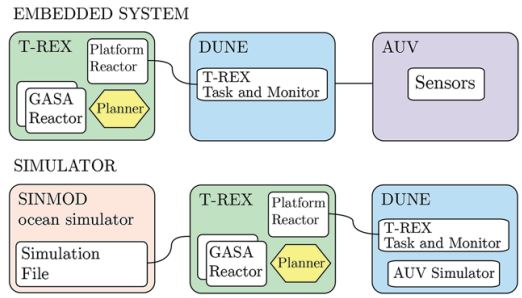


**FIGURE 8** A block diagram layout comparing the embedded and simulated systems used

**ALGORITHM 1** The GASA algorithm.

```
Initialize GP, Graph: G
update_GP_bias()                                   %Runs only once
while active do
    if goal is reached then
        for survey line in G do
            Evaluate objective function (Eqn. (6)).
        end
        Find the best survey line.
        Set the corresponding node as the goal.
        Add dynamic uncertainty component in spatial GP model.
    else
        Continue towards goal.
        Collect data.
        Update model (Eqn. (5)).
    end
end
```

In an operational scenario, once the AUV is deployed, it will need to travel to the starting point of the survey graph, before initiation of the algorithm, having time to update the bias for the prior mean on its way. To avoid overfitting, the bias correction will only occur if the observed model discrepancy is above $\pm 1\,^{\circ}\mathrm{C}$. Once the starting point is reached, the algorithm activates and begins evaluating the alternative survey lines available at its current location. Once the objective values have been calculated, the best survey line and the corresponding node is set as a waypoint goal for the AUV to visit.

## 4.6 | Implementation

Prior to the deployment, the GASA algorithm was tested in a simulated environment, identical to the embedded system in the AUV. The setup consists of three essential components; a virtual ocean simulator, an AUV vehicle simulator and an autonomous agent architecture (Figure 8).

An interface that directly couples the SINMOD model provides 3D ocean data that are used to simulate sensor readings, reproducing actual ocean conditions at a given time, depth, and location. The Unified Navigation Environment in DUNE (Pinto et al., 2012), handles the AUV simulation, and is used for navigation, control, vehicle supervision, communication, and interaction with actuators—DUNE is running onboard the AUV as well. On top of the hierarchy sits the autonomous agent architecture T-REX (Teleo-Reactive EXecutive), which synthesizes plans and uses an artificial intelligence based automated planning/execution temporal framework to execute tasks continuously, as sensing and control data are fed to it. Details of T-REX are beyond the scope of this work; readers are encouraged to refer to Py, Rajan, and McGann (2010), Rajan and Py (2012), and Rajan, Py, and Berreiro (2012). The communication between DUNE and T-REX is handled by the LSTS toolchain (Pinto et al., 2013)[¶], which provides the back-seat driver API to DUNE allowing external controllers, such as T-REX, to provide desired poses for the platform while receiving progress updates on their attainability.

[¶] http://lsts.pt/toolchain.

**TABLE 1** Results from running 1,000 mission simulations

| Run | Mean criteria score[a] | RMSE[b] |
|---|---|---|
| Random route | +0.15 | 0.61 |
| GASA: both variance and gradient | −0.21 | 0.36 |
| Only variance (gradient kept constant −0.33) | −0.06 | 0.37 |
| Only gradient (variance kept constant +0.33) | −0.15 | 0.49 |

*Note.* RMSE = root mean square error.
[a]The mean score from the objective function for each chosen alternative.
[b]The root mean square estimation error between the underlying temperature field and the estimated Gaussian process (GP) temperature field.

GASA and dependencies were implemented as *reactors* that are internal control loops in the T-REX framework capable of producing goals that the planner integrates in a series of actions (e.g., Goto, Arrive_at …), which are finally collected to form a plan. This plan is then distributed through the framework and checked for errors such as operational limitations, before dispatch to DUNE, which handles low level control and execution. The mission is hence continuously monitored by T-REX, as it follows the *Sense* → *Plan* → *Act* control methodology.

## 4.7 | Simulation

We conducted an empirical study comparing the GASA algorithm and preplanned randomly generated routes to assess performance, along with simulations using SINMOD nowcast data to provide further insight into the resulting behavior, using the same GP parameters, graph, and objective function as in the at-sea experiments. The following procedure was used for the empirical simulations:

1. Generate a random GP temperature field.
2. Simulate 1,000 different missions visiting five nodes using GASA with randomly chosen routes.
3. Collect the criteria score and the final root mean square error (RMSE).

The drawn temperature fields had a variation 1.5°C. If larger temperature differences are expected, one should evaluate to reduce the influence of the gradient term.

As shown in Table 1, the random route has a high criteria score and a high RMSE; this was to be expected. Using only variance results in a lower RMSE as it will seek to explore rather than exploit. In contrast, using only the gradient will put emphasis on exploitation, yielding higher RMSE results. When using both terms, the resulting behavior is a balance.

In addition, various simulations were conducted using both hindcast, and forecast (nowcast) data from the Froan area. However, for the sake of clarity, analysis of simulations using nowcast data from May 4, 2017 is presented, where the example illustrates the interplay and influence of the variance and gradient components. To demonstrate this, three simulations were carried out with the objective function considering: only variance, only gradient, and finally both (shown as Simulations 1–3 in Table 2). The simulation considers a route of five consecutive nodes to be visited in a prioritized fashion depending on their objective value.

**TABLE 2** Simulated routes using different terms in the objective function

| Run | Route (nodes) | Remarks | Visual path |
|---|---|---|---|
| Simulation 1: variance | 2, 3, 0, 2, 1 | Variance only |  |
| Simulation 2: gradient | 3, 2, 0, 1, 2 | Gradient only |  |
| Simulation 3: both | 2, 3, 0, 2, 3 | Variance and gradient |  |

The underlying nowcast covers the sea state for May 4, 2017. Because the algorithm only updates using measurements from the 70 to- 90 m depth interval, the temperature is expected to be relatively homogeneous, except in areas with the influx of AW. Two clear trends are visible in the prior variance (Figure 9a) and mean (Figure 9c). Both variance and temperature gradients are higher toward the north, suggesting that the AUV should start by mapping here first. The prior variance and mean, both derived from May 2016 hindcast data, were kept constant, both during simulation and during field deployments.

Using only the variance (Simulation 1) for navigation, results in a maximum reduction of the prior uncertainty and the nodes: 2, 3, 0, 2, 1, thus prioritizing the high-variance hot spots close to nodes 2 and 3. Using only the gradient (Simulation 2) leads to a route favoring the survey lines with the greatest temperature change. The gradient follows the outer edges of the graph, visiting the north region first following the nodes: 3, 2, 0, 1, 2. Because the gradient depends on the collected temperature measurements from the nowcast, the gradient is using in situ information to change its path, in contrast to the variance, having a predetermined track based only on prior knowledge.

Combining both influence from variance and gradient in Simulation 3 shows the interplay between the two information measures. The executed path, visible as Simulation 3 in Table 2 and Figure 9b, shows priority of exploring the north-south axis. As the gradients are weighted by the prediction accuracy, the initial path choices are dominated by variance because the gradients will have high uncertainty. Then, as measurements reduce the uncertainty of the mean estimation, the gradient effect becomes more influential. Still, because the temperature distribution is relatively homogeneous for this example, the gradients are approximately the same for each alternative, resulting in a dominance of variance right until the end where the gradient changes the choice to node 3. As the model only updates if measurements are within 70 to- 90 m depth, the estimated fields in Figure 9b and d are uneven, leaving only parts of the grid updated, because the AUV is traveling in a yo-yo pattern. In addition, the covariance range is limited and locally changing as a result of the covariance modification in Equation 3, allowing the information to be "spread" nonuniformly, hence the uneven spots in Figure 9b. Differences in paths for various mean, variance, and correlation models were also studied prior to deployment.

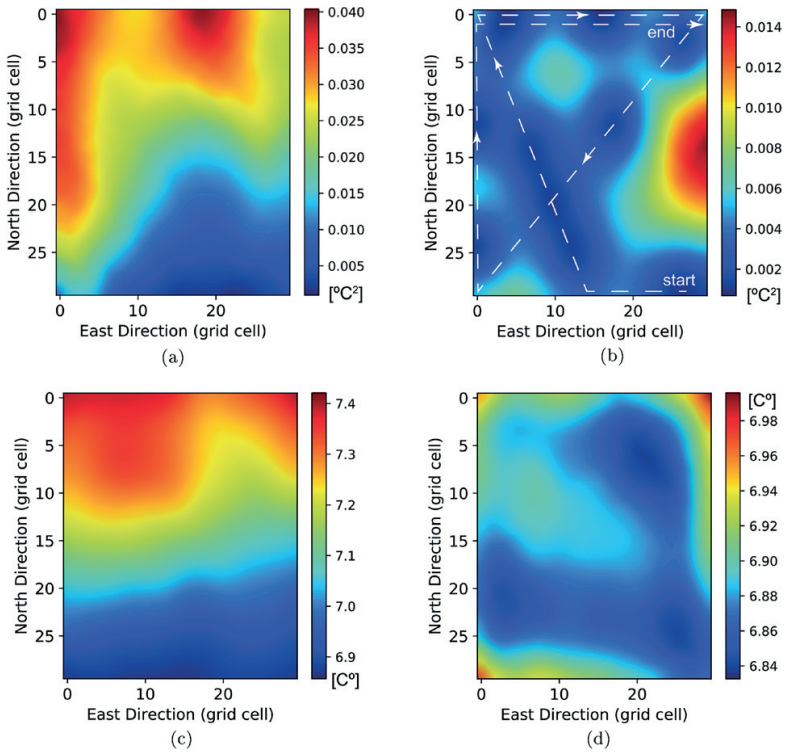


**FIGURE 9** Simulation prior to deployment using both terms in the objective function with nowcast data from May 4th, 2017 at ~10 a.m. Temperature variance for operational area *at start*. Note the location of the highest variance. (b) The final estimated variance and the traveled path *at end*. Note the spots of low variance. (c) The estimated temperature at the survey area *prior to deployment*. (d) The final GP regression of the temperature field *at end*

For a discussion on GP sensitivity to variance and correlation parameters for sequential sampling schemes, see Eidsvik et al. (2018). Note that the dynamic nature of the processes studied here would be highly nonlinear and non-Gaussian over a longer spatial and temporal range, and in the future one can imagine having more complex spatiotemporal proxy models on-board the AUV itself.

## 5 | FIELD EXPERIMENTS

The experiments at sea aimed to verify our algorithm's ability to adapt mission execution based on in situ measurements, and demonstrate its capability to spatially prioritize data collection, using ocean model driven predictions encapsulated in a stochastic model. They were carried out between the May 4 and 12, 2017, using the operational area and waypoint graph shown in Figures 7 and 10 of the Froan archipelago.

Inclement weather on the Norwegian west coast led to numerous postponed deployments, but two full missions, referred to as Surveys 1 and 2, were conducted during this period. Both surveys used the same prior data (variance and mean from Figure 9). Doing so was important for demonstrating adaptability toward the environmental conditions while keeping the initial conditions the same for both surveys.

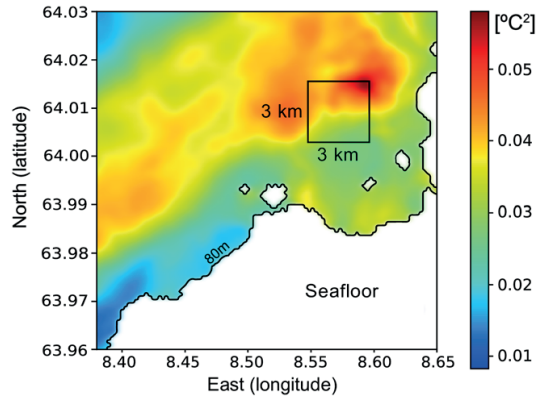


**FIGURE 10** The distribution of temperature variance across the Froan coastal region with the operational area indicated; note the 80-m isobath

### 5.1 | Experimental setup

Our scientific focus was the upper water-column and the effect of physical forcings on phytoplankton dynamics of the Froan coastal region, which we targeted using temperature variability. Consequently,

**FIGURE 11** NTNU's light AUV platform (*Harald*) for upper water-column exploration used in our work—the CTD is visible in the nose. The AUV has an excess of 24 hr in-water operational capacity with a range of sensors in addition to the CTD

before bringing the system to the field, an approach similar to Sakov and Oke (2008) was used to identify an operational area where shifts in temperature would be prominent and hence interesting from both a model and oceanographic perspective. The input data to this analysis were hindcast realizations from SINMOD (May 2016), reflecting the changing temperature distribution at 80-m depth using a planned deployment time between 8:00 a.m. and 2:00 p.m., where the empirical variance was estimated by applying Equation 3 and shown in Figure 10.

The survey area was confined to the eastern region close to the point of highest empirical variance, but also sufficiently near the shallower waters in the event an emergency recovery of the AUV and/or dealing with unfavorable weather conditions. To operate safely the waypoint graph $G$ (Figure 7) was limited within the operational area $3 \times 3$ km$^2$ to $2.5 \times 2.5$ km$^2$ (allowing a 500-m drift margin), permitting a reduced search area and enabling the AUV to be monitored using acoustics from a vessel stationed at the center of the survey pattern. Although the experiments were constrained by this one graph for these pilot deployments, the framework is general and can be extended to a series of connected graphs of any shape. In addition, having a greedy (one-step look ahead) planner as well as a simple waypoint graph allowed us to work with a constant and reliable computational load on the AUVs CPU, while maintaining communication to the vehicle in the harsh conditions offshore.

Our robotic platform consisted of a light AUV (Sousa et al., 2012) equipped with a 16 Hz Seabird "Fastcat 49" active conductivity, temperature, and depth (CTD) sensor providing temperature and salinity measurements, see Figure 11. The CTD is active as it continuously pumps water, ensuring that a fresh sample is observed. The accuracy of the CTD instrument is $\pm 0.0003$ S/m (conductivity), $\pm 0.002$°C (temperature). The AUV was also equipped with a Wetlabs EcoPuck for chlorophyll *a* concentration, color dissolved organic matter (cDOM) and total suspended matter (TSM). The embedded system in Figure 8 hosting the GASA framework was operating on a multicore GPU NVIDIA Jetson TX1 single board computer, specifically developed for autonomous systems. With a lithium polymer battery bank, the AUV had an operational capacity in the water column exceeding 24 hr of continuous operation.

**TABLE 3** Executed routes and deployment times, May 2017

| Run | Route (nodes) | Deployment time |
|---|---|---|
| Survey 1—May 9 | 2, 3, 0, 1, 3 | 10:02 a.m. |
| Survey 2—May 12 | 2, 1, 3, 0, 2 | 10:15 a.m. |

Each survey took 4 hr to complete, with five nodes to visit during this period. Restricting the adaptation to only five choices, and within the waypoint graph, was necessary to manage deployment and recovery within limited weather windows. Because full coverage of the region could be attained with the AUV, we emphasize that the results from the field operations should be seen as applicable to cases in which intensive sampling is not feasible.

The GP model used a grid resolution of $30 \times 30$ on a $2.5 \times 2.5$ km$^2$ region ($83 \times 83$ m$^2$). The GP model was configured with a prior mean and variance (seen in Figure 9) associated with the temperature distribution at 70 to 90 m depth. Updating these priors was limited to measurements collected from this depth. Limiting the information used by the objective function to these depths was to specifically target the temperature dynamics induced from warmer AW, as discussed in Section 3.4.

## 5.2 | Results and evaluation

This section first presents the AUV data and the details related to the GASA algorithm, followed by a comparison to SINMOD model forecasts (nowcasts) and data from remote sensing, buoy, and ship-based measurements.

Figure 12 shows recorded temperature versus depth taken along the transect for the two surveys, along with the maps of the executed survey path superimposed on the SINMOD model predictions for both deployment days. The survey paths from the maps are collected and shown in Table 3, along with the deployment time and date. The objective values used to differentiate the route choices is presented in Figure 13.

We observe that two different strategies have been executed, underpinned by the GP priors and the assimilated temperature measurements. As the GP priors are the same, the observed difference between the paths are provided by separate temperature conditions. This is apparent in Figure 12a and c, with Survey 2 clearly having a more shallow prominence of warmer AW, depicting the thermocline (dashed lines) shifting from 65 to 40 m, the same shift predicted by SINMOD in Figure 5. The deep salinity measurements come close to 35.0, suggesting the water is of Atlantic origin, which is distinctly more saline than FW ($\lesssim$32) and CW (32 $\lesssim$ 35). This is also confirmed from the CTD measurements taken from the R/V *Gunnerus* shown in Figure 17. There is also a visible difference in surface warming, which is traceable in both buoy and remote sensing data.

Evaluating the adaptive behavior, as in simulation, node 2 is always taken as the first node to visit. This is expected as the prior data are identical at this point, and no measurements are assimilated; objective values for the first node choice in Figure 13a and b confirm this. After reaching node 2, the recorded data come into consideration because exposure to the warm water influx is different, each survey will have a

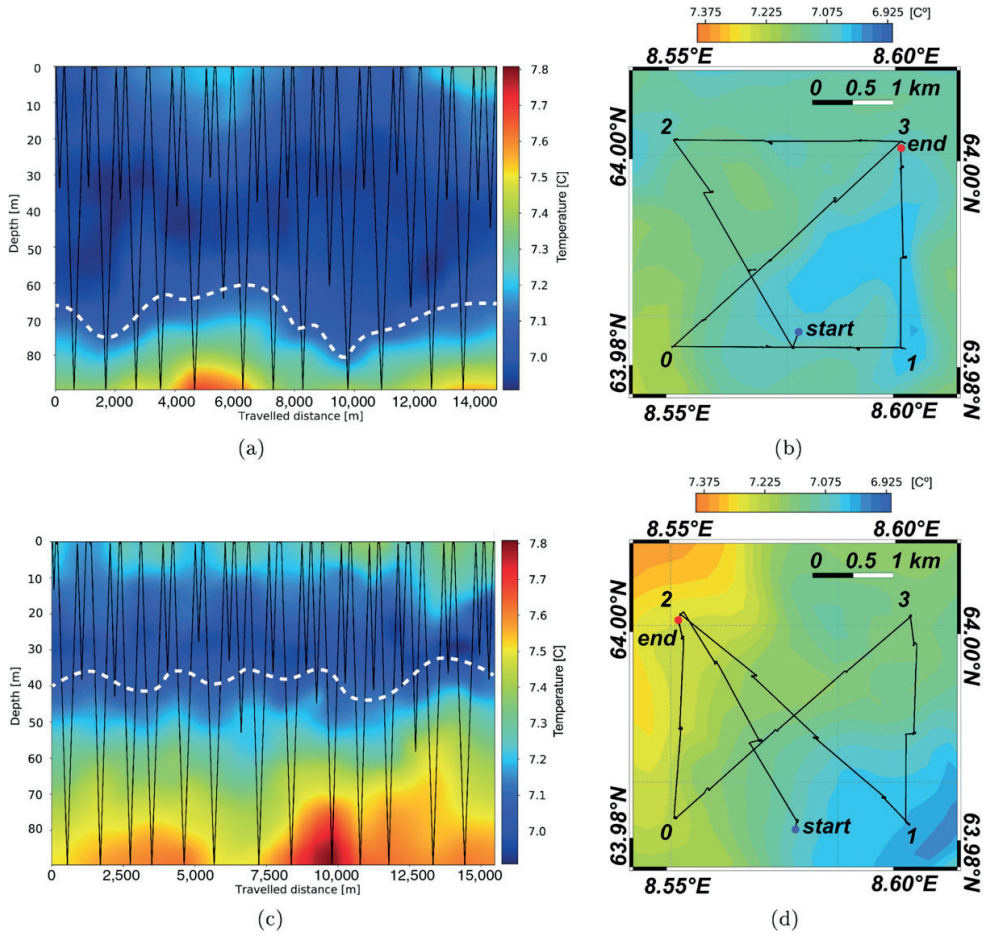


**FIGURE 12** Results from the AUV survey on the May 9th (Survey 1) and May 12th, 2017 (Survey 2). Yo-yo pattern (black line) and the temperature distribution for Survey 1. (b) Map of the executed path for Survey 1, SINMOD realization for May 9th in background. (c) Yo-yo pattern and temperature for Survey 2. (d) Executed path for Survey 2, SINMOD realization for May 12th in background. In (a) and (c), temperature distribution in the survey area and thermocline (white lines) influenced by AW (temperatures are interpolated to cover the plot surface) is shown. In (b) and (d), the path generated by the GASA algorithm for the two surveys is shown. The gaps in the position on the plots are surfacing events to correct for drift and navigational errors in the water column

distinctive posterior mean temperature field and hence gradient influence. Consequently, the intensity and direction of the gradient will also be different. After reaching node 2, the first decision with posterior information is made. This choice is the most intuitive to consider and interpret, as only the data along the first survey line are assimilated into the onboard GP model. Evaluated from node 2, a transect toward node 3 would be most beneficial for reducing the variance (comparing with simulations in Table 2), if no strong temperature trends are to be observed. This is the case for Survey 1, which tracks to node 3, after node 2. More interestingly, Survey 2 tracks back toward node 1. Clearly, this is not optimal for reducing the variance as several measurement locations will be close to the first survey line. One can therefore argue that this choice is dominated by the influence from the recorded temperature data, which is visible as a difference in score at the second evaluation step in Figure 13b.

Additionally, because the uncertainty is low around the first transect, this gradient is weighted higher compared to other gradients with larger uncertainty. After reaching node 1, the AUV in Survey 2, tracks toward following the paths associated with Survey 1, visiting nodes 3 and 0, which suggests that the influence of variance is dominant. As observed in Figure 12b and d, Survey 2 has a hourglass pattern, while Survey 1 has a more mixed survey pattern. These characteristics will be compared to the model and external data in the following sections.

## 5.3 | Model correspondence with AUV data

Deviation between recorded data and the simulated predictions is to be expected. Considering assimilation back to the model, the question is as follows: Can the observed discrepancies contain contextual information that can augment the model and enhance ocean prediction?

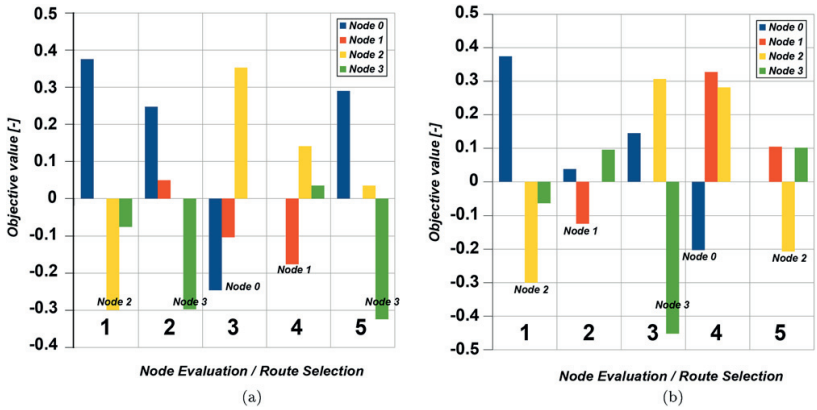


**FIGURE 13** Values for the objective/utility function used to evaluate the different survey alternatives (negative score is preferred). (a) Survey 1 and (b) Survey 2. The choices correspond to the executed paths in Table 3

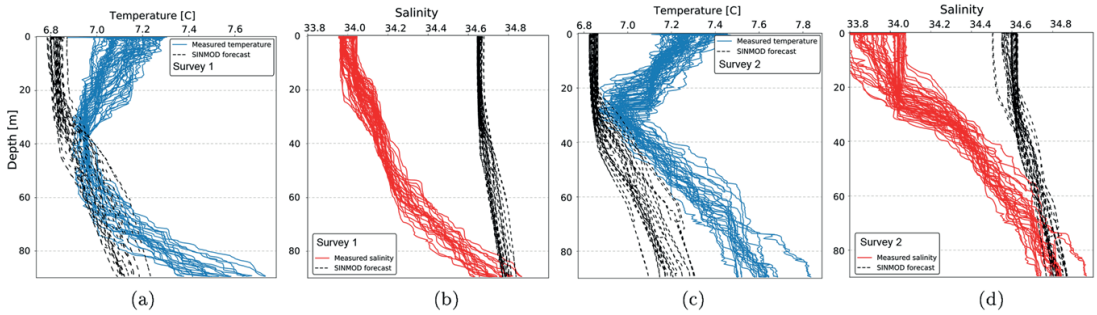


**FIGURE 14** Vertical comparison of AUV measurements with SINMOD nowcast data. (a) Temperatures for Survey 1. (b) Salinity for Survey 1. (c) Temperatures for Survey 2. (d) Salinity for Survey 2

Although a full diagnosis of the model accuracy is not within the scope of this work, a general overview and direct comparisons are shown on which to base further analysis. Because undue reliance on one data source increases the risk of erroneous comparisons, consequently in this section we compare SINMOD data and AUV observations, followed by Section 5.4, where we provide supporting data from ship, buoy, and remote sensing from the same spatiotemporal domain.

During the field experiment period SINMOD provided nowcasts (48-hr forecasts) used to cross-validate the in situ measurements and study the experienced behavior. Comparing the executed paths to the 80-m SINMOD nowcasts (shown in the background in Figure 12b and d) suggests that Survey 2 accounts for a temperature trend that is warming toward west, crossing the gradients in a manner one would expect. More uniform conditions are predicted for Survey 1, which results in a more variance dominated survey.

Figure 14 presents temperature and salinity measurements from the AUV with the SINMOD nowcasts superimposed (dashed lines). The immediate impression is that the model shows a tendency to *underestimate* the surface warming present in the AUV data; a bias in salinity is also present. The correspondence is good in the 70 to 90 m depth in which the GP data assimilation and GASA algorithm were active.

The temperature difference is easier to study using Figure 15, presenting the temperature deviation spatially within the survey area (birds-eye view). Figure 15a and b makes it possible to study, where in the survey area, the temperature deviation between the nowcasts and reality was the highest. The northeastern corner of the model was the weakest in terms of predicting ocean temperature, for both surveys, being warmer than expected. This may explain why GASA in both cases chose to cross over from node 3 to node 0. The deviation between the measurements and the nowcast is not influencing the AUV behavior directly because the objective function only evaluates the balance between variance and gradient. However, if the number of nodes to visit is higher (e.g., more than 5), we would expect this region to be revisited as the objective value would favor the temperature gradient. Indirectly, this would result in a higher sampling density where model discrepancy would potentially be high, as a result of this gradient. The region corresponds to the maximum-variance hot spot (Figure 10), which suggests a connection between temperature variation and model uncertainty, important for validating our approach in developing the objective function.

Figures 14 and 15 can be used to give the first impression of the discrepancies, but cannot be used as the proof of model error, as a range of sources may contribute to the mismatch, including

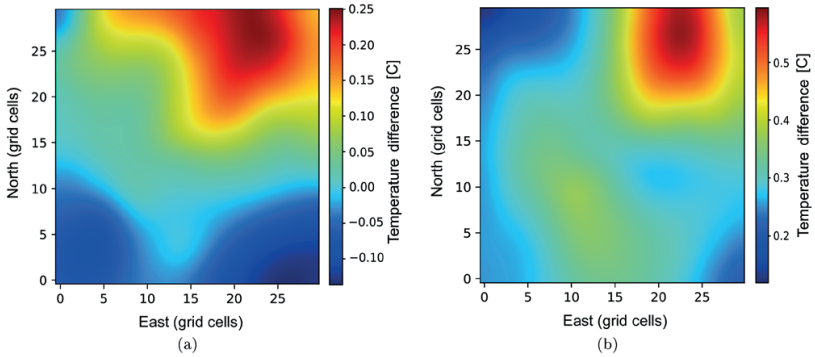


**FIGURE 15** Subparts (a) and (b) show the spatial comparison of predicted SINMOD nowcast and the estimated GP temperature field (survey area seen from above at 80 m depth). (a) Temperature discrepancy Survey 1. (b) Temperature discrepancy Survey 2

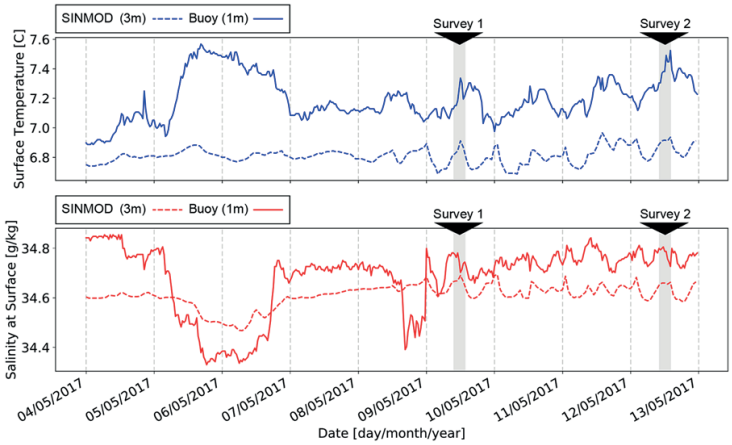


**FIGURE 16** Results from a moored buoy, from May 4 to 11, 2017. Temperature and salinity measurements from the buoy at 1 m depth during the operational period, overlayed on SINMOD predictions at 3 m depth; Surveys 1 and 2 are indicated in grey

errors in initial conditions. The results nevertheless demonstrate how adaptive and data-driven approaches can improve ocean modeling, by revising a priori uncertainty assumptions and providing information that can greatly focus analysis of model shortcomings and inaccuracies.

## 5.4 | Buoy, ship-based, and remote sensing data

To get a full picture of the environment and ground truth the SINMOD and AUV data, supporting data sets from the other marine platforms are presented in this section. The measurements from a moored buoy in Figure 16 show the long-term fluctuation in the area. The buoy is located further inshore, 3 km from the AUV survey area; see Figure 19b.

The buoy data show a trend of sun-driven surface warming during the AUV deployments, with Survey 2 having a higher peak temperature during the deployment corresponding to sea SST products from remote sensing. The SINMOD nowcast prediction at the buoy location, shown with the dashed line, follows the trends well albeit with some bias, although certain events such as the salinity drop before May 9, 2017, is not picked up by the model.

The results from Surveys 1 and 2 indicate a significant difference in the influence from AW, visible in the thermocline line in Figure 12a and d. Comparing these results with CTD measurements made from the R/V *Gunnerus* in Figure 17 and the SINMOD prediction in Figure 5, the same thermocline dynamics can be found. Most notably for the outermost stations (2 and 6), both taken at high tide, there is a large shift in both temperature and salinity between May 9 and 10, 2017.

A significant difference in chlorophyll *a* concentration (Figure 18) for the two deployments is captured in the remote sensing data. Due to cloud cover, the retrieved data area is patchy; despite this, there is clearly more chlorophyll *a* concentrated in the surface during Survey 1, in agreement with the in situ chlorophyll measurements from the AUV and the *R/V Gunnerus*.

It is important to stress that the peak chlorophyll concentration at 15 to 20 m depth cannot be detected from space and that sparse coverage from ship-based sampling can be augmented with AUV data to render a more precise in-depth picture of chlorophyll

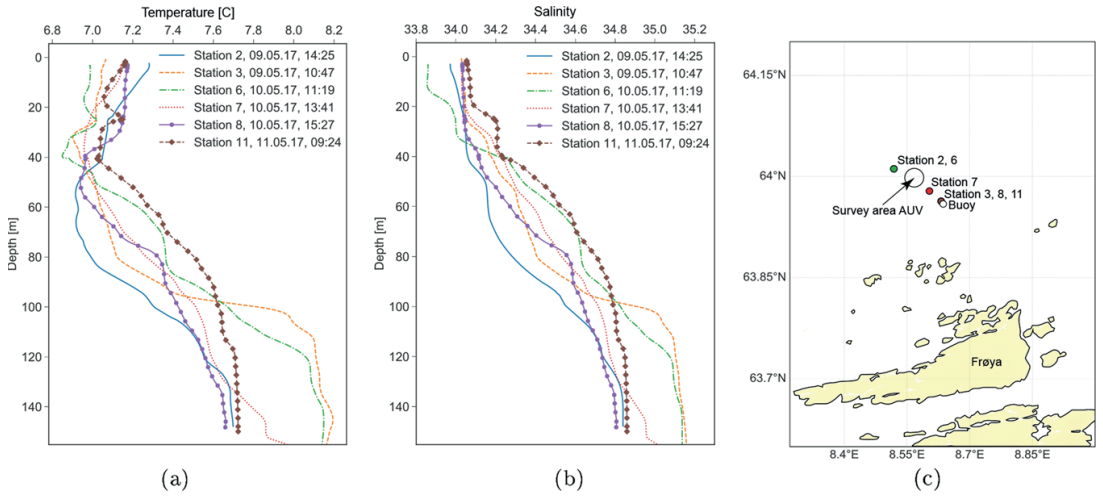


**FIGURE 17** Results from the R/V *Gunnerus* operations from May 9 to 11, 2017 (a) Temperature profiles. (b) Salinity profiles. (c) CTD cast locations. Vertical profiles from CTD measurements made by *Gunnerus* with temperature variability showing the influx of AW moving up and down in the water column

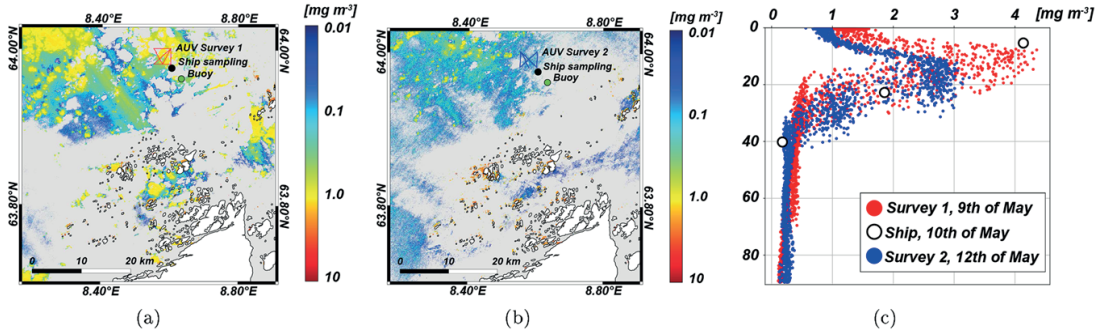


**FIGURE 18** Chlorophyll *a* concentration for May 9 and 12, 2017, processed from Copernicus Sentinel Data (Sentinel-2A) *OC2* (Vanhellemont & Ruddick, 2016) compared with in situ measurements from AUV and the research vessel (a) Sentinel-2A , CHL OC2, May 9, 2017, 10:56 a.m. (b) Sentinel-2A , CHL OC2, May 12, 2017, 11:13 a.m. (c) AUV and vessel R/V *Gunnerus*, May 9, 2017

structure. This demonstrates why we need to combine information from several sources to arrive at a deeper understanding of ongoing processes.

Comparing across the different measurement platforms, Figure 19 shows the nowcasted temperature for the entire upper 3-m model area, side by side with remote sensing, AUV, and buoy measurements. The remote sensing data are filtered for quality and only compared to locations within the model domain (Figure 19b, orange area). Some days had full overcast (May 9, 2017) and therefore no remote sensing data are available. Some of the variations is related to difference in space, as the buoy is further inshore compared to the AUV, and time, because the AUV and remote sensing data were collected somewhat apart. However, there is a clear tendency of SINMOD to underestimate the surface temperature during the campaign; this is supported by both AUV data (Figure 14) and buoy time series (Figure 16).

## 6 | DISCUSSION

Our work shows the synergies to be exploited between data-driven sampling and synthetic ocean models, making oceanographic observations and data collection more efficient, by providing comparison of in-field data to augment and cross-validate model predictability, while also enabling greater capability to study and understand oceanographic processes and events. Using stochastic surrogate models, such as the GP model derived in this paper, allows the unification of both in situ measurements, data assimilation, and uncertainty quantification of the full hydrodynamic model, presenting scientists with a powerful framework for efficient experiment design.

As Zhang and Sukhatme (2007) pointed out, interpolation/kriging is required to estimate the value where no direct measurements are available; hence a bias is inevitable. Consequently, the algorithm will be exposed to high gradients as a result of failing to initialize the prior with

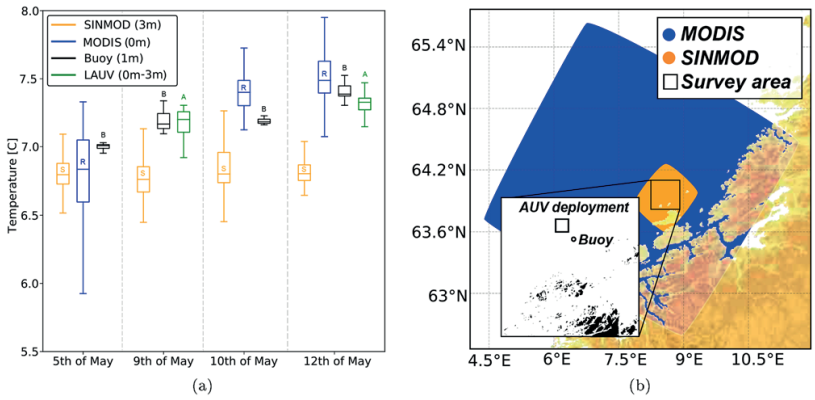


**FIGURE 19** The 3-m water temperature nowcast from SINMOD compared to remote sensing SST products (MODIS), buoy measurements at 1 m depth, and AUV data from the surface layer 0–3 m, at noon. (a) Recorded temperatures at noon. S, R, B, and A denote SINMOD, remote sensing, buoy, and the AUV measurements, respectively. (b) Coverage and location map for the campaign at Froan (midway)

realistic values because prior and measured temperatures in unexplored locations typically deviate causing each update to generate a gradient peak that may not actually be realistic. Therefore, the objective function presented in this work counterbalances the gradient estimate with the corresponding uncertainty in $\boldsymbol{P}_{t,d_j}$, while also performing a one-time-only bias correction of the prior mean estimate to avoid this effect.

Independent of the cost function, the algorithm used in this paper uses a one-step planning horizon, greedily choosing the path with the best objective value, for which an adverse effect can be attraction to local optima—there are a number of reasons for making this choice.

First, there are factors related to computational load, which grow exponentially for recursive approaches, originating from the combinatoric complexity as the graph network size increases. In the proposed approach, the graph is small and compute time is not an issue; however, as the method is devised for larger graphs, this is important to keep in mind, as some greedy-recursive approaches contemplate solutions shown to have better performance, see e.g., Ma, Liu, and Sukhatme (2016). So for larger graphs or limited computation, greedy approaches may provide "good enough" solutions (Binney et al., 2013) and acceptable performance, as shown in Krause et al. (2008). Second, as the methods used depend on ocean models, which are approximate, the inherent model uncertainty and integrated error effects will reduce the advantage gained in using a longer planning horizon. In some cases, this may cause the performance to become worse (Binney et al., 2013). The regional spatial and temporal scales on which to operate also come into consideration as upper water-column and coastal variability can neither be sampled nor modeled on a sustained and substantial basis (Lermusiaux, 2006). Some of these constraints can be managed; examples of nonmyopic approaches, such as Krause (2007) and Hoang, Low, Jaillet, and Kankanhalli (2014), can be used for active sampling, with complexity bounds on the exploration phase.

In terms of applicability, the end-to-end method presented in this work is general in the sense that the pipeline starting with (a) the discretization and spatial modeling of the phenomena using ocean model data, (b) formulation of the objective function toward a scientific context, and (c) algorithmic implementation can easily be tailored to other environmental attributes or a combination of several, depending on the phenomena and scientific goals, where the perspective is the combination of ocean model data and in situ measurements. In our field experiment, both surveys showed a large variation with thermocline shift from 65 to 40 m, a spread in salinity from 33.0 to 34.9, and chlorophyll concentrations from 1 to 4 mg/m$^3$. This observed variability across a range of environmental signatures demonstrates that using another type of environmental variable is possible and that to resolve different ocean phenomena measurements from several assets needs to be considered.

## 7 | CONCLUSIONS AND FUTURE WORK

In this work, we have presented methods for coupling ocean models with in situ data to achieve efficient sampling of coastal processes, with specific focus on the physical–biological coupling active in the Froan region, using ocean temperature as an information utility. Based on high-resolution hindcast data from the SINMOD ocean model, a stochastic proxy model using GPs was formulated, and a location-based covariance function was implemented to improve the assimilation of in situ measurements. To consolidate the GP model with the phenomena of interest for adaptive sampling, a variance and gradient-based objective function that accounts for uncertainty in the estimated gradients was established. The sampling algorithm, being both data- and model-driven, was tested in simulation and in sea trials, onboard an AUV. The experiments show that the algorithm differentiated between alternative survey strategies, having good agreement with model forecasts. The recorded data indicate correspondence between ocean model and AUV in determining a thermocline shift from influx of AW. Finally, we present supporting data from remote sensing, buoy, and ship-based measurements, and discuss how the combined data sources can be used improve ocean models.

Because only information from a specific depth region is utilized, we plan to extend the integration to several depths, which can be done

without significantly increasing the complexity of the system. This is also the case for extending the current GP model to include more complex spatiotemporal dynamics. A more advanced bias correction scheme will also be considered as several covariates and information sources can be included to contribute to augment the prior forecast coming from the model. Additionally, recursive approaches flanked by model or phenomena-based heuristics, which have a limited computational footprint, are also improvements that will be explored.

## ACKNOWLEDGMENTS

This work was part of the ENTiCE project funded by the Research Council of Norway Project #255303/E40,[#] the Nansen Legacy Program, project number #27272, and the AMOS, Center of Excellence funding scheme, project number #223254. We are grateful to the captain and crew of NTNU's research vessel, the R/V *Gunnerus*. We thank the anonymous reviewers for their insightful comments that significantly improved this paper. And finally, the authors are grateful for the support of João Sousa, João Pereira, Tiago Marques, and LSTS from the University of Porto, prior and subsequent to the field experiments in this work. LSTS' work was partially funded by the the European Union's Seventh Framework Programme (FP7/2007–2013) under grant agreement #270180 (NOPTILUS).

## ORCID

*Trygve Olav Fossum* http://orcid.org/0000-0003-3468-9638

## REFERENCES

Albretsen, J. (2011). *NorKyst-800 Report No. 1: User manual and technical descriptions. Fisken og havet*. Bergen: Institute of Marine Research.

Asplin, L., Salvanes, A. G. V., & Kristoffersen, J. B. (1999). Nonlocal wind-driven fjord-coast advection and its potential effect on plankton and fish recruitment. *Fisheries Oceanography*, 8(4), 255–263.

Baafi, E., & Schofield, N. (1997). *Geostatistics. Geostatistics Wollongong'96*. Berlin: Springer Science and Business Media.

Banerjee, S., Carlin, B. P., & Gelfand, A. E. (2014). *Hierarchical modeling and analysis for spatial data*. Boca Raton, FL: CRC Press.

Barth, J. A., Hebert, D., Dale, A. C., & Ullman, D. S. (2004). Direct observations of along-isopycnal upwelling and diapycnal velocity at a shelfbreak front. *Journal of Physical Oceanography*, 34(3), 543–565.

Bhattacharjya, D., Eidsvik, J., & Mukerji, T. (2013). The value of information in portfolio problems with dependent projects. *Decision Analysis*, 10(4), 341–351.

Binney, J., Krause, A., & Sukhatme, G. S. (2010). Informative path planning for an autonomous underwater vehicle. *IEEE International Conference on Robotics and Automation* (pp. 4791–4796), Anchorage, Alaska.

Binney, J., Krause, A., & Sukhatme, G. S. (2013). Optimizing waypoints for monitoring spatiotemporal phenomena. *International Journal of Robotics Research*, 32(8), 873–888.

Broch, O. J., Ellingsen, I. H., Forbord, S., Wang, X., Volent, Z., Alver, M. O., … Skjermo, J. (2013). Modelling the cultivation and bioremediation potential of the kelp saccharina latissima in close proximity to an exposed salmon farm in Norway. *Aquaculture Environment Interactions*, 4(2), 187–206.

[#] https://www.sintef.no/en/projects/entice/.

Broch, O. J., Slagstad, D., & Smit, M. (2013). Modelling produced water dispersion and its direct toxic effects on the production and biomass of the marine copepod *Calanus finmarchicus*. *Marine Environmental Research*, 84(Supplement C), 84–95.

Cao, N., Low, K. H., & Dolan, J. M. (2013). Multi-robot informative path planning for active sensing of environmental phenomena: A tale of two algorithms. *Proceedings of the 2013 International Conference on Autonomous Agents and Multi-agent Systems, AAMAS'13* (pp. 7–14), Richland, SC.

Chang, D., Zhang, F., & Edwards, C. R. (2015). Real-time guidance of underwater gliders assisted by predictive ocean models. *Journal of Atmospheric and Oceanic Technology*, 32(3), 562–578.

Chekuri, C., & Pal, M. (2005). A recursive greedy algorithm for walks in directed graphs. *46th Annual IEEE Symposium on Foundations of Computer Science, 2005, FOCS 2005* (pp. 245–253), Piscataway, NJ: IEEE.

Cressie, N. A. C., & Wikle, C. K. (2011). Statistics for spatio-temporal data. *Probability and Statistics*. New York: Wiley.

Curtin, T. B., Bellingham, J. G., Catipovic, J., & Webb, D. (1993). Autonomous oceanographic sampling networks. *Oceanography*, 6(3), 86–94.

Das, J., Py, F., Harvey, J. B. J., Ryan, J. P., Gellene, A., Graham, R., … Sukhatme, G. S. (2015). Data-driven robotic sampling for marine ecosystem monitoring. *International Journal of Robotics Research*, 34(12), 1435–1452.

Das, J., Py, F., Maughan, T., Messie, M., O'Reilly, T., Ryan, J., … Rajan, K. (2012). Coordinated sampling of dynamic oceanographic features with AUVs and drifters. *International Journal of Robotics Research*, 31, 626–646.

Das, J., Rajan, K., Frolov, S., Ryan, J. P., Py, F., Caron, D. A., and Sukhatme, G. S. (2010). Towards marine bloom trajectory prediction for AUV mission planning. *IEEE International Conference on Robotics and Automation (ICRA)*, Anchorage, Alaska.

Davis, R. A. (2014). *Gaussian process: Theory* (pp. 1–6). Hoboken, NJ: John Wiley & Sons.

Donlon, C., Berruti, B., Buongiorno, A., Ferreira, M.-H., Féménias, P., Frerick, J., … Sciarra, R. (2012). The global monitoring for environment and security (gmes) sentinel-3 mission. *Remote Sensing of Environment*, 120, 37–57.

Eidsvik, J., Martinelli, G., & Bhattacharjya, D. (2018). Sequential information gathering schemes for spatial risk and decision analysis applications. *Stochastic Environmental Research and Risk Assessment*, 32(4), 1163–1177.

Eidsvik, J., Mukerji, T., & Bhattacharjya, D. (2015). *Value of information in the earth sciences: Integrating spatial modeling and decision analysis*. Cambridge: Cambridge University Press.

Ellingsen, I., Dalpadado, P., Slagstad, D., & Loeng, H. (2008). Impact of climatic change on the biological production in the Barents Sea. *Climate Change*, 87(1), 155–175.

Ellingsen, I., Slagstad, D., & Sundfjord, A. (2009). Modification of water masses in the Barents Sea and its coupling to ice dynamics: A model study. *Ocean Dynamics*, 59(6), 1095–1108.

Forristall, G. (2011). *Lofoten and Vesteralen currents (LOVECUR): Comparison of hindcasts with measurements* (Technical report). Camden, ME: Forristall Ocean Engineering, Inc.

Franks, P. J. S. (1992). Sink or swim: Accumulation of biomass at fronts. *Marine Ecology Progress Series*, 82, 1–12.

Frolov, S., Paduan, J., Cook, M., & Bellingham, J. (2012). Improved statistical prediction of surface currents based on historic HF-radar observations. *Ocean Dynamics*, 62(7), 1111–1122.

Gordoa, A., Masó, M., & Voges, L. (2000). *Satellites, oceanography and society* (Vol. 63). Amsterdam: Elsevier Science.

Graham, R., Py, F., Das, J., Lucas, D., Maughan, T., & Rajan, K. (2012). Exploring space-time tradeoffs in autonomous sampling for marine robotics. *International Symposium on Experimental Robotics (ISER)*, Quebec City, Canada.

Guestrin, C., Krause, A., & Singh, A. P. (2005). Near-optimal sensor placements in Gaussian processes. *Proceedings of the 22nd International Conference on Machine Learning* (Vol. 1, pp. 1–8).

Hoang, T. N., Low, B. K. H., Jaillet, P., & Kankanhalli, M. (2014). Nonmyopic $\epsilon$-Bayes-optimal active learning of Gaussian processes. *International Conference on Machine Learning* (pp. 739–747).

Holt, J. T., Allen, J. I., Proctor, R., & Gilbert, F. (2005). Error quantification of a high-resolution coupled hydrodynamic-ecosystem coastal-ocean model: Part 1 model overview and assessment of the hydrodynamics. *Journal of Marine Systems*, 57(1), 167–188.

Howe, B. M., Chao, Y., Arabshahi, P., Roy, S., McGinnis, T., & Gray, A. (2010). A smart sensor web for ocean observation: Fixed and mobile platforms, integrated acoustics, satellites and predictive modeling. *IEEE Journal of Selected Topics in Applied Earth Observations and Remote Sensing*, 3(4), 507–521.

Ikeda, M., Johannessen, J. A., Lygre, K., & Sandven, S. (1989). A process study of mesoscale meanders and eddies in the Norwegian coastal current. *Journal of Physical Oceanography*, 19(1), 20–35.

Krause, A. (2007). Nonmyopic active learning of Gaussian processes: An exploration–exploitation approach. *Proceedings of the IEEE International Conference on Machine Learning* (pp. 449–456), Pittsburgh, PA.

Krause, A., Guestrin, C., Gupta, A., & Kleinberg, J. (2006). Near-optimal sensor placements: maximizing information while minimizing communication cost. *2006 5th International Conference on Information Processing in Sensor Networks* (pp. 2–10), Nashville, TN.

Krause, A., Singh, A., & Guestrin, C. (2008). Near-optimal sensor placements in Gaussian processes: Theory, efficient algorithms and empirical studies. *Journal of Machine Learning Research*, 9, 235–284.

Leonard, N. E., Paley, D. A., Lekien, F., Sepulchre, R., Fratantoni, D. M., & Davis, R. E. (2007). Collective motion, sensor networks, and ocean sampling. *Proceedings of the IEEE*, 95(1), 48–74.

Lermusiaux, P. F. J. (2006). Uncertainty estimation and prediction for interdisciplinary ocean dynamics. *Journal of Computational Physics*, 217(1), 176–199.

Lévy, M. (2003). Mesoscale variability of phytoplankton and of new production: Impact of the large-scale nutrient distribution. *Journal of Geophysical Research: Oceans*, 108(C11). https://doi.org/10.1029/2002JC001577.

Ling, C. K., Low, K. H., & Jaillet, P. (2016). Gaussian process planning with Lipschitz continuous reward functions: Towards unifying Bayesian optimization, active learning, and beyond. *Proceedings Association for the Advancement of Artificial Intelligence* (pp. 1860–1866), Phoenix, AZ.

Low, K. H., Dolan, J. M., & Khosla, P. (2011). Active Markov information-theoretic path planning for robotic environmental sensing. *The 10th International Conference on Autonomous Agents and Multiagent Systems, AAMAS'11* (Vol. 2, pp. 753–760), Taipei, Taiwan.

Ma, K.-C., Liu, L., & Sukhatme, G. S. (2016). An information-driven and disturbance-aware planning method for long-term ocean monitoring. *2016 IEEE/RSJ International Conference on Intelligent Robots and Systems (IROS)* (pp. 2102–2108). Piscataway, NJ: IEEE.

Marchant, R., Ramos, F., Sanner, S., et al. (2014). Sequential Bayesian optimisation for spatial-temporal monitoring. *Proceedings Uncertainty in Artificial Intelligence* (pp. 553–562), Quebec City, Quebec.

Matérn, B. (2013). Spatial variation. *Meddelanden från Statens Skogsforskningsinstitut*, 36(5), 1–144.

Minnett, P., & Kaiser-Weiss, A. (2012). Near-surface oceanic temperature gradients (GHRSST Discussion Doc.).

Moses, W. J., Ackleson, S. G., Hair, J. W., Hostetler, C. A., & Miller, W. D. (2016). Spatial scales of optical variability in the coastal ocean: Implications for remote sensing and in situ sampling. *Journal of Geophysical Research: Oceans*, 121(6), 4194–4208.

Müller, M., Homleid, M., Ivarsson, K.-I., Køltzow, M. A., Lindskog, M., Midtbø, K. H., … Vignes, O. (2017). Arome-metcoop: A nordic convective-scale operational weather prediction model. *Weather and Forecasting*, 32(2), 609–627.

Pinto, J., Calado, P., Braga, J., Dias, P., Martins, R., Marques, E., & Sousa, J. (2012). Implementation of a control architecture for networked vehicle systems. *IFAC Proceedings Volumes*, 45(5), 100–105.

Pinto, J., Diasand, P. S., Martins, R., Fortuna, J., Marques, E., & Sousa, J. (2013). The LSTS toolchain for networked vehicle systems. *MTS/IEEE Oceans* (pp. 1–9). Piscataway, NJ: IEEE.

Py, F., Rajan, K., & McGann, C. (2010). A systematic agent framework for situated autonomous systems. *International Conference on Autonomous Agents and Multiagent Systems (AAMAS)*, Toronto, Canada.

Rajan, K., & Py, F. (2012). T-REX: Partitioned inference for AUV mission control. In G. N. Roberts & R. Sutton (Eds.), *Further advances in unmanned marine vehicles*. Michael Faraday House, Stevenage: The Institution of Engineering and Technology (IET).

Rajan, K., Py, F., & Berreiro, J. (2012). Towards deliberative control in marine robotics. In M. Seto (Ed.), *Marine robot autonomy*. Berlin: Springer.

Ramp, S. R., Davis, R. E., Leonard, N. E., Shulman, I., Chao, Y., Robinson, A. R., … Li, Z. (2009). Preparing to predict: The Second Autonomous Ocean Sampling Network (AOSN-II) experiment in the Monterey Bay. *Deep-Sea Research Part II: Topical Studies in Oceanography*, 56(3-5), 68–86.

Rao, D., & Williams, S. B. (2009). Large-scale path planning for underwater gliders in ocean currents. *Australasian Conference on Robotics and Automation (ACRA)*, Sydney.

Sætre, R. (1999). Features of the central norwegian shelf circulation. *Continental Shelf Research*, 19(14), 1809–1831.

Sætre, R. (2007). *The Norwegian coastal current: Oceanography and climate*. Bergen: The Institute of Marine Research, Tapir Academic Press.

Sakov, P., & Oke, P. R. (2008). Objective array design: Application to the tropical indian ocean. *Journal of Atmospheric and Oceanic Technology*, 25(5), 794–807.

Sakshaug, E., Johnsen, G., & Kovacs, K. (2009). *Ecosystem Barents Sea. Physical oceanography*. Trondheim: Tapir Academic Press.

Savtchenko, A., Ouzounov, D., Ahmad, S., Acker, J., Leptoukh, G., Koziana, J., & Nickless, D. (2004). Terra and Aqua MODIS products available from NASA GES DAAC. *Advances in Space Research*, 34(4), 710–714.

Shchepetkin, A. F., & McWilliams, J. C. (2005). The regional oceanic modeling system (ROMS): A split-explicit, free-surface, topography-following-coordinate oceanic model. *Ocean Modelling*, 9(4), 347–404.

Singh, A., Krause, A., Guestrin, C., & Kaiser, W. J. (2009). Efficient informative sensing using multiple robots. *Journal of Artificial Intelligence Research*, 34, 707–755.

Skarðhamar, J., Slagstad, D., & Edvardsen, A. (2007). Plankton distributions related to hydrography and circulation dynamics on a narrow continental shelf off Northern Norway. *Estuarine, Coastal and Shelf Science*, 75(3), 381–392.

Slagstad, D., & McClimans, T. A. (2005). Modeling the ecosystem dynamics of the Barents Sea including the marginal ice zone: I. Physical and chemical oceanography. *Journal of Marine Systems*, 58(1–2), 1–18.

Slagstad, D., Wassmann, P. F., & Ellingsen, I. (2015). Physical constrains and productivity in the future arctic ocean. *Frontiers in Marine Science*, 2, 85.

Smith, R. N., Das, J., Yi, C., Caron, D. A., Jones, B. H., & Sukhatme, G. S. (2010). *Cooperative multi-AUV tracking of phytoplankton blooms based on ocean model predictions*. Sydney: IEEE Oceans.

Smith, R. N., Py, F., Cooksey, P., Sukhatme, G., & Rajan, K. (2016). *Adaptive path planning for tracking ocean fronts with an autonomous underwater vehicle*. Morocco: International Symposium on Experimental Robotics (ISER).

Smith, R. N., Schwager, M., Smith, S. L., Jones, B. H., Rus, D., & Sukhatme, G. S. (2011). Persistent ocean monitoring with underwater gliders: Adapting sampling resolution. *Journal of Field Robotics*, 28(5), 714–741.

Sousa, A., Madureira, L., Coelho, J., Pinto, J., Pereira, J., Sousa, J., and Dias, P. (2012). LAUV: The man-portable autonomous underwater vehicle. Navigation, Guidance and Control of Underwater Vehicles (Vol. 3, pp. 268–274). https://doi.org/10.3182/20120410-3-PT-4028.00045.

Stein, M. L. (2005). *Nonstationary spatial covariance functions (CISES Technical Report 21)*. Chicago, IL: University of Chicago.

Stein, M. L., Chi, Z., & Welty, L. J. (2004). Approximating likelihoods for large spatial data sets. *Journal of the Royal Statistical Society: Series B (Statistical Methodology)*, 66(2), 275–296.

Stewart, R. (2009). *Introduction to physical oceanography*. Gainesville, FL: University Press of Florida.

Sverdrup, K. A., Duxbury, A., & Duxbury, A. C. (2006). *Fundamentals of oceanography*. New York: McGraw-Hill Higher Education.

Trenberth, K. (1992). *Climate system modeling*. Cambridge: Cambridge University Press.

Troccoli, A. (2003). *A proposal for correcting the wind stress forcing of an ocean model*. Nice, France: EGS-AGU-EUG Joint Assembly.

Vanhellemont, Q., & Ruddick, K. (2016). Acolite for sentinel-2: Aquatic applications of MSI imagery. *Proceedings of the ESA Living Planet Symposium* (pp. 9–13), Prague, Czech Republic.

Wassmann, P., Slagstad, D., & Ellingsen, I. (2010). Primary production and climatic variability in the European sector of the arctic ocean prior to 2007: Preliminary results. *Polar Biology*, 33(12), 1641–1650.

Wassmann, P., Slagstad, D., Riser, C. W., & Reigstad, M. (2006). Modelling the ecosystem dynamics of the Barents Sea including the marginal ice zone: II. *Carbon flux and interannual variability. Journal of Marine Systems*, 59(1–2), 1–24.

Werdell, P. J., & Bailey, S. W. (2005). An improved in-situ bio-optical data set for ocean color algorithm development and satellite data product validation. *Remote Sensing of Environment*, 98(1), 122–140.

Wunsch, C., & Heimbach, P. (2007). Practical global oceanic state estimation. *Physica D: Nonlinear Phenomena*, 230(1–2), 197–208.

Yilmaz, N. K., Evangelinos, C., Lermusiaux, P. F., & Patrikalakis, N. M. (2008). Path planning of autonomous underwater vehicles for adaptive sampling using mixed integer linear programming. *IEEE Journal of Oceanic Engineering*, 33(4), 522–537.

Zamuda, A., Hernandez Sosa, J. D., & Adler, L. (2016). Constrained differential evolution optimization for underwater glider path planning in submesoscale eddy sampling. *Applied Soft Computing*, 42, 93–118.

Zhang, B., & Sukhatme, G. S. (2007). Adaptive sampling for estimating a scalar field using a robotic boat and a sensor network. *Proceedings 2007 IEEE International Conference on Robotics and Automation* (pp. 3673–3680), Piscataway, NJ: IEEE.

Zhang, B., Sukhatme, G. S., & Requicha, A. A. (2004). Adaptive sampling for marine microorganism monitoring. *Proceedings Intelligent Robots and Systems (IROS)* (Vol. 2, pp. 1115–1122). Piscataway, NJ: IEEE.

**How to cite this article:** Fossum TO, Eidsvik J, Ellingsen I, Alver MO, Fragoso GM, Johnsen G, Mendes R, Ludvigsen M, Rajan K. Information-driven robotic sampling in the coastal ocean. *J Field Robotics*. 2018;1–21. https://doi.org/10.1002/rob.21805

# Article B

## Towards Adaptive Robotic Sampling of Phytoplankton in the Coastal Ocean

**Trygve Olav Fossum**, Glaucia M. Fragoso, Emlyn J. Davies, Jenny E. Ullgren, Renato Mendes, Geir Johnsen, Ingrid Ellingsen, Jo Eidsvik, Martin Ludvigsen and Kanna Rajan.



This article is published in
*Science Robotics*, Volume 4, Issue 27, $13^{th}$ February 2019,
doi: 10.1126/scirobotics.aav3041

UNDERSEA ROBOTS

# Toward adaptive robotic sampling of phytoplankton in the coastal ocean

Trygve O. Fossum[1,2,*], Glaucia M. Fragoso[3], Emlyn J. Davies[4], Jenny E. Ullgren[5], Renato Mendes[6,7,8], Geir Johnsen[2,3,9], Ingrid Ellingsen[4], Jo Eidsvik[10], Martin Ludvigsen[1,2,9], Kanna Rajan[2,6,11]



**Currents, wind, bathymetry, and freshwater runoff are some of the factors that make coastal waters heterogeneous, patchy, and scientifically interesting—where it is challenging to resolve the spatiotemporal variation within the water column. We present methods and results from field experiments using an autonomous underwater vehicle (AUV) with embedded algorithms that focus sampling on features in three dimensions. This was achieved by combining Gaussian process (GP) modeling with onboard robotic autonomy, allowing volumetric measurements to be made at fine scales. Special focus was given to the patchiness of phytoplankton biomass, measured as chlorophyll a (Chla), an important factor for understanding biogeochemical processes, such as primary productivity, in the coastal ocean. During multiple field tests in Runde, Norway, the method was successfully used to identify, map, and track the subsurface chlorophyll a maxima (SCM). Results show that the algorithm was able to estimate the SCM volumetrically, enabling the AUV to track the maximum concentration depth within the volume. These data were subsequently verified and supplemented with remote sensing, time series from a buoy and ship-based measurements from a fast repetition rate fluorometer (FRRf), particle imaging systems, as well as discrete water samples, covering both the large and small scales of the microbial community shaped by coastal dynamics. By bringing together diverse methods from statistics, autonomous control, imaging, and oceanography, the work offers an interdisciplinary perspective in robotic observation of our changing oceans.**

## INTRODUCTION

Processes controlling the growth and accumulation of phytoplankton are central to nutrient, carbon, and energy cycling; these provide the foundations for marine and human food webs (*1*, *2*). Despite their ubiquitous presence across the upper water column in the global ocean, phytoplankton presents a remarkable heterogeneity in spatial distribution (we will refer to this heterogeneity as patchiness) that is observable in microscale [subcentimeter, (*3*)], kilometer scale (*4*), and up to more than 600 km (*5*). Sampling at such a wide range of spatial scales is both challenging and interesting, because patchiness has been shown to strongly influence ecosystem stability (*6*), diversity (*7*), and productivity (*8*). Furthermore, measuring phytoplankton is complicated because observations have their basis in the proxy measurement of peak absorption of light at 675 nm, originating from photosynthetic chlorophyll a (Chla) inside planktonic cells.

With the growing capabilities of robotic vehicles, adaptive coverage of the water column is increasingly viable, although they continue to be challenging to operate in the harsh confines of the water column and the dynamic coastal ocean. Motivated by this, this work describes the use of propelled robotic platforms, known as autonomous underwater vehicles (AUVs), for optimizing mapping of water-column features in three dimensions. Such volumetric surveys of the water column are of substantial scientific interest because they provide better insight for understanding and measuring factors such as primary productivity, a vital indicator for ocean health.

[1]Department of Marine Technology, Norwegian University of Science and Technology (NTNU), Trondheim, Norway. [2]Centre for Autonomous Marine Operations and Systems (AMOS), Trondheim, Norway. [3]Department of Biology, NTNU, Trondheim, Norway. [4]SINTEF Ocean AS, Trondheim, Norway. [5]Runde Environmental Centre, Runde, Norway. [6]Underwater Systems and Technology Laboratory, Faculty of Engineering, University of Porto, Porto, Portugal. [7]CIIMAR, University of Porto, Porto, Portugal. [8]CESAM, Department of Physics, University of Aveiro, Aveiro, Portugal. [9]University Centre in Svalbard (UNIS), Longyearbyen, Norway. [10]Department of Mathematical Sciences, NTNU, Trondheim, Norway. [11]Department of Engineering Cybernetics, NTNU, Trondheim, Norway.
*Corresponding author. Email: trygve.o.fossum@ntnu.no

To do so, we concentrated on volumetric sampling of subsurface chlorophyll a maxima (SCM) using adaptive sampling methods. In particular, the goal was to develop adaptive behavior for AUVs that can enable increased sampling resolution of water-column processes in three dimensions by focusing sampling efforts in regions of interest. We limited the survey to a bounding box with a certain size, introducing both spatial and temporal constraints, similar to the enclosure criterion used in (*9*). Shortening the survey time means that the temporal effects will be minimal, and the error contributions from currents, navigation drift, and other time-dependent effects will be bounded, allowing complex time variability to be mitigated. This then transforms into a purely spatial problem of finding the relevant sampling locations within the surveyed volume, given a scientific context (for our case, the maximum Chla concentration depths). Assuming that only limited previous information is available, obtaining an a priori estimate of the SCM feature has substantial benefits, contrary to conducting an adaptive survey directly using interior [inside the three-dimensional (3D) volume] measurements. This direct approach is ineffective due to two main reasons. First, the AUV will have no forward-looking data to guide adaptation, resulting in coverage that is subject to a "hit-or-miss" trade-off. Given the limited volume of the survey, the adaptation distance available for such an approach is not present. Second, a key driver is the need to survey the most interesting aspects of the feature as fast and accurately as possible to reduce time-dependent effects. Building up an accurate estimate of the interior will be central to achieving this goal, because both the probability of losing track of the feature and the survey time can be reduced.

The method suggested in this work is designed to adhere to these ideas by separating the survey into a dedicated exploration and exploitation phase as follows: The AUV first starts by covering the sides of the bounding box volume in an initial phase dubbed MODE 1, followed by an adaptive survey of the interior volume, dubbed MODE 2, capitalizing on the learned information captured in a Gaussian process (GP) model, during MODE 1 (full details are given in Materials and Methods). Thus,

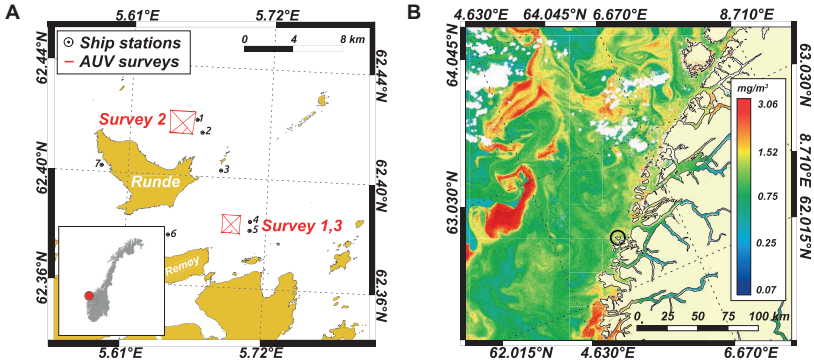


**Fig. 1. Survey area and Chla distribution.** (**A**) Map of the operational area with the three AUV surveys indicated [surveys 1 and 3 (southeast of Runde) and survey 2 (north of Runde)], whereas the ship-based sampling stations are denoted by numbers (stations 1 to 7). In the lower corner, a small map of Norway is shown with Runde marked in red. (**B**) Chla (OC4ME) product from Ocean and Land Color Instrument, a multispectral medium-resolution instrument on board ESA's Sentinel-3. The image from 2 May shows the Chla patchiness in the coastal zone, some months before the surveys. Runde is shown encircled in black.

the exploitation phase is a single-calculated maneuver based on the available information, allowing the AUV to survey a region of interest in the water column in a fast and focused manner, toward attaining a quasi-synoptic snapshot of the feature.

Our experiments were conducted in Runde, Norway, in June 2017 (see Fig. 1) with the algorithm embedded on an AUV to detect and to map the SCM, providing a 3D map of the Chla concentration, denoted as [Chla]. Note that we specifically define concentration with [Chla]. This is different from "Chla," which is an abbreviation for chlorophyll a. The measurements were complemented with photophysiological data derived from a fast repetition rate fluorometer (FRRf) and two particle imaging systems (SINTEF) (*10*) with different magnifications. These were profiled from a winch, together with a CTD (conductivity, temperature, and depth) sensor and water samples taken from the research vessel *R/V Gunnerus* at stations around Runde. An overview of the involved systems, scales, and platforms is given in fig. S2.

In situ measurements of the size, concentration, and type of particulate material in the water column are critical to resolve spatial distributions of the particles in question while minimizing disruption to them (*11*). A wide range of techniques could be used for such measurements: optical backscatter, fluorescence, laser diffraction (*12*), digital holography (*13*), and telecentric transmittance imaging (*10*, *14*), each providing specific information about suspended particulate material. However, it is not possible for a single instrument to obtain measurements of the entire size range of suspended material present in natural seawater, making it necessary to combine multiple techniques to monitor the full range of size and types. By combining measurements, a detailed picture of the water column can be rendered with both biometric and volumetric information, providing fine detail for resolving the in situ features while reducing errors related to aliasing and patchiness.

## Related work

Methods for tracking and sampling biomass distributions using autonomous platforms are still in their infancy. However, methodological studies are regularly reported, and several experiments have been conducted in the recent past. Moline *et al.* (*15*) introduced AUV-based sampling for ecophysiological work. Focusing on harmful algal blooms (HABs), Robbins *et al.* (*16*) combined AUV surveys with remote sensing toward attaining 3D information about bloom conditions. Similarly, Zhang *et al.* (*17*) used a long-endurance AUV to sample the peak Chla layer along horizontal cross sections for HAB monitoring using onboard gene processing equipment. Ryan *et al.* (*18*) used hidden Markov models to enable online estimation of water-column properties, enabling water samples to be triggered under certain upwelling conditions in Monterey Bay. The same region was explored in (*9*), where a GPS-tracked Lagrangian drifter was used in combination with AUVs for coordinated sampling of dynamic oceanic features, trying to follow the sides of a volume of water as it moved with subsurface currents. More decision-based efforts in sampling were presented in (*19*), where GPs were used in an online optimal choice approach to adaptively decide where to trigger water samples in the water column based on biomass concentration. In (*20*), cooperative tracking of phytoplankton blooms using buoyancy-driven gliders driven by ocean model predictions was articulated. This was developed further in (*21*), where the sampling resolution was modified by adjusting the undulation angle of a glider while accounting for ocean currents, with the aim to characterize and sample blooms. Graham *et al.* (*22*) discussed problems related to estimating spatiotemporal correlation in time-varying fields and compared Euclidean and Lagrangian approaches using AUV and drifter information to perform spatial interpolation. Feature tracking of patches and plumes was also discussed in (*23*), where a plan-based policy was learned, tested, and evaluated using simulated patches of Chla and then sampled in 2D in the open ocean. In (*24*), the combined use of satellite measurement, AUV, and research vessel data was used to describe advection of phytoplankton cells from open waters transported under the sea ice in the Arctic linking Chla presence, photosynthesis, and biodiversity. Spatial and temporal decorrelation scales in phytoplankton bloom magnitude were reviewed in (*25*), focusing on the U.S. West Coast. Sahlin *et al.* (*26*) gave an overview of different 3D interpolation strategies for oceanic data, with the conclusion that kriging is the preferred method for studying the marine pelagic environment.

Our work presents a practical real-world implementation of a sampling approach for the upper water column, capable of adapting to distributions in three dimensions. Such uncertain environments require a trade-off between exploration and exploitation; the proposed method presents a solution by splitting the survey into two dedicated phases within a limited volume, bounding time-variability effects. Under these conditions, the AUV can map the region of interest in the water column in an efficient quasi-synoptic manner. We demonstrated the method in a field experiment together with additional sampling on board a ship, showing the potential of collaborative mapping of planktonic distributions in a dynamic coastal environment.

## Sampling Chla in the water column

Planktonic patchiness can be a result of complex interplay of physical (stirring and mixing), chemical (nutrient availability, $CO_2$, $O_2$, and trace

metals), and biological (growth, movement, and mortality) processes, which can rapidly change in marine ecosystems and vary across multiple spatiotemporal scales (*27*). These interacting processes create a broad spectrum of patchiness, which can occur in small vertical layers [SCM layers (SCMLs)] (*28*) or in bigger plumes (*29*, *30*) that can only be partially visible in remote-sensing imagery (Fig. 1). Phenomena such as eddies can interrupt these layers by upwelling or downwelling and potentially create deep Chla maxima layers (DCMs) (*31*). Details about the difference between SCMLs and DCMs can be found in (*32*).

Knowing where and when to sample is vital to accurately resolve processes. Furthermore, data collection will, in some cases (especially Lagrangian buoys and floats), itself be influenced by the same forces, such as currents and winds, in addition to the physical limitations of the platform (speed, battery, depth rating, etc.) affecting the spatiotemporal coverage. Capturing synoptic information is therefore a major challenge. Remote-sensing data can only obtain coverage at the very surface, omitting valuable information in the depth dimension and, consequently, features such as the SCM. Furthermore, remote-sensing products rarely reach the subkilometer resolution, which is vital for evaluation of oceanographic phenomena that control coastal primary productivity at fine scales (*33*).

## Chla patchiness, distributions, and interpretation

The advent of fluorometry as a proxy for measuring Chla fluorescence, in addition to the progress of remote-sensing approaches, has provided a significant advance in the study of plankton distributions (*34*, *35*) providing continuous measurements, where Chla is used as a common "currency" for biomass estimation. Biomass is a broad and practical term used to describe the amount of living material in the water column. We use the concentration of Chla as an indicator of the phytoplankton biomass (organic carbon, expressed as milligrams per cubic meter); hence, the terms [Chla] and phytoplankton biomass, or just biomass, are used interchangeably in this text. Although Chla is used as an indicator of phytoplankton biomass worldwide, variability of cellular Chla content is expected to occur as a function of light intensity, species composition, and nutrient availability (*36*, *37*).

The use of Chla fluorescence measured in vivo, i.e., in live cells measured in situ, as a proxy of phytoplankton biomass and patchiness, needs to be interpreted carefully. When phytoplankton cells are exposed to high light levels (for instance, those usually found at the surface ocean, particularly near mid-day during summer), some of the excess of energy absorbed is dissipated as heat (*38*). Part of this is related to a photoprotective process, called nonphotochemical quenching (NPQ), that occurs as a rapid response to high light and results in the reduction of fluorescence emission at the surface (*39*). Thus, a subsurface Chla fluorescence maximum observed in a vertical profile may not necessarily reflect biomass accumulation; rather, it can be a spurious representation of patchiness. To circumvent this challenge, we compared in vivo fluorescence Chla collected in situ from the AUVs and FRRf measurements with in vitro Chla, which is derived from filtered water samples and methanol extraction to check whether a subsurface Chla maximum is present at the sampled locations.

At first glance, the complex spatial structure of the phytoplankton distribution occurs as a result of biological and physical processes and interactions in the water column. The spatial distribution of phytoplankton biomass, its intensity, morphology, and scale dependence [such as the open ocean (10 to 100 km, mesoscale) or coastal zones (10 m to 1 km, submesoscale)] is substantially driven by processes, such as turbulent advection, upwelling, convergence, and vertical mixing (*27*, *40*). For example, local processes such as upwelling zones can bring deep water nutrients to the surface layer and nurture phytoplankton, creating regional hot spots (with high biomass concentration), at scales ranging from 5 to 10 km (*41*) or even ≤1 km for complex coastal zones (*42*). In the open ocean, the same aggregation can range from 70 to 140 km (spatial correlation) in the horizontal plane; vertically, persistent upper water-column stratification may lead to a subsurface maxima, where phytoplankton is concentrated in the bottom of the pycnocline (density gradient) to better use light and nutrients (*43*). Vertical correlation is much weaker due to stratification effects (*26*). Figure 1B shows the surface distribution of [Chla] for 2 May 2017 along the Norwegian coast, depicting the spatial patterns at the mesoscale.

Regardless of the physical processes taking place, spatial heterogeneity must be "seeded" from external factors that trigger phytoplankton growth, such as nutrient availability and light levels (*4*), in addition to intrinsic evolutionary and physiological traits of the species (e.g., buoyancy, vertical migration, and daily cycles of photosynthesis) (*3*), reinforcing the role of physiology on shaping phytoplankton patchiness. Many fluorometers [such as pulse amplitude modulated (PAM) and FRRf] offer the opportunity to study the health of phytoplankton communities, which allow examination of the physiological state of a community and, when combined with reconstructions from AUV surveys, are powerful assets to investigate the spatial structure of phytoplankton distributions (*24*).

Zooplankton grazing is another biological process that accounts for patchiness as it relates to phytoplankton mortality. Although extremely important, it is difficult to study the effect of such grazing on patchiness due to the nonlinear nature of biological interactions and the scarcity of observations that constrain models (*4*). Like phytoplankton, zooplankton themselves are patchily distributed, either occurring in swarms or vertically migrating in the water column, which complicates the interpretation of abundance due to undersampling—that is, being below the Nyquist sampling rate, so that the dynamics of a phenomena is not captured at a level necessary for reconstructing the original distribution (aliasing). The development of acoustic sensors, such as Acoustic Doppler Velocity Profiler and Acoustic Zooplankton Fish Profiler, and particle counters capable of collecting continuous zooplankton counts provides an opportunity to assess abundance and the phytoplankton influence.

## Experimental setting

Our study site is in the coastal zone of the southern Norwegian Sea. In this region, the Norwegian Atlantic Current approaches the coast bringing saline Atlantic water onto the narrow continental shelf (*44*). The Norwegian Coastal Current, carrying fresh water from the outflow of the Baltic and receiving additional fresh water from land runoff as it flows northward along the coast, also enters the shelf in the Møre region (*44*, *45*). Both the volume transport of the Norwegian Coastal Current and the lateral location of the interface between Atlantic and coastal water vary seasonally and are strongly affected by wind (*46*, *47*); there is also considerable mesoscale variability in the coastal current system (*47*, *48*). Mesoscale eddies play an essential role in ocean dynamics and significantly affect ocean biology and biogeochemistry (*49*). Although mesoscale eddies, from a few to a few hundred kilometers, are known to have a strong effect on plankton distributions, community structure, and diversity (*49*), smaller instabilities can locally enhance vertical mixing (*50*). Such submesoscale processes, on spatial scales of 0.1 to 10 km, can enhance both phytoplankton productivity and its variance on time scales of a few days (*50*).

Repeated sampled temperature and salinity profiles from Skinnbrokleia (7 km southeast of our AUV surveys) were used to place the AUV

observations in a local and seasonal setting. Meteorological and oceanographic (metocean) time series from a stationary buoy at Breisundet (14 km northeast of the AUV surveys) were also used. The buoy, placed in 345-m water depth in an inlet between two islands, measures surface waves, wind, current velocity, salinity, and temperature at selected depths.

In the weeks preceding the field campaign, the hydrographic conditions in the study area were typical of early summer (*51*, *52*). Upper layer salinity was low, and a shallow seasonal thermocline had formed in the upper 10 m (seen in data from a monitoring station on 8 June, 16 km southeast from the survey site). The beginning of the cruise, however, coincided with the onset of stronger winds, around 10 m/s with gusts up to 16 m/s, that prevailed throughout the first half of that week (Fig. 2B). The fresh breeze was accompanied by increasing wave height, up to 2 m (as measured at the stationary metocean buoy in Breisundet). Wind stirring during this event caused a deepening of the mixed layer. Time series of temperature and salinity from the metocean buoy revealed that the mixing started immediately with the onset of stronger winds on 17 June and progressed during the following days until eventually temperature and salinity were homogenized down to the 40-m depth level (Fig. 2A).

The AUV and ship-based CTD profiles taken on the same day showed a 30-m-deep well-mixed layer (Fig. 3). The water-column structure was similar in the AUV survey area and at the ship-based CTD stations some 400 m away. In the thermocline between depths of 30 and 40 m, we found some features that were different, such as local temperature inversions, and that were seen at one site (CTD stations) but not at the other (AUV surveys). The different measurement methods lead to small variations between the profiles: The AUV captured the surface layer from the top centimeter down, whereas the CTD profile excluded the uppermost meter. On the other hand, the CTD profiles reached deeper than the AUV's maximum dive depth of 50 m. The many profiles from the AUV survey form an envelope that indicates the small-scale spatial variability of temperature and salinity. The difference in water mass properties between the CTD sites and the AUV survey is comparable with the variability within the AUV survey area, which, in turn, is comparable in size with the distance between CTD stations and the AUV survey (Fig. 1A).

### GP model of the distribution of Chla

We used a spatial statistical model in the form of a GP to model the SCM. The GP formulation is widely used for dealing with spatial applications in the ocean (*22*, *53*). Its popularity is largely due to the simple yet flexible modeling formulation, which allows consistent and efficient data conditioning. In contrast to a full numerical ocean model, a GP can operate with limited computational resources on board an AUV and assimilate measurements on the fly.

Measurements were coherently assimilated to render a more detailed representation of the SCM as the survey progressed. The SCM is predicted by a GP in 3D space (latitude, longitude, and depth), by assimilating the identified SCM depth into a 2D grid, of which the detailed steps are explained in Materials and Methods. For environmental applications, a GP is typically discretized to a grid map with a certain resolution describing variation in space. This map is, in essence, a collection of random variables (on the grid) with a multivariate normal probability density function, where the spatial dependence is captured by a covariance model.

The stochastic process $\{x(s), s \in \Omega\}$, with $\Omega$ being an indexed grid set $\Omega \subset \mathbb{R}^3$, is a GP if, for any finite choice of $n$ distinct locations $s_1, \ldots, s_n \in \Omega$,

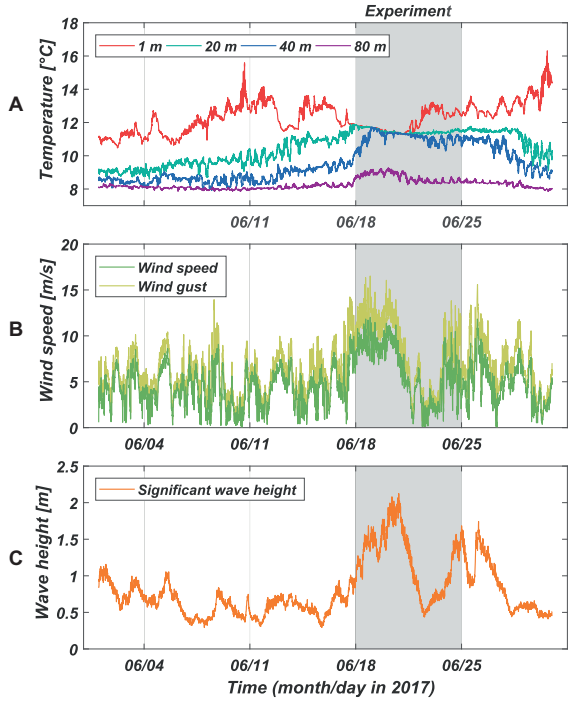


**Fig. 2. Environmental conditions from buoy data.** Time series of (**A**) water temperature at four different depths, (**B**) wind speed and wind gust, and (**C**) significant wave height, measured at a buoy located some 14 km inshore of the AUV survey area. The entire month of June 2017 is shown, with gray background marking the period of AUV and ship measurements.

the random vector $\mathbf{x} = [x(\mathbf{s}_1), \ldots, x(\mathbf{s}_n)]$ has a multivariate normal probability density function

$$p(\mathbf{x}) = \mathcal{N}(\boldsymbol{\mu}, \boldsymbol{\Sigma}) = \frac{1}{(2\pi)^{\frac{n}{2}}|\boldsymbol{\Sigma}|^{\frac{1}{2}}} e^{-\frac{1}{2}(\mathbf{x}-\boldsymbol{\mu})^T \boldsymbol{\Sigma}^{-1}(\mathbf{x}-\boldsymbol{\mu})} \quad (1)$$

defined by the mean vector $\boldsymbol{\mu} = E(\mathbf{x})$ and the symmetric positive definite covariance matrix $\boldsymbol{\Sigma} = \mathrm{cov}(\mathbf{x}, \mathbf{x})$. The prior mean $\boldsymbol{\mu} = [\mu_1, \ldots, \mu_n]$ constitutes a 3D surface (latitude, longitude, and depth) of the estimated peak Chla layers. The covariance matrix $\boldsymbol{\Sigma}$ is given as

$$\boldsymbol{\Sigma} = \begin{bmatrix} \Sigma_{11} & \Sigma_{12} & \ldots & \Sigma_{1n} \\ \Sigma_{21} & \Sigma_{22} & \ldots & \Sigma_{2n} \\ \vdots & \vdots & \ddots & \vdots \\ \Sigma_{n1} & \Sigma_{n2} & \ldots & \Sigma_{nn} \end{bmatrix}$$

where $\Sigma_{ij} = \sigma^2 \mathcal{K}(i,j)$. The stationary covariance has entries depending on the pairwise distance between grid locations. The kernel is defined as

$$\mathcal{K}(i,j) = (1 + \phi h_{ij}) e^{-\phi h_{ij}}$$

with distance $h_{ij} = |\mathbf{s}_i - \mathbf{s}_j|$ and $\phi$ a model parameter indicative of the correlation range (*54*). Capturing the correct spatial correlation is

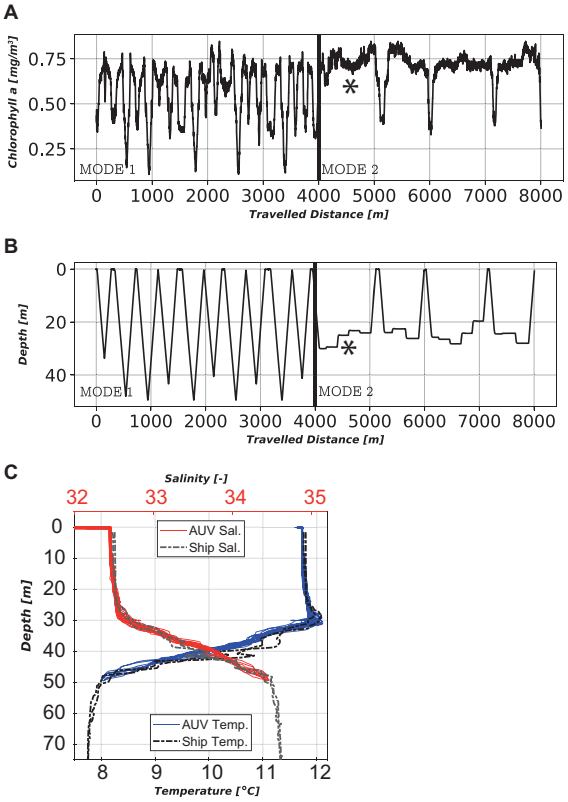


**Fig. 3. Data from survey 1 (MODE 1.fixed) using fixed tracking of the 3D Chla surface.** Asterisks mark a point where the AUV behavior transitions, as the depth adjustment is followed by increased [Chla]. This is also shown in Fig. 4. (**A**) Chla concentration versus traveled distance accumulated over ground. (**B**) Temperature and salinity curves from AUV and the *R/V Gunnerus* from the same area. (**C**) AUV depth versus traveled distance. Note the adjustment of survey depth as the AUV follows the 3D surface (in 200-m increments).

important, because this will affect how the measurements are interpolated. In our experiments, the effective correlation range was set to $\phi \sim 1000$ m based on the east-west variogram results from (*42*), investigating the Chla scale dependency for coastal zones using high-resolution remote sensing [notably, this implies having correlation across the smallest survey area ($\sqrt{700^2 + 700^2} = 990$ m)]. Here, both larger (*26*) and smaller (*55*) correlation ranges can be defined, depending on the scale of heterogeneity, type of marine system being studied, and previous insight of the water body and ambient conditions.

As measurements are assimilated, the 3D mean surface is adjusted toward the derived Chla maximum depth, and prediction variances are reduced (details are provided in Materials and Methods). The SCM peak depth is found for each vertical crossing as the AUV undulates via a "yo-yo" maneuver in the water column, where $d_t$ is the AUV location at time $t$ with the corresponding SCM peak. The measurement model for time $t$ is given by

$$\mathbf{y}_{t,d_t} = \mathbf{G}_{t,d_t}\mathbf{x} + \mathbf{v}_t \tag{2}$$

where $\mathbf{y}_{t,d_t}$ is a length $m_{t,d_t}$ vector of the survey line observation and the $m_{t,d_t} \times n$ matrix $\mathbf{G}_{t,d_t}$ contains "1" entries only at the designated $d_t$ indices and 0 otherwise. The error term $\mathbf{v}_t \sim \mathcal{N}(0, \mathbf{R}_{t,d_t})$ represents measurement noise. The covariance matrix $\mathbf{R}_{t,d_t}$ is set to a constant diagonal matrix (*56*), and there is no dependence of measurement error terms over assimilation time.

Under Gaussian linear modeling assumptions, the sequential updating of survey data leads to the Gaussian conditional distribution $p(\mathbf{x}|\mathbf{y}_{1,d_1}, \ldots, \mathbf{y}_{t,d_t})$, defined by conditional mean $\mathbf{m}_{t,d_t}$ and covariance $\mathbf{P}_{t,d_t}$. These equations are recursive over the data-gathering steps:

$$\begin{aligned}
\mathbf{S}_{t,d_t} &= \mathbf{G}_{t,d_t}\mathbf{P}_{t-1,d_{t-1}}\mathbf{G}^t_{t,d_t} + \mathbf{R}_{t,d_t} \\
\mathbf{K}_{t,d_t} &= \mathbf{P}_{t-1,d_{t-1}}\mathbf{G}^t_{t,d_t}\mathbf{S}^{-1}_{t,d_t} \\
\mathbf{m}_{t,d_t} &= \mathbf{m}_{t-1,d_{t-1}} + \mathbf{K}_{t,d_t}(\mathbf{y}_{t,d_t} - \mathbf{G}_{t,d_t}\mathbf{m}_{t-1,d_{t-1}}) \\
\mathbf{P}_{t,d_t} &= \mathbf{P}_{t-1,d_{t-1}} - \mathbf{K}_{t,d_t}\mathbf{G}_{t,d_t}\mathbf{P}_{t-1,d_{t-1}}
\end{aligned} \tag{3}$$

where the mean and covariance matrix are initialized by $\mathbf{m}_{0,d_0} = \boldsymbol{\mu}$ and $\mathbf{P}_{0,d_0} = \boldsymbol{\Sigma}$.

## RESULTS

### Experimental setup

The AUV platform used in our experiments was an OceanScan Light AUV (LAUV) (*57*), capable of upward 24-hour in-water operation (fig. S1). A WET Labs ECO Puck was the main sensor payload measuring Chla concentration (470-nm excitation and 695-nm emission peak of Chla) with supplementary sensors including cDOM (color dissolved organic matter), TSM (total suspended matter), a 16-Hz Sea-Bird FastCAT 49 pumping CTD, and Aanderaa 4831 oxygen optode. The Chla tracking algorithm was hosted on a multicore graphics processing unit (GPU) NVIDIA Jetson TX1 single-board computer.

Alongside AUV measurements, both FRRf and two SilCam camera systems were used to resolve details of the water column, as well as allowing cross-reference and verification of AUV measurements and behavior in addition to the algorithm embedded onboard. These systems were deployed from a winch, together with a CTD. The FRRf measures irradiance and [Chla], in addition to photophysiological parameters of the phytoplankton community. The SilCam systems imaged a particle size range spanning 28 μm to 4 cm in equivalent diameter, enabling characterization of particle size over a range covering three orders of magnitude in diameter. For accurate fluorescence-based Chla determination and calibration of the FRRf, water samples were collected every 10 m in the upper 60 m on the upward CTD casts using 5-liter Niskin bottles mounted on a rosette frame. Water samples were immediately filtered onto 25-mm glass fiber filters (from GF/F Whatman Inc.) and stored in a −20°C freezer until analyzed in the laboratory 1 month later. [Chla] was extracted in 100% methanol for about 4 hours at 10°C and fluorometrically determined using a Turner Designs fluorometer. This sampling activity was conducted from the research vessel *R/V Gunnerus*. The survey map and sampling stations are shown in Fig. 1A.

### AUV surveys

The adaptive AUV surveys took ~1.5 hours to complete (survey 2 covered a larger volume), with a mean vehicle speed of 1.6 m/s over ground; details are provided in Table 1. To follow the GP model estimate of the SCM 3D surface, we explored two strategies: (i) using fixed depth (MODE 1.fixed) and (ii) using an undulating/yo-yo motion, ±2.5 m across the 3D surface (MODE 2.undulating). Although finer

**Table 1. AUV survey information and details.**

| Survey | Date and time | Duration | Mean velocity (m/s) | Area ($m^2$) | Mode |
|---|---|---|---|---|---|
| 1 | 20.06.17, 10:02 a.m. | 1 hour 33 min | 1.5 | 700 | Fixed depth |
| 2 | 20.06.17, 12:10 a.m. | 1 hour 58 min | 1.5 | 900 | Fixed depth |
| 3 | 22.06.17, 11:06 a.m. | 1 hour 27 min | 1.6 | 700 | Undulating ±2.5 m |

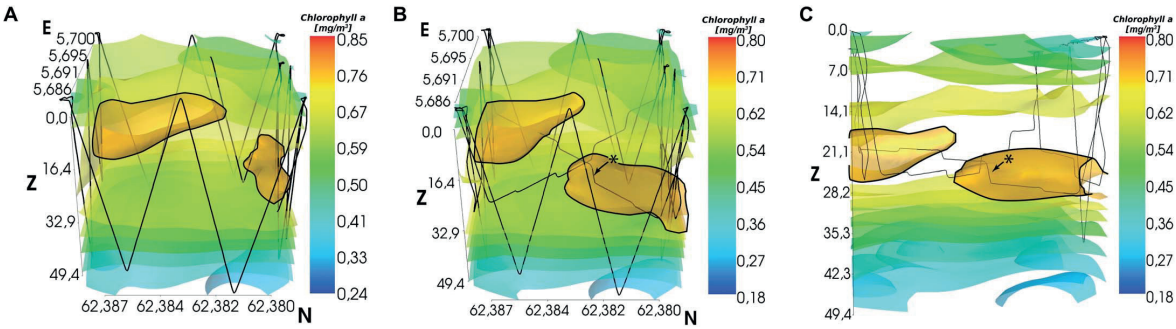


**Fig. 4. Volumetric estimate and AUV path.** (**A**) Volumetric representation (3D kriging) of the [Chla] isosurfaces after the initial survey phase (MODE 1) covering the sides of the volume. The AUV path is overlaid (black line), and N, E, and Z are labels for north, east, and depth, respectively. (**B**) Volume after the adaptive survey of the internal volume (MODE 2), rendering more of the internal [Chla] structure. The depth adjustment (marked with asterisk) in the interior made the AUV stay in the region of high concentration. (**C**) Side view of the same volume as in (B) to highlight the adaptive depth adjustments performed by the AUV. The color scale of the interior isosurfaces is affected by the transparency. Plots constructed in Mayavi (*65*).

discretization is possible, given the uncertainty due to current speed and direction, as well as natural stratification, the SCM depth estimates from the GP surface (~23-m resolution) were discretized into 200-m segments for the AUV to follow.

A detailed analysis of the approach is presented focusing on survey 1, using fixed depth control, and comparing that with survey 3, tracking the 3D surface using an undulating/yo-yo pattern. Results from survey 2 are shown in fig. S3.

In Fig. 3B, the first ~4 km is used to cover the sides of the volume (MODE 1), gathering an estimate of the SCM, before MODE 2 tracks this estimate by either fixed or undulating/yo-yo behavior. MODE 2, in turn, trails an hourglass pattern in the interior of the volume for the next ~4 km (see Materials and Methods for more details). The second half of Fig. 3B shows the AUV adjusting its depth according to the SCM estimate, with periodic surfacing events when reaching the corner points of the survey box. Both survey 1 (Figs. 3A and 4) and survey 3 (Fig. 5A) confirm that the [Chla] concentrations were higher during the tracking phase of MODE 2, with the AUV sampling between the 20- and 30-m depth range. These depths correspond to the SCM found from analysis of the water samples taken from the research vessel and shown together in Fig. 6 with FRRf data. The temperature and salinity data in Fig. 3C suggest that the water column was well mixed down to 30 m, where an abrupt gradient is present. This interface influences the distribution of biomass in the water column (*58*).

Because the first phase (MODE 1) took ~40 min to complete, some of the estimates were likely affected by current velocity and direction. It is therefore important to verify that the depth adjustments result in an increase of [Chla]. Elevated levels of [Chla] can be seen throughout the second phase of the missions, but to verify this further, in Figs. 3 (A and B) and 4 (B and C), an asterisk shows the first part of the SCM tracking and the successful depth adjustment that results in elevated levels of [Chla]. The first part is chosen, because the earliest observations have the highest probability of being affected, due to their high lag between the initial measurements and revisitation, affected by current.

Furthermore, by comparing the volumetric estimate before (Fig. 4A) and after (Fig. 4, B and C) the interior survey, we can see the distribution change in light of the new measurements. The isosurfaces (marked with black lines in Fig. 4) changed, resolving the interior information with finer detail. The change is greatest within the volume, which is expected, because these locations are unsurveyed, previously estimated on the basis of the data from the sides. The main features and distribution are largely similar before and after the initial survey. This coherence supports the credibility of the design premise, limiting the survey size to effectively handle time dynamics, as well as the shared information between the interior and boundary used to focus sampling.

Comparing the results with survey 3 using the undulating/yo-yo depth tracking shows that survey 3 also has elevated concentrations while tracking the SCM. Because the undulating/yo-yo approach is less sensitive to errors in the depth estimate while providing higher sampling density at the SCM, it is more practical for mapping the structure of the SCM but only subject to a certain current regime; with strong currents, a fixed depth approach would likely be preferable because of shorter survey times.

## FRRf measurements

Figure 6 shows a vertical profile of the in vitro (extracted) and the in vivo (measured in situ) [Chla] derived from the FRRf deployed at stations 4 and 5 and from AUV survey 1 indicated on the map in Fig. 1A; all FRRf surveys are shown in Table 2. Details on intercalibration can be found in (*24*). In the in situ assessments (FRRf and AUV), [Chla] is higher

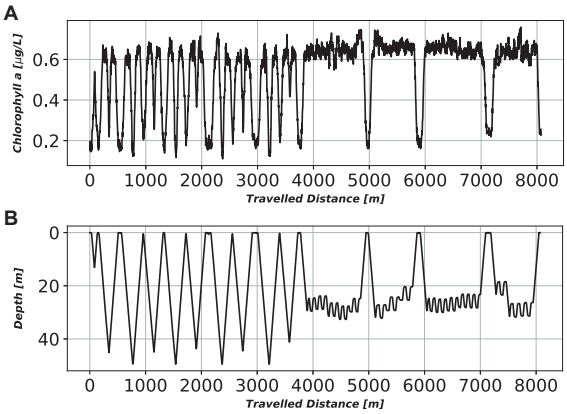


**Fig. 5. Survey 3 using undulating tracking control during the survey.** (**A**) [Chla] versus traveled distance accumulated over ground. (**B**) AUV depth versus traveled distance.

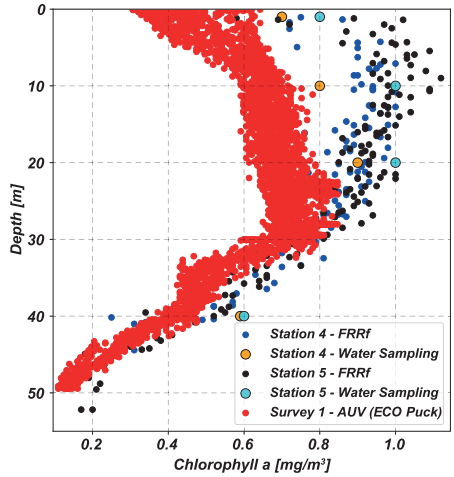


**Fig. 6. Comparisons of in situ [Chla] derived from the AUV (ECO Puck), FRRf profiling measurements, and in vitro [Chla] extracted from water samples.** The differences in [Chla] at the surface between the two sensors are due to the hydrography of the two stations despite proximity.

(>0.6 mg $m^{-3}$) at the upper 30 m, decreasing gradually below this depth (<0.8 mg $m^{-3}$). The vertical structure of [Chla] is in agreement with salinity profiles, confirming that the depth of the mixed layer approaches 30 m. At stations 4 and 5, the in situ observations (from the FRRf) agreed with the results from the in vitro [Chla]. Both measurements reveal a similar vertical pattern, such as a subsurface maximum (from 10 to 25 m), suggesting a higher concentration of phytoplankton cells at this depth, although this trend is much less pronounced than for the AUV data. When compared with AUV survey 1, [Chla] varies slightly in the upper 30 m (a difference of 0.2 mg $m^{-3}$ of [Chla]), which could imply that the hydrography was different between stations 4 and 5 and survey 1, despite the proximity of sites. This result reemphasizes the need for robotic sampling to monitor the variability and patchiness of phytoplankton distributions.

A quenching (reduction) of the fluorescence signal in live cells (in situ) is commonly found in surface waters during summer, when phytoplankton are exposed to high light levels. This occurs to protect the cells' photosystems [a process called NPQ (*38*)], by converting part of the excess energy to heat. Results from this study show that the in vitro [Chla] presented approximately the same vertical pattern as the in situ measurements, with a subsurface maximum at depths of 20 to 30 m. This suggests that NPQ processes were not evident in this study, possibly because of cloudy conditions. Clouds reduce the amount of light that reaches the surface water; consequently, such conditions do not interfere as much with the in situ fluorescence measurements derived from the sensors.

## SilCam observations

In situ [Chla] derived from the FRRf and the AUV provided relevant information regarding phytoplankton patchiness, but there may exist some linkages to biological activity (e.g., grazing) at higher trophic levels and thus larger particle sizes. Results from the two SilCam particle imaging systems provided in situ images of suspended material, allowing insight into the presence and distribution of larger phytoplankton and zooplankton, in addition to other material in the water column, such as marine snow and suspended sediments.

Figure 7 shows particle number distribution and sample images recorded within the diameter range of 30 to 10,000 µm at stations 4 and 5 using the two SilCams with different magnifications. With an average exponent ($m$) of 3 (shown by the dashed lines in Fig. 7), the size distribution follows approximately that of a Junge distribution (*59*):

$$n(D) = kD^{-m} \quad (4)$$

where $n(D)$ is the number of particles of diameter $D$, $k$ is a constant that scales according to the particle concentration, and $m$ is the slope of the distribution. In the simplest form, the Junge distribution is an approximation of the particle size distribution, made up of a series of multiple log-normal distributions with varying median sizes that arise from subpopulations of particulate material such as specific types of phytoplankton, zooplankton, or marine snow (*60*). In Fig. 7, the observed distributions show many points of variation from this average Junge slope, with one peak at just over 100 µm that corresponds to a high abundance of the dinoflagellate genus *Ceratium* (indicated by the red shaded region), which can be seen in the middle column of

**Table 2. FRRf survey data gathered from stations 1 to 7, shown in Fig. 1A.**

| Name | Area | Tide |
|---|---|---|
| Station 1—19.06.17, 10:15 a.m. | Survey 2 | Ebb |
| Station 2—19.06.17, 13:55 a.m. | Survey 2 | Low |
| Station 3—19.06.17, 16:15 a.m. | Between S2 and S1 | Rise |
| Station 4—20.06.17, 10:30 a.m. | Survey 1 | Ebb |
| Station 5—20.06.17, 13:05 a.m. | Survey 1 | Low |
| Station 6—21.06.17, 10:10 a.m. | West of S1 | High |
| Station 7—21.06.17, 14:45 a.m. | West and between S2 and S1 | Low |

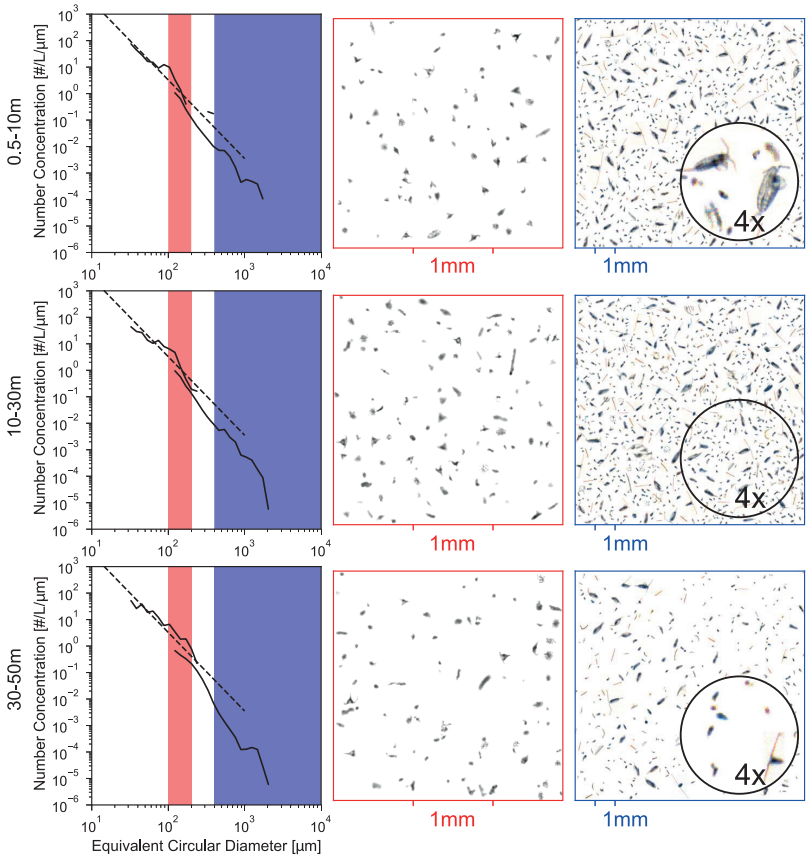


**Fig. 7. Sample imaging information from the SilCam obtained at stations 4 and 5.** Data presented are averaged from both stations and discretized into three depth ranges from 0.5 to 10 m (top), 10 to 30 m (middle), and 30 to 50 m (bottom). The left column shows the particle number distribution from the two magnifications of SilCam that were deployed, with the montages of particles from the red shaded region presented in the images in the middle column of the figure and the blue shaded region in the images in the right column of the figure. The dashed line in the particle number distributions represents the average fitted Junge distribution (*59*) (between 100 and 300 µm) from all depths.

the figure. The copepod genus *Calanus* is also highly abundant (indicated by the blue shaded region) and can be seen in the rightmost column of the figure. In the montages of particle images (right two columns of Fig. 7), individual particle images are packaged into the plot by randomly sampling from the recorded size distribution so as to maintain the ratio of large to small particles, albeit without being representative of the true concentration of particles, which was more sparse in situ.

Most particulate material is present within the top 10 m, and it is where relative abundance of *Ceratium* appears greatest because the 100-µm peak in the particle number distribution is most prominent. *Ceratium* is still present in approximately the same concentration between 10 and 30 m but is surrounded by a higher concentration of other material also present within this depth range. This is evidenced by the reduced dominance of the 100-µm peak. Below the thermocline at 30 m, the *Ceratium* peak in the number distribution is not discernible, and there is less total material in suspension. With such a high dominance of biological material in the water, the reduced concentrations below 30 m, observed by the SilCam, agree well with the reduced [Chla]. The highest load of particulates observed by particle imaging was within the 10- to 30-m depth range, which also corresponds to the SCM. However, the small difference in the concentrations of material at 100 µm between the 0.5- to 10-m and 10- to 30-m depth ranges suggests that other smaller phytoplankton species (possibly not captured by the imaging system), in addition to *Ceratium*, are contributing to the SCM.

## DISCUSSION

We have presented methods for autonomously mapping spatial heterogeneity of phytoplankton biomass in 3D using AUVs by combining GP models and robotic sampling. The method is shown to successfully estimate and track layers of high Chla concentration, focusing sampling efforts and increasing resolution along important features such as the SCM. We used spatial modeling and interpolation to reconstruct the distribution in 3D. This volumetric estimate was then augmented with in situ images of suspended particles, fluorometry, and discrete water samples taken co-temporally from a research vessel. Comparison of in-field data shows correspondence between AUV data and behavior, providing a broad and extensive perspective of the pelagic activity. The results demonstrate the complexity of conducting interdisciplinary coastal ecology and support unification of marine data sources to achieve a detailed environmental picture of the water column.

### Limitations and future steps

The largest source of sampling uncertainty comes from the effects of currents (speed and direction), making the observations time-dependent. The AUV used in this study is fast enough to find and make use of spatial structure, but not so fast as that it can capture the full spatial field at any time, because an AUV is not a synoptic measurement platform. Ideally, the AUV should therefore try to "stay" with the same water mass, working in a Lagrangian frame of reference to reduce these effects. Lagrangian correction is, however, nontrivial, and, unless a good proxy measurement of advection can be provided (such as from a surface drifter), there is limited value in adding to experimental complexity [see (*22*) for a more detailed discussion]. A simple and effective measure to account for this is to limit the method/survey area to subkilometer size, setting a bound on these uncertainties similar to the enclosure criterion used in (*9*). Use of this strategy allows us to use directed Euclidean sampling of the interior volume while increasing sampling resolution and determining SCM variability. This can be seen by looking at the recorded data and comparing

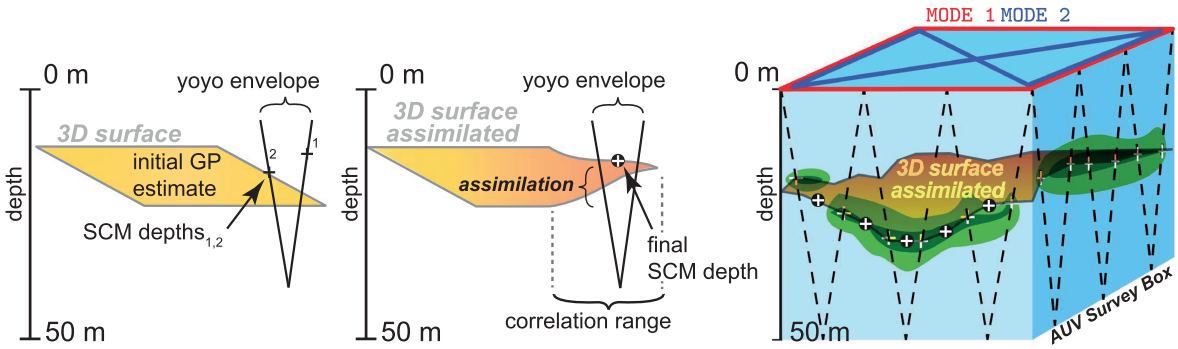


**Fig. 8. A 3D conceptual view of our approach.** (**Left**) After each yo-yo envelope, two SCM peak depths are found and the final SCM is determined. (**Middle**) The final SCM depth is then assimilated into the GP model's 3D SCM surface. (**Right**) AUV transects (black dashed line), peak detection (black/white crosses), MODE 1 [red lines (box)], MODE 2 [blue lines (hourglass)], and true distribution (green blobs), with the 3D surface of the SCM depth shown as the tan surface.

the estimated Chla distribution before and after the initial survey, as in Fig. 4, where only a minor current influence was discernible (except at unobserved locations).

Furthermore, the approach is designed with two modes: MODE 1 that is purely exploratory and MODE 2 that is exploitative. Consequently, the most interesting part of the volume is surveyed last. This is important because previous data from MODE 1 allow sampling (the interior) to proceed with higher survey speed and reduced probability of losing track of the feature. The number of yo-yo envelopes is platform dependent, and the spacing, depth, and number of envelopes could be used to further optimize the time spent finding an adequate estimate. In addition, forsaking some surfacing events could help reduce survey time, if more accurate navigation is possible. At the cost of a greatly increased operational complexity, additional assets such as another AUV could be used to increase coverage capacity and sampling density, should sharing of information between assets be available [e.g., (*55*)].

The AUV does not update the survey depths based on measurements inside the volume due to the previously mentioned factors such as hit-or-miss consequences and time-variability effects. Using the measurements from the interior (within the defined volume) survey can be considered in future work, although the value of this information is limited because of the small survey area and correlation scales present in the coastal ocean. Thus, making use of these data can be challenging. One possible use would, for instance, be to improve the undulating depth from a fixed oscillation to a data-adjusted offset. It is also the case that variability in the ocean is higher along the vertical axis, motivating the use of such capabilities. However, this variability depends on a host of factors and can be hard to estimate correctly without the aforementioned drawbacks. Furthermore, the results from this work show that platforms such as AUVs can make measurements adequate to resolve fine-scale features using an enclosure criterion. This is also apparent in the results presented, which shows spatial coherence throughout the mission (see Fig. 4).

The volumetric results from kriging (such as Fig. 4) are dependent on the accuracy of the correlation parameters used. The values used in this paper are based on the variogram from (*42*) and can only give a suggestive estimate for conducting similar experiments. Aspects of spatial correlation and use of marine sensor fusion toward description of the water column on the submesoscale require effort that is not within the scope of this work. This includes looking at the time dependence of the data, as well as using previous historical data sources (*25*, *61*).

Future integration of particle imaging instruments on board the AUV would greatly change how volumetric surveys can be conducted, enabling adaptation based on taxonomically descriptive data (targeting HABs or other materials such as suspended plastics) as well as reducing the current sensitivity to patchiness arising from ship-based winch deployment.

## MATERIALS AND METHODS

The aim of the study is to obtain a fine-resolution synoptic view of a water-column feature, using a single AUV, by concentrating sampling efforts in the water column. In our case, the feature of interest is the SCM. To achieve this, we split sampling into two modes or phases: an initial phase dubbed MODE 1 that is explorative, followed by a second phase (MODE 2) that exploits the information from the first phase to sampling a feature of interest, using the data to plan the survey. By this design, the most interesting part of the volume is surveyed last, allowing the time spent mapping it at high resolution to be minimized. This is a subtle but important point because this reduces both spatial and temporal uncertainty of the most critical measurements. To avoid redundant data collection, we also split sampling of the volume between the modes. MODE 1 surveys the sides of the volume, whereas MODE 2 surveys the interior. MODE 1 uses a spatial model (GP) to estimate the SCM distribution inside the volume so that MODE 2 can follow these estimates subsequently. The following and Fig. 8 show these steps in detail:

**Step 1)** MODE 1

*Aim*: Estimate the SCM inside the volume using the GP model.

*Behavior*: Survey the sides (red square shown in Fig. 8) of the volume while doing yo-yo envelopes from 0 to 50 m in depth.

*Tasks*:

MODE 1.peak—Identify the depth of the Chla peak.

MODE 1.assimilate—Assimilate SCM depths into a GP surface.

**Step 2)** MODE 2

*Aim*: Use the learned information from MODE 1 to perform a detailed survey.

*Behavior*: Track the GP SCM depth 3D surface inside the AUV survey volume following an hourglass pattern (shown as blue lines in

Fig. 8) chosen to specifically cover as much of the interior in as short a time.

*Tasks*:

MODE 2.fixed—Follow the estimate using fixed depth control.
MODE 2.undulating—Follow the estimate using undulating depth control.

MODE 1 comprises the initial phase, where the location and depths of the SCM are to be identified and assimilated (MODE 1. assimilate) into the GP SCM depth 3D surface. During each full yo-yo envelope (one descent and one ascent), the final SCM depth is to be found and stored as [latitude, longitude, depth, Chla concentration]. It is the task of the subroutine MODE 1.peak to do this analysis. The function will decide the final SCM depth based on the following logic:

1) Segment the concentration measurements into depth bins with average measurements. Collecting five data points in one bin, with an average depth.
2) Find the two depths corresponding to the largest ($depth_1$) and second largest ($depth_2$) concentration spikes.
3) Calculate the depth difference between these spikes.
4) If the depth difference is less than 10 m, the SCM depth is set to the depth of the largest concentration: $SCM_{depth} = depth_1$. If not, the SCM depth is set to a weighted mean, as $SCM_{depth} = depth_1 * 0.70 + depth_2 * 0.30$. This is based on the fact that about 70% of normally distributed values are within 1 SD of the mean.

The subsequent subroutine MODE 1.assimilate will integrate the final $SCM_{depth}$ into the GP model (Eq. 3) using the observation location (lat, lon → grid cell) and "lifting" or "lowering" the depth estimate at the surrounding locations/grid cells within the correlation range. These two concepts are encapsulated in Fig. 8.

Once the GP SCM depth 3D surface has been established, the AUV switches to MODE 2 and depth tracking mode, where the goal is to provide a high-resolution volumetric representation of the Chla structure by tracking this 3D surface in either MODE 2.fixed or MODE 2. undulating following a 3D path. This enables an effective and improved way of mapping detail within the SCM. The biomass patchiness can thus be evaluated and augmented with supporting ship-based samples, allowing organism community structure to be described more accurately.

### Kriging in 3D

Using kriging (*54*), we can construct a 3D representation of the volume, conditioned on the data. The kriging surface is the interpolated prediction given as the conditional mean of the GP while providing the conditional prediction covariance in an explicit form.

Spatial correlation is an essential component of kriging, and this is incorporated by a kernel function that relies on the distance between pairs of locations, $h_{ij} = |\mathbf{s}_i - \mathbf{s}_j|$; in this work, this is measured in 3D $[x, y, z]$ coordinates. Compared with the more common 1D or 2D applications of kriging, this means a considerable increase in the size of the covariance matrices required for data conditioning—assimilating all the samples from the survey is therefore not practical when doing the interpolation. In our approach, a pruned version of the assimilated 1700 samples from this volume was used, with a square size of 2700 covariance matrix (reflecting the $[30 \times 30 \times 30]$ volume grid).

The interpolation time on a Dell Latitude E7540 i7 took about 1.5 min with these parameters, resulting in figures such as Fig. 4. To capture the difference between horizontal and vertical correlation distance, we artificially exaggerated the $z$ dimension by a factor of about 20 based on (*26*). The horizontal correlation was, as previously discussed, based on the east-west variogram from (*42*). Although there are methods for handling memory and computational time challenges for 3D GPs, our focus was on an applied study using MODE 1 to define a region of interest.

## SUPPLEMENTARY MATERIALS

robotics.sciencemag.org/cgi/content/full/4/27/eaav3041/DC1
Fig. S1. LAUV platform.
Fig. S2. Experiment overview.
Fig. S3. Survey 2 data.

## REFERENCES AND NOTES


1. P. G. Falkowski, R. T. Barber, V. Smetacek, Biogeochemical controls and feedbacks on ocean primary production. *Science* **281**, 200–206 (1998).
2. M. Dowd, E. Jones, J. Parslow, A statistical overview and perspectives on data assimilation for marine biogeochemical models. *Environmetrics* **25**, 203–213 (2014).
3. W. M. Durham, E. Climent, M. Barry, F. De Lillo, G. Boffetta, M. Cencini, R. Stocker, Turbulence drives microscale patches of motile phytoplankton. *Nat. Commun.* **4**, 2148 (2013).
4. A. P. Martin, Phytoplankton patchiness: The role of lateral stirring and mixing. *Prog. Oceanogr.* **57**, 125–174 (2003).
5. E. K. Hovland, H. M. Dierssen, A. S. Ferreira, G. Johnsen, Dynamics regulating major trends in Barents Sea temperatures and subsequent effect on remotely sensed particulate inorganic carbon. *Mar. Ecol. Prog. Ser.* **484**, 17–32 (2013).
6. A. Bracco, A. Provenzale, I. Scheuring, Mesoscale vortices and the paradox of the plankton. *Proc. R. Soc. Lond. B Biol. Sci.* **267**, 1795–1800 (2000).
7. C. Perruche, P. Rivière, P. Pondaven, X. Carton, Phytoplankton competition and coexistence: Intrinsic ecosystem dynamics and impact of vertical mixing. *J. Mar. Sys.* **81**, 99–111 (2010).
8. S. J. Brentnall, K. J. Richards, J. Brindley, E. Murphy, Plankton patchiness and its effect on larger-scale productivity. *J. Plankton Res.* **25**, 121–140 (2003).
9. J. Das, F. Py, T. Maughan, T. O'Reilly, M. Messié, J. Ryan, G. S. Sukhatme, K. Rajan, Coordinated sampling of dynamic oceanographic features with underwater vehicles and drifters. *Int. J. Rob. Res.* **31**, 626–646 (2012).
10. E. Davies, P. J. Brandvik, F. Leirvik, R. Nepstad, The use of wide-band transmittance imaging to size and classify suspended particulate matter in seawater. *Mar. Pollut. Bull.* **115**, 105–114 (2017).
11. L. Stemmann, E. Boss, Plankton and particle size and packaging: From determining optical properties to driving the biological pump. *Annu. Rev. Mar. Sci.* **4**, 263–290 (2012).
12. Y. C. Agrawal, H. C. Pottsmith, Instruments for particle size and settling velocity observations in sediment transport. *Mar. Geol.* **168**, 89–114 (2000).
13. G. W. Graham, W. A. M. Nimmo-Smith, The application of holography to the analysis of size and settling velocity of suspended cohesive sediments. *Limnol. Oceanogr. Methods* **8**, 1–15 (2010).
14. H. M. Sosik, R. J. Olson, Automated taxonomic classification of phytoplankton sampled with imaging-in-flow cytometry. *Limnol. Oceanogr. Methods* **5**, 204–216 (2007).
15. M. A. Moline, S. M. Blackwell, C. von Alt, B. Allen, T. Austin, J. Case, N. Forrester, R. Goldsborough, M. Purcell, R. Stokey, Remote environmental monitoring units: An autonomous vehicle for characterizing coastal environments. *J. Atmos. Ocean. Technol.* **22**, 1797–1808 (2005).
16. I. Robbins, G. J. Kirkpatrick, S. M. Blackwell, J. Hillier, C. A. Knight, M. A. Moline, Improved monitoring of HABs using autonomous underwater vehicles (AUV). *Harmful Algae* **5**, 749–761 (2006).
17. Y. Zhang, B. Kieft , R. McEwen , J. Stanway , J. Bellingham , J. Ryan, B. Hobson, D. Pargett, J. Birch, C. Scholin, Tracking and sampling of a phytoplankton patch by an autonomous underwater vehicle in drifting mode, in *OCEANS 2015 MTS/IEEE Washington* (IEEE, 2015), pp. 1–5.
18. J. P. Ryan, S. B. Johnson, A. Sherman, K. Rajan, F. Py, H. Thomas, J. B. J. Harvey, L. Bird, J. D. Paduan, R. C. Vrijenhoek, Mobile autonomous process sampling within coastal ocean observing systems. *Limnol. Oceanogr. Methods* **8**, 394–402 (2010).
19. J. Das, F. Py, J. B. J. Harvey, J. P. Ryan, A. Gellene, R. Graham, D. A. Caron, K. Rajan, G. S. Sukhatme, Data-driven robotic sampling for marine ecosystem monitoring. *Int. J. Rob. Res.* **34**, 1435–1452 (2015).
20. R. N. Smith, J. Das, C. Yi, D. A. Caron, B. H. Jones, G. S. Sukhatme, Cooperative multi-AUV tracking of phytoplankton blooms based on ocean model predictions, in *OCEANS'10 IEEE SYDNEY* (IEEE, 2010), pp. 1–10.

21. R. N. Smith, M. Schwager, S. L. Smith, B. H. Jones, D. Rus, G. S. Sukhatme, Persistent ocean monitoring with underwater gliders: Adapting sampling resolution. *J. Field Robot.* **28**, 714–741 (2011).
22. R. Graham, F. Py, J. Das, D. Lucas, T. Maughan, K. Rajan, Exploring space-time tradeoffs in autonomous sampling for marine robotics, in *Experimental Robotics: The 13th International Symposium on Experimental Robotics*, J. P. Desai, G. Dudek, O. Khatib, V. Kumar, Eds. (vol. 88 of Springer Tracts in Advanced Robotics, Springer, 2013), pp. 819–839.
23. D. Magazzeni, F. Py, M. Fox, D. Long, K. Rajan, Policy learning for autonomous feature tracking. *Auton. Robot.* **37**, 47–69 (2014).
24. G. Johnsen, M. Norli, M. Moline, I. Robbins, C. von Quillfeldt, K. Sørensen, F. Cottier, J. Berge, The advective origin of an under-ice spring bloom in the Arctic Ocean using multiple observational platforms. *Polar Biol.* **41**, 1197–1216 (2018).
25. S. Frolov, R. M. Kudela, J. G. Bellingham, Monitoring of harmful algal blooms in the era of diminishing resources: A case study of the U.S. West Coast. *Harmful Algae* **21–22**, 1–12 (2013).
26. J. Sahlin, M. A. Mostafavi, A. Forest, M. Babin, Assessment of 3D spatial interpolation methods for study of the marine pelagic environment. *Mar. Geod.* **37**, 238–266 (2014).
27. S. van Gennip, A. P. Martin, M. A. Srokosz, J. T. Allen, R. Pidcock, S. C. Painter, M. C. Stinchcombe, Plankton patchiness investigated using simultaneous nitrate and chlorophyll observations. *J. Geophys. Res. Oceans* **121**, 4149–4156 (2016).
28. J. J. Cullen, Subsurface chlorophyll maximum layers: Enduring enigma or mystery solved? *Annu. Rev. Mar. Sci.* **7**, 207–239 (2015).
29. W. M. Durham, R. Stocker, Thin phytoplankton layers: Characteristics, mechanisms, and consequences. *Annu. Rev. Mar. Sci.* **4**, 177–207 (2012).
30. W. O. Smith Jr., D. J. Demaster, Phytoplankton biomass and productivity in the Amazon River plume: Correlation with seasonal river discharge. *Cont. Shelf Res.* **16**, 291–319 (1996).
31. J. B. Weiss, A. Provenzale, Transport and mixing in geophysical flows, in *Lecture Notes in Physics* (Springer Berlin Heidelberg, 2007).
32. A. Morel, J.-F. Berthon, Surface pigments, algal biomass profiles, and potential production of the euphotic layer: Relationships reinvestigated in view of remote-sensing applications. *Limnol. Oceanography* **34**, 1545–1562 (1989).
33. V. S. Hemsley, T. J. Smyth, A. P. Martin, E. Frajka-Williams, A. F. Thompson, G. Damerell, S. C. Painter, Estimating oceanic primary production using vertical irradiance and chlorophyll profiles from ocean gliders in the North Atlantic. *Environ. Sci. Technol.* **49**, 11612–11621 (2015).
34. C. J. Lorenzen, A method for the continuous measurement of in vivo chlorophyll concentration. *Deep-Sea Res. Oceanogr. Abstr.* **13**, 223–227 (1966).
35. R. C. Smith, K. S. Baker, P. Dustan, Fluorometric techniques for the measurement of oceanic chlorophyll in the support of remote sensing (SIO Ref. 81-17, Visibility Laboratory, Scripps Institution of Oceanography, University of California, San Diego, 1981).
36. J. J. Cullen, The deep chlorophyll maximum: Comparing vertical profiles of chlorophyll *a*. *Can. J. Fish. Aquat. Sci.* **39**, 791–803 (1982).
37. M. Felip, J. Catalan, The relationship between phytoplankton biovolume and chlorophyll in a deep oligotrophic lake: Decoupling in their spatial and temporal maxima. *J. Plankton Res.* **22**, 91–106 (2000).
38. J. J. Cullen, J. G. MacIntyre, Behavior, physiology and the niche of depth-regulating phytoplankton. *NATO ASI Ser. G* **41**, 559–580 (1998).
39. S. Roy, C. A. Llewellyn, E. S. Egeland, G. Johnsen, *Phytoplankton Pigments: Characterization, Chemotaxonomy and Applications in Oceanography* (Cambridge Univ. Press, 2011).
40. D. L. Mackas, K. L. Denman, M. R. Abbott, Plankton patchiness: Biology in the physical vernacular. *Bull. Mar. Sci.* **37**, 652–674 (1985).
41. A. P. Martin, K. J. Richards, A. Bracco, A. Provenzale, Patchy productivity in the open ocean. *Glob. Biogeochem. Cycles* **16**, 9 (2002).
42. R. D. Hedger, T. J. Malthus, A. M. Folkard, Spatial dynamics of chlorophyll-a and sea surface temperature in a coastal zone as revealed by high-resolution remote sensing, in *Remote Sensing of the Ocean and Sea Ice 2002* (International Society for Optics and Photonics, 2003), pp. 146–158.
43. G. M. Silsbe, S. Y. Malkin, Where light and nutrients collide: The global distribution and activity of subsurface chlorophyll maximum layers, in *Aquatic Microbial Ecology and Biogeochemistry: A Dual Perspective* (Springer, 2016), pp. 141–152.
44. R. Sætre, R. Ljøen, The Norwegian coastal current, in *Proceedings of the First International Conference on Port and Ocean Engineering Under Arctic Conditions* (The Technical University of Norway, 1972), pp. 514–535.
45. O. P. Pedersen, K. S. Tande, D. Slagstad, A model study of demography and spatial distribution of *Calanus finmarchicus* at the Norwegian coast. *Deep Sea Res. II* **48**, 567–587 (2001).
46. R. Sætre, J. Aure, R. Ljøen, Wind effects on the lateral extension of the Norwegian Coastal Water. *Cont. Shelf Res.* **8**, 239–253 (1988).
47. M. Mork, Circulation phenomena and frontal dynamics of the Norwegian coastal current. *Philos. Trans. R. Soc. Lond. A* **302**, 635–647 (1981).
48. J. A. Johannessen, E. Svendsen, S. Sandven, O. M. Johannessen, K. Lygre, Three-dimensional structure of mesoscale eddies in the Norwegian Coastal Current. *J. Phys. Oceanogr.* **19**, 3–19 (1989).
49. J. D. McGillicuddy Jr., Mechanisms of physical-biological-biogeochemical interaction at the oceanic mesoscale. *Annu. Rev. Mar. Sci.* **8**, 125–159 (2016).
50. A. Mahadevan, The impact of submesoscale physics on primary productivity of plankton. *Annu. Rev. Mar. Sci.* **8**, 161–184 (2016).
51. H. Svendsen, *Ecology of Fjords and Coastal Waters*, H. R. Skjoldal, C. Hopkins, K. E. Erikstad, H. P. Leinaas, Eds. (Elsevier Science B.V., 1995).
52. P. Wassmann, H. Svendsen, A. Keck, M. Reigstad, Selected aspects of the physical oceanography and particle fluxes in fjords of northern Norway. *J. Mar. Syst.* **8**, 53–71 (1996).
53. J. Binney, A. Krause, G. S. Sukhatme, Optimizing waypoints for monitoring spatiotemporal phenomena. *Int. J. Robot. Res.* **32**, 873–888 (2013).
54. N. Cressie, C. K. Wikle, *Wiley Series in Probability and Statistics: Statistics for Spatio-Temporal Data* (Wiley, 2011).
55. S. Kemna, "Multi-robot strategies for adaptive sampling with autonomous underwater vehicles," thesis, University of Southern California (2018).
56. C. Wunsch, P. Heimbach, Practical global oceanic state estimation. *Phys. D* **230**, 197–208 (2007).
57. A. Sousa, L. Madureira, J. Coelho, J. Pinto, J. Pereira, J. Sousa, P. Dias, LAUV: The man-portable autonomous underwater vehicle. *IFAC Proc. Vol.* **3**, 268–274 (2012).
58. L. C. Lund-Hansen, Subsurface chlorophyll maximum (SCM) location and extension in the water column as governed by a density interface in the strongly stratified Kattegat estuary. *Hydrobiologia* **673**, 105–118 (2011).
59. H. Bader, The hyperbolic distribution of particle sizes. *J. Geophys. Res.* **75**, 2822–2830 (1970).
60. M. Jonasz, G. Fournier, Approximation of the size distribution of marine particles by a sum of log-normal functions. *Limnol. Oceanogr.* **41**, 744–754 (1996).
61. S. Frolov, B. Garau, J. Bellingham, Can we do better than the grid survey: Optimal synoptic surveys in presence of variable uncertainty and decorrelation scales. *J. Geophys. Res. Oceans* **119**, 5071–5090 (2014).
62. Runde Environmental Centre (Norway); http://rundecentre.no.
63. SINTEF Ocean AS, ENTiCE project webpage (2016); https://sintef.no/prosjekter/entice/.
64. Centre for Autonomous Marine Operations and Systems (AMOS); https://ntnu.edu/amos.
65. P. Ramachandran, G. Varoquaux, Mayavi: A package for 3D visualization of scientific data. *Comput. Sci. Eng.* **13**, 40–51 (2011).


**Acknowledgments:** We are grateful to the resident scientists at the Runde Environmental Centre (*62*) and the captain and crew of Ophelia and NTNU's research vessel, the *R/V Gunnerus*. The metocean buoy data were obtained from the Norwegian Meteorological Institute. The monitoring station data were collected by R. Kvalsund at the Runde Environmental Centre on commission from the Norwegian Institute for Water Research (NIVA), as part of the Ecosystem Monitoring of Coastal Waters programme financed by the Norwegian Environment Agency. **Funding:** This work was part of the ENTiCE project (*63*) funded by the Research Council of Norway (project number 255303/E40), the Nansen Legacy Program (project number 27272), and AMOS (*64*), Center of Excellence (project number 223254). **Author contributions:** T.O.F., G.M.F., E.J.D., J.E.U., R.M., G.J., I.E., J.E., M.L., and K.R. contributed to the manuscript. T.O.F. and M.L. performed the field expriments. G.M.F., E.J.D., and G.J. were responsible for SilCam and FRRf operations and subsequent data analysis. R.M. was responsible for remote sensing. Oceanography of the Runde region was articulated by J.E.U. and I.E. **Competing interests:** The authors declare that they have no competing financial interests. **Data and materials availability:** All data needed to evaluate the conclusions in the paper are present in the paper or the Supplementary Materials.

Submitted 6 September 2018
Accepted 20 December 2018
Published 13 February 2019
10.1126/scirobotics.aav3041

**Citation:** T. O. Fossum, G. M. Fragoso, E. J. Davies, J. E. Ullgren, R. Mendes, G. Johnsen, I. Ellingsen, J. Eidsvik, M. Ludvigsen, K. Rajan, Toward adaptive robotic sampling of phytoplankton in the coastal ocean. *Sci. Robot.* **4**, eaav3041 (2019).

Science Robotics

# Toward adaptive robotic sampling of phytoplankton in the coastal ocean

Trygve O. Fossum, Glaucia M. Fragoso, Emlyn J. Davies, Jenny E. Ullgren, Renato Mendes, Geir Johnsen, Ingrid Ellingsen, Jo Eidsvik, Martin Ludvigsen and Kanna Rajan

*Sci. Robotics* **4**, eaav3041.
DOI: 10.1126/scirobotics.aav3041

# Article C

## Compact models for Adaptive Sampling in Marine Robotics.

**Trygve Olav Fossum**, John Ryan, Tapan Mukerji, Jo Eidsvik, Thom Maughan, Martin Ludvigsen and Kanna Rajan



This article is submitted to *International Journal of Research Robotics*, February $12^{th}$ 2018.

Journal Title
XX(X):1–14

DOI: 10.1177/ToBeAssigned
www.sagepub.com/
SAGE

# Compact Models for Adaptive Sampling in Marine Robotics

**Trygve Olav Fossum[1,7], John Ryan[2], Tapan Mukerji[3], Jo Eidsvik[4], Thom Maughan[2], Martin Ludvigsen[1,5] and Kanna Rajan[6,7,8]**

**Abstract**

Finding high-value locations for *in-situ* data collection is of substantial importance in ocean science, where diverse bio-physical processes interact to create dynamically evolving phenomenon. These cover a variable spatial extent, are sparse, and difficult to predict. Autonomous robotic platforms can sustain themselves in harsh conditions with persistent presence, but require deployment at the right place and time. To that end, we consider the use of remote sensing data for building compact models that can improve skill in predicting sub-mesoscale features and inform onboard sampling. The model enables prediction of regional patterns based on sparse *in-situ* data, a capability that is essential in regions where use of satellite remote sensing in real time is often limited by cloud cover. Our model is based on classification of sea-surface temperature (SST) images, but the technique is general across any remotely sensed parameter. Images having similar magnitude and spatial patterns are grouped into a compact set of conditional means representing the dominant states. The classification is *unsupervised* and uses a combination of dictionary learning and hierarchical clustering. The method is demonstrated using SST images from Monterey Bay, California. The consistency of the classification result is verified and compared with oceanographic forcing using historical wind measurements. The established model is then shown working in a real application using measurements from an autonomous surface vehicle (ASV), together with forecast and sampling strategies. Finally an analysis of the model prediction error is presented and compared across different paths and survey duration.

**Keywords**

Machine Learning, Sampling, Ocean Modeling, Marine Robotics

## 1 Introduction

Effective and informative sampling of the ocean requires data gathering strategies that can resolve the spatial and temporal variations of phenomena. This is a formidable challenge due to the dynamic and unstructured nature of the ocean, with spatio-temporal scales spanning many orders of magnitude, making it unrealistic to observe the dynamics in detail. Additionally, coastal waters are often heterogeneous in composition due to bathymetry, river discharge, land run-off, and oceanic circulation. Methodologically this drives a requirement for using compact spatial models to inform more effective sampling strategies, capable of running on robotic platforms, utilizing prior and current *in-situ* observations. There are numerous ways to build spatial models. The essential goal is to exploit the underlying spatial correlation structures and try to reconstruct the environment, so that future sensing locations can be determined accordingly.

Earth observing satellites offer the possibility to observe large spatial extent and various ocean parameters, such as sea-surface temperature (SST), sea-surface height (SSH), salinity, and ocean color, from which a number of ocean processes can be discerned and characterized; including algal blooms, fronts, eddies, internal waves, and numerous water quality parameters (Johannessen et al. 2000). Consequently, there is enormous potential for using such data to perform large scale automated analysis of the spatial patterns in the ocean. However, a major challenge using modern machine learning techniques is the reliance on labeled data sets (Gonalves et al. 2008). In remote sensing applications, this challenge is further exacerbated in having to work with a limited number of training samples (Mountrakis et al. 2011), especially when concentrating on a specific area of scientific interest. It is therefore valuable to use unsupervised methods that provide the ability to learn the inherent structure of the data without using explicitly provided labels.

[1]Department of Marine Technology, Norwegian University of Science and Technology (NTNU), Trondheim, Norway.
[2]Monterey Bay Aquarium Research Institute, California, US.
[3]Stanford University, Department of Energy Resources Engineering and Department of Geophysics by courtesy, California, US.
[4]Department of Mathematical Sciences, NTNU, Trondheim, Norway.
[5]University Centre in Svalbard (UNIS), Longyearbyen, Norway.
[6]Department of Engineering Cybernetics, NTNU, Trondheim, Norway.
[7]Centre for Autonomous Marine Operations and Systems (AMOS), Trondheim, Norway.
[8]Underwater Systems and Technology Laboratory, Faculty of Engineering, University of Porto, Portugal.

**Corresponding author:**
Trygve Olav Fossum, Department of Marine Technology, Norwegian University of Science and Technology, Trondheim, Norway.
Email: trygve.o.fossum@ntnu.no

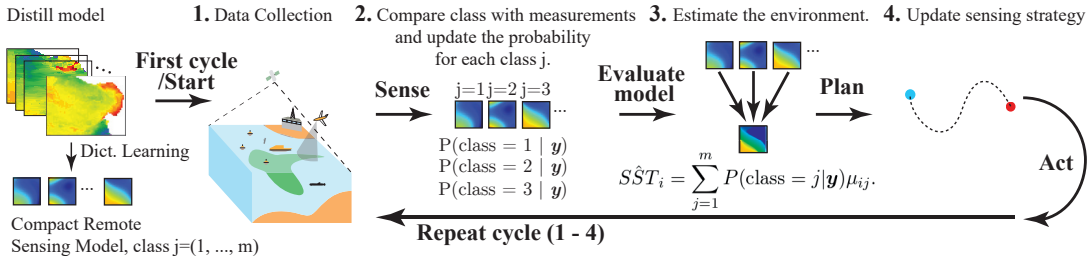


**Figure 1.** The main concept and flow diagram for using compact remote sensing models in robotic sampling. The details are explained in Section 6.

Given the challenge with *undersampling* in oceanography (Munk 2002) and the limited availability of accurate real time information, it is essential to call for capabilities that can estimate spatial and temporal variations in the ocean environment on the fly. Building compact spatial models using prior data sources such as remote sensing and ocean model output therefore one such opportunity. Towards this end, we present a method for building such a model using remotely sensed SST data, as well as examples of how this model can be used in a robotic sampling framework. Images based on sea-surface temperature are chosen specifically due to their synoptic properties providing repeated large-scale surface observations with reasonably high resolution. The model aims at predicting the current state of the environment using a superposition of states, referred to as *classes* or *scenarios*, where each state is established from a similar set of SST images that represent recurring states of oceanographic conditions. The environment is assumed to be equal to a superposition of states, found by evaluating the likelihood of these states against observations. A conceptual view of this approach is presented in Fig. 1 below, showing how the model can inform sampling in a *sense-plan-act* structure.

It is important that this type of data reduction (unsupervised clustering) cover the common dominant spatial patterns seen in the images, i.e. in the form of several distinct classes of *conditional means*, that is comparable to the variation in the underlying environment. Using a combination of dictionary learning (Aharon et al. 2006), sparse coding (Mairal et al. 2009), and (agglomerative) hierarchical clustering (Everitt et al. 2011) we propose an unsupervised classifier that can group images with similar oceanographic characteristics, using spatial patterns and the magnitude of temperature from SST images. The idea is not only to automate this process, but also to provide new insight into the underlying processes themselves. Subsequently, the classified SST images are used to distill a compact model of the dominant features by computing conditional means within these classes. One potential drawback to this approach is the lack of uniformity in data acquisition due to cloud cover and lack of satellite coverage. These factors limit the ability to do repeated and systematic observations of a region of interest, which in the worst case can impede the construction of such spatial models. As a mitigation, data from a three year spring period is used (see Fig. 2), such that we obtain a relatively continuous data coverage for a season.

The applicability of such compact models is an effective characterization of key ocean states, especially when SST data from satellites is not available. In this work we show an example of this, determining large scale conditions for a given day, using data gathered from a WaveGlider ASV. We also examine the model prediction error, by computing the expected mis-classification rates for different sampling design strategies.

The structure of this paper is as follows: in Section 2 we introduce related work, along with some of the challenges that underpin the motivation for this paper. Section 3 presents some background on both the data sources and methods used. Section 4 presents the proposed classification methodology, with the results shown in Section 5. Section 6 presents model implementation and usage towards adaptive sampling. We conclude in Section 7 with a summary, followed by a discussion of future work.

## 2 Related Work

Much of the work on automated analysis of remote sensing data is focused on thematic mapping for terrestrial applications, with numerous applications such as agriculture (Mulla 2013), mapping of urban environments (Saritha and Kumar 2017) and vegetation (Xie et al. 2008), and geared towards change detection (Walter 2004). Typically, the general objective is to categorize regions of an image into one of various land cover classes or themes. Dictionary based classification has been explored for terrestrial hyper-spectral thematic mapping in Chen et al. (2011). Similar approaches such as sparse reconstruction-based classification (SRC) have been applied to high resolution images of the sea floor, taken with synthetic aperture Sonar (SAS) in McKay et al. (2016). Despite an abundance of approaches Wilkinson (2005) demonstrates through evaluation of fifteen-years of remote sensing research, related to classification, that no technique displays any significant advantage over another, showing no trend in improvement of the classification results, including results from artificial neural networks. Limited contexts, increasing complexity of data sets, lack of embodiment into best practice, the difference between low-level features and high-level user requirement, and imperfect human processes (such as labeling and ground truthing) are some explanations proposed for this lack of progress.

Compared to terrestrial or seafloor applications, some additional challenges exist in the upper ocean domain, namely: i) the non-static boundaries and surface features

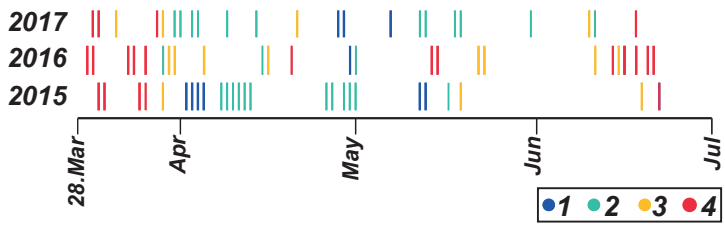


**Figure 2.** The dates of usable SST images from Monterey Bay for 2015, 2016, and 2017, in the period March until July. Each image is indicated with a vertical line, colored according to the initial classification results (class 1, 2, 3, and 4), see Section 5.1.

present in the environment (Blondeau-Patissier et al. 2014), ii) the lower signal-to-noise ratio for signals arising from water masses, and iii) the presence of surface effects such as sun, and sky glint (Emberton et al. 2016). Studying ocean surface features for analysis of surface slicks, currents, fronts, waves, and wind interactions are discussed in Ryan et al. (2010) and Chen (2012), with an emphasis on synthetic aperture radar images. High frequency (HF) radar is also combined with remote sensing in Das et al. (2010), where the sampling and hotspot prediction of harmful algal blooms (HABs) is examined. This is also studied in Bernstein et al. (2013), where a shore-based recognition pipeline is suggested, building on remote sensing data for event detection, feature localization, and trajectory prediction. Frolov et al. (2013) analyzes the spatial and temporal decorrelation scales seen in marine algal blooms using fluorescence line height imagery, to strategize monitoring of such episodic events. Frolov et al. (2012) investigates short-term prediction of surface currents using HF-radar observations to develop a linear autoregression model, where the climatology of conditional mean flow-fields for upwelling, downwelling, and relaxation in Monterey Bay is presented. Optical water types were found using fuzzy clustering analysis on spectral information in Eleveld et al. (2017), aimed towards identifying different types of lakes, e.g. clear versus turbid waters. At large spatial scales, Oliver and Irwin (2008) uses remote sensing data to automatically resolve different oceanic regions with certain spatiotemporal characteristics, to monitor the effect of El Niño events.

A number of approaches have been explored combining onboard models and remote sensing to guide sampling in the ocean. Smith et al. (2010) utilizes forecasts from a high resolution ocean model combined with remote sensing to pre-plan missions with multiple AUVs. Areas with high concentration of Chlorophyll *a* (a proxy for phytoplankton abundance) is identified from the satellite imagery and simulated forward in time using an ocean model. Presenting only simulated results, the paper shows the potential and also the challenges of leveraging prior data. Issues related to small scale discrepancy between model simulation (used for planning) and the actual conditions, aligns with the assumptions in our work, and on the fact that we are focusing on predicting and planning based on large scale features. Chao et al. (2017), provides a discussion and preliminary results towards a closed loop between numerical ocean models, robotic platform sampling, and data assimilation. Multiple information streams are proposed to update and improve sampling strategies without human intervention. However, the robotic assets depend on human involvement and robust communications using shore-based assimilation and planning schemes. Consequently, this drives the need towards elevated levels of autonomy and onboard sampling strategies for situational awareness, such as presented in our work.

This paper describes a novel way of building compact ocean models using remote sensing products for use in robotic sampling. As our work uses pre-processed data (1 day average SST), some of the raw information (e.g. quality flags) is forsaken for practical purposes of obtaining and working with the data. The proposed method is original and provides the ability to work directly with both temperature and spatial patterns, as this information is carried along throughout the analysis. Contrary to other work, the classification results are confirmed and verified by an independent marine data source (preceding wind history), allowing oceanographic processes to be tied to the subsequent analysis and use of the data. Wind drives horizontal and vertical circulations, which in turn determines magnitudes, gradients, and spatial patterns in SST (Rosenfeld et al. 1994). The method is unsupervised and can be used with a small number of images ($\leq 100$).

## 3 Preliminaries

### 3.1 Satellite Data Sources

The SST remote sensing images used as a basis for this model are provided from a high resolution radiometer onboard the Polar-orbiting Operational Environmental Spacecrafts (POEs) NOAA-17 and NOAA-18. The data is processed and mapped to an equal angle grid (0.0125 degrees latitude by 0.0125 degrees longitude) using a simple arithmetic mean, producing both individual and composite images from 1 to 14 days duration. This may provide some averaging artifacts, see Fig. 15a. The nominal accuracy is about 0.7 degrees Celsius (C), covering the west coast of North America.*

We used one-day average SST images, as in Fig. 3a, from 2015, 2016, and 2017 in this work covering Monterey Bay, California (marked in Fig. 3b), for a 100 day period from March until the start of August, yielding 300 images

*The data is publicly available through the National Oceanic and Atmospheric Administration (NOAA) NWS Monterey Regional Forecast Office and the CoastWatch program, from their ERDDAP server https://bit.ly/2ngyP6c.

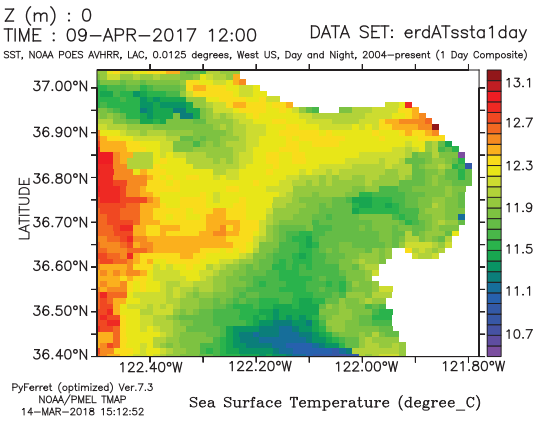


**(a)** Example of a SST image that was used to make the compact model.


**(b)** Map of California and Monterey Bay with the SST region marked.

**Figure 3.** (a) A SST image from NOAA NWS Monterey Regional Forecast Office showing Monterey Bay (between 36.65 and 37°N). (b) Map of California and Monterey Bay with the SST region marked.

in total. This period of the year was chosen because wind-driven coastal upwelling and associated thermal signatures are strongest. Due to cloud cover, only about 25% of the images had a quality that was useful for our application, giving us a total of 74 images to work with. Local cloud and fog cover can limit the data availability; henceforth longer time periods should be considered for inclusion in the data sources, if highly exposed to these factors. Equally, too much exposure can create data gaps that introduce bias into the final model, as images and their spatial patterns are left out of the analysis. Cloud and fog cover, are further a motivating factor for actually deploying autonomous vehicles that can aid in estimating ocean conditions. Although the SST images in this analysis are limited to spring and summer, coastal upwelling circulation in this region continues into the fall season and is closely linked to coastal land features (Rosenfeld et al. 1994). Therefore, the interpretation of structure information by these methods should be similarly applicable during fall. However, SST magnitude shifts during fall due to seasonal warming throughout the region. This aspect of the environment motivates a seasonally dependent method, using images that are consistent seasonally.

The time stamp of images in Fig. 2, shows availability over sequential days, and therefore the likelihood of having a similar mean temperature. However, SST patterns can be vastly different in sequential days because energetic currents change water mass distributions rapidly, motivating the case for looking at spatial similarities.

### 3.2 Unsupervised learning and classification of SST images

In order to quantify different spatial patterns in SST images, we use an unsupervised classification method based on sparse representations of the images. The compressed representations are obtained from employing dictionary learning techniques. Before hierarchical clustering (Everitt et al. 2011) is performed in several steps. The approach aims at classifying images with the same SST pattern into dominant/archetypical classes, having distinct oceanographic significance. Clustering the raw image data (pixels) is not effective, due to their high dimensionality. Using bulk characteristics, such as the mean, min, and max temperature, is also possible. This approach can get good results, but leads to unnecessary smoothing/blur (in the conditional mean) as classes are combined without spatial information. To demonstrate this, a comparison of the classification variability is presented in Section 4.2. Consequently, clustering a compressed/sparse representation is more viable, as both temperature magnitude and spatial information can be combined together. Moreover, the dimension can be kept low, making it easier to cluster and hence identify and differentiate between the characteristics of each image.

### 3.3 Dictionary Learning

Sparse dictionary learning (Aharon et al. 2006; Mairal et al. 2009) is a method that can be used to build sparse representations of the input data. The resulting format is a set of coefficients, collected as a *sparse code*. Dictionary learning is similar to *Principal Component Analysis* (PCA) (Jolliffe 2011) (also known as *Empirical Orthogonal Functions*) in that the coefficients form a linear combination of certain basic elements, referred to here as *atoms*. The atoms can be considered as instances of "characteristic patterns" that can be combined to reconstruct the input. The combined matrix of atoms is called a *dictionary*, usually denoted as $\boldsymbol{D}$, while the sparse codes are usually noted as $\boldsymbol{\alpha}$, having the relationship

$$\boldsymbol{x}_k = \boldsymbol{D}\boldsymbol{\alpha}_k, \tag{1}$$

where $\boldsymbol{x}_k$ is the raw image $k$, with $\boldsymbol{D}$ as the dictionary, and $\boldsymbol{\alpha}_k$ as the unique coding for that specific image. We use `MiniBatchDictionaryLearning` or `MBDL` from (Pedregosa et al. 2011) to find the dictionary using the least angle regression method (LARS) Mairal et al. (2009), while the sparse codes are found using an orthogonal matching

pursuit (OMP) algorithm that greedily selects the dictionary atoms sequentially, through computation of the inner products between the image and dictionary columns. This is accomplished by repeatedly iterating over mini-batches of input images, fed in as block patches, with a specific size, taken from the original image. The size of these patches will influence the result and needs to be selected based on the small- and large-scale similarities in the input images. Sensitivity analysis should therefore be used to identify this size parameter (see Section 4.1). Finding the dictionary $\boldsymbol{D}$ using the `MiniBatchDictionaryLearning` library involves an iterative process that uses a random state to initiate the model, hence reproducible results require using the same pre-defined random seed. More details can be found in the reference documentation [†].

## 4 Methods

### 4.1 Proposed Classification Methodology

In separating and collecting dominant spatial patterns from SST images an important aspect that we emphasize in this work is that images sharing a common oceanographical evolution should be identifiable. This implies finding images that share a mutual historic progression of, for example, wind and currents, that contributed to shaping a particular ocean condition. Involvement of local oceanographic expertise and knowledge is therefore essential in finding a separation scheme that is justifiable. This is especially true since the images are snapshots of a continuous process and separation into classes will imply some form of discretization.

The classification method builds off the idea of classifying images based on sparse codes, instead of high dimensional pixel space. The methodology, illustrated in Fig. 4, can be seen as a branching graph with a new dictionary and sparse coding generated after each separation step. Making a new conditional dictionary after the initial classification allows us to reach a new level of similarity, as this refinement step will be based on a dictionary with more similar content. Here, both magnitude and large scale similarities matter less as these have been addressed in the initial classification. The subsequent classification can therefore separate the images further based on the latent spatial patterns. The detailed steps involved can be described as follows, for image $k$ and each class $j = 1, \ldots, m$:

1. Normalize all images with the global mean and standard deviation.
2. Extract a fixed number of patches from the SST image (e.g. 260 patches of size $40 \times 40$ pixels), and stack these in a 1D vector.
3. The 1D vectors are collected in the data matrix and fed into the `MBDL` subroutine to retrieve the initial dictionary $\boldsymbol{D}_j$.
4. Each SST image is then compressed using the dictionary $\boldsymbol{D}_j$ to form a unique sparse coding for the image $\boldsymbol{\alpha}_j^k$.
5. These first $\boldsymbol{\alpha}_j^k$ coefficients are then classified using hierarchical clustering.
6. Step 2-3 is then repeated for the images within the derived classes to retrieve a new sub-class specific dictionary $\tilde{\boldsymbol{D}}_j$.
7. Step 4 is repeated using the sub-class specific dictionary $\tilde{\boldsymbol{D}}_j$ to obtain the final sparse codes $\tilde{\boldsymbol{\alpha}}_j^k$.
8. The final sparse coding $\tilde{\boldsymbol{\alpha}}_j^k$ is now further classified into sub-groups with a higher level of similarity using another step of hierarchical clustering. This is the secondary classification as seen in Fig. 4. This final classification is subject to a criteria where the mean number of images across the final classes should be at least 3.0 (explained below), if not the images are flagged as being too distinct.

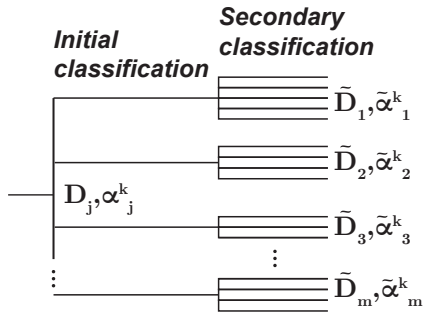


**Figure 4.** Based on the dictionary $\boldsymbol{D}$ a sparse code $\boldsymbol{\alpha}$ is found. These codes are used to classify images into distinct classes. After an initial classification this step is repeated, with a new dictionary and codes generated from the images within a class; branching into smaller sub-classes with higher levels of similarity.

As noted in *Step 8*, it is important to ensure that the final classification result is not too distinct, e.g. having only one image in a class, resulting in loss of effectiveness towards building a compact model. It is therefore important to consider the *separation distance* (`SD`) used in hierarchical clustering – the similarity of the classified images is controlled by this distance metric. A practical aspect of using hierarchical clustering is that compared to clustering algorithms such as *k-means* (MacQueen 1967), where the number of clusters to detect must be specified in advance, hierarchical clustering can use the dendrogram to consider the clustering structure. Consider therefore the dendrogram in Fig. 5 used for finding `SD` in the initial step. Lowering the `SD` yields more classes with fewer images and vice-versa. The distance metric used for clustering is the Ward sum-of-squares minimization metric (Ward Jr 1963). The Ward metric was chosen as it is more permissive in terms of cluster shape/size assumptions (Anderberg 1973), which performed better on the sparse codes. In using this distance measure it is important that the data vectors we are operating on are normalized by the mean and standard deviation (Wilks 2011), hence *Step 1* above. The `SD` for the initial clustering is found based on the dendrogram and evaluation of the separation results. As noted in Wilks (2011), setting the

[†] `https://bit.ly/2KS0OY2`

| Parameter | Value | Comment |
|---|---|---|
| Input data set | 74 images, size: $52 \times 59$ pixels | Type: 1 km, 1 day average SST |
| Patch size $[x_{pa}]$ | $40 \times 40$ | The patch pixel size |
| Sample count | 260 | The number of sample patches from each image |
| Dict. size $[x_{ds}]$ (initial) | 4 | Number of atoms in the dictionary |
| Dict. size $[x_{ds}]$ (secondary) | 8 | Number of atoms in the dictionary |
| Distance metric | Ward | The distance metric used by the hierarchical clustering |

**Table 1.** Classification parameters.

SD usually requires a subjective choice that depends on the goal of the classification. There exist various statistical machine learning tools that consider the bias versus variance trade-offs (e.g. James et al. (2013)), but there is no single "best" approach. Since this initial grouping is followed by a secondary classification, this initial grouping is not as decisive a factor, as the secondary clustering, as only the major features are to be identified. Nevertheless, local oceanographic expertise and knowledge should be involved to find a justifiable separation scheme. For the first step of the classification, a general rule of thumb would be to avoid a SD that yields too sparse a set of classes.

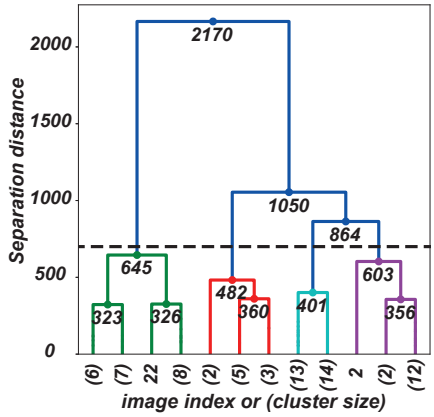


**Figure 5.** The dendrogram for the initial clustering step. Four classes are being separated using a distance measure set to 700. The numbers on the x-axis are either image index or cluster size (in parentheses).

For the secondary clustering step, finding a SD that does not result in an unbalanced variance (too big/small classes) becomes important. The goal here is to find similar images that can be used in a conditional mean, while also excluding images that are too distinct – similarity is, as noted, controlled by the SD. To achieve an adequate final result we iteratively change the SD until we reach a classification result where the mean number of images across the sub-classes is above or equal to a certain threshold, which we have set to 3.0. This threshold is chosen to establish a criterion that ensures we are generating classes that span several images, while not creating classes with a too dissimilar image basis. For example, if a secondary classification with 12 images starts with a SD$= 500$ and yields the sub-classes $[1, 2, 3, 4, 5]$ with associated image counts of $[5, 4, 1, 1, 1]$, the mean number of images in each class equals 2.4, and three classes have only one image. This does not satisfy our criterion, and the SD can therefore be increased, relaxing the measure of how similar the images need to be. The SD is relaxed until one of the classes containing only one image is combined into one of the other five, as this reaches our criterion.

Parameters that are associated with the above procedure, are shown in Table 1. The patch and dictionary size can be adjusted to yield different results. The relationship between the patch size $x_{pa}$, dictionary size $x_{ds}$, and code length $x_{cl}$ is given, using the fixed dimensions $52 \times 59$ for the images, as $x_{cl} = ((52 - x_{pa} + 1) \times (59 - x_{pa} + 1)) \times x_{ds}$. From this, we can see that the code length depends on the patch size squared, while increasing linearly with the dictionary size. This code length is important as clustering becomes more complex and may lead to degraded classification accuracy for higher dimensional vectors, as can be seen in Fig. 6a.

Parameter selection was done by comparing the intra-class variability (ICV) for each class $j = 1, \ldots, m$ measuring how different the images within a class are by comparing the temperature variability at each location across the images, given as:

$$\begin{aligned} \mathrm{ICV}_j &= \sum_i \sigma_{ij}^2, \\ \sigma_{ij}^2 &= \frac{1}{n_j} \sum_{k \in \otimes_j} (x_{ik} - \mu_{ij})^2 \\ \mu_{ij} &= \frac{1}{n_j} \sum_{k \in \otimes_j} x_{ik}, \end{aligned} \tag{2}$$

where $x_{ik}$ is the temperature at location $i$ in image $k$, $\otimes_j$ is the set of images belonging to class $j$, and $n_j$ is the number of images in this set. Moreover, $\mu_{ij}$ and $\sigma_{ij}^2$ are the sample mean and variance in temperature at location $i$ for class $j$. Using ICV as a metric, the patch and dictionary size is chosen based on the settings that give the lowest ICV after several iterations for each setting with a non-constant random seed. The patch size sensitivity visible in Fig. 6a, suggests that running the method with larger patch sizes performs better –hence a patch size of $40 \times 40$ pixels is used. For choosing the dictionary size, Fig. 6b shows that a dictionary size of 4.0 is enough to achieve both low ICV spread and value. Having a larger patch size and smaller dictionary size is also positive for reducing computational load. For the secondary classification the dictionary size is increased because the number of images being classified are fewer and their similarity is higher (filtered by the initial classification), hence a more descriptive code can be applied.

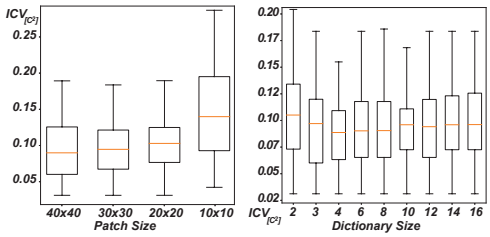


**(a)** ICV sensitivity to patch size. **(b)** ICV sensitivity to dictionary size.

**Figure 6.** Intra-Class Variability (ICV) sensitivity using different patch size $x_{pa}$ and dictionary size $x_{ds}$. Fig. 6a shows a box plot of the ICV spread for different patch sizes; larger $x_{pa}$ tend to yield lower ICV values. Fig. 6b shows the ICV variation for different dictionary sizes. A dictionary size of 4 would be a good choice, indicating low ICV spread and value.

### 4.2 Enhancement of Classification by Structural Information

The performance of the methodology is compared by using only temperature *minimum, maximum, min-max range,* and *mean* as a classification vector. The magnitude-only classification is done using hierarchical clustering directly (i.e. no sparse codes), while the sparse dictionary classes are a result of the proposed method in Section 4.1. As the temperature values of SST can contain several strong separating factors, some initial categorization can be achieved, but defining conditional means from these classes leads to unnecessary variability as spatial information is neglected. By comparing the ICV given in Eq. (2) between the sparse dictionary- and magnitude-only derived classes, this effect is shown in Fig. 7 which shows the ICV for $m = 13$ classes using the two approaches, where each unit block in the histogram is a class with a corresponding ICV.

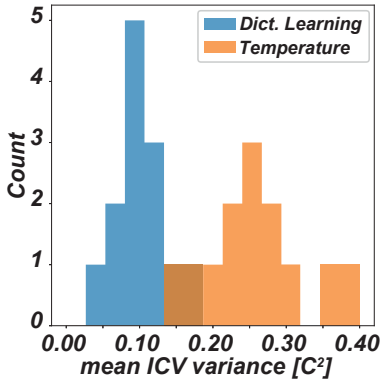


**Figure 7.** Histogram of the ICV for the sparse dictionary- and temperature derived classes.

As seen in Fig. 7, classifying only using temperature characteristics leads to higher variance, as images within the classes are less similar. Since the proposed classification method not only considers images with the same temperature magnitude, but also how this temperature is distributed spatially, the variance is lower when using the dictionary learning approach.

## 5 Classification Results

The final classification groups are used to make different conditional means that together constitute a compact model. An important aspect of the approach is to verify that images which are classified together share a common formation history; having been influenced by the same sequence of physical processes. Having a shared evolution of oceanographic conditions also implies that there exists a common and distinct spatial pattern that can be clustered together to make what we choose to call a *condition*. Wind observations can be used for this purpose for two important reasons: i) wind influences a range of oceanographic processes and is the dominant driver of SST variability in this region of study; ii) ambient conditions like the wind are common oceanographic measurement provided by a range of maritime platforms. The use of other sources of data, rather than wind, is also possible and will vary depending on the study region. The comparison and verification is shown in Fig. 8 together with the initial clustering result.

### 5.1 Initial Classification

The initial classification is dominated by the temperature magnitude, as this is a stronger separating factor than spatial patterns. The SD used in hierarchical clustering was found using the dendrogram in Fig. 5, producing four classes. Fig. 8 shows these together with the aggregated 4 day preceding wind history. The images appear in arrangement going from *cold* to *warm*, or in the oceanographic context, from *upwelled* to *relaxation* dominated waters. The associated winds confirm this by showing a correspondence between the upwelled (class 1 – cold) SST images with strong north-westerly winds, and weaker more spread wind pattern for the relaxation (class 4 – warm) SST images.

Fig. 9 shows the average u- and v-components of the wind [‡] history for each class. Similar to Fig. 8, the average trend shows class 1 has the strongest average winds, and class 4 the weakest. A strongly negative v component of the wind is equivalent to north-westerly, i.e. blowing from the northwest and upwelling favorable. There is also a strong diurnal signal in the winds, evident in all classes in the u component (Fig. 9). This predominantly east-west "sea-breeze" is driven by differential heating of land and ocean through day/night. The intermediate classes comprise images covering the transition between these oceanographic conditions. This initial classification shows that some structure follows from the temperature, but as seen in Section 4.2, using temperature alone will not achieve the best clustering result. Magnitude information helps us avoid a pitfall where images that have a similar pattern but different temperature magnitude are clustered together, disrupting the conditional means by averaging images that represent different oceanographic states.

[‡] The u signifies the zonal velocity component of the wind, while v the meridional component.

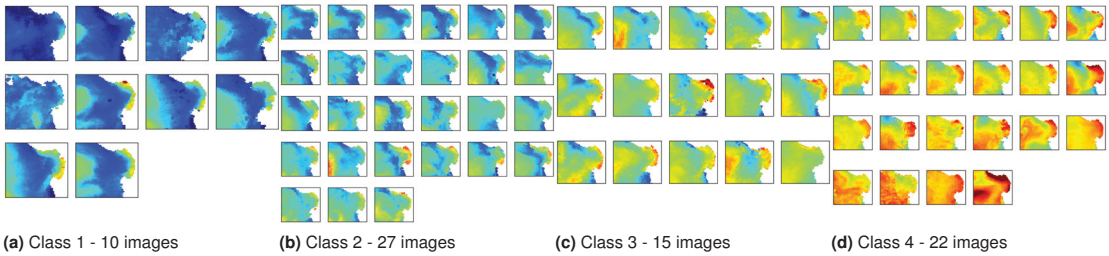

**(a)** Class 1 - 10 images **(b)** Class 2 - 27 images **(c)** Class 3 - 15 images **(d)** Class 4 - 22 images

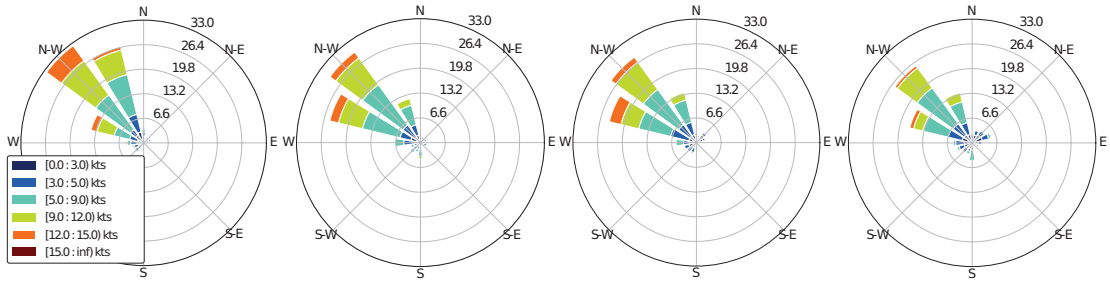


**(e)** Wind rose 1 **(f)** Wind rose 2 **(g)** Wind rose 3 **(h)** Wind rose 4

**Figure 8.** The four classes derived from the initial classification shown with the associated wind history during the 4 days preceding each image within a class. The wind rose plots represent a summary of wind speeds and the directions from which it was blowing. Wind speeds are defined by color (legend) and percentage of speeds in a given range are shown by occupancy of each color. Cold upwelled class 1 has stronger north-westerly winds, while warm relaxation class 4 has weaker magnitude and greater spread in direction. The temperature images are all using the same temperature scale from $10°\mathrm{C}$ to $16°\mathrm{C}$.

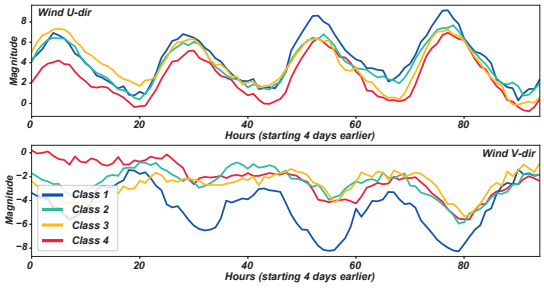


**Figure 9.** The average 4 day wind history for each class given in terms of u- and v-components also show a significant difference between the classes. Note the strong 2 day amplitude for class 1.

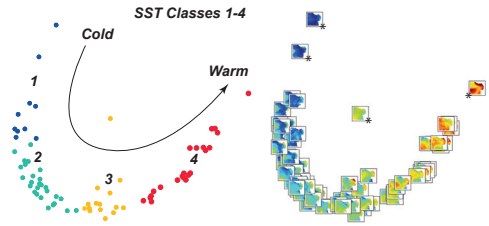


**(a)** PCA projection. **(b)** PCA projection - image scatter

**Figure 10.** The initial classification shown as projected into 2D using PCA, shown with the classified label color and class membership. It is evident that the images represent a continuous process which can be expressed as progress from cold to warm conditions. Note also potential outlier images (marked *).

To understand this classification further Fig. 10 shows the projection of the sparse codes using principal component analysis (PCA) projected into a 2D plane, visualizing the information contained in the vectors. As previously noted, as the SST images are covering a continuous process some images are "overlapping" and could potentially be associated with more than one class. It is also possible to identify certain images that can be deemed as outliers. The colors in Fig. 10a show where the hierarchical clustering distance, SD, is making the distinction.

## 5.2 Secondary Classification Refinement

The images in each class are to be further distinguished in the secondary classification. The images in this step are now already sorted according to matching temperature, which we have shown, by comparing the wind history, can be traced to distinct evolution of oceanographic conditions. Within each class, a new dictionary $\tilde{\boldsymbol{D}}_j$ can now be found, that can specialize in finding a final sparse code $\tilde{\boldsymbol{\alpha}}_j^k$ that factors in more spatial information, which is shown in Fig. 7. The parameters for the secondary classification, found in Table 1, are similar to the initial classification apart from a larger dictionary size. As noted, the dictionary size has increased because the number of images being classified are fewer and their similarity is higher in this step, hence a more descriptive code can be applied.

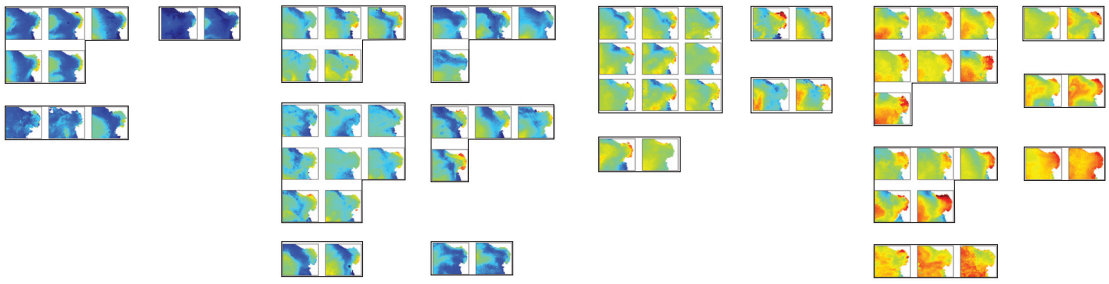

**(a)** Sub-Classes 1 **(b)** Sub-Classes 2 **(c)** Sub-Classes 3 **(d)** Sub-Classes 4

**Figure 11.** The results from the secondary classification with 19 sub-classes. Four initial classes have been further sub-divided into sub-classes based on their class $j$ dependent $\tilde{\boldsymbol{D}}_j$ and $\tilde{\boldsymbol{\alpha}}_j^k$ dictionary and code. Note the number of groups is only the valid sub-classes, as some of the images are left out from the compact model, deemed to be too distinct.

| Classification | Classes | Image Count | Mean Class Size | ICV |
|---|---|---|---|---|
| 1st | [1 2 3 4] | [22 10 27 15] | 18.5 | 0.30 |
| 2nd - Class 1 | [1 2 3] | [3 2 5] | 3.33 | 0.12 |
| 2nd - Class 2 | [1 2 3 4 5 6 7*] | [2 3 5 2 2 7 1*] | 3.14 | 0.09 |
| 2nd - Class 3 | [1 2 3 4] | [2 2 2 9] | 3.75 | 0.13 |
| 2nd - Class 4 | [1 2* 3* 4 5 6 7 8] | [2 1* 1* 4 4 2 8 5] | 3.37 | 0.13 |

**Table 2.** Classification Results. The $ICV$, given in Eq. (2), measures the mean sub-class variability. (*) marks groups with only 1 image considered too distinct that are removed.

Fig. 11 shows the resulting secondary classification, with a total of 19 sub-classes (see Table 2). The classes containing only one image are deemed too distinct for further inclusion into the compact model. As expected the mean class size is above 3.0 as specified from the criteria in *Step 8*, with $ICV$ values from $0.09 - 0.13$. It is also apparent that images are now sorted both by temperature as well as spatial features (see e.g. the upper left corner of Fig. 11c). However, cloud cover can pose challenges. In some cases, this "false" pattern match can be such a dominating feature that images with a similar "false" features are classified together, (e.g. the lower group in Fig. 11a) as shown in Fig. 12.

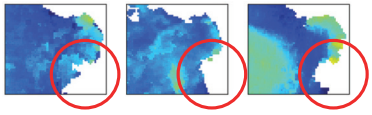

**Figure 12.** The misclassification of images due to cloud cover. The last image should be in the first group in Fig. 11a, rather than the lower group.

Taking the average across each sub-class in Fig. 11, yields the different conditional means and the final compact model, shown in Fig. 13b. Rather than relying on the means from the initial classification in Fig. 13a, these representations hold more spatial information that is advantageous when trying to predict the current state of the environment. From these conditional means one can observe not only the transition from cold to warm conditions, but also the varying spatial structure that develops within and outside Monterey Bay.

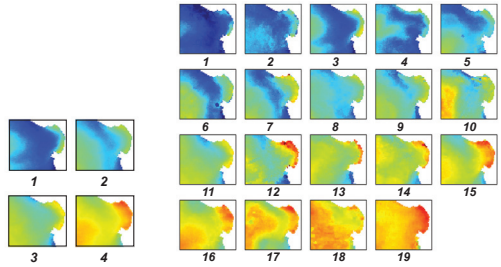


**(a)** Initial conditional means **(b)** Secondary conditional means

**Figure 13.** The conditional means derived from the initial and secondary classification.

## 6 Forecast and Sampling Policies

We now use these conditional means as a compact model from which a prediction of the environment, specifically the SST field, can be made. Having the capability to compare *in-situ* data with the model provides a way to determine which types of historical conditions that best fits this data. On this basis an estimate of the current state can be formed, usually taken as a weighted combination of the "best" class candidates. A common method for verifying the reliability of the prediction is to compare the root-mean-square error (RMSE) of the class mean to the average class spread, as suggested in Fortin et al. (2014); the idea is that the standard deviation of the class spread should be approximately equal to the RMSE. We further study how the

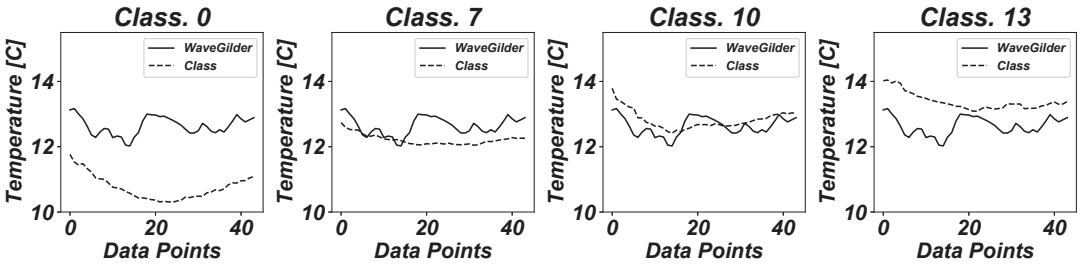


**Figure 14.** The *in-situ* temperature profile superimposed on the temperature profile for class 0, 7, 10, and 13.

prediction probabilities of different states depend on the data, and how this can be used in designing sampling strategies.

### 6.1 Predicting the Environment

From Fig. 1, an intuitive way to predicting the environment is by combining one or several classes using a weighted average. During robotic vehicle operations such as that provided by a WaveGlider ASV, the prediction is done conditional on data $\boldsymbol{y} = (y_1, \ldots, y_{n_p})$, where $p$ is the number of measurements made during the survey. Based on satellite data, the probability $P(\text{class} = j)$ is estimated as the fraction of images in each class over the total number of images, $P(\text{class} = j) = n_j/n$. Conditional on data $\boldsymbol{y}$ the probability of class $j$ becomes:

$$P(\text{class} = j|\boldsymbol{y}) = \frac{p(\boldsymbol{y}|j)P(\text{class} = j)}{p(\boldsymbol{y})} \qquad (3)$$
$$p(\boldsymbol{y}) = \sum_j p(\boldsymbol{y}|j)P(\text{class} = j).$$

The class likelihood, in Eq. (3) above, is approximated as a *multivariate normal distribution*:

$$p(\boldsymbol{y}|j) = \frac{1}{\sqrt{(2\pi)^{n_p}|\boldsymbol{\Sigma}_j|}} e^{\left(-\frac{1}{2}(\boldsymbol{y}-\boldsymbol{\mu}_j)^T\boldsymbol{\Sigma}_j^{-1}(\boldsymbol{y}-\boldsymbol{\mu}_j)\right)}, \qquad (4)$$

where $\boldsymbol{\mu}_j = (\mu_{1j}, \ldots, \mu_{n_p j})$ is the class-$j$ vector of mean values along the survey trajectory, and $\boldsymbol{\Sigma}_j$ is the associated covariance matrix at these $p$ sampling locations. This covariance is defined by elements $\boldsymbol{\Sigma}_j(i,i') = \text{diag}(\sigma_{ij})\ \boldsymbol{R}\ \text{diag}(\sigma_{i'j})$, where $\boldsymbol{R}$ is a distance based correlation matrix (Matérn 2013), i.e. $R(i,i') = (1 + \phi h_{ii'})e^{-\phi h_{ii'}}$, where $h_{ii'}$ is the Euclidean distance between sampling locations $i$ and $i'$, and $\phi$ is indicative of the correlation range. In this paper we use ∼15 km, based on Frolov et al. (2014, Fig. 4b) showing decorrelation scales for Monterey Bay.

Prediction is done using class probabilities as a function of the data gathering window. This means that we integrate one more observation at every step, and re-calculate the probability over the classes, given this growing subset of data. Because of the spatial correlation in the model, induced via $\boldsymbol{R}$, the assimilation of one more observation will not have the same effect as it would for independent data. The final prediction at location $i$, based on available data data $\boldsymbol{y}$, is a weighted average according to the conditional distribution in Eq. (3),

$$\hat{SST}_i = \sum_{j=1}^{m} P(\text{class} = j|\boldsymbol{y})\mu_{ij}. \qquad (5)$$

where $\mu_{ij}$ is the conditional mean in class $j$. A brief example using this approach is presented using data from a WaveGlider. This vehicle records the temperature at 0.4 m depth using a Seabird CTD (conductivity, temperature, and depth) sensor, which we will use to predict the SST.

We use data from the $17^{th}$ of May, 2018 in Monterey Bay, during the **CANON**[§] field experiment. The prediction, using Eq. (5), is compared to the actual 1 day average SST for that day. Fig. 14 shows the recorded temperature profile across the survey locations (the survey path is shown in Fig. 15a) together with the corresponding profile from class 0, 7, 10, and 13. Clearly, some classes match the data better than others. Class 7 and 10 follow closely throughout, while class 0 and 13 has a poor correspondence. We use this data to predict the environment using $P(\text{class} = j|\boldsymbol{y})$ as the weights. Thus, the likelihood is therefore expected to be high around class 7 and 10, and low for the others. The prediction is shown in Fig. 15b, together with the actual SST image in Fig. 15a. The accuracy of the prediction is, as expected, better on the large scale, with some smaller spatial features that are not captured by the model. Fig. 15d shows this temperature difference spatially. Note that the the nominal accuracy of the SST images is about 0.7 degrees Celsius. As the original daily composite SST image is not without error, e.g. noise from daily averaging, some regions will show exaggerated difference. It is also reasonable to assume that there is a discrepancy between the WaveGlider data and the daily average SST, which also contribute to estimation error. This can be seen with closer inspection of Fig. 15a, as the track and overlaid temperature are colder than the average SST. Fig. 15c shows the RMSE and together with the likelihood $P(\text{class} = j|\boldsymbol{y})$. The RMSE is calculated as:

$$RMSE(j, \boldsymbol{y}) = \sqrt{\frac{\sum_{i=1}^{n_p}(y_i - \mu_{ij})^2}{p}}. \qquad (6)$$

There is a correspondence between the likelihood $P(\text{class} = j|\boldsymbol{y})$ and the RMSE. As expected the maximum

[§] https://bit.ly/2KHpfCH

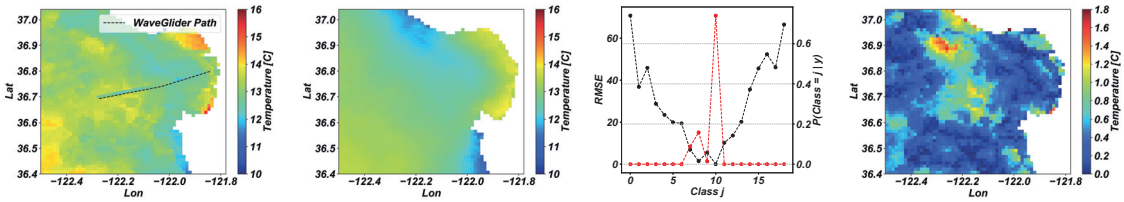


**(a)** True SST 2018-05-17. **(b)** Estimated SST. **(c)** Likelihood and RMSE. **(d)** Estimation error.

**Figure 15.** The results from evaluating the classes by using the likelihood and the RMSE. The true SST (15a), estimated SST (15b), the likelihood and RMSE for each class (15c), and the spatial temperature difference (15d) are shown. The track of the WaveGlider is shown in panel (15a) with the observed temperatures overlaid. There is some averaging artifacts in the true SST that shows up in the estimation error (15d).

likelihood and the lowest RMSE occur around class 10. As the likelihood adjusts for spatial correlation and prior probability $P(\text{class} = j)$, there is some difference between the two measures of similarity (e.g. class 9). Comparing the mean RMSE of the estimated SST against the class spread (0.45 vs. 0.77), indicate that we are in accordance with the reliability measure discussed in the beginning of this section.

## 6.2 Evaluation of Model Prediction Error

For discrete models, such as the one developed here or Lilleborge et al. (2016), the intent of data collection is to pull the predictive probabilities closer to 0 or 1 (Eidsvik et al. 2015). The *a priori* prediction error (before any data is recorded) is given via the most likely ocean state class as $j^* = \text{argmax}_j\{P(\text{class} = j)\}$ as:

$$PE = 1 - P(\text{class} = j^*). \tag{7}$$

Conditional on data $\boldsymbol{y}$ the prediction error is $PE(\boldsymbol{y}) = 1 - P(\text{class} = j^*(\boldsymbol{y})|\boldsymbol{y})$, where now the most likely ocean state is given as $j^*(\boldsymbol{y}) = \text{argmax}_j\{P(\text{class} = j|\boldsymbol{y})\}$, with probabilities defined in Eqn. (3).

Before sampling, which data $\boldsymbol{y}$ to collect is not known. The sampling strategy is hence evaluated up-front, based on the model, and the average posterior prediction error is obtained by integrating over all possible data. This gives

$$\begin{aligned} PE(\boldsymbol{y}) &= E\{1 - P(\text{class} = j|\boldsymbol{y})\} \\ &= \int (1 - P(\text{class} = j^*(\boldsymbol{y})|\boldsymbol{y})p(\boldsymbol{y}))dy, \end{aligned} \tag{8}$$

where $j^*(\boldsymbol{y})$ is the class with largest probabilities conditional on $\boldsymbol{y}$. The improvement made by data collection can now be compared over various experimental designs (survey paths) using the Monte Carlo approach outlined in Eidsvik et al. (2015, Ch. 5.6). To analyze the effect of data gathering we start by generating synthetic data from the model. This entails drawing a random class $j^b$ from probabilities $P(\text{class} = j)$, $j = 1, \ldots, m$, and next drawing data $\boldsymbol{y}^b$ conditional on this class. This is based on the likelihood model in Eq. (4). We set:

$$\boldsymbol{y}^b = \boldsymbol{\mu}_{j^b} + \boldsymbol{L}_{j^b}\boldsymbol{z}. \tag{9}$$

This approach uses the Cholesky factorization (Nash 1990) of the covariance matrix $\boldsymbol{\Sigma}_j = \boldsymbol{L}_j\boldsymbol{L}_j^T$ along with a length $n_p$ vector $\boldsymbol{z}$ of independent $N(0, 1)$ variables. Examples of generated data can be seen in Fig. 16. The final error prediction can now be computed using the generated data in a Monte Carlo approximation.

$$PE(\boldsymbol{y}) \sim \frac{1}{B}\sum_{b=1}^{B}(1 - p(j^*(\boldsymbol{y}^b)|\boldsymbol{y}^b)), \tag{10}$$

where $B$ is the number of iterations (we used $B = 500$).

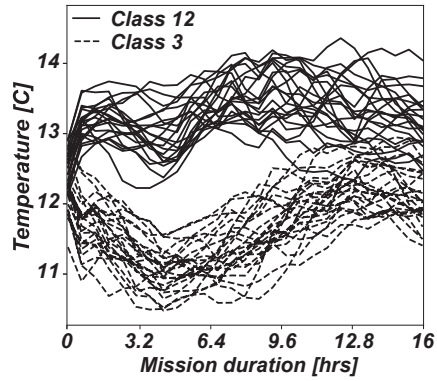


**Figure 16.** An example of 50 synthetic survey lines data for class $j = 12$ and $j = 3$, with missions lasting 16 hours.

It is now possible for a practical comparison of the reduction of prediction error for different survey times (the effect of gathering more data) and survey locations (survey trajectories). The results are shown in Fig. 17, as a function over the survey duration, and for three different survey paths, using the WaveGlider and assuming a platform speed of approximately 2.2 kts. Using this, different lengths of surveys can be correlated to mission time.

Fig. 17a shows the prediction error for a given mission duration. Naturally, longer missions result in more observations and less error, reflecting the amount of data that is available. The effect of different survey paths is shown by using three different routes, shown together in Fig. 17b, with their evolution and final $PE(\boldsymbol{y})$, as shown in Fig. 17a. Path 1, that is both crossing the inner and outer bay, produces the lowest prediction error ($PE(\boldsymbol{y}) \sim 0.15$).

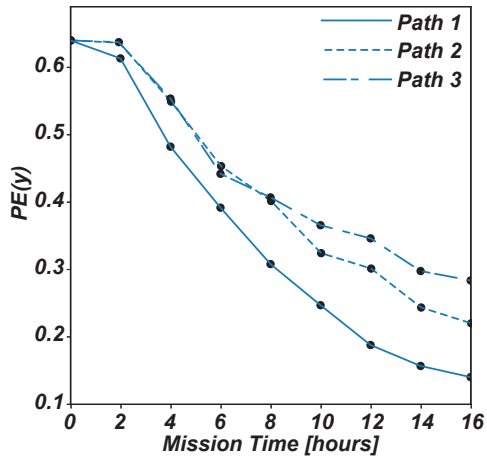


**(a)** Predicted error vs. mission time.

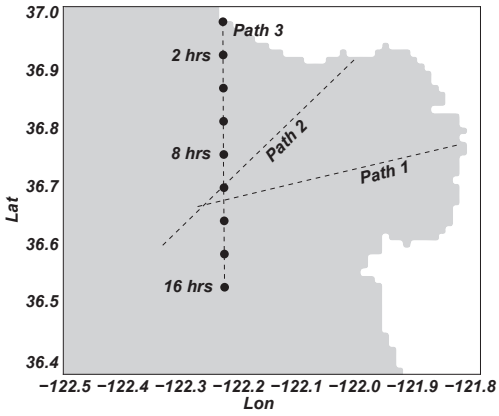


**(b)** The different mission paths.

**Figure 17.** (17a) The effect of gathering more data (expressed as mission duration) on the prediction error, calculated for each of the three paths. The error drops (from close to the prior probability $PE \sim 0.64$) as more information is obtained. (17b) By comparing different survey paths, one can observe that some locations are more informative than others, showing difference in $PE$-curves.

A possible reason for this is that path 1 crosses both gradients inside the bay, as well as gradients that are prominent further offshore, covering the usual band where up-welling fronts occur. The curve starts at the prior probability $PE \sim 0.64$, which arises from Eq. (7), estimated as the fraction of images in each scenario over the total number of images. This type of investigation useful, since it provides an estimate of both the value of mission duration and location, which is often an unknown when planning survey campaigns. Such an analysis can also be conducted across platforms; each platform can be evaluated by simulating a different coverage (survey speed), spatial correlation ($\phi$), measurement noise, etc. Optimization of coverage versus cost is also possible, finding effective solutions that maximize the cost per observation. This type of reasoning ("What is the value of the data and how much data is enough?") is often referred to as *value of information*-analysis (Eidsvik et al. 2015).

## 7 Discussion

In the absence of remote sensing, description of regional *high resolution* data may be unavailable. A compact model, as the one developed in this work, and the supporting statistical tools, can help provide contextual *low resolution* information, by using *in-situ* observations. Reducing the global uncertainty is necessary for enabling efficient planning of vehicle surveys, that rely on evaluating the current state at unexplored locations, as well as variability and associated correlation structures. With this in mind, some aspects of the presented approach are discussed, in order to shed light on the potential benefits and pitfalls.

Assimilation using an onboard numerical ocean model that accounts for time is currently not possible or practical due to time and computational limitations, hence compact or reduced order models are needed. The current compact model is static, i.e. the classes themselves are not modified during the mission. In practice, this means that small scale features will not be well resolved. One could use *Gaussian Process* regression (Rasmussen and Williams 2006) to assimilate the observations and correct this locally. However, the primary capability and goal is to predict large-scale features, hence updating each class locally has limited value, as it is the prediction at unobserved locations that is most interesting towards future planning of sampling. Prediction works by taking a weighted average, using a likelihood function. There exist several strategies for finding an alternative weighting scheme. The current approach can be improved by including co-variates (e.g. wind measurements) to further determine some of the global conditions and find the weights conditioned on this. The weighting can also be found using optimization such as Sequential Least SQuares Programming (SLSQP) (Nocedal and Wright 2000) to minimize the error between the observations and a weighted combination of the classes.

Another interesting application, once a model is established, is to calculate a vehicle trajectory that results in the greatest level of class separation, that is, a path that best reduces the uncertainty in the model by fast convergence to a ranking (a probable scenario); similar to the analysis in Fig. 17a. Finding such a route can improve prediction of the oceanographic state by gathering temperature data in areas that will enhance discrimination, and can locate areas where multidisciplinary sensing from in situ platforms will be most informative. Criterion such as expected reduction of variance, mutual information, or entropy can be used to find these locations.

Regional factors such as wind, bathymetry, and currents contribute to shaping the spatial patterns used for classification, which contribute to shaping SD and other parameters. Local oceanographic expertise is therefore necessary for validation. The method also involves some work related to tuning of hyperparameters, that will need supervision by oceanographers to ensure that a physically sound separation is used for building the model. Once configured, the method can operate on its own, and be

automatically set to digest new SST images. We use different settings for the dictionary size in the initial and secondary classification. This increases the length of the sparse codes, but allows for more spatial/pattern based information to be used in classification; initially this might not be necessary as the temperature dominates.

## 8 Conclusion

We have developed a new methodology for classifying remote sensing products such as SST towards building compact models that can be utilized by autonomous vehicles to provide environmental estimates. The method allows continuous processes to be segmented and compressed into a basis of classes/scenarios that can be used as a framework for informing trajectory planning and sampling design. This approach can enhance the effectiveness of ocean observing campaigns and in the end help scientists understand the regional oceanographic influences. We show examples using real data from Monterey Bay, where the compact model is combined with in-situ data to predict regional oceanographic states and bulk features. The results show that local observations can be used to yield information on a synoptic scale, but is limited to only resolving low frequency details. We have also evaluated the prediction error of the model and demonstrated the sensitivity to data, from the perspective of an ASV like the WaveGlider.

### References


Aharon M, Elad M and Bruckstein A (2006) k-SVD: an algorithm for designing overcomplete dictionaries for sparse representation. *IEEE Transactions on signal processing* 54(11): 4311–4322.

Anderberg MR (1973) Cluster analysis for applications. *Probability and Mathematical Statistics, New York Academic Press, 1973* .

Bernstein M, Graham R, Cline D, Dolan JM and Rajan K (2013) Learning-based event response for marine robotics. *IEEE International Conference on Intelligent Robots and Systems* : 3362–3367DOI:10.1109/IROS.2013.6696835.

Blondeau-Patissier D, Gower JF, Dekker AG, Phinn SR and Brando VE (2014) A review of ocean color remote sensing methods and statistical techniques for the detection, mapping and analysis of phytoplankton blooms in coastal and open oceans. *Progress in Oceanography* 123: 123 – 144. DOI:https://doi.org/10.1016/j.pocean.2013.12.008. URL http://www.sciencedirect.com/science/article/pii/S0079661114000020.

Chao Y, Chien S, Kinsey J, Flexas MM, Erickson ZK, Farrara J, Fratantoni D, Branch A, Chu S, Troesch M, Claus B and Society TO (2017) Satellites to Seafloor: Towards fully autonomous ocean sampling. *Oceanography* 30(2): 160–168.

Chen C (2012) *Signal and Image Processing for Remote Sensing, Second Edition*. Electrical engineering / remote sensing. Taylor & Francis. ISBN 9781439855966. URL https://books.google.no/books?id=QQDH13L867QC.

Chen Y, Nasrabadi NM and Tran TD (2011) Hyperspectral image classification using dictionary-based sparse representation. *IEEE Transactions on Geoscience and Remote Sensing* 49(10): 3973–3985. DOI:10.1109/TGRS.2011.2129595.

Das J, Rajan K, Frolov S, Ryan JP, Py F, Caron DA, Sukhatme GS, Ryan JP, Caron DA and Sukhatme GS (2010) Towards marine bloom trajectory prediction for AUV mission planning. *Proceedings - IEEE International Conference on Robotics and Automation* : 4784–4790DOI:10.1109/ROBOT.2010.5509930.

Eidsvik J, Mukerji T and Bhattacharjya D (2015) *Value of Information in the Earth Sciences: Integrating Spatial Modeling and Decision Analysis*. Cambridge: Cambridge University Press. ISBN 9781139628785. DOI:10.1017/CBO9781139628785. URL https://www.cambridge.org/core/books/value-of-information-in-the-earth-sciences/61119AB2F707D557E49E00BF9FD6FE39.

Eleveld MA, Ruescas AB, Hommersom A, Moore TS, Peters SWM and Brockmann C (2017) An optical classification tool for global lake waters. *Remote Sensing* 9(5). DOI:10.3390/rs9050420. URL http://www.mdpi.com/2072-4292/9/5/420.

Emberton S, Chittka L, Cavallaro A and Wang M (2016) Sensor capability and atmospheric correction in ocean colour remote sensing. *Remote Sensing* 8(1). DOI:10.3390/rs8010001. URL http://www.mdpi.com/2072-4292/8/1/1.

Everitt B, Landau S, Leese M and Stahl D (2011) *Cluster Analysis*. Wiley Series in Probability and Statistics. Wiley. ISBN 9780470978443. URL https://books.google.no/books?id=w3bE1kqd-48C.

Fortin V, Abaza M, Anctil F and Turcotte R (2014) Why should ensemble spread match the rmse of the ensemble mean? *Journal of Hydrometeorology* 15(4): 1708–1713.

Frolov S, Garau B and Bellingham J (2014) Can we do better than the grid survey: Optimal synoptic surveys in presence of variable uncertainty and decorrelation scales. *Journal of Geophysical Research: Oceans* 119: 5071–5090. DOI:10.1002/2013JC009521.Received.

Frolov S, Kudela RM and Bellingham JG (2013) Monitoring of harmful algal blooms in the era of diminishing resources: A case study of the u.s. west coast. *Harmful Algae* 21-22: 1 – 12. DOI:https://doi.org/10.1016/j.hal.2012.11.001. URL http://www.sciencedirect.com/science/article/pii/S1568988312001503.

Frolov S, Paduan J, Cook M and Bellingham J (2012) Improved statistical prediction of surface currents based on historic HF-radar observations. *Ocean Dynamics* 62(7): 1111–1122. DOI:10.1007/s10236-012-0553-5.

Gonalves ML, Netto MLA, Costa JAF and Jnior JZ (2008) An unsupervised method of classifying remotely sensed images using kohonen selforganizing maps and agglomerative hierarchical clustering methods. *International Journal of Remote Sensing* 29(11): 3171–3207. DOI:10.1080/01431160701442146. URL https://doi.org/10.1080/01431160701442146.

James G, Witten D, Hastie T and Tibshirani R (2013) *An introduction to statistical learning*, volume 112. Springer.

Johannessen OM, Sandven S, Jenkins AD, Durand D, Pettersson LH, Espedal H, Evensen G and Hamre T (2000) Satellite earth observation in operational oceanography. *Coastal Engineering* 41(1-3): 155–176. DOI:10.1016/S0378-3839(00)00030-2.

Jolliffe I (2011) Principal component analysis. In: *International encyclopedia of statistical science*. Springer, pp. 1094–1096.

Lilleborge M, Hauge R and Eidsvik J (2016) Information gathering in bayesian networks applied to petroleum prospecting.

*Mathematical Geosciences* 48(3): 233–257.

MacQueen J (1967) Some methods for classification and analysis of multivariate observations. In: *Proceedings of the fifth Berkeley symposium on mathematical statistics and probability*, volume 1. pp. 281–297.

Mairal J, Bach F, Ponce J and Sapiro G (2009) Online dictionary learning for sparse coding. In: *Proceedings of the 26th annual international conference on machine learning*. ACM, pp. 689–696.

Matérn B (2013) Spatial variation. *Meddelanden från Statens Skogsforskningsinstitut* 36(5): 1–144.

McKay J, Monga V and Raj R (2016) Robust sonar atr with pose corrected sparse reconstruction-based classification. In: *OCEANS 2016 MTS/IEEE Monterey*. pp. 1–5. DOI:10.1109/OCEANS.2016.7761189.

Mountrakis G, Im J and Ogole C (2011) Support vector machines in remote sensing: A review. *ISPRS Journal of Photogrammetry and Remote Sensing* 66(3): 247 – 259. DOI:https://doi.org/10.1016/j.isprsjprs.2010.11.001. URL http://www.sciencedirect.com/science/article/pii/S0924271610001140.

Mulla DJ (2013) Twenty five years of remote sensing in precision agriculture: Key advances and remaining knowledge gaps. *Biosystems Engineering* 114(4): 358 – 371. DOI: https://doi.org/10.1016/j.biosystemseng.2012.08.009. URL http://www.sciencedirect.com/science/article/pii/S1537511012001419. Special Issue: Sensing Technologies for Sustainable Agriculture.

Munk W (2002) Testimony to the U.S. Commission on Ocean Policy. URL http://govinfo.library.unt.edu/oceancommission/meetings/apr18_19_02/munk_statement.pdf.

Nash J (1990) The cholesky decomposition. *Compact numerical methods for computers: Linear algebra and function minimisation* 2.

Nocedal J and Wright S (2000) *Numerical Optimization*. Springer Series in Operations Research and Financial Engineering. Springer New York. ISBN 9780387987934. URL https://books.google.no/books?id=epc5fX0lqRIC.

Oliver MJ and Irwin AJ (2008) Objective global ocean biogeographic provinces. *Geophysical Research Letters* 35(15). DOI:10.1029/2008GL034238. URL https://agupubs.onlinelibrary.wiley.com/doi/abs/10.1029/2008GL034238.

Pedregosa F, Varoquaux G, Gramfort A, Michel V, Thirion B, Grisel O, Blondel M, Prettenhofer P, Weiss R, Dubourg V, Vanderplas J, Passos A, Cournapeau D, Brucher M, Perrot M and Duchesnay E (2011) Scikit-learn: Machine learning in Python. *Journal of Machine Learning Research* 12: 2825–2830.

Rasmussen EC and Williams CKI (2006) *Gaussian Processes for Machine Learning*. 1 edition. MIT Press. ISBN 026218253X. DOI:10.1142/S0129065704001899.

Rosenfeld LK, Schwing FB, Garfield N and Tracy DE (1994) Bifurcated flow from an upwelling center: a cold water source for monterey bay. *Continental Shelf Research* 14(9): 931–964.

Ryan JP, Fischer AM, Kudela RM, McManus MA, Myers JS, Paduan JD, Ruhsam CM, Woodson CB and Zhang Y (2010) Recurrent frontal slicks of a coastal ocean upwelling shadow. *Journal of Geophysical Research: Oceans* 115(12): 1–15. DOI: 10.1029/2010JC006398.

Saritha S and Kumar GS (2017) Inter-spectral and intra-spectral features for effective classification of remotely sensed images. *Procedia Computer Science* 115: 549 – 555. DOI:https://doi.org/10.1016/j.procs.2017.09.113. URL http://www.sciencedirect.com/science/article/pii/S1877050917319415. 7th International Conference on Advances in Computing & Communications, ICACC-2017, 22-24 August 2017, Cochin, India.

Smith RN, Das J, Yi C, Caron DA, Jones BH and Sukhatme GS (2010) Cooperative multi-AUV tracking of phytoplankton blooms based on ocean model predictions. *OCEANS'10 IEEE Sydney, OCEANSSYD 2010* DOI:10.1109/OCEANSSYD.2010.5603594.

Walter V (2004) Object-based classification of remote sensing data for change detection. *ISPRS Journal of Photogrammetry and Remote Sensing* 58: 225–238.

Ward Jr JH (1963) Hierarchical grouping to optimize an objective function. *Journal of the American Statistical Association* 58(301): 236–244.

Wilkinson GG (2005) Results and implications of a study of fifteen years of satellite image classification experiments. *IEEE Transactions on Geoscience and Remote Sensing* 43(3): 433–440. DOI:10.1109/TGRS.2004.837325.

Wilks DS (2011) Cluster analysis. In: *International geophysics*, volume 100. Elsevier, pp. 603–616.

Xie Y, Sha Z and Yu M (2008) Remote sensing imagery in vegetation mapping: a review. *Journal of Plant Ecology* 1(1): 9–23. DOI:10.1093/jpe/rtm005. URL http://dx.doi.org/10.1093/jpe/rtm005.

## Acknowledgements

This work was part of the ENTiCE project [¶] funded by the Research Council of Norway Project # 255303/E40, the *Nansen Legacy Program*, project number # 27272, and AMOS [‖], Center of Excellence, project number # 223254. TM acknowledges support from the Stanford Center for Earth Resources Forecasting and from the Dean of the Stanford School of Earth, Energy, and Environmental Sciences. MBARI authors are funded by a block grant from the David and Lucile Packard Foundation. The WaveGlider data was provided from the MBARI **CANON** campaign with support from Christopher Wahl, Devon Northcott, and Francisco Chavez. Finally, the authors are grateful for the support from MBARI engineering, science, and marine operations.

¶ http://sintef.no/en/projects/entice/

‖ https://www.ntnu.edu/amos

# Article D

## Autonomous Robotic Intervention using ROV: An Experimental Approach

**Trygve Olav Fossum**, Martin Ludvigsen, Stein M. Nornes,
Ida Rist-Christensen and Lars Brusletto



This article is published in the proceedings of
*MTS/IEEE OCEANS 2016*. Monterey, CA, USA, 19-22$^{th}$ September 2016.
doi: 10.1109/OCEANS.2016.7761178

# Article E

## Adaptive Sampling of Ocean Processes Using an AUV with a Gaussian Proxy Model.

Gunhild Elisabeth Berget, **Trygve Olav Fossum**, Tor Arne Johansen, Jo Eidsvik and Kanna Rajan.



This article is published in the proceedings of
*11th IFAC Conference on Control Applications in Marine Systems, Robotics, and Vehicles CAMS 2018*, Opatija, Croatia, 10-12$^{th}$ September 2018.
doi: 10.1016/j.ifacol.2018.09.509

Available online at www.sciencedirect.com

ScienceDirect

IFAC PapersOnLine 51-29 (2018) 238–243

IFAC Papers Online CONFERENCE PAPER ARCHIVE

# Adaptive Sampling of Ocean Processes Using an AUV with a Gaussian Proxy Model

**Gunhild Elisabeth Berget** * **Trygve Olav Fossum** ** **Tor Arne Johansen** * **Jo Eidsvik** *** **Kanna Rajan** *

* *Department of Engineering Cybernetics, Center for Autonomous Marine Operations and Systems, Norwegian University of Science and Technology, 7491 Trondheim, Norway*
** *Department of Marine Technology, Center for Autonomous Marine Operations and Systems, Norwegian University of Science and Technology, 7491 Trondheim, Norway*
*** *Department of Mathematical Sciences, Norwegian University of Science and Technology, 7491 Trondheim, Norway*
*(E-mail: gunhild.berget@ntnu.no, trygve.o.fossum@ntnu.no, tor.arne.johansen@ntnu.no, jo.eidsvik@ntnu.no, kanna.rajan@ntnu.no).*

**Abstract:** This paper presents methods for building and exploiting compact spatial models on board an autonomous underwater vehicle (AUV) towards tracking suspended material plumes. The research is aiming to improve real-time monitoring of dispersal dynamics connected to marine industries such as oil and mine tailing. By exploiting in-situ information from sensors, the AUV is able to assimilate and adapt the mission capitalizing on all the information available. The spatial model is built using Gaussian process approximations and an objective function for path planning is suggested to maximize the value of the collected information.



*Keywords:* Gaussian processes, Adaptive sampling, AUV, Oceanography

## 1. INTRODUCTION

Creating models describing the ocean is challenging because of its large scale nonlinear processes and high spatio-temporal variability. Existing models continuously refine numerical methods towards improving accuracy, (Griffies et al., 2000). Still, model verification and data assimilation continues to be a challenge that prompts the need for data sampled from the ocean. Such data is commonly obtained using either remote sensing, ships or buoys. This data is usually expensive to acquire and process. Hence, the ocean tends to be *undersampled* and strategic planning of missions are essential to retrieve as much information as possible. Planning of missions are usually based on historical data or simulation data from numerical models, but often the real world differs much from these data. Hence, being able to adapt the mission in real-time, adjusting the plan based on current observations, will likely improve the modeling efficiency.

In this paper we focus on a method using an AUV for sampling in-situ oceanographic data with a goal of tracking suspended material plumes, and being able to adjust the mission in real-time. To obtain real-time adaption, a faster-than-real-time particle model onboard the AUV is required. The numerical models have a high computational load, making them unfit for running on embedded robotic systems with both data processing and storage constraints. Hence, a simpler, more compact model approximating the processes is built based on Gaussian processes (GP). This simplified proxy model represents the current state of the ocean at the time, and can be updated when new information are added.

In addition to the GP proxy model, this paper presents an objective function for path planning aiming to maximize the value of information from the samples. The objective function explores the area by choosing locations assumed to be information rich, and also considers the limitations of the AUV.

As a case study, an area in Frænfjorden, Norway containing a seafill for submarine mine tailings is investigated. The goal is to track the particle dispersal near this seafill, aiming to improve real-time monitoring of dispersal dynamics. Two existing numerical ocean models, SINMOD and DREAM, are used to train the GP proxy model creating a prior proxy model of the particle concentration. Having the prior model ready, the AUV can be deployed, and sensor readings can be used to update the proxy model onboard the AUV in real-time. In this paper a simulation study is done using data from the numerical models as sensor readings for the AUV. Figure 1 gives an overview

⋆ This work was supported by the Research Council of Norway through Centers of Excellence funding scheme, Project number 223254 - Centre for Autonomous Marine Operations and Systems (NTNU-AMOS), and the INDORSE project 267793.


10.1016/j.ifacol.2018.09.509

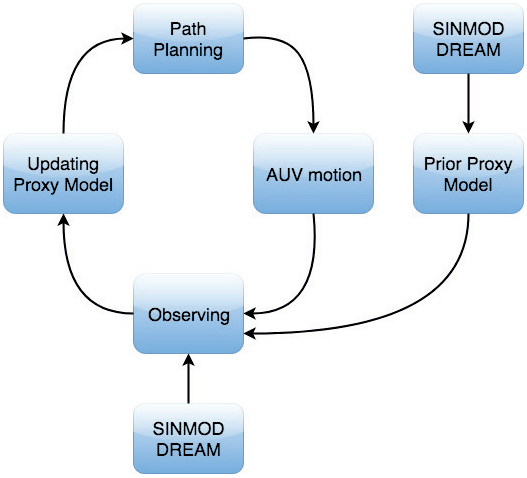


Fig. 1. Block diagram showing the simulation routine. A prior GP proxy model is built using training data from SINMOD and DREAM. Then sensor readings are used to update the proxy model real-time onboard the AUV, and the updated model is used to find the next sampling locations. In the simulation study, the sensor readings are provided by a test data set from SINMOD and DREAM.

of the method proposed in this paper, showing a block diagram of the simulation routine.

### *1.1 Related work and contribution*

GPs (Cressie and Wikle, 2011; Eidsvik et al., 2015) are powerful for creating non-parametric, simple and time-effective models, and are widely used when creating a simplified spatial model. Using GPs for environmental sensing is among others explored in Krause et al. (2008); Zhang et al. (2012); Binney et al. (2010); Das et al. (2015).

In Krause et al. (2008), a method for static sensor placements is suggested using GPs and maximization of mutual information. Others use moving sensors attached to robotic vehicles, as in Zhang et al. (2012) where an AUV is used to track an upwelling front, or in Das et al. (2015) which use an AUV to collect samples for ex-situ analysis, selecting the sampling locations based on previous missions and maximizing a utility function.

When introducing robotic vehicles for sampling, path planning is required to obtain the optimal sampling path. This is among others discussed in Binney et al. (2010) which use the measure of mutual information to optimize information gain along a 2D path for a marine glider. This is further elaborated and tested with a surface vehicle in Binney et al. (2013), where a comparison of greedy vs. recursive greedy approaches is explored for a similar problem.

Zhang and Sukhatme (2007) create an adaptive sampling algorithm based on local linear regression and minimizing estimation error for a sensor network including static sensors and an AUV. Yilmaz et al. (2008); Jadaliha and Choi (2013) discuss environmental sensing and adaptive sampling using more than one robotic vehicle.

A common approach when building a GP model is to assume stationary variance, but when modeling particle transportation there is reason to believe that some sites vary more than others. In this paper an approach using non-stationary variance is suggested, using empirical variance from numerical models as training data for the model variance.

Section 2 presents preliminaries explaining the spatial model and data assimilation procedures. The method used is presented in section 3, before section 4 presents simulation results.

## 2. MODELLING

Having a complex numerical model describing the ocean onboard the AUV is not practical due to computational limitations. Keeping an onboard representation of the environment is resolved using a simpler proxy model, based on Gaussian processes (GP). This section gives a short introduction to the spatiotemporal modelling, and the data assimilation methods used in this paper.

### *2.1 Numerical oceanographic models*

Numerical oceanographic models are in this paper used both to train the proxy model and for simulation purposes. SINMOD and DREAM are two existing models that describe ocean dynamics, and the release and transport of drill cuttings, respectively. SINMOD is a fully coupled hydrodynamic, sea ice and ecological ocean model (Slagstad and McClimans, 2005; Lindstrøm et al., 2009). It is based on the fundamental NavierStokes equations and uses a nesting technique where high resolution models obtain their boundary conditions from larger model domains with lower resolution. This can be repeated in several steps to achieve high resolution for selected areas. SINMOD is established in configurations with horizontal resolutions ranging from 20 km to 32 m. DREAM is a Lagrangian particle transport model which can be used to simulate behaviour and fate of marine pollutants, including particulate discharges from drilling operations (Rye et al., 1998, 2008). It provides time series of both concentrations of released materials in the water column, as well as deposition of these materials onto the sea floor. Input to the DREAM model includes hydrodynamic data, which will be delivered by SINMOD, as well as information about the release (amount, rate, densities, grain size distribution).

For generating the forecast data as input for the AUVs onboard model, SINMOD has been set up with 32 m resolution. Bathymetry data is based on DBM Sør-Norge, supplemented by OLEX data recorded by SINTEF Materials and Chemistry inside Frænfjorden. The atmospheric input data is produced using the Weather Research and Forecasting (WRF) (http://www.wrf-model.org/index.php) model simulated with boundary values from the ERA-Interim reanalysis, and climatologic data for freshwater run-off is used. This data is then forwarded and used as input for the DREAM model. The model area is Frænfjorden (Norway) and the data is from two consecutive days April 1st and April 2nd 2013. Data from 1st April is used

as training data for the proxy model, and data from 2nd April is used as test data in the simulation study.

### 2.2 Spatial Model

A GP is chosen to model the underlying spatial dependencies of the particle concentration. The 2-dimensional domain is divided into a regular grid with $N$ grid points $[s_1, \dots, s_N]$, and the particle concentration in location $s_i$ are assumed to be Gaussian with mean $\mu_i$ and variance $\sigma_i^2$. The random variable defining the concentration at location $s_i$ is denoted $x(s_i)$. Hence, the joint distribution of the state at all the locations $\boldsymbol{x} = [x(s_1), \dots, x(s_n)]$ is multivariate Gaussian

$$\boldsymbol{x} \sim N(\boldsymbol{\mu}, \boldsymbol{\Sigma}) \tag{1}$$

with mean vector $\boldsymbol{\mu} = [\mu_1, \dots, \mu_N]^T$ and a positive definite covariance matrix $\boldsymbol{\Sigma}$. The diagonal of the covariance matrix contains the variances $\sigma_i^2$, and the off-diagonal elements describe the covariance between the locations. The fundamental concept of modelling spatial correlation needs to fulfill two main properties: i) that correlation decays with distance and ii) that the covariance matrix is positive definite. To achieve this, it is common to use known correlation functions or kernels. By comparing covariance functions with the empirical covariance of the training data, Matern (3/2) kernel (Matérn, 2013) is chosen. The function is given by

$$R_{ij} = (1 + \phi h_{ij}) \exp(-\phi h_{ij}), \tag{2}$$

where $h_{ij} = |s_i - s_j|$ is the Euclidian distance between two locations and $\phi$ is a constant meta-parameter regulating the correlation decay with the distance. The best value for $\phi$ is estimated using training data by choosing the best fit of the covariance function to the empirical covariance in the data.

### 2.3 Prior distribution

The model is assumed to be updated sequentially for time steps $t = 1, \dots, T$ adding information from observations in every time step. The initial prior belief at $t = 0$ ($\boldsymbol{\mu}_0$ and $\boldsymbol{\Sigma}_0$) is found using the training data from the numerical models (SINMOD/DREAM). The empirical mean of the training data in each location is used as the prior mean $\boldsymbol{\mu}_0$. Assuming $M$ data $[y^*_{i,1}, \dots, y^*_{i,M}]$ in location $s_i$, this is given by

$$\mu_i^* = \frac{1}{M} \sum_m y^*_{i,m}, \tag{3}$$

and the prior mean of the proxy model is obtained as the vector $\boldsymbol{\mu}_0 = [\mu_1^*, \dots, \mu_N^*]^T$.

A common approach for GPs is to simplify and assume the same variance in each location. However, when modeling ocean processes factors such as topology, currents, wind patterns, and freshwater run-off in coastal areas imply that some locations will have elevated variability. Thus, the prior variance of the state in each location is chosen to be the empirical variance from the training data (Stein, 2005)

$$\sigma_i^{*2} = \frac{1}{M-1} \sum_m (y^*_{i,m} - \mu_i^*)^2. \tag{4}$$

The entries of the prior covariance matrix $\boldsymbol{\Sigma}_0$ are given by

$$\boldsymbol{\Sigma}_0(i,j) = \sigma_i^* \sigma_j^* R_{ij} \tag{5}$$

where $R_{ij}$ defines the correlation between points $s_i$ and $s_j$ as defined by (2).

### 2.4 Data assimilation

To model the temporal changes, a simple Markovian process is suggested

$$\boldsymbol{x}_t = \boldsymbol{x}_{t-1} + \boldsymbol{q}_t, \tag{6}$$

where $\boldsymbol{q}_t \sim N_N(0, V\boldsymbol{\Sigma}_0)$ is a N-dimensional normally distributed vector with zero mean and covariance matrix $V\boldsymbol{\Sigma}_0$ where $V > 0$ is a constant parameter. This temporal model assumes that the current step in time is similar to the previous with an increase in variance proportional to the prior covariance matrix $\boldsymbol{\Sigma}_0$. In this way, parts of the spatial correlation between the locations is maintained, and the increase in variance due to the dynamics of the particle transportation is modeled. The constant value $V$ determines the size of the increase in variance, and this value can be tuned to fit the modelled domain. This temporal process alone does not model the dynamics of the process, and hence, we rely on the observations from the AUV to catch the changes.

The observation model is given by

$$\boldsymbol{y}_t = \boldsymbol{G}_t \boldsymbol{x}_t + \boldsymbol{\epsilon}_t. \tag{7}$$

Here, $\boldsymbol{G}_t$ is the sampling design, a matrix that contains 1 entries only at the sampled indices, otherwise it is 0. $\boldsymbol{\epsilon}_t \sim N_N(0, \boldsymbol{\Omega})$ is a normally distributed error term with zero-mean and covariance $\boldsymbol{\Omega}$, assumed to be Gaussian, describing the measurement noise.

Since a GP is fully represented by its mean and covariance matrix, these are the only thing that needs to be updated in each time step. Exploiting the properties of the Gaussian distribution, the conditional updated mean and covariance matrix at time step $t$: $\boldsymbol{\mu}_t = E(\boldsymbol{x}_t | \boldsymbol{y}_1, \dots, \boldsymbol{y}_t)$ and $\boldsymbol{\Sigma}_t = \mathrm{Cov}(\boldsymbol{x}_t | \boldsymbol{y}_1, \dots, \boldsymbol{y}_t)$ can be found by (Rasmussen and Williams, 2005)

$$\begin{aligned} \boldsymbol{K}_t &= \boldsymbol{\Sigma}_{t-1} \boldsymbol{G}_t^T (\boldsymbol{G}_t \boldsymbol{\Sigma}_{t-1} \boldsymbol{G}_t^T + \boldsymbol{\Omega})^{-1} \\ \boldsymbol{\mu}_t &= \boldsymbol{\mu}_{t-1} + \boldsymbol{K}_t (\boldsymbol{y}_t - \boldsymbol{G}_t \boldsymbol{\mu}_{t-1}) \\ \boldsymbol{\Sigma}_t &= \boldsymbol{\Sigma}_{t-1} - \boldsymbol{K}_t \boldsymbol{G}_t \boldsymbol{\Sigma}_{t-1} + V\boldsymbol{\Sigma}_0. \end{aligned} \tag{8}$$

## 3. METHOD

Having set the foundation by suggesting a proxy spatial model in section 2, we now proceed to explain the adaptive sampling method, including the path planning method using an objective function and the overall sampling algorithm.

### 3.1 Objective function

To obtain an information rich path for the AUV, an objective function is suggested. The function is created based on three criteria.

(1) Locations with high variance are preferred
(2) Locations close to the previous sampling location are preferred
(3) Locations with high predicted concentration are preferred

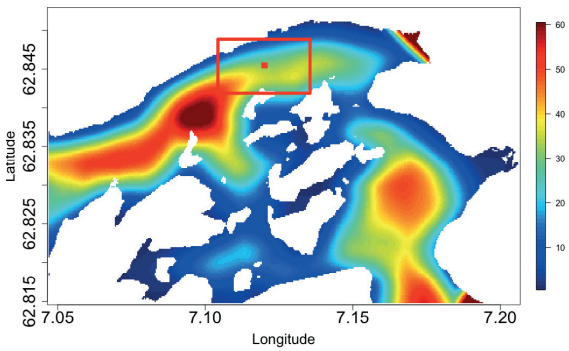


Fig. 2. Plot of the bathymetry of Frænfjorden. The red rectangle shows the selected area, and the red dot indicates the location of the seafill.

The first criterion is chosen because observing in areas with high variance leads to a reduction in total variance, hence creating a more accurate model. This criterion also ensures that the AUV travels to areas that are unexplored. The second criteron comes from the energy and speed limitation of the AUV. When choosing the next sample location, it is essential that the AUV does not travel too far. The last criterion makes the method adaptive. When studying the simulation results of the particle transport from the complex model, it is clear that the variability is highest where there is a high concentration of particles. Hence, this last criterion is inspired by this observation, and assumes that locations with high predicted concentration will be rich with information.

The suggested objective function is then created by having a term for each of these criteria. At time step $t$ for location $s_i$ given the previous sampling location $S_{t-1}$, the objective function is given by

$$f_t(s_i) = \theta_1 \sigma^2_{i,t} - \theta_2 |S_{t-1} - s_i| + \theta_3 \mu_{i,t} \tag{9}$$

where the constant parameters $\boldsymbol{\theta} = [\theta_1, \theta_2, \theta_3]$ defines the weighting for each of the three criteria. These parameters together with the parameter $V$ in the updating equations (8) are tuned by trial and error to obtain the desired behavior of the AUV.

### *3.2 The algorithm*

The sampling location $S_t$ at time step $t$ is chosen as the location that maximizes the objective function $f_t(s_i)$ for $s_i \in [s_1, \dots, s_N]$,

$$S_t = \text{argmax}_{s_i}(f_t(s_i)). \tag{10}$$

The details of the sampling method are given in Algorithm 1.

The method is a greedy method that sequentially chooses the best sampling location. First, the spatial GP model is created using training data from simulations. Then the sampling starts by evaluating the objective function and choosing the location which maximizes it. After reaching the desired location and doing observations, the GP model is updated and the variance is increased in the unobserved locations.

**Algorithm 1** Sampling method

```
procedure SAMPLING
    Initialize GP
    for t = 1, ..., T do
        for s = s_1, ..., s_N do
            Evaluate f_t(s)
        Choose S_t = argmax_s(f_t(s))
        Go to location S_t
        Retrieve observations from S_t
        Assimilate data according to (8)
```

## 4. SIMULATION RESULTS

Data for April 1st 2013 describing the particle concentration in the fjord obtained from DREAM was used to train the GP, and to create the prior mean $\boldsymbol{\mu}_0$ and covariance $\boldsymbol{\Sigma}_0$. For simplicity, only a small area around the seafill was considered (2560 m × 1280 m) and the area was divided into a regular grid with grid cells of size 32 m × 32 m (the same grid as for the simulation data). Also, in this initial simulation only one depth layer was considered at ≈ 15 m depth, but this could be expanded to 3 dimension considering multiple snapshots in different depth layers. Figure 2 shows the bathymetry of the fjord and the selected area as a red rectangle. From the training data it was observed that the distribution of particles in the location of the seafill was rapidly changing and had very little correlation with the neighboring sites. Thus, this location was disregarded in our model. When plotting the results, this was handled by setting the variance to 0 in the location, and using the true value from the test data as the mean.

The spatial model and the sampling method was implemented using the language R (R Core Team, 2017), and test data from DREAM (April 2nd) was used as sensor readings for the AUV. Hence, for this simulation we consider the test data from DREAM to be the true distribution at all time. The time step was discretized into intervals of 5 minutes. A total of 54 updates were simulated, which corresponds to monitoring the outlets for 4.5 hours (270 minutes). The values used for the tuning parameters was $\boldsymbol{\theta} = [1, 125, 100]$ and $V = 0.05$.

The results of the simulation study are shown in Figure 3, showing results at four different time steps. The particle concentration is measured in $\mu g/L$, and the color bar shows the intensity at each location. The x-and y-axis shows the distance in metres from the seafill. The first column of plots shows the true values from DREAM. The predicted particle concentration is shown in the second column, and the third column shows the prediction variance together with the path of the AUV showing the 10 most recent sampling locations as small white dots and the current position of the AUV as a large white dot.

Comparing the predicted particle concentration with the truth from the test data it can be seen that the sampling method generally gives a smooth prediction that coincides quite well with our "true" distribution. Still, many of the finer details are overlooked, and more samples are needed to model these details.

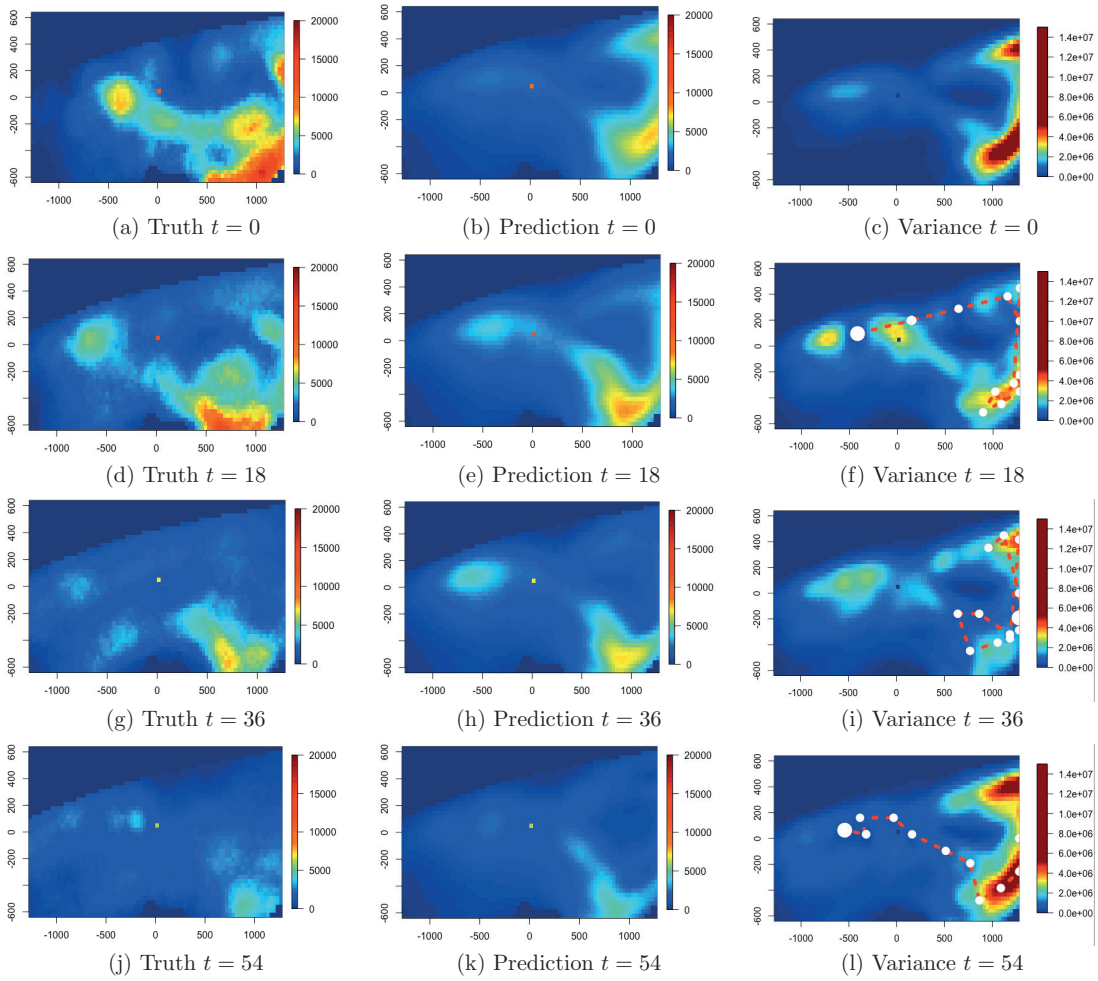


Fig. 3. Results of the simulation study at four different time steps $t = 0, 18, 36, 54$ corresponding to [0,90,180, 270] minutes. The particle concentration is measured in $\mu g/L$, and the color bar shows the intensity at each location. The x-and y-axis shows the distance in metres from the seafill. The first column of plots corresponds to the true values (a),(d),(g) and (j). The predicted mean particle concentration is shown in the second column (b), (e), (h) and (k), and the third column corresponds to the prediction variance (c), (f), (i) and(l). The path of the AUV is plotted as a red line, the small white dots shows the 10 most recent sampling locations and the large dot indicates the current position of the AUV.

Considering the path of the AUV together with the prediction variance, it can be seen that the variance is decreased near the recently sampled locations. The increase in variance proportional to the prior variance can also be clearly seen in the prediction variance plots.

The objective function controls the AUV path in an intuitive way, leading it to unexplored areas on the one hand, and in most cases assuring a reasonable travel speed for the AUV between sampling locations. The travel distance of the AUV lies between 100-400 metres for most time steps, which is a suitable distance given the time step length and the AUV speed.

An issue with the model, is that it does not seem to keep up with the rapid changing of the ocean process. Since the model relies on the observations from the AUV to catch the change in the particle concentration, the prediction results far from recently sampled locations will be inaccurate. When the dynamics of the particle transportation are fast, we will get a delay in the updating of the model. As an example, the prediction results in the upper left area can be considered. At t=18, the prediction in this area shows a smaller concentration than the true value. Then at t=36, the predicted concentration has increased in this area, but in the true model the particles have moved resulting in a low density. Finally, at t=54 the predicted and the true value is quite similar. This example shows the delay in the predicted values.

## 5. CONCLUSION AND FUTURE WORK

A method for adaptive sampling of ocean processes using an AUV is suggested, and tested using simulation data from numerical models of particle transportation near a seafill. The spatial model reconstructs the true field quite well, showing the same tendencies as the true field. Still, the temporal variability of the particle transporting is faster than the AUV can keep up with, indicating that more samples from multiple vehicles or buoys and/or a better temporal model is useful.

Future work includes expanding the model such that it considers the temporal variability of particle transportation, such that the the non-stationarity of the model is not driven by the collected data alone. Path planning can be improved both by considering optimizing for a sequence of points instead of only choosing one sampling location at a time. Fieldwork is also planned, enabling testing of the method in real ocean conditions. This will give insight in how the method works in the real world, and how this differs from simulation.

## ACKNOWLEDGEMENTS

The authors would like to thank Finn Are Michelsen and Raymond Nepstad from SINTEF Ocean AS for running the numerical models SINMOD and DREAM, and supplying the data sets used in section 4.

## REFERENCES

Binney, J., Krause, A., and Sukhatme, G.S. (2010). Informative path planning for an autonomous underwater vehicle. In *2010 IEEE International Conference on Robotics and Automation*, 4791–4796. doi: 10.1109/ROBOT.2010.5509714.

Binney, J., Krause, A., and Sukhatme, G.S. (2013). Optimizing waypoints for monitoring spatiotemporal phenomena. *The International Journal of Robotics Research*, 32(8), 873–888. doi:10.1177/0278364913488427.

Cressie, N. and Wikle, C. (2011). *Statistics for Spatio-Temporal Data*. CourseSmart Series. Wiley.

Das, J., Py, F., Harvey, J.B., Ryan, J.P., Gellene, A., Graham, R., Caron, D.A., Rajan, K., and Sukhatme, G.S. (2015). Data-driven robotic sampling for marine ecosystem monitoring. *The International Journal of Robotics Research*, 34(12), 1435–1452. doi: 10.1177/0278364915587723.

Eidsvik, J., Mukerji, T., and Bhattacharjya, D. (2015). *Value of information in the earth sciences : integrating spatial modeling and decision analysis*. Cambridge University Press, Cambridge.

Griffies, S.M., Böning, C., Bryan, F.O., Chassignet, E.P., Gerdes, R., Hasumi, H., Hirst, A., Treguier, A.M., and Webb, D. (2000). Developments in ocean climate modelling. *Ocean Modelling*, 2, 123–192. doi:10.1016/S1463-5003(00)00014-7.

Jadaliha, M. and Choi, J. (2013). Environmental monitoring using autonomous aquatic robots: Sampling algorithms and experiments. *IEEE Transactions on Control Systems Technology*, 21(3), 899–905. doi: 10.1109/TCST.2012.2190070.

Krause, A., Singh, A., and Guestrin, C. (2008). Near-optimal sensor placements in gaussian processes: Theory, efficient algorithms and empirical studies. *J. Mach. Learn. Res.*, 9, 235–284.

Lindstrøm, U., Smout, S., Howell, D., and Bogstad, B. (2009). Modelling multi-species interactions in the barents sea ecosystem with special emphasis on minke whales and their interactions with cod, herring and capelin. *Deep Sea Research Part II: Topical Studies in Oceanography*, 56(21), 2068 – 2079. doi: https://doi.org/10.1016/j.dsr2.2008.11.017. The Proceedings of the ECONORTH Symposium on Ecosystem Dynamics in the Norwegian Sea and Barents Sea.

Matérn, B. (2013). Spatial variation. *Meddelanden från Statens Skogsforskningsinstitut*, 36(5), 1–144.

R Core Team (2017). *R: A Language and Environment for Statistical Computing*. R Foundation for Statistical Computing, Vienna, Austria. URL `https://www.R-project.org/`.

Rasmussen, C.E. and Williams, C.K.I. (2005). *Gaussian Processes for Machine Learning (Adaptive Computation and Machine Learning)*. The MIT Press.

Rye, H., Reed, M., and Ekrol, N. (1998). The partrack model for calculation of the spreading and deposition of drilling mud, chemicals and drill cuttings. *Environmental Modelling Software*, 13(5), 431 – 441. doi: https://doi.org/10.1016/S1364-8152(98)00048-6.

Rye, H., Reed, M., Frost, T., Smit, M., Durgut, I., Johansen, O., and Ditlevsen, M. (2008). Development of a numerical model for calculating exposure to toxic and nontoxic stressors in the water column and sediment from drilling discharges. *Integrated environmental assessment and management*, 4, 194–203.

Slagstad, D. and McClimans, T. (2005). Modeling the ecosystem dynamics of the barents sea including the marginal ice zone: I. physical and chemical oceanography. 58, 1–18.

Stein, M.L. (2005). Nonstationary spatial covariance functions. *University of Chicago, CISES Technical Report 21*.

Yilmaz, N.K., Evangelinos, C., Lermusiaux, P.F.J., and Patrikalakis, N.M. (2008). Path planning of autonomous underwater vehicles for adaptive sampling using mixed integer linear programming. *IEEE Journal of Oceanic Engineering*, 33(4), 522–537. doi: 10.1109/JOE.2008.2002105.

Zhang, B. and Sukhatme, G.S. (2007). Adaptive sampling for estimating a scalar field using a robotic boat and a sensor network. In *Proceedings 2007 IEEE International Conference on Robotics and Automation*, 3673–3680. doi:10.1109/ROBOT.2007.364041.

Zhang, Y., Godin, M.A., Bellingham, J.G., and Ryan, J.P. (2012). Using an autonomous underwater vehicle to track a coastal upwelling front. *IEEE Journal of Oceanic Engineering*, 37(3), 338–347. doi: 10.1109/JOE.2012.2197272.

# Article F

## Autonomous Optical Survey Based on Unsupervised Segmentation of Acoustic Backscatter.

Øystein Sture, **Trygve Olav Fossum**, Martin Ludvigsen and Martin Syre Wiig.



This article is published in the proceedings of
*OCEANS - MTS/IEEE*, Kobe Techno-Oceans (OTO), Kobe, 2018, pp. 1-8.
doi: 10.1109/OCEANSKOBE.2018.8559211

# Previous PhD theses published at the Department of Marine Technology

## Previous PhD theses published at the Department of Marine Technology (earlier: Faculty of Marine Technology) NORWEGIAN UNIVERSITY OF SCIENCE AND TECHNOLOGY

| Report No. | Author | Title |
|---|---|---|
| | Kavlie, Dag | Optimization of Plane Elastic Grillages, 1967 |
| | Hansen, Hans R. | Man-Machine Communication and Data-Storage Methods in Ship Structural Design, 1971 |
| | Gisvold, Kaare M. | A Method for non-linear mixed -integer programming and its Application to Design Problems, 1971 |
| | Lund, Sverre | Tanker Frame Optimalization by means of SUMT-Transformation and Behaviour Models, 1971 |
| | Vinje, Tor | On Vibration of Spherical Shells Interacting with Fluid, 1972 |
| | Lorentz, Jan D. | Tank Arrangement for Crude Oil Carriers in Accordance with the new Anti-Pollution Regulations, 1975 |
| | Carlsen, Carl A. | Computer-Aided Design of Tanker Structures, 1975 |
| | Larsen, Carl M. | Static and Dynamic Analysis of Offshore Pipelines during Installation, 1976 |
| UR-79-01 | Brigt Hatlestad, MK | The finite element method used in a fatigue evaluation of fixed offshore platforms. (Dr.Ing. Thesis) |
| UR-79-02 | Erik Pettersen, MK | Analysis and design of cellular structures. (Dr.Ing. Thesis) |
| UR-79-03 | Sverre Valsgård, MK | Finite difference and finite element methods applied to nonlinear analysis of plated structures. (Dr.Ing. Thesis) |
| UR-79-04 | Nils T. Nordsve, MK | Finite element collapse analysis of structural members considering imperfections and stresses due to fabrication. (Dr.Ing. Thesis) |
| UR-79-05 | Ivar J. Fylling, MK | Analysis of towline forces in ocean towing systems. (Dr.Ing. Thesis) |
| UR-80-06 | Nils Sandsmark, MM | Analysis of Stationary and Transient Heat Conduction by the Use of the Finite Element Method. (Dr.Ing. Thesis) |
| UR-80-09 | Sverre Haver, MK | Analysis of uncertainties related to the stochastic modeling of ocean waves. (Dr.Ing. Thesis) |
| UR-81-15 | Odland, Jonas | On the Strength of welded Ring stiffened cylindrical Shells primarily subjected to axial Compression |
| UR-82-17 | Engesvik, Knut | Analysis of Uncertainties in the fatigue Capacity of |

| | | |
|---|---|---|
| | | Welded Joints |
| UR-82-18 | Rye, Henrik | Ocean wave groups |
| UR-83-30 | Eide, Oddvar Inge | On Cumulative Fatigue Damage in Steel Welded Joints |
| UR-83-33 | Mo, Olav | Stochastic Time Domain Analysis of Slender Offshore Structures |
| UR-83-34 | Amdahl, Jørgen | Energy absorption in Ship-platform impacts |
| UR-84-37 | Mørch, Morten | Motions and mooring forces of semi submersibles as determined by full-scale measurements and theoretical analysis |
| UR-84-38 | Soares, C. Guedes | Probabilistic models for load effects in ship structures |
| UR-84-39 | Aarsnes, Jan V. | Current forces on ships |
| UR-84-40 | Czujko, Jerzy | Collapse Analysis of Plates subjected to Biaxial Compression and Lateral Load |
| UR-85-46 | Alf G. Engseth, MK | Finite element collapse analysis of tubular steel offshore structures. (Dr.Ing. Thesis) |
| UR-86-47 | Dengody Sheshappa, MP | A Computer Design Model for Optimizing Fishing Vessel Designs Based on Techno-Economic Analysis. (Dr.Ing. Thesis) |
| UR-86-48 | Vidar Aanesland, MH | A Theoretical and Numerical Study of Ship Wave Resistance. (Dr.Ing. Thesis) |
| UR-86-49 | Heinz-Joachim Wessel, MK | Fracture Mechanics Analysis of Crack Growth in Plate Girders. (Dr.Ing. Thesis) |
| UR-86-50 | Jon Taby, MK | Ultimate and Post-ultimate Strength of Dented Tubular Members. (Dr.Ing. Thesis) |
| UR-86-51 | Walter Lian, MH | A Numerical Study of Two-Dimensional Separated Flow Past Bluff Bodies at Moderate KC-Numbers. (Dr.Ing. Thesis) |
| UR-86-52 | Bjørn Sortland, MH | Force Measurements in Oscillating Flow on Ship Sections and Circular Cylinders in a U-Tube Water Tank. (Dr.Ing. Thesis) |
| UR-86-53 | Kurt Strand, MM | A System Dynamic Approach to One-dimensional Fluid Flow. (Dr.Ing. Thesis) |
| UR-86-54 | Arne Edvin Løken, MH | Three Dimensional Second Order Hydrodynamic Effects on Ocean Structures in Waves. (Dr.Ing. Thesis) |
| UR-86-55 | Sigurd Falch, MH | A Numerical Study of Slamming of Two-Dimensional Bodies. (Dr.Ing. Thesis) |
| UR-87-56 | Arne Braathen, MH | Application of a Vortex Tracking Method to the Prediction of Roll Damping of a Two-Dimension Floating Body. (Dr.Ing. Thesis) |

| | | |
|---|---|---|
| UR-87-57 | Bernt Leira, MK | Gaussian Vector Processes for Reliability Analysis involving Wave-Induced Load Effects. (Dr.Ing. Thesis) |
| UR-87-58 | Magnus Småvik, MM | Thermal Load and Process Characteristics in a Two-Stroke Diesel Engine with Thermal Barriers (in Norwegian). (Dr.Ing. Thesis) |
| MTA-88-59 | Bernt Arild Bremdal, MP | An Investigation of Marine Installation Processes – A Knowledge - Based Planning Approach. (Dr.Ing. Thesis) |
| MTA-88-60 | Xu Jun, MK | Non-linear Dynamic Analysis of Space-framed Offshore Structures. (Dr.Ing. Thesis) |
| MTA-89-61 | Gang Miao, MH | Hydrodynamic Forces and Dynamic Responses of Circular Cylinders in Wave Zones. (Dr.Ing. Thesis) |
| MTA-89-62 | Martin Greenhow, MH | Linear and Non-Linear Studies of Waves and Floating Bodies. Part I and Part II. (Dr.Techn. Thesis) |
| MTA-89-63 | Chang Li, MH | Force Coefficients of Spheres and Cubes in Oscillatory Flow with and without Current. (Dr.Ing. Thesis |
| MTA-89-64 | Hu Ying, MP | A Study of Marketing and Design in Development of Marine Transport Systems. (Dr.Ing. Thesis) |
| MTA-89-65 | Arild Jæger, MH | Seakeeping, Dynamic Stability and Performance of a Wedge Shaped Planing Hull. (Dr.Ing. Thesis) |
| MTA-89-66 | Chan Siu Hung, MM | The dynamic characteristics of tilting-pad bearings |
| MTA-89-67 | Kim Wikstrøm, MP | Analysis av projekteringen for ett offshore projekt. (Licenciat-avhandling) |
| MTA-89-68 | Jiao Guoyang, MK | Reliability Analysis of Crack Growth under Random Loading, considering Model Updating. (Dr.Ing. Thesis) |
| MTA-89-69 | Arnt Olufsen, MK | Uncertainty and Reliability Analysis of Fixed Offshore Structures. (Dr.Ing. Thesis) |
| MTA-89-70 | Wu Yu-Lin, MR | System Reliability Analyses of Offshore Structures using improved Truss and Beam Models. (Dr.Ing. Thesis) |
| MTA-90-71 | Jan Roger Hoff, MH | Three-dimensional Green function of a vessel with forward speed in waves. (Dr.Ing. Thesis) |
| MTA-90-72 | Rong Zhao, MH | Slow-Drift Motions of a Moored Two-Dimensional Body in Irregular Waves. (Dr.Ing. Thesis) |
| MTA-90-73 | Atle Minsaas, MP | Economical Risk Analysis. (Dr.Ing. Thesis) |
| MTA-90-74 | Knut-Aril Farnes, MK | Long-term Statistics of Response in Non-linear Marine Structures. (Dr.Ing. Thesis) |
| MTA-90-75 | Torbjørn Sotberg, MK | Application of Reliability Methods for Safety Assessment of Submarine Pipelines. (Dr.Ing. |

| | | |
|---|---|---|
| | | Thesis) |
| MTA-90-76 | Zeuthen, Steffen, MP | SEAMAID. A computational model of the design process in a constraint-based logic programming environment. An example from the offshore domain. (Dr.Ing. Thesis) |
| MTA-91-77 | Haagensen, Sven, MM | Fuel Dependant Cyclic Variability in a Spark Ignition Engine - An Optical Approach. (Dr.Ing. Thesis) |
| MTA-91-78 | Løland, Geir, MH | Current forces on and flow through fish farms. (Dr.Ing. Thesis) |
| MTA-91-79 | Hoen, Christopher, MK | System Identification of Structures Excited by Stochastic Load Processes. (Dr.Ing. Thesis) |
| MTA-91-80 | Haugen, Stein, MK | Probabilistic Evaluation of Frequency of Collision between Ships and Offshore Platforms. (Dr.Ing. Thesis) |
| MTA-91-81 | Sødahl, Nils, MK | Methods for Design and Analysis of Flexible Risers. (Dr.Ing. Thesis) |
| MTA-91-82 | Ormberg, Harald, MK | Non-linear Response Analysis of Floating Fish Farm Systems. (Dr.Ing. Thesis) |
| MTA-91-83 | Marley, Mark J., MK | Time Variant Reliability under Fatigue Degradation. (Dr.Ing. Thesis) |
| MTA-91-84 | Krokstad, Jørgen R., MH | Second-order Loads in Multidirectional Seas. (Dr.Ing. Thesis) |
| MTA-91-85 | Molteberg, Gunnar A., MM | The Application of System Identification Techniques to Performance Monitoring of Four Stroke Turbocharged Diesel Engines. (Dr.Ing. Thesis) |
| MTA-92-86 | Mørch, Hans Jørgen Bjelke, MH | Aspects of Hydrofoil Design: with Emphasis on Hydrofoil Interaction in Calm Water. (Dr.Ing. Thesis) |
| MTA-92-87 | Chan Siu Hung, MM | Nonlinear Analysis of Rotordynamic Instabilities in Highspeed Turbomachinery. (Dr.Ing. Thesis) |
| MTA-92-88 | Bessason, Bjarni, MK | Assessment of Earthquake Loading and Response of Seismically Isolated Bridges. (Dr.Ing. Thesis) |
| MTA-92-89 | Langli, Geir, MP | Improving Operational Safety through exploitation of Design Knowledge - an investigation of offshore platform safety. (Dr.Ing. Thesis) |
| MTA-92-90 | Sævik, Svein, MK | On Stresses and Fatigue in Flexible Pipes. (Dr.Ing. Thesis) |
| MTA-92-91 | Ask, Tor Ø., MM | Ignition and Flame Growth in Lean Gas-Air Mixtures. An Experimental Study with a Schlieren System. (Dr.Ing. Thesis) |
| MTA-86-92 | Hessen, Gunnar, MK | Fracture Mechanics Analysis of Stiffened Tubular Members. (Dr.Ing. Thesis) |

| | | |
|---|---|---|
| MTA-93-93 | Steinebach, Christian, MM | Knowledge Based Systems for Diagnosis of Rotating Machinery. (Dr.Ing. Thesis) |
| MTA-93-94 | Dalane, Jan Inge, MK | System Reliability in Design and Maintenance of Fixed Offshore Structures. (Dr.Ing. Thesis) |
| MTA-93-95 | Steen, Sverre, MH | Cobblestone Effect on SES. (Dr.Ing. Thesis) |
| MTA-93-96 | Karunakaran, Daniel, MK | Nonlinear Dynamic Response and Reliability Analysis of Drag-dominated Offshore Platforms. (Dr.Ing. Thesis) |
| MTA-93-97 | Hagen, Arnulf, MP | The Framework of a Design Process Language. (Dr.Ing. Thesis) |
| MTA-93-98 | Nordrik, Rune, MM | Investigation of Spark Ignition and Autoignition in Methane and Air Using Computational Fluid Dynamics and Chemical Reaction Kinetics. A Numerical Study of Ignition Processes in Internal Combustion Engines. (Dr.Ing. Thesis) |
| MTA-94-99 | Passano, Elizabeth, MK | Efficient Analysis of Nonlinear Slender Marine Structures. (Dr.Ing. Thesis) |
| MTA-94-100 | Kvålsvold, Jan, MH | Hydroelastic Modelling of Wetdeck Slamming on Multihull Vessels. (Dr.Ing. Thesis) |
| MTA-94-102 | Bech, Sidsel M., MK | Experimental and Numerical Determination of Stiffness and Strength of GRP/PVC Sandwich Structures. (Dr.Ing. Thesis) |
| MTA-95-103 | Paulsen, Hallvard, MM | A Study of Transient Jet and Spray using a Schlieren Method and Digital Image Processing. (Dr.Ing. Thesis) |
| MTA-95-104 | Hovde, Geir Olav, MK | Fatigue and Overload Reliability of Offshore Structural Systems, Considering the Effect of Inspection and Repair. (Dr.Ing. Thesis) |
| MTA-95-105 | Wang, Xiaozhi, MK | Reliability Analysis of Production Ships with Emphasis on Load Combination and Ultimate Strength. (Dr.Ing. Thesis) |
| MTA-95-106 | Ulstein, Tore, MH | Nonlinear Effects of a Flexible Stern Seal Bag on Cobblestone Oscillations of an SES. (Dr.Ing. Thesis) |
| MTA-95-107 | Solaas, Frøydis, MH | Analytical and Numerical Studies of Sloshing in Tanks. (Dr.Ing. Thesis) |
| MTA-95-108 | Hellan, Øyvind, MK | Nonlinear Pushover and Cyclic Analyses in Ultimate Limit State Design and Reassessment of Tubular Steel Offshore Structures. (Dr.Ing. Thesis) |
| MTA-95-109 | Hermundstad, Ole A., MK | Theoretical and Experimental Hydroelastic Analysis of High Speed Vessels. (Dr.Ing. Thesis) |
| MTA-96-110 | Bratland, Anne K., MH | Wave-Current Interaction Effects on Large-Volume Bodies in Water of Finite Depth. (Dr.Ing. Thesis) |
| MTA-96-111 | Herfjord, Kjell, MH | A Study of Two-dimensional Separated Flow by a Combination of the Finite Element Method and |

| | | |
|---|---|---|
| | | Navier-Stokes Equations. (Dr.Ing. Thesis) |
| MTA-96-112 | Æsøy, Vilmar, MM | Hot Surface Assisted Compression Ignition in a Direct Injection Natural Gas Engine. (Dr.Ing. Thesis) |
| MTA-96-113 | Eknes, Monika L., MK | Escalation Scenarios Initiated by Gas Explosions on Offshore Installations. (Dr.Ing. Thesis) |
| MTA-96-114 | Erikstad, Stein O., MP | A Decision Support Model for Preliminary Ship Design. (Dr.Ing. Thesis) |
| MTA-96-115 | Pedersen, Egil, MH | A Nautical Study of Towed Marine Seismic Streamer Cable Configurations. (Dr.Ing. Thesis) |
| MTA-97-116 | Moksnes, Paul O., MM | Modelling Two-Phase Thermo-Fluid Systems Using Bond Graphs. (Dr.Ing. Thesis) |
| MTA-97-117 | Halse, Karl H., MK | On Vortex Shedding and Prediction of Vortex-Induced Vibrations of Circular Cylinders. (Dr.Ing. Thesis) |
| MTA-97-118 | Igland, Ragnar T., MK | Reliability Analysis of Pipelines during Laying, considering Ultimate Strength under Combined Loads. (Dr.Ing. Thesis) |
| MTA-97-119 | Pedersen, Hans-P., MP | Levendefiskteknologi for fiskefartøy. (Dr.Ing. Thesis) |
| MTA-98-120 | Vikestad, Kyrre, MK | Multi-Frequency Response of a Cylinder Subjected to Vortex Shedding and Support Motions. (Dr.Ing. Thesis) |
| MTA-98-121 | Azadi, Mohammad R. E., MK | Analysis of Static and Dynamic Pile-Soil-Jacket Behaviour. (Dr.Ing. Thesis) |
| MTA-98-122 | Ulltang, Terje, MP | A Communication Model for Product Information. (Dr.Ing. Thesis) |
| MTA-98-123 | Torbergsen, Erik, MM | Impeller/Diffuser Interaction Forces in Centrifugal Pumps. (Dr.Ing. Thesis) |
| MTA-98-124 | Hansen, Edmond, MH | A Discrete Element Model to Study Marginal Ice Zone Dynamics and the Behaviour of Vessels Moored in Broken Ice. (Dr.Ing. Thesis) |
| MTA-98-125 | Videiro, Paulo M., MK | Reliability Based Design of Marine Structures. (Dr.Ing. Thesis) |
| MTA-99-126 | Mainçon, Philippe, MK | Fatigue Reliability of Long Welds Application to Titanium Risers. (Dr.Ing. Thesis) |
| MTA-99-127 | Haugen, Elin M., MH | Hydroelastic Analysis of Slamming on Stiffened Plates with Application to Catamaran Wetdecks. (Dr.Ing. Thesis) |
| MTA-99-128 | Langhelle, Nina K., MK | Experimental Validation and Calibration of Nonlinear Finite Element Models for Use in Design of Aluminium Structures Exposed to Fire. (Dr.Ing. Thesis) |
| MTA-99- | Berstad, Are J., MK | Calculation of Fatigue Damage in Ship Structures. |

| | | |
|---|---|---|
| 129 | | (Dr.Ing. Thesis) |
| MTA-99-130 | Andersen, Trond M., MM | Short Term Maintenance Planning. (Dr.Ing. Thesis) |
| MTA-99-131 | Tveiten, Bård Wathne, MK | Fatigue Assessment of Welded Aluminium Ship Details. (Dr.Ing. Thesis) |
| MTA-99-132 | Søreide, Fredrik, MP | Applications of underwater technology in deep water archaeology. Principles and practice. (Dr.Ing. Thesis) |
| MTA-99-133 | Tønnessen, Rune, MH | A Finite Element Method Applied to Unsteady Viscous Flow Around 2D Blunt Bodies With Sharp Corners. (Dr.Ing. Thesis) |
| MTA-99-134 | Elvekrok, Dag R., MP | Engineering Integration in Field Development Projects in the Norwegian Oil and Gas Industry. The Supplier Management of Norne. (Dr.Ing. Thesis) |
| MTA-99-135 | Fagerholt, Kjetil, MP | Optimeringsbaserte Metoder for Ruteplanlegging innen skipsfart. (Dr.Ing. Thesis) |
| MTA-99-136 | Bysveen, Marie, MM | Visualization in Two Directions on a Dynamic Combustion Rig for Studies of Fuel Quality. (Dr.Ing. Thesis) |
| MTA-2000-137 | Storteig, Eskild, MM | Dynamic characteristics and leakage performance of liquid annular seals in centrifugal pumps. (Dr.Ing. Thesis) |
| MTA-2000-138 | Sagli, Gro, MK | Model uncertainty and simplified estimates of long term extremes of hull girder loads in ships. (Dr.Ing. Thesis) |
| MTA-2000-139 | Tronstad, Harald, MK | Nonlinear analysis and design of cable net structures like fishing gear based on the finite element method. (Dr.Ing. Thesis) |
| MTA-2000-140 | Kroneberg, André, MP | Innovation in shipping by using scenarios. (Dr.Ing. Thesis) |
| MTA-2000-141 | Haslum, Herbjørn Alf, MH | Simplified methods applied to nonlinear motion of spar platforms. (Dr.Ing. Thesis) |
| MTA-2001-142 | Samdal, Ole Johan, MM | Modelling of Degradation Mechanisms and Stressor Interaction on Static Mechanical Equipment Residual Lifetime. (Dr.Ing. Thesis) |
| MTA-2001-143 | Baarholm, Rolf Jarle, MH | Theoretical and experimental studies of wave impact underneath decks of offshore platforms. (Dr.Ing. Thesis) |
| MTA-2001-144 | Wang, Lihua, MK | Probabilistic Analysis of Nonlinear Wave-induced Loads on Ships. (Dr.Ing. Thesis) |
| MTA-2001-145 | Kristensen, Odd H. Holt, MK | Ultimate Capacity of Aluminium Plates under Multiple Loads, Considering HAZ Properties. (Dr.Ing. Thesis) |
| MTA-2001-146 | Greco, Marilena, MH | A Two-Dimensional Study of Green-Water |

| | | |
|---|---|---|
| | | Loading. (Dr.Ing. Thesis) |
| MTA-2001-147 | Heggelund, Svein E., MK | Calculation of Global Design Loads and Load Effects in Large High Speed Catamarans. (Dr.Ing. Thesis) |
| MTA-2001-148 | Babalola, Olusegun T., MK | Fatigue Strength of Titanium Risers – Defect Sensitivity. (Dr.Ing. Thesis) |
| MTA-2001-149 | Mohammed, Abuu K., MK | Nonlinear Shell Finite Elements for Ultimate Strength and Collapse Analysis of Ship Structures. (Dr.Ing. Thesis) |
| MTA-2002-150 | Holmedal, Lars E., MH | Wave-current interactions in the vicinity of the sea bed. (Dr.Ing. Thesis) |
| MTA-2002-151 | Rognebakke, Olav F., MH | Sloshing in rectangular tanks and interaction with ship motions. (Dr.Ing. Thesis) |
| MTA-2002-152 | Lader, Pål Furset, MH | Geometry and Kinematics of Breaking Waves. (Dr.Ing. Thesis) |
| MTA-2002-153 | Yang, Qinzheng, MH | Wash and wave resistance of ships in finite water depth. (Dr.Ing. Thesis) |
| MTA-2002-154 | Melhus, Øyvin, MM | Utilization of VOC in Diesel Engines. Ignition and combustion of VOC released by crude oil tankers. (Dr.Ing. Thesis) |
| MTA-2002-155 | Ronæss, Marit, MH | Wave Induced Motions of Two Ships Advancing on Parallel Course. (Dr.Ing. Thesis) |
| MTA-2002-156 | Økland, Ole D., MK | Numerical and experimental investigation of whipping in twin hull vessels exposed to severe wet deck slamming. (Dr.Ing. Thesis) |
| MTA-2002-157 | Ge, Chunhua, MK | Global Hydroelastic Response of Catamarans due to Wet Deck Slamming. (Dr.Ing. Thesis) |
| MTA-2002-158 | Byklum, Eirik, MK | Nonlinear Shell Finite Elements for Ultimate Strength and Collapse Analysis of Ship Structures. (Dr.Ing. Thesis) |
| IMT-2003-1 | Chen, Haibo, MK | Probabilistic Evaluation of FPSO-Tanker Collision in Tandem Offloading Operation. (Dr.Ing. Thesis) |
| IMT-2003-2 | Skaugset, Kjetil Bjørn, MK | On the Suppression of Vortex Induced Vibrations of Circular Cylinders by Radial Water Jets. (Dr.Ing. Thesis) |
| IMT-2003-3 | Chezhian, Muthu | Three-Dimensional Analysis of Slamming. (Dr.Ing. Thesis) |
| IMT-2003-4 | Buhaug, Øyvind | Deposit Formation on Cylinder Liner Surfaces in Medium Speed Engines. (Dr.Ing. Thesis) |
| IMT-2003-5 | Tregde, Vidar | Aspects of Ship Design: Optimization of Aft Hull with Inverse Geometry Design. (Dr.Ing. Thesis) |
| IMT- | Wist, Hanne Therese | Statistical Properties of Successive Ocean Wave |

| | | |
|---|---|---|
| 2003-6 | | Parameters. (Dr.Ing. Thesis) |
| IMT-2004-7 | Ransau, Samuel | Numerical Methods for Flows with Evolving Interfaces. (Dr.Ing. Thesis) |
| IMT-2004-8 | Soma, Torkel | Blue-Chip or Sub-Standard. A data interrogation approach of identity safety characteristics of shipping organization. (Dr.Ing. Thesis) |
| IMT-2004-9 | Ersdal, Svein | An experimental study of hydrodynamic forces on cylinders and cables in near axial flow. (Dr.Ing. Thesis) |
| IMT-2005-10 | Brodtkorb, Per Andreas | The Probability of Occurrence of Dangerous Wave Situations at Sea. (Dr.Ing. Thesis) |
| IMT-2005-11 | Yttervik, Rune | Ocean current variability in relation to offshore engineering. (Dr.Ing. Thesis) |
| IMT-2005-12 | Fredheim, Arne | Current Forces on Net-Structures. (Dr.Ing. Thesis) |
| IMT-2005-13 | Heggernes, Kjetil | Flow around marine structures. (Dr.Ing. Thesis |
| IMT-2005-14 | Fouques, Sebastien | Lagrangian Modelling of Ocean Surface Waves and Synthetic Aperture Radar Wave Measurements. (Dr.Ing. Thesis) |
| IMT-2006-15 | Holm, Håvard | Numerical calculation of viscous free surface flow around marine structures. (Dr.Ing. Thesis) |
| IMT-2006-16 | Bjørheim, Lars G. | Failure Assessment of Long Through Thickness Fatigue Cracks in Ship Hulls. (Dr.Ing. Thesis) |
| IMT-2006-17 | Hansson, Lisbeth | Safety Management for Prevention of Occupational Accidents. (Dr.Ing. Thesis) |
| IMT-2006-18 | Zhu, Xinying | Application of the CIP Method to Strongly Nonlinear Wave-Body Interaction Problems. (Dr.Ing. Thesis) |
| IMT-2006-19 | Reite, Karl Johan | Modelling and Control of Trawl Systems. (Dr.Ing. Thesis) |
| IMT-2006-20 | Smogeli, Øyvind Notland | Control of Marine Propellers. From Normal to Extreme Conditions. (Dr.Ing. Thesis) |
| IMT-2007-21 | Storhaug, Gaute | Experimental Investigation of Wave Induced Vibrations and Their Effect on the Fatigue Loading of Ships. (Dr.Ing. Thesis) |
| IMT-2007-22 | Sun, Hui | A Boundary Element Method Applied to Strongly Nonlinear Wave-Body Interaction Problems. (PhD Thesis, CeSOS) |
| IMT-2007-23 | Rustad, Anne Marthine | Modelling and Control of Top Tensioned Risers. (PhD Thesis, CeSOS) |
| IMT-2007-24 | Johansen, Vegar | Modelling flexible slender system for real-time simulations and control applications |
| IMT-2007-25 | Wroldsen, Anders Sunde | Modelling and control of tensegrity structures. |

| | | |
|---|---|---|
| | | (PhD Thesis, CeSOS) |
| IMT-2007-26 | Aronsen, Kristoffer Høye | An experimental investigation of in-line and combined inline and cross flow vortex induced vibrations. (Dr. avhandling, IMT) |
| IMT-2007-27 | Gao, Zhen | Stochastic Response Analysis of Mooring Systems with Emphasis on Frequency-domain Analysis of Fatigue due to Wide-band Response Processes (PhD Thesis, CeSOS) |
| IMT-2007-28 | Thorstensen, Tom Anders | Lifetime Profit Modelling of Ageing Systems Utilizing Information about Technical Condition. (Dr.ing. thesis, IMT) |
| IMT-2008-29 | Refsnes, Jon Erling Gorset | Nonlinear Model-Based Control of Slender Body AUVs (PhD Thesis, IMT) |
| IMT-2008-30 | Berntsen, Per Ivar B. | Structural Reliability Based Position Mooring. (PhD-Thesis, IMT) |
| IMT-2008-31 | Ye, Naiquan | Fatigue Assessment of Aluminium Welded Box-stiffener Joints in Ships (Dr.ing. thesis, IMT) |
| IMT-2008-32 | Radan, Damir | Integrated Control of Marine Electrical Power Systems. (PhD-Thesis, IMT) |
| IMT-2008-33 | Thomassen, Paul | Methods for Dynamic Response Analysis and Fatigue Life Estimation of Floating Fish Cages. (Dr.ing. thesis, IMT) |
| IMT-2008-34 | Pákozdi, Csaba | A Smoothed Particle Hydrodynamics Study of Two-dimensional Nonlinear Sloshing in Rectangular Tanks. (Dr.ing.thesis, IMT/ CeSOS) |
| IMT-2007-35 | Grytøyr, Guttorm | A Higher-Order Boundary Element Method and Applications to Marine Hydrodynamics. (Dr.ing.thesis, IMT) |
| IMT-2008-36 | Drummen, Ingo | Experimental and Numerical Investigation of Nonlinear Wave-Induced Load Effects in Containerships considering Hydroelasticity. (PhD thesis, CeSOS) |
| IMT-2008-37 | Skejic, Renato | Maneuvering and Seakeeping of a Singel Ship and of Two Ships in Interaction. (PhD-Thesis, CeSOS) |
| IMT-2008-38 | Harlem, Alf | An Age-Based Replacement Model for Repairable Systems with Attention to High-Speed Marine Diesel Engines. (PhD-Thesis, IMT) |
| IMT-2008-39 | Alsos, Hagbart S. | Ship Grounding. Analysis of Ductile Fracture, Bottom Damage and Hull Girder Response. (PhD-thesis, IMT) |
| IMT-2008-40 | Graczyk, Mateusz | Experimental Investigation of Sloshing Loading and Load Effects in Membrane LNG Tanks Subjected to Random Excitation. (PhD-thesis, CeSOS) |
| IMT-2008-41 | Taghipour, Reza | Efficient Prediction of Dynamic Response for Flexible amd Multi-body Marine Structures. (PhD- |

| | | |
|---|---|---|
| | | thesis, CeSOS) |
| IMT-2008-42 | Ruth, Eivind | Propulsion control and thrust allocation on marine vessels. (PhD thesis, CeSOS) |
| IMT-2008-43 | Nystad, Bent Helge | Technical Condition Indexes and Remaining Useful Life of Aggregated Systems. PhD thesis, IMT |
| IMT-2008-44 | Soni, Prashant Kumar | Hydrodynamic Coefficients for Vortex Induced Vibrations of Flexible Beams, PhD thesis, CeSOS |
| IMT-2009-45 | Amlashi, Hadi K.K. | Ultimate Strength and Reliability-based Design of Ship Hulls with Emphasis on Combined Global and Local Loads. PhD Thesis, IMT |
| IMT-2009-46 | Pedersen, Tom Arne | Bond Graph Modelling of Marine Power Systems. PhD Thesis, IMT |
| IMT-2009-47 | Kristiansen, Trygve | Two-Dimensional Numerical and Experimental Studies of Piston-Mode Resonance. PhD-Thesis, CeSOS |
| IMT-2009-48 | Ong, Muk Chen | Applications of a Standard High Reynolds Number Model and a Stochastic Scour Prediction Model for Marine Structures. PhD-thesis, IMT |
| IMT-2009-49 | Hong, Lin | Simplified Analysis and Design of Ships subjected to Collision and Grounding. PhD-thesis, IMT |
| IMT-2009-50 | Koushan, Kamran | Vortex Induced Vibrations of Free Span Pipelines, PhD thesis, IMT |
| IMT-2009-51 | Korsvik, Jarl Eirik | Heuristic Methods for Ship Routing and Scheduling. PhD-thesis, IMT |
| IMT-2009-52 | Lee, Jihoon | Experimental Investigation and Numerical in Analyzing the Ocean Current Displacement of Longlines. Ph.d.-Thesis, IMT. |
| IMT-2009-53 | Vestbøstad, Tone Gran | A Numerical Study of Wave-in-Deck Impact usin a Two-Dimensional Constrained Interpolation Profile Method, Ph.d.thesis, CeSOS. |
| IMT-2009-54 | Bruun, Kristine | Bond Graph Modelling of Fuel Cells for Marine Power Plants. Ph.d.-thesis, IMT |
| IMT 2009-55 | Holstad, Anders | Numerical Investigation of Turbulence in a Sekwed Three-Dimensional Channel Flow, Ph.d.-thesis, IMT. |
| IMT 2009-56 | Ayala-Uraga, Efren | Reliability-Based Assessment of Deteriorating Ship-shaped Offshore Structures, Ph.d.-thesis, IMT |
| IMT 2009-57 | Kong, Xiangjun | A Numerical Study of a Damaged Ship in Beam Sea Waves. Ph.d.-thesis, IMT/CeSOS. |
| IMT 2010-58 | Kristiansen, David | Wave Induced Effects on Floaters of Aquaculture Plants, Ph.d.-thesis, CeSOS. |

| | | |
|---|---|---|
| IMT 2010-59 | Ludvigsen, Martin | An ROV-Toolbox for Optical and Acoustic Scientific Seabed Investigation. Ph.d.-thesis IMT. |
| IMT 2010-60 | Hals, Jørgen | Modelling and Phase Control of Wave-Energy Converters. Ph.d.thesis, CeSOS. |
| IMT 2010- 61 | Shu, Zhi | Uncertainty Assessment of Wave Loads and Ultimate Strength of Tankers and Bulk Carriers in a Reliability Framework. Ph.d. Thesis, IMT/ CeSOS |
| IMT 2010-62 | Shao, Yanlin | Numerical Potential-Flow Studies on Weakly-Nonlinear Wave-Body Interactions with/without Small Forward Speed, Ph.d.thesis,CeSOS. |
| IMT 2010-63 | Califano, Andrea | Dynamic Loads on Marine Propellers due to Intermittent Ventilation. Ph.d.thesis, IMT. |
| IMT 2010-64 | El Khoury, George | Numerical Simulations of Massively Separated Turbulent Flows, Ph.d.-thesis, IMT |
| IMT 2010-65 | Seim, Knut Sponheim | Mixing Process in Dense Overflows with Emphasis on the Faroe Bank Channel Overflow. Ph.d.thesis, IMT |
| IMT 2010-66 | Jia, Huirong | Structural Analysis of Intect and Damaged Ships in a Collission Risk Analysis Perspective. Ph.d.thesis CeSoS. |
| IMT 2010-67 | Jiao, Linlin | Wave-Induced Effects on a Pontoon-type Very Large Floating Structures (VLFS). Ph.D.-thesis, CeSOS. |
| IMT 2010-68 | Abrahamsen, Bjørn Christian | Sloshing Induced Tank Roof with Entrapped Air Pocket. Ph.d.thesis, CeSOS. |
| IMT 2011-69 | Karimirad, Madjid | Stochastic Dynamic Response Analysis of Spar-Type Wind Turbines with Catenary or Taut Mooring Systems. Ph.d.-thesis, CeSOS. |
| IMT - 2011-70 | Erlend Meland | Condition Monitoring of Safety Critical Valves. Ph.d.-thesis, IMT. |
| IMT – 2011-71 | Yang, Limin | Stochastic Dynamic System Analysis of Wave Energy Converter with Hydraulic Power Take-Off, with Particular Reference to Wear Damage Analysis, Ph.d. Thesis, CeSOS. |
| IMT – 2011-72 | Visscher, Jan | Application of Particla Image Velocimetry on Turbulent Marine Flows, Ph.d.Thesis, IMT. |
| IMT – 2011-73 | Su, Biao | Numerical Predictions of Global and Local Ice Loads on Ships. Ph.d.Thesis, CeSOS. |
| IMT – 2011-74 | Liu, Zhenhui | Analytical and Numerical Analysis of Iceberg Collision with Ship Structures. Ph.d.Thesis, IMT. |
| IMT – 2011-75 | Aarsæther, Karl Gunnar | Modeling and Analysis of Ship Traffic by Observation and Numerical Simulation. Ph.d.Thesis, IMT. |

| | | |
|---|---|---|
| Imt – 2011-76 | Wu, Jie | Hydrodynamic Force Identification from Stochastic Vortex Induced Vibration Experiments with Slender Beams. Ph.d.Thesis, IMT. |
| Imt – 2011-77 | Amini, Hamid | Azimuth Propulsors in Off-design Conditions. Ph.d.Thesis, IMT. |
| IMT – 2011-78 | Nguyen, Tan-Hoi | Toward a System of Real-Time Prediction and Monitoring of Bottom Damage Conditions During Ship Grounding. Ph.d.thesis, IMT. |
| IMT- 2011-79 | Tavakoli, Mohammad T. | Assessment of Oil Spill in Ship Collision and Grounding, Ph.d.thesis, IMT. |
| IMT- 2011-80 | Guo, Bingjie | Numerical and Experimental Investigation of Added Resistance in Waves. Ph.d.Thesis, IMT. |
| IMT- 2011-81 | Chen, Qiaofeng | Ultimate Strength of Aluminium Panels, considering HAZ Effects, IMT |
| IMT- 2012-82 | Kota, Ravikiran S. | Wave Loads on Decks of Offshore Structures in Random Seas, CeSOS. |
| IMT- 2012-83 | Sten, Ronny | Dynamic Simulation of Deep Water Drilling Risers with Heave Compensating System, IMT. |
| IMT- 2012-84 | Berle, Øyvind | Risk and resilience in global maritime supply chains, IMT. |
| IMT- 2012-85 | Fang, Shaoji | Fault Tolerant Position Mooring Control Based on Structural Reliability, CeSOS. |
| IMT- 2012-86 | You, Jikun | Numerical studies on wave forces and moored ship motions in intermediate and shallow water, CeSOS. |
| IMT- 2012-87 | Xiang ,Xu | Maneuvering of two interacting ships in waves, CeSOS |
| IMT- 2012-88 | Dong, Wenbin | Time-domain fatigue response and reliability analysis of offshore wind turbines with emphasis on welded tubular joints and gear components, CeSOS |
| IMT- 2012-89 | Zhu, Suji | Investigation of Wave-Induced Nonlinear Load Effects in Open Ships considering Hull Girder Vibrations in Bending and Torsion, CeSOS |
| IMT- 2012-90 | Zhou, Li | Numerical and Experimental Investigation of Station-keeping in Level Ice, CeSOS |
| IMT- 2012-91 | Ushakov, Sergey | Particulate matter emission characteristics from diesel enignes operating on conventional and alternative marine fuels, IMT |
| IMT- 2013-1 | Yin, Decao | Experimental and Numerical Analysis of Combined In-line and Cross-flow Vortex Induced Vibrations, CeSOS |

| | | |
|---|---|---|
| IMT-2013-2 | Kurniawan, Adi | Modelling and geometry optimisation of wave energy converters, CeSOS |
| IMT-2013-3 | Al Ryati, Nabil | Technical condition indexes doe auxiliary marine diesel engines, IMT |
| IMT-2013-4 | Firoozkoohi, Reza | Experimental, numerical and analytical investigation of the effect of screens on sloshing, CeSOS |
| IMT-2013-5 | Ommani, Babak | Potential-Flow Predictions of a Semi-Displacement Vessel Including Applications to Calm Water Broaching, CeSOS |
| IMT-2013-6 | Xing, Yihan | Modelling and analysis of the gearbox in a floating spar-type wind turbine, CeSOS |
| IMT-7-2013 | Balland, Océane | Optimization models for reducing air emissions from ships, IMT |
| IMT-8-2013 | Yang, Dan | Transitional wake flow behind an inclined flat plate-----Computation and analysis, IMT |
| IMT-9-2013 | Abdillah, Suyuthi | Prediction of Extreme Loads and Fatigue Damage for a Ship Hull due to Ice Action, IMT |
| IMT-10-2013 | Ramìrez, Pedro Agustìn Pèrez | Ageing management and life extension of technical systems-<br>Concepts and methods applied to oil and gas facilities, IMT |
| IMT-11-2013 | Chuang, Zhenju | Experimental and Numerical Investigation of Speed Loss due to Seakeeping and Maneuvering. IMT |
| IMT-12-2013 | Etemaddar, Mahmoud | Load and Response Analysis of Wind Turbines under Atmospheric Icing and Controller System Faults with Emphasis on Spar Type Floating Wind Turbines, IMT |
| IMT-13-2013 | Lindstad, Haakon | Strategies and measures for reducing maritime CO2 emissons, IMT |
| IMT-14-2013 | Haris, Sabril | Damage interaction analysis of ship collisions, IMT |
| IMT-15-2013 | Shainee, Mohamed | Conceptual Design, Numerical and Experimental Investigation of a SPM Cage Concept for Offshore Mariculture, IMT |
| IMT-16-2013 | Gansel, Lars | Flow past porous cylinders and effects of biofouling and fish behavior on the flow in and around Atlantic salmon net cages, IMT |
| IMT-17-2013 | Gaspar, Henrique | Handling Aspects of Complexity in Conceptual Ship Design, IMT |
| IMT-18-2013 | Thys, Maxime | Theoretical and Experimental Investigation of a Free Running Fishing Vessel at Small Frequency of Encounter, CeSOS |
| IMT-19-2013 | Aglen, Ida | VIV in Free Spanning Pipelines, CeSOS |

| | | |
|---|---|---|
| IMT-1-2014 | Song, An | Theoretical and experimental studies of wave diffraction and radiation loads on a horizontally submerged perforated plate, CeSOS |
| IMT-2-2014 | Rogne, Øyvind Ygre | Numerical and Experimental Investigation of a Hinged 5-body Wave Energy Converter, CeSOS |
| IMT-3-2014 | Dai, Lijuan | Safe and efficient operation and maintenance of offshore wind farms ,IMT |
| IMT-4-2014 | Bachynski, Erin Elizabeth | Design and Dynamic Analysis of Tension Leg Platform Wind Turbines, CeSOS |
| IMT-5-2014 | Wang, Jingbo | Water Entry of Freefall Wedged – Wedge motions and Cavity Dynamics, CeSOS |
| IMT-6-2014 | Kim, Ekaterina | Experimental and numerical studies related to the coupled behavior of ice mass and steel structures during accidental collisions, IMT |
| IMT-7-2014 | Tan, Xiang | Numerical investigation of ship's continuous- mode icebreaking in leverl ice, CeSOS |
| IMT-8-2014 | Muliawan, Made Jaya | Design and Analysis of Combined Floating Wave and Wind Power Facilities, with Emphasis on Extreme Load Effects of the Mooring System, CeSOS |
| IMT-9-2014 | Jiang, Zhiyu | Long-term response analysis of wind turbines with an emphasis on fault and shutdown conditions, IMT |
| IMT-10-2014 | Dukan, Fredrik | ROV Motion Control Systems, IMT |
| IMT-11-2014 | Grimsmo, Nils I. | Dynamic simulations of hydraulic cylinder for heave compensation of deep water drilling risers, IMT |
| IMT-12-2014 | Kvittem, Marit I. | Modelling and response analysis for fatigue design of a semisubmersible wind turbine, CeSOS |
| IMT-13-2014 | Akhtar, Juned | The Effects of Human Fatigue on Risk at Sea, IMT |
| IMT-14-2014 | Syahroni, Nur | Fatigue Assessment of Welded Joints Taking into Account Effects of Residual Stress, IMT |
| IMT-1-2015 | Bøckmann, Eirik | Wave Propulsion of ships, IMT |
| IMT-2-2015 | Wang, Kai | Modelling and dynamic analysis of a semi-submersible floating vertical axis wind turbine, CeSOS |
| IMT-3-2015 | Fredriksen, Arnt Gunvald | A numerical and experimental study of a two-dimensional body with moonpool in waves and current, CeSOS |
| IMT-4-2015 | Jose Patricio Gallardo Canabes | Numerical studies of viscous flow around bluff bodies, IMT |

| | | |
|---|---|---|
| IMT-5-2015 | Vegard Longva | Formulation and application of finite element techniques for slender marine structures subjected to contact interactions, IMT |
| IMT-6-2015 | Jacobus De Vaal | Aerodynamic modelling of floating wind turbines, CeSOS |
| IMT-7-2015 | Fachri Nasution | Fatigue Performance of Copper Power Conductors, IMT |
| IMT-8-2015 | Oleh I Karpa | Development of bivariate extreme value distributions for applications in marine technology,CeSOS |
| IMT-9-2015 | Daniel de Almeida Fernandes | An output feedback motion control system for ROVs, AMOS |
| IMT-10-2015 | Bo Zhao | Particle Filter for Fault Diagnosis: Application to Dynamic Positioning Vessel and Underwater Robotics, CeSOS |
| IMT-11-2015 | Wenting Zhu | Impact of emission allocation in maritime transportation, IMT |
| IMT-12-2015 | Amir Rasekhi Nejad | Dynamic Analysis and Design of Gearboxes in Offshore Wind Turbines in a Structural Reliability Perspective, CeSOS |
| IMT-13-2015 | Arturo Jesùs Ortega Malca | Dynamic Response of Flexibles Risers due to Unsteady Slug Flow, CeSOS |
| IMT-14-2015 | Dagfinn Husjord | Guidance and decision-support system for safe navigation of ships operating in close proximity, IMT |
| IMT-15-2015 | Anirban Bhattacharyya | Ducted Propellers: Behaviour in Waves and Scale Effects, IMT |
| IMT-16-2015 | Qin Zhang | Image Processing for Ice Parameter Identification in Ice Management, IMT |
| IMT-1-2016 | Vincentius Rumawas | Human Factors in Ship Design and Operation: An Experiential Learning, IMT |
| IMT-2-2016 | Martin Storheim | Structural response in ship-platform and ship-ice collisions, IMT |
| IMT-3-2016 | Mia Abrahamsen Prsic | Numerical Simulations of the Flow around single and Tandem Circular Cylinders Close to a Plane Wall, IMT |
| IMT-4-2016 | Tufan Arslan | Large-eddy simulations of cross-flow around ship sections, IMT |

| | | |
|---|---|---|
| IMT-5-2016 | Pierre Yves-Henry | Parametrisation of aquatic vegetation in hydraulic and coastal research,IMT |
| IMT-6-2016 | Lin Li | Dynamic Analysis of the Instalation of Monopiles for Offshore Wind Turbines, CeSOS |
| IMT-7-2016 | Øivind Kåre Kjerstad | Dynamic Positioning of Marine Vessels in Ice, IMT |
| IMT-8-2016 | Xiaopeng Wu | Numerical Analysis of Anchor Handling and Fish Trawling Operations in a Safety Perspective, CeSOS |
| IMT-9-2016 | Zhengshun Cheng | Integrated Dynamic Analysis of Floating Vertical Axis Wind Turbines, CeSOS |
| IMT-10-2016 | Ling Wan | Experimental and Numerical Study of a Combined Offshore Wind and Wave Energy Converter Concept |
| IMT-11-2016 | Wei Chai | Stochastic dynamic analysis and reliability evaluation of the roll motion for ships in random seas, CeSOS |
| IMT-12-2016 | Øyvind Selnes Patricksson | Decision support for conceptual ship design with focus on a changing life cycle and future uncertainty, IMT |
| IMT-13-2016 | Mats Jørgen Thorsen | Time domain analysis of vortex-induced vibrations, IMT |
| IMT-14-2016 | Edgar McGuinness | Safety in the Norwegian Fishing Fleet – Analysis and measures for improvement, IMT |
| IMT-15-2016 | Sepideh Jafarzadeh | Energy effiency and emission abatement in the fishing fleet, IMT |
| IMT-16-2016 | Wilson Ivan Guachamin Acero | Assessment of marine operations for offshore wind turbine installation with emphasis on response-based operational limits, IMT |
| IMT-17-2016 | Mauro Candeloro | Tools and Methods for Autonomous Operations on Seabed and Water Coumn using Underwater Vehicles, IMT |
| IMT-18-2016 | Valentin Chabaud | Real-Time Hybrid Model Testing of Floating Wind Tubines, IMT |
| IMT-1-2017 | Mohammad Saud Afzal | Three-dimensional streaming in a sea bed boundary layer |
| IMT-2-2017 | Peng Li | A Theoretical and Experimental Study of Wave-induced Hydroelastic Response of a Circular Floating Collar |
| IMT-3-2017 | Martin Bergström | A simulation-based design method for arctic maritime transport systems |

| | | |
|---|---|---|
| IMT-4-2017 | Bhushan Taskar | The effect of waves on marine propellers and propulsion |
| IMT-5-2017 | Mohsen Bardestani | A two-dimensional numerical and experimental study of a floater with net and sinker tube in waves and current |
| IMT-6-2017 | Fatemeh Hoseini Dadmarzi | Direct Numerical Simualtion of turbulent wakes behind different plate configurations |
| IMT-7-2017 | Michel R. Miyazaki | Modeling and control of hybrid marine power plants |
| IMT-8-2017 | Giri Rajasekhar Gunnu | Safety and effiency enhancement of anchor handling operations with particular emphasis on the stability of anchor handling vessels |
| IMT-9-2017 | Kevin Koosup Yum | Transient Performance and Emissions of a Turbocharged Diesel Engine for Marine Power Plants |
| IMT-10-2017 | Zhaolong Yu | Hydrodynamic and structural aspects of ship collisions |
| IMT-11-2017 | Martin Hassel | Risk Analysis and Modelling of Allisions between Passing Vessels and Offshore Installations |
| IMT-12-2017 | Astrid H. Brodtkorb | Hybrid Control of Marine Vessels – Dynamic Positioning in Varying Conditions |
| IMT-13-2017 | Kjersti Bruserud | Simultaneous stochastic model of waves and current for prediction of structural design loads |
| IMT-14-2017 | Finn-Idar Grøtta Giske | Long-Term Extreme Response Analysis of Marine Structures Using Inverse Reliability Methods |
| IMT-15-2017 | Stian Skjong | Modeling and Simulation of Maritime Systems and Operations for Virtual Prototyping using co-Simulations |
| IMT-1-2018 | Yingguang Chu | Virtual Prototyping for Marine Crane Design and Operations |
| IMT-2-2018 | Sergey Gavrilin | Validation of ship manoeuvring simulation models |
| IMT-3-2018 | Jeevith Hegde | Tools and methods to manage risk in autonomous subsea inspection,maintenance and repair operations |
| IMT-4-2018 | Ida M. Strand | Sea Loads on Closed Flexible Fish Cages |
| IMT-5-2018 | Erlend Kvinge Jørgensen | Navigation and Control of Underwater Robotic Vehicles |

| | | |
|---|---|---|
| IMT-6-2018 | Bård Stovner | Aided Intertial Navigation of Underwater Vehicles |
| IMT-7-2018 | Erlend Liavåg Grotle | Thermodynamic Response Enhanced by Sloshing in Marine LNG Fuel Tanks |
| IMT-8-2018 | Børge Rokseth | Safety and Verification of Advanced Maritime Vessels |
| IMT-9-2018 | Jan Vidar Ulveseter | Advances in Semi-Empirical Time Domain Modelling of Vortex-Induced Vibrations |
| IMT-10-2018 | Chenyu Luan | Design and analysis for a steel braceless semi-submersible hull for supporting a 5-MW horizontal axis wind turbine |
| IMT-11-2018 | Carl Fredrik Rehn | Ship Design under Uncertainty |
| IMT-12-2018 | Øyvind Ødegård | Towards Autonomous Operations and Systems in Marine Archaeology |
| IMT-13-2018 | Stein Melvær Nornes | Guidance and Control of Marine Robotics for Ocean Mapping and Monitoring |
| IMT-14-2018 | Petter Norgren | Autonomous Underwater Vehicles in Arctic Marine Operations: Arctic marine research and ice monitoring |
| IMT-15-2018 | Minjoo Choi | Modular Adaptable Ship Design for Handling Uncertainty in the Future Operating Context |
| MT-16-2018 | Ole Alexander Eidsvik | Dynamics of Remotely Operated Underwater Vehicle Systems |
| IMT-17-2018 | Mahdi Ghane | Fault Diagnosis of Floating Wind Turbine Drivetrain- Methodologies and Applications |
| IMT-18-2018 | Christoph Alexander Thieme | Risk Analysis and Modelling of Autonomous Marine Systems |
| IMT-19-2018 | Yugao Shen | Operational limits for floating-collar fish farms in waves and current, without and with well-boat presence |
| IMT-20-2018 | Tianjiao Dai | Investigations of Shear Interaction and Stresses in Flexible Pipes and Umbilicals |
| IMT-21-2018 | Sigurd Solheim Pettersen | Resilience by Latent Capabilities in Marine Systems |
| IMT-22-2018 | Thomas Sauder | Fidelity of Cyber-physical Empirical Methods. Application to the Active Truncation of Slender Marine Structures |
| IMT-23-2018 | Jan-Tore Horn | Statistical and Modelling Uncertainties in the Design of Offshore Wind Turbines |

| | | |
|---|---|---|
| IMT-24-2018 | Anna Swider | Data Mining Methods for the Analysis of Power Systems of Vessels |
| IMT-1-2019 | Zhao He | Hydrodynamic study of a moored fish farming cage with fish influence |
| IMT-2-2019 | Isar Ghamari | Numerical and Experimental Study on the Ship Parametric Roll Resonance and the Effect of Anti-Roll Tank |
| IMT-3-2019 | Håkon Strandenes | Turbulent Flow Simulations at Higher Reynolds Numbers |
| IMT-4-2019 | Siri Mariane Holen | Safety in Norwegian Fish Farming – Concepts and Methods for Improvement |
| IMT-5-2019 | Ping Fu | Reliability Analysis of Wake-Induced Riser Collision |
| IMT-6-2019 | Vladimir Krivopolianskii | Experimental Investigation of Injection and Combustion Processes in Marine Gas Engines using Constant Volume Rig |
| IMT-7-2019 | Anna Maria Kozlowska | Hydrodynamic Loads on Marine Propellers Subject to Ventilation and out of Water Condition. |
| IMT-8-2019 | Hans-Martin Heyn | Motion Sensing on Vessels Operating in Sea Ice: A Local Ice Monitoring System for Transit and Stationkeeping Operations under the Influence of Sea Ice |
| IMT-9-2019\| | Stefan Vilsen | Method for Real-Time Hybrid Model Testing of Ocean Structures – Case on Slender Marine Systems |
| IMT-10-2019 | Finn-Christian W. Hanssen | Non-Linear Wave-Body Interaction in Severe Waves |
| IMT-11-2019 | Trygve Olav Fossum | Adaptive Sampling for Marine Robotics |